

**IMPROVING ADOPTIVE CELL THERAPY TO OVERCOME TUMOR  
RESISTANCE**

**MS-275 ENHANCES ANTITUMOR IMMUNITY DURING ADOPTIVE CELL  
THERAPY TO OVERCOME TUMOR RESISTANCE**

By ANDREW NGUYEN, M.Sc

A Thesis Submitted to the School of Graduate Studies in  
Partial Fulfillment of the Requirements for the Degree Doctor of Philosophy

DOCTOR OF PHILOSOPHY (2021) (Medical Sciences)

McMaster University Hamilton, Ontario

TITLE: MS-275 enhances antitumor immunity during adoptive cell therapy to overcome tumor resistance

AUTHOR: Andrew Nguyen, M.Sc (McMaster University)

SUPERVISOR: Dr. Yonghong Wan

NUMBER OF PAGES: xix, 229

**Lay Abstract:**

The host immune system has the ability to recognize and destroy tumor cells. Therapeutic platforms that leverage antitumor immune cells, specifically T cells, have shown potency in the elimination of cancer. In the clinic, cancer immunotherapies have demonstrated early success against hematological malignancies; however, are unreliable in the treatment of solid tumors. Solid tumors utilize intrinsic and adapted mechanisms of resistance to mitigate the effectiveness of cancer immunotherapy. This thesis pursues research questions aimed at understanding how tumors resist immunotherapy, what mechanisms are utilized, and how to overcome these obstacles. We anticipate that these results will contribute to the development and incorporation of strategies to subvert tumor resistance and potentiate T cells against solid tumors.

**Abstract:**

Cancer immunotherapy has gained attention in recent years for its successes in potentiating immune responses that can elicit tumor control. In particular, adoptive cell therapy (ACT), which involves the autologous/allogeneic transplant of *ex vivo*-cultivated tumor-specific T lymphocytes, can mediate potent tumor recognition and killing; however, durable clinical responses are often difficult to obtain in solid tumors. Solid tumors and their unique microenvironments have the capacity to evade and suppress antitumor immune responses and represent significant hurdles for effective ACT. Recently, we have discovered that chemical inhibition of histone deacetylases via MS-275 (Entinostat) during ACT can subvert tumor resistance to foster potent, broad-spectrum antitumor immunity. Overall, the work described supports the efficacy of ACT in the treatment of immunosuppressive, solid tumors; however, consistency in durable clinical outcomes can only be achieved through the concurrent therapeutic targeting of tumor resistance mechanisms.

This thesis uses pre-clinical models to describe how tumor resistance to ACT can manifest, and demonstrates that concurrent MS-275 delivery drives extensive immunomodulation to promote sustained tumor clearance. This includes:

- 1) The polarization of tumor-infiltrating myeloid cells into cytotoxic effectors with the ability to reject immune escape variants
- 2) The inflammatory remodeling of the tumor microenvironment to potentiate epitope spreading against secondary tumor antigens
- 3) The transcriptional reprogramming of adoptively transferred T cells to overcome tumor-burden-dependent exhaustion

We expect that the results will help facilitate the development of next-generation ACT platforms that will feature strategies for multi-mechanistic perturbation of tumor resistance.

### **Acknowledgements:**

To say that this experience has been not fraught with emotional hardship would be to undersell the effort my mentors have undertaken to guide me to where I am today. The anxiety, the self-doubt, the frustration... in spite of all these feelings that persist to this day, at this moment, I am filled with nothing but gratitude.

Thank you, Dr. Yonghong Wan. It may have been a rocky road, but I am glad that you were patient with me and allowed me the autonomy to develop my own scientific interests and skills. No one loves science more than you, and it has really shaped my research intentions both during my time here and moving forward. Although I still do not know where my path may lead, I will retain that spirit of genuine curiosity and passion for research for as long as I am able. After I defend, let us go for that walk and talk about where our journeys will take us next.

Thank you, Dr. Jonathan Bramson and Dr. Matt Miller. I appreciate both of you taking the time to act as members of my supervisory committee. Your guidance has strengthened my development as a researcher and my confidence in discussing my scientific insights. I hope to one day match the caliber of mentorship that you both have displayed during my study period.

Thank you, Dr. Sam Workenhe and Dr. Scott Walsh. You both have been pivotal presences during my time in the laboratory. I learned much from your approaches to scientific inquiry and your perspectives on this career path. More importantly, you were both gracious in our discussions despite my naivety as a junior scientist. Sam – I wish you continued success and know that you will run your lab with an iron fist. Just stop investing in crypto... Scott – Despite little Owen occupying all of your time these days, you are still as productive as ever and have grown so much as a leadership presence. I know you will find success wherever your career takes you.

Thank you, Dr. Lan Chen, Omar, and all the members of Wan Lab. Thank you for enriching my academic experience. I know our paths will cross again someday.

## Table of Contents:

### Preliminary Pages:

Title Page .....	i
Descriptive Note .....	ii
Lay Abstract.....	iii
Abstract .....	iv
Acknowledgements.....	v
Table of Contents .....	vi-viii
List of Figures and Tables.....	ix-xii
List of All Abbreviations and Symbols .....	xiii-xvi
Declaration of Academic Achievement .....	xvii
Preface.....	xviii-xix

### Main Text:

<b>1.0 Chapter One – Introduction .....</b>	<b>1-16</b>
1.1 Background .....	1
1.1.1 The Threat of Cancer .....	1
1.1.2 Tumorigenesis and the Hallmarks of Cancer .....	1
1.1.3 Cancer Immunosurveillance .....	1
1.1.4 Cancer Immunoediting.....	2
1.2 Cancer Immunotherapy as a Platform for Tumor Control.....	3
1.2.1 Adoptive Cell Therapy .....	3
1.2.2 Cancer Vaccines.....	4
1.2.3 The Marriage between ACT and Cancer Vaccination .....	6
1.3 The Challenges Facing Cancer Immunotherapy.....	6
1.3.1 Tumor-induced Immunosuppression .....	6
1.3.2 Regulatory T Cells .....	7
1.3.3 Myeloid-Derived Suppressor Cells (MDSCs) .....	8

1.3.4	Immune Selection and Escape .....	10
1.3.5	T cell exhaustion .....	11
1.4	The Prospect of Combination Therapy .....	11
1.4.1	Histone Acetylation as a Target for Gene Regulation .....	12
1.4.2	The Therapeutic Potential of HDAC Inhibitors .....	13
1.4.3	Benzamides and MS-275 (Entinostat) .....	14
1.4.4	HDACi for Cancer Immunotherapy .....	15
1.5	Thesis Scope and Content .....	15

## **2.0 Chapter Two – HDACi Delivery Reprograms Tumor-Infiltrating**

<b>Myeloid Cells to Eliminate Antigen-Loss Variants .....</b>		<b>17-74</b>
2.1	Introduction .....	17
2.2	Manuscript status, copyright, and citation .....	17
2.3	Published journal article .....	18-74

## **3.0 Chapter Three – HDACi promotes inflammatory remodeling of the tumor microenvironment to enhance epitope spreading and antitumor immunity.....75-118**

3.1	Introduction .....	75
3.2	Manuscript status, copyright, and citation .....	75
3.3	Article pre-print .....	76-118

## **4.0 Chapter Four – T cell transcriptional reprogramming overcomes tumor burden induced cellular exhaustion.....119-176**

4.1	Introduction .....	119
4.2	Manuscript status, copyright, and citation .....	119
4.3	Article pre-print .....	120-176

## **5.0 Chapter Five – Conclusions .....**

5.1	Tumor resistance can supersede potent therapy-driven antitumor immune responses .....	177
-----	---------------------------------------------------------------------------------------	-----



5.2	TME reprogramming induces a cascade of pro-inflammatory events that disrupt tumor immunosuppression and potentiate antitumor immunity .	177
5.3	Selective inhibition of Class I HDACs may ubiquitously promote antitumor programmes .....	178
5.4	Reinvigoration of endogenous T cells is critical for cancer immunotherapy in resistant tumors .....	179
5.5	The Future of HDAC Inhibition in Cancer Immunotherapy .....	179
5.6	Desired Post-activation T Cell Phenotypes for Cancer Immunotherapy .	180
<b>6.0 Chapter Six – References .....</b>		<b>181-204</b>
<b>7.0 Chapter Seven – Appendix.....</b>		<b>205-229</b>
7.1	Functional analysis of tumor-infiltrating myeloid cells by flow cytometry and adoptive transfer.....	205-217
7.2	De novo necroptosis creates an inflammatory environment mediating tumor susceptibility to immune checkpoint inhibitors .....	218-229

## **Lists of Figures and Tables:**

### **2.0 Chapter Two – HDACi Delivery Reprograms Tumor-Infiltrating Myeloid Cells to Eliminate Antigen-Loss Variants**

Figure 1: ACT+OV-mediated CD8 <sup>+</sup> T cell expansion regressed tumors, but subsequent loss of antigen recognition promotes tumor relapse	51
Figure 2: Concomitant MS-275 delivery prevents tumor relapse by mediating the elimination of gene-loss variants	52
Figure 3: Concomitant MS-275 delivery induces a pro-inflammatory phenotype within tumor-infiltrating CD11b <sup>+</sup> Ly6Chi Ly6G <sup>-</sup> myeloid cells	53
Figure 4: Pro-inflammatory tumor-infiltrating myeloid cells display decreased suppressiveness and demonstrate tumor killing capacity	54
Figure 5: ACT+OV and ACT+OV+MS-275 reprogram tumor-infiltrating myeloid cells from an M2 phenotype to an M1 phenotype	55
Figure 6: Concomitant MS-275 delivery enhances M1 polarization further through heightened local IFN $\gamma$ /IFN $\gamma$ R signaling	56
Table 1: GO enrichment analysis for differentially expressed genes in ACT+OV+MS-275 vs ACT+OV-treated tumors	57-58
Figure S1, related to Figure 1A: Efficacy of ACT+OV in additional tumor models	59
Figure S2: Concomitant MS-275 does not alter T cell magnitude or phenotype	60
Figure S3: Concomitant MS-275 does not improve T cell killing	61
Figure S4, related to Figure 3D, E: Reprogrammed pro-inflammatory tumor-infiltrating myeloid cell phenotype in the CMS-5 tumor model	62
Figure S5, related to Figure 4E: Pro-inflammatory tumor-infiltrating	63

myeloid cells kill through cell-contact dependent mechanisms	
Figure S6, related to Figure 6C: Concomitant MS-275 delivery alters the intratumoral concentrations of select inflammatory-related cytokines	64
Figure S7, related to Figure 6E: Elevated IFN $\gamma$ in the context of MS-275 is attributed to tumor-infiltrating CD8 $^+$ T cells	65
Figure S8, related to Figure 3B: Enumeration of myeloid cell subsets during ACT + OV + MS-275 treatment	66
Table S1: M1/M2 Gene Profile, related to Figure 5	67
Table S2: Differentially expressed genes from the Nanostring nCounter inflammatory gene codeset, related to Figure 5	68-74
<b>3.0 Chapter Three – HDACi promotes inflammatory remodeling of the tumor microenvironment to enhance epitope spreading and antitumor immunity</b>	
Figure 1: Concomitant MS-275 delivery prevents tumor relapse during adoptive cell therapy	107
Figure 2: MS-275 remodels the inflammatory landscape of the tumor microenvironment to promote antigen processing and presentation	108
Figure 3: MS-275 alters myeloid cell composition within the tumor/dLN and enhances co-stimulation	109
Figure 4: Epitope spreading mobilizes tumor-rejecting p15E-specific endogenous CD8 $^+$ T cell responses	110
Figure 5: Reduced local immunosuppressive signals coincide with reduced regulatory T cell infiltration	111
Figure 6: Regulatory T cells selectively obstruct the magnitude of	112

endogenous responses from epitope spreading and their depletion promotes sustained tumor regression	
Figure S1, related to Figure 2: Connectivity mapping of differentially expressed (DE) genes	113
Figure S2, related to Figure 2C: Fully-annotated curated gene sets (C2) enrichment map	114
Figure S3, related to Figure 2D: Gene module ranking based on MS-275 up-regulation	115
Figure S4, related to Figure 2F: Fully-annotated immunologic signatures (C7) enrichment map	116
Table S1: Custom inflammatory gene sets, related to Figure 2A	117
Table S2: Enriched custom gene sets after gene set enrichment analysis (GSEA), related to Figure 2A	117
Table S3: Modules derived from the network of differentially expressed genes, related to Figure 2D	118
<b>4.0 Chapter Four – T cell transcriptional reprogramming overcomes tumor burden-induced cellular exhaustion</b>	
Figure 1: Tumor burden potentiates immunotherapeutic resistance and decreased clinical outcomes through the expression of a unique pathway signature	160
Figure 2: MS275 promotes tissue homeostasis and in conjunction with ACT restores therapeutic efficacy in large, immunosuppressive tumors	161
Figure 3: T cell reinvigoration is associated with increased proliferation and cytotoxicity	162
Figure 4: T cell whole transcriptome analysis reveals enhanced activation-dependent signaling	163

Figure 5: Tim-3 up-regulation is associated with reduced exhaustion and polarization towards terminal effector lineage differentiation	164
Table 1: Cox regression analysis of prognostic factors for SKCM T1/T4 patients	165
Figure S1: Transferred T cell proliferation and cell death over time, related to Figure 3D, E	166
Figure S2: Enriched Hallmark pathways using the Module (M2) list, related to Figure 4D	167
Figure S3: Differentially expressed genes when comparing ACT+MS-275- to ACT-treated T cells, related to Figure 4D	168
Figure S4: DUSP22-pathway correlation, related to Figure 4I, J	169
Table S1: Overrepresented GO terms associated with Module 2 (M2), related to Figure 4E, F	170
Table S2: Gene lists of T cell signatures, related to Figure 5E	171-176

## List of All Abbreviations:

### Abbreviations:

ACT	adoptive cell therapy
ANOVA	analysis of variance
APC	antigen presenting cell
BRCA	breast invasive carcinoma
CAR	chimeric antigen receptor
CFSE	carboxyfluorescein succinimidyl ester
CTL	cytotoxic lymphocyte
CTLA-4	cytotoxic T-lymphocyte-associated protein 4
DC	dendritic cell
DCT	dopachrome tautomerase
DE	differentially expressed
DEREG	depletion of regulatory T cell
DISC	death-induced signaling complex
DNA	deoxyribonucleic acid
DOX	doxorubicin
DT	diphtheria toxin
DTR	diphtheria toxin receptor
FADD	fas-associated protein with death domain
FC	fold change
FDA	Food and Drug Administration
FDR	false discovery rate
FI	fluorescence intensity
FISH	fluorescence <i>in situ</i> hybridization
GDAC	Genome Data Analysis Center
GEO	Gene Expression Omnibus
GFP	green fluorescence protein
GNAT	Gcn5-related <i>N</i> -acetyl transferase
GO	gene ontology
GOBP	gene ontology biological processes
GSEA	gene set enrichment analysis
HDAC	histone deacetylase
HIF	hypoxia-inducible factor
HLA	human leukocyte antigen
HNSC	head-neck squamous cell carcinoma
HR	hazard ratio

ICOS	inducible T cell costimulator
ICOSL	inducible T cell costimulator ligand
IDO	indoleamine 2,3-dioxygenase
IF	immunofluorescence
IFN	interferon
IFNG	interferon gamma
IFNGR	interferon gamma receptor
IHC	immunohistochemistry
IMC	immature myeloid cell
IV	intravenous
IVIS	<i>in vivo</i> imaging system
JAK	janus kinase
KRAS	kirsten rat sarcoma virus
LCMV	lymphocytic choriomeningitis virus
LMP	latent membrane protein
LPS	lipopolysaccharide
MAGE	melanoma antigen gene
MAPK	mitogen-activated protein kinase
MART-1	melanoma antigen recognized by T cells 1
MDSC	myeloid derived suppressor cell
MEM	memory
MHC	major histocompatibility complex
MICA	MHC class I chain-related protein A
MICB	MHC class I chain-related protein B
MMP	matrix metalloproteinase
MTT	3-(4,5-dimethylthiazol-2-yl)-2,5-diphenyltetrazolium bromide
NCOR	nuclear receptor co-repressor 1
NK	natural killer cell
NKT	natural killer T cell
NO	nitric oxide
NS	not significant
OV	oncolytic virus
PCA	principal component analysis
PCR	polymerase chain reaction
PGE2	prostaglandin E2
PMN	polymorphonuclear
PPI	protein-protein interaction
RAG2	recombination activating gene 2

RIN	RNA integrity number
RMA	robust multichip average
RNA	ribonucleic acid
ROC	receiver operating characteristic
ROS	reactive oxygen species
SAHA	suberanilohydroxamic acid
SKCM	skin cutaneous melanoma
SOD	superoxide dismutase
SST	signal-space transformation
STAT	signal transducer and activator of transcription
TAA	tumor associated antigen
TAC	Transcriptome Analysis Console
TADC	tumor-associated dendritic cell
TAM	tumor-associated macrophage
TAN	tumor-associated neutrophil
TCGA	The Cancer Genome Atlas
TCM	central memory T cells
TCR	T-cell receptor
TEFF	effector T cells
TEMRA	effector memory T cells re-expresses CD45RA
TEX	exhausted T cells
TGF $\beta$	tumor growth factor $\beta$
TIGIT	T cell immunoreceptor with Ig and ITIM domains
TIL	tumor infiltrating lymphocyte
TIM	T-cell immunoglobulin and mucin-domain
TLR	toll-like receptor
TME	tumor microenvironment
TMEM	memory T cell
TMPEC	memory precursor effector T cell
TNF $\alpha$	tumor necrosis factor $\alpha$
TOX	thymocyte selection associated high mobility group box
TRAIL	tumor necrosis factor-related apoptosis-inducing ligand
TRP-2	tyrosinase-related protein 2
TSA	trichostatin A
TSLEC	short-lived effector T cell
t-SNE	t-distributed stochastic neighbor embedding
TTEC	Tim-3hi effector-like cells
TTMC	Tim-3hi memory-like cells



VEGF	vascular endothelial growth factor
VSV	vesicular stomatitis virus
WHO	World Health Organization
WT	wild-type

**Declaration of Academic Achievement:**

I, Andrew Nguyen, declare that I have independently authored and assembled the contents of this thesis, with editorial assistance from Dr. Yonghong Wan. With respect to the scholarly works presented in Chapter Two – Four, a detailed breakdown of my academic contributions, as well as my co-authors', is provided in the Preface.

## **Preface:**

This thesis contains five scholarly works (Chapter Two – Four, Appendix). My academic contributions (**bold text**) as well as my co-authors' are detailed as follows:

Chapter Two: **Nguyen, A**, Ho, L, Workenhe, ST, Chen, L, Samson, J, Walsh, SR, Pol, J, Bramson, JL, Wan, Y (2018). “HDACi Delivery Reprograms Tumor-Infiltrating Myeloid Cells to Eliminate Antigen-Loss Variants.” *Cell Reports* 24(3): 642-654.

- **A.N. designed and conducted the majority of the experiments described and wrote the manuscript.** L.H. prepared the samples for microarray analysis. L.C. monitored the therapeutic efficacy of ACT + OV + MS-275 in DCT and mERK models. J.S. conducted the FISH staining on treated tumor sections. J.P. constructed the VSV-gp33 viral vector and S.R.W. constructed the VSV-mERK viral vector. S.T.W. and J.L.B. participated in the conception of experimental designs and manuscript writing. Y.W. supervised the study and participated in the conception of experimental designs and manuscript writing.
- This work was conducted from 2014-2016.

Chapter Three: **Nguyen, A**, Ho, L, Walsh, S, Hogg, R, Chen, L, Wan, Y (2021). “HDACi promotes inflammatory remodeling of the tumor microenvironment to enhance epitope spreading and antitumor immunity.” *Science Advances*. In submission.

- **A.N. designed and conducted the majority of the experiments described and wrote the manuscript.** L.H. prepared the samples for microarray analysis and qRT-PCR. S.W. constructed the VSV-gp33 viral vector. R.H. constructed the MCA102-p15E cell line. L.C. helped monitor the therapeutic efficacy of ACT+MS-275 in the gp33 model. Y.W. supervised the study, and participated in the conception of experimental designs
- This work was conducted from 2017-2019.

Chapter Four: **Nguyen, A**, Brown, D, Krishnan, R, Walsh, SR, Bastin, D, Deng, L, Chen, L, Bramson, JL, Wan, Y (2021). “T cell transcriptional reprogramming overcomes tumor burden-induced cellular exhaustion.” *Immunity*. In submission.

- **A.N. designed and performed the majority of the experiments and wrote the manuscript.** D.B. and R.K. performed animal experiments. S.W. constructed the viral vectors used in the study. D.B. transduced cultured TCM to express luciferase. D.L. performed the cytotoxicity assay. L.C. assisted with in vitro TCM culture and tissue processing. J.L.B. provided guidance during manuscript preparation. Y.W. supervised the study and participated in the conception of experimental designs and manuscript writing.
- This work was conducted from 2019-2021.

Appendix:

**Nguyen, A,** Salem, O, Wan, Y (2021). “Functional Analysis of Tumor-Infiltrating Myeloid Cells by Flow Cytometry and Adoptive Transfer.” *Journal of Visualized Experiments* (169).

- **A.N. wrote the manuscript.** O.S. contributed to the design of key figures. Y.W. supervised the methodology and manuscript writing.
- This work was conducted from 2020.

Workenhe, ST, **Nguyen, A,** Bakhshinyan, D, Wei, J, Hare, DN, MacNeill, KL, et. al. (2020). "De novo necroptosis creates an inflammatory environment mediating tumor susceptibility to immune checkpoint inhibitors." *Communications Biology* 3(1): 645.

- S.T.W., **A.N.,** Y.W., J.L.B, and K.L.M. **conceived the study and designed experiments.** S.T.W, **A.N.,** A.V, N.E, A.N., D.N.H., J.W., A.O., Kelly L.M., D.N.H. **developed the methodologies, conducted the experiments.** S.T.W, K.L.M, **A.N.,** A.O., J.A.N, A.G.M. S.K.S, D.B. **analyzed and interpreted the experimental results.** S.T.W, A.O., Y.W, J.L.B, and K.L.M. wrote and revised the manuscript.
- This work was conducted from 2020.

## **1.0 Chapter One – Introduction**

This work can be considered a continuation of the Master's thesis (Nguyen, 2013). Parts of the background information in this section were adapted from the Master's thesis.

### **1.1 Background**

#### **1.1.1 The Threat of Cancer**

Cancer malignancies encompass some of the most life-threatening and prevalent diseases across the globe and are a driving force in medical research. The World Health Organization (WHO) has reported that cancer is the second leading cause of death in industrialized countries and third worldwide (1). While established therapies such as surgical resection of primary tumors, radiation therapy, and chemotherapy have improved throughout the years, cancer is still responsible for 25% of mortalities (2). Approximately 1% of patients diagnosed with cancer will die on an annual basis (2). Five-year survival rates range from 10–20% for lung, esophagus and stomach cancer, to 40–60% for colon, bladder and cervix cancer, and 60–80% for breast and prostate cancer (2). Consequently, the relative ineffectiveness of current therapeutic methods underscores an ever-increasing need for clinically promising treatments against cancer.

#### **1.1.2 Tumorigenesis and the Hallmarks of Cancer**

The tumorigenic process that defines the transformation of a normal cell into a cancer cell can be divided into three distinct stages: tumor initiation, tumor promotion, and tumor progression. During tumor initiation, growth-regulatory genes undergo genetic or epigenetic mutations. This results in the activation of oncogenes (such as Ras and Myc) or inactivation of tumor-suppressors (such as p53 and Rb). The second stage of tumorigenesis, tumor promotion, is dependent on the clonal expansion of tumor-initiated cells as a result of increased proliferative capacity or decreased ability to undergo cell death. Lastly, tumor progression is characterized by an increased rate of growth and invasiveness due to acquisition of a malignant phenotype. Traditionally, the characterization of malignant tumor cells was relegated to six specific criteria (3): 1) self-sufficiency in growth signals, 2) insensitivity to anti-growth signals, 3) evasion of apoptosis 4) limitless replicative potential 5) sustained angiogenesis, and 6) tissue invasiveness and metastasis. However, Schreiber and colleagues proposed that the avoidance of immunosurveillance could be the seventh hallmark of cancer (4).

### 1.1.3 Cancer Immunosurveillance

Paul Ehrlich was the first to suggest that the immune system could repress the majority of carcinomas (5), but the idea of immunological control of neoplastic diseases was not further explored until the mid-twentieth century. Thomas and Burnett were responsible for coining the term “immunosurveillance” and proposing the idea that the immune system protects the host against cancer development from a non-viral origin (6). This was based on early work showing that mice could be immunized against syngeneic transplants of tumors induced by chemical carcinogens, viruses, and other means (7, 8). While caveated studies with immunocompromised athymic nude mice by several investigators dampened enthusiasm to the idea (9-11), key observations by Schreiber *et al* renewed interest in the concept of immunosurveillance (12-14). He further suggested that host immunity could modulate the immunogenicity of developing tumors by a process in which he termed, “immunoediting” (15).

### 1.1.4 Cancer Immunoediting

Given that immunosurveillance can actively prevent tumor formation, it is relatively unclear why cancer can occur in immunocompetent individuals. Schreiber suggests that the immune system may select for variants that are better suited to survive in an immunologically intact environment, resulting in an outgrowing population that possesses low immunogenicity (15). He proposes a dual role of the immune system in host-protecting and tumor-sculpting which he described as “immunoediting”. This is envisaged as a result of three distinct processes: 1) elimination, 2) equilibrium, and 3) escape.

The elimination process encompasses the original concept of cancer immunosurveillance, whereby the host immune response attempts to successfully delete the developing tumor. Minor disruption in surrounding tissue induces inflammatory signals, leading to innate cell recruitment (natural killer (NK), NKT,  $\gamma\delta$  T cells, macrophages, and dendritic cells (DCs)) to the tumor site (16-18). Tumor cell recognition by infiltrating lymphocytes (NKT, NK or  $\gamma\delta$  T cells) through danger-associated molecular patterns (DAMPs), dying/damaged tissues (ex. HMGB1), and expressed stress ligands (ex. natural killer cell protein group 2D (NKG2D) ligands such as major histocompatibility class I (MHC class I) chain-related molecules A/B (MICA/B)) induces the production and secretion of interferon  $\gamma$  (IFN $\gamma$ ) (19-21), which may facilitate tumor death by anti-proliferative (22) and apoptotic (23) mechanisms. Early tumor cell death by (non)immunologic mechanisms can release debris which is taken up by dendritic cells, leading to the activation and recruitment of tumor-specific CD4+ and CD8+ T cells (24, 25).

Any tumor cell variant that has survived elimination enters into a dynamic equilibrium. At this stage, the adaptive immune system prevents immediate outgrowth of the tumor, but is insufficient for complete elimination. Darwinian selection dictates that while much of the original tumor population is destroyed, tumor cells with genetic and epigenetic traits conferring heightened immune resistance are granted a growth and survival advantage. At the escape stage of cancer immunoediting, tumor cells that can escape immunological detection and/or elimination due to genetic or epigenetic changes begin to grow rapidly, resulting in disease that is clinically observable.

Avoidance of immunosurveillance through successful immunoediting forms the crux of Schreiber's seventh hallmark of cancer. Host immunity can thus play an active role in shaping the development of immune-resistant tumor phenotypes during outgrowth and malignancy. However, it is also apparent that the immune system plays a fundamental role in controlling tumor growth. This may suggest that strategies which aim to stimulate antitumor immunity may be therapeutically viable and should undergo further investigation.

## 1.2 Cancer Immunotherapy as a Platform for Tumor Control

Utilizing host immunity for the purpose of combating cancer is not a novel concept. In 1891, New York surgeon William Coley treated sarcoma patients by vaccinating them intratumorally with a mixture of attenuated *Streptococcus pyogenes* and *Serratia marcescens* which became known as Coley's toxin (26, 27). Similarly, it was found that intravesical injection of live bacillus Calmette-Gu in after surgical resection of superficial bladder cancer was able to extend the survival of patients (28-30). In the 1950s, Burnett demonstrated that the immune system could mount antitumor responses and suggested that transplantation antigens expressed on tumor cells could elicit the generation of protective immunity (31, 32).

Cancer immunotherapy aims to restore the reactivity of the host's immune system to combat cancer in a non-specific (Coley's toxin) or tumor-specific manner. Tumor-targeted therapeutic designs elicit immune responses that are specific for cancer antigens expressed on tumors. Tumor-specific antigens (TSA) are a small group exemplified by cancer-testis antigens (ex. melanoma antigen gene, MAGE) (33, 34). These are silent in normal tissue but are expressed in cancer cells. Tumor-associated antigens (TAA) are expressed by normal cells but are overexpressed in cancer (ex. MART-1 (35), gp100 (36), TRP-2 (37)). Mutational antigens can arise from point mutations of growth-regulatory genes such as the p53 oncogene that render the tumor cell immunogenically distinct from normal cells (38, 39). Lastly, certain viruses have an oncogenic capacity (HPV Type 16) and the gene

products encoded by these viruses (E6 and E7 proteins) are distinct from normal cells and are immunogenic (40). Cancer immunotherapy can be implemented in many different ways, whereby each strategy offers a unique method of propagating immune attack on the tumor; however, it is apparent that side-effects and limited clinical efficacy emphasize an ever urgent need to improve current strategies for safe and reliable therapeutic outcomes.

### 1.2.1 Adoptive Cell Therapy

Adoptive cell therapy begins with the identification of autologous or allogenic lymphocytes with antitumor activity (from peripheral blood, tumor-draining lymph nodes, or directly from the tumor mass). These cells are then expanded *in vitro* and re-infused into the tumor-bearing patient. ACT is normally preceded by a preparative, non-myeloablative lymphodepleting regimen (total body irradiation or cytotoxic drugs) to eliminate regulatory T cells (Tregs) and normal endogenous lymphocytes that compete with the transferred cells for homeostatic cytokines (IL-7, IL-15). T cell growth factors such as IL-2 are administered during ACT to stimulate the survival and expansion of transferred cells *in vivo* (41-43). Studies have shown that the differentiation state of adoptively transferred T cells can affect the success of therapy. Cells that are less differentiated (ex. memory T cells) have been shown to have greater proliferative capacity and antitumor efficacy (44-48). Furthermore, lymphocytes can be gene-modified prior to adoptive transfer to confer properties that will enhance their therapeutic efficacy. This includes the insertion of genes that confer antigen reactivity/specificity (49), enhance co-stimulation (50), prevent apoptosis (51), induce inflammation or homeostatic proliferation (52, 53), and/or promote T cell migration to the tumor site (54).

While objective clinical response rates to autologous tumor-infiltrating lymphocytes (TIL) were encouraging in patients with stage IV melanoma, a large number of patients did not respond favorably to treatment (55-57). Furthermore, the efficacy of naturally occurring TILs appears restricted to melanoma for unknown reasons. The use of gene-engineered T cells may induce off-target toxicities as a result of recognition of unintended structures (58-62). Also, toxicities have been associated with the use of nonspecific preconditioning regimens based on chemotherapy and radiation (43). On a practical side, ACT is a highly personalized treatment, is labor-intensive, is expensive, and requires laboratory expertise (41).

### 1.2.2 Cancer Vaccines



The aim of active cancer immunotherapy is to induce an endogenous, robust, and long-lasting tumor antigen-specific immune response. Since some cancers originate from chronic infections, therapies that prevent the infection prior to tumor formation are defined as prophylactic (ex. HBV and HPV/16/18 vaccines against liver and cervical cancers) (63). The development of therapeutic cancer vaccines, which aim to clear tumors once they have been established, is much more challenging. This vaccination approach requires defined TAAs or material obtained from direct tumor biopsies rather than a foreign antigen expressed by the infectious agent. Therefore, the efficacy of treatment is dependent on the ability of the vaccine to prime an immune response that can overcome host immune tolerance for the TAA, which is a self-antigen. While many approaches have been implemented, they have a commonality shared across all active immunotherapeutics in that a priming response is initiated against the tumor antigen.

CD8<sup>+</sup> effector T cells have a central role in the elimination of tumors. Immature DCs mature after being exposed to inflammatory signals (ex. TNF $\alpha$ , IL-1 $\beta$ , IL-6, Type I IFN), DAMPs (eg, HMGB1, heat-shock proteins (HSPs)), or pathogen-associated molecular patterns (PAMPs) (ex. LPS, dsRNA). Resulting mature DCs have improved antigen-presenting abilities, increased expression of co-stimulatory molecules, and acquire migratory potential to secondary lymphoid tissue. Presentation of antigen on MHC class II to cognate CD4<sup>+</sup> T cells and CD40-CD40L interaction completes DC maturation in a process known as *licensing* (64).

Naïve CD8<sup>+</sup> T cells express T-cell receptors (TCRs) which interact with mature DCs via 8-10 amino acid long peptides buried in the antigen-presenting groove of MHC class I molecules. This interaction initiates the priming of the naïve CD8<sup>+</sup> T cell and provides the first signal for T cell activation. However, CD8<sup>+</sup> T cell-mediated tumor rejection requires additional DC-CD8<sup>+</sup> T cell signals. CD28 co-stimulatory receptors expressed on T cells interact with CD80/CD86 ligands on DCs to produce a second signal, the absence of which would provoke T cell anergy. Additional co-stimulatory receptor-ligand interactions that are crucial for optimal T cell activation include ICOSL-ICOS, OX40L-OX40, and CD137L-CD137 among others. Lastly, the presence of IL-12 and/or IFN $\alpha/\beta$  during T cell priming provides the third signal for optimal CD8<sup>+</sup> T cell activation, leading to the differentiation and expansion of tumor-specific cytotoxic T lymphocytes (CTLs) (65).

CTL infiltration into the tumor microenvironment is followed by tumor killing through various mechanisms. Recognition of target tumor cells leads to the release of apoptosis-inducing cytotoxins (perforin, granzymes, granulysin). Also, cell-surface interactions may also lead to surface expression of Fas ligand (FasL). Fas-FasL interaction can induce apoptosis of the tumor cell through recruitment of death-induced signaling complex (DISC) and Fas-associated death domain (FADD) (66, 67). Therefore, it is clear that cytotoxic T

cells play a major role in the clearance of established tumors. Several strategies will be described which attempt to elicit high quality tumor-specific CD8<sup>+</sup> T cell responses but, like previously described strategies, have had limited success in terms of therapeutic efficacy and positive clinical responses.

Viral vectors are considered an attractive choice as an antigen delivery system for cancer immunotherapy. They are able to mimic natural infection and provide potent danger signals which are necessary for the activation of innate immune responses (68). Furthermore, many types of recombinant viruses have been shown to infect professional APCs and express various transgenes (69-74), leading to enhanced tumor antigen presentation and increased frequency and avidity of the antitumor CTL response. Recombinant viruses are also produced more easily compared to whole tumor vaccines and DC vaccines due to ease of production, purification, and storage (75). On the other hand, multiple injections of the same recombinant virus can promote host-induced neutralizing antibodies to the vector itself, severely limiting its continued use (76). The existence of pre-existing immunity towards many commonly used viral vectors poses a similar challenge due to the production of neutralizing antibodies (76). Numerous recombinant viral vector systems (ex. vaccinia, avipox, adenovirus) have been developed and encode a diverse array of cytokine/co-stimulatory molecules and/or TAAs (ex. CEA, gp100, MART-1) (76, 77). Unfortunately, monotherapies with recombinant viral vectors have not been conducive to significant objective response rates during clinical investigation (78).

### **1.2.3 The Marriage between ACT and Cancer Vaccination**

In order to improve clinical responses to immunotherapy, antigen restimulation in the context of ACT may facilitate maximal tumor regression (79). Indeed, cancer vaccination has been shown to enhance the *in vivo* antitumor efficacy of adoptively transferred T cells in both preclinical (80-84) and clinical studies (85, 86). However, a consistent benefit to combination therapy with mono-specific vaccines and ACT was not commonly observed. This could be attributed to the use of relatively weak immunogens such as peptide vaccines with oil-in-water emulsion adjuvants (87). By contrast, recombinant poxviruses, fowlpox viruses, and vaccinia viruses encoding human gp100 are strong immunogens that could be rationally combined with ACT to provide an enhanced antitumor immune response (88). Indeed, it was found that the viral vaccine titer associated with these vectors correlated with the strength of *in vivo* antigen restimulation during ACT as well as the slope of tumor regression (88). Therefore, adoptive cell therapy delivered in tandem with viral vaccination may represent a more optimized immunotherapeutic platform.

### 1.3 The Challenges Facing Cancer Immunotherapy

However, the design of clinically effective anticancer immune therapies still faces significant challenges. Despite increasing the magnitude and potency of antitumor immune effector cells, generating a higher number of tumor-specific immune effector cells may not necessarily correlate with tumor regression in pre-clinical studies or objective responses in clinical trials. Tumors have evolved mechanisms to inherently evade and suppress antitumor immune responses. It is apparent that current paradigms of immunotherapeutic design should now also consider the elimination of inhibitory factors and prevention of immunoresistant phenotypes.

#### 1.3.1 Tumor-induced Immunosuppression

Tumors can subvert endogenously- or exogenously-induced antitumor immunity by a variety of immunosuppressive mechanisms. Secretion of paracrine mediators such as VEGF-A (89, 90), adenosine (91), prostaglandin E2 (PGE2) (92, 93), IL-10 (94, 95), and TGF $\beta$  (96-98) can indirectly inhibit T-cell penetration into the tumor bed, suppress effector T cell activation, and promote Treg function. Furthermore, these factors may inhibit DC differentiation and maturation through suppression of nuclear factor kappa-light-chain enhancer of activated B cells (NF $\kappa$ B) signaling (99, 100). Cancer-associated fibroblasts can also promote the recruitment of immunosuppressive cells through the secretion of CCL2 and CXCL2 and suppress effector T cell function through TGF $\beta$  (101-103).

Tumor cells may also directly up-regulate surface ligands which can mediate T-cell anergy by binding to inhibitory T-cell receptors. Programmed death 1 (PD-1) protein is such a receptor with distinct biological function and ligand specificity and is expressed on activated T cells. It has two known ligands, PD-L1 (B7-H1) and PD-L2 (B7-DC), the former being selectively expressed on many tumors and cells within the tumor microenvironment in response to inflammation. PD-1 ligation inhibits cytokine production and cytolytic activity from tumor-infiltrating antigen-specific CD4<sup>+</sup> and CD8<sup>+</sup> T cells (104-110). Though controversial, another mechanism of tumor-induced immunosuppression is the expression of death receptor ligands by tumor cells. A variety of cancer cells (lung carcinoma, melanoma, colon carcinoma, and hepatocellular carcinoma) have been shown to express FasL, which induces apoptosis of Fas-susceptible target cells including activated T cells (111-118).

Tumors can also potentiate the infiltration and activity of immunomodulatory leukocyte subsets in order to suppress tumor antigen-specific T-cell responses. While IL-10-producing B cells, B regulatory cells, Type II NKT cells, NK cells, and  $\gamma\delta$  T cells have

been implicated in the down-regulation of antitumor activity (101), Treg cells and myeloid lineage cells have received the most consideration in the design of effective cancer immunotherapeutics.

### 1.3.2 Regulatory T Cells

Previous observations have shown that the onset of cancer can often be correlated with an accumulation of Tregs in tumor-bearing hosts. Questions have arisen whether or not this could be attributed as a host response to endogenous antitumor immunity which is sensed as an auto-reactive immune response, or if the tumor is actively manipulating and accumulating Tregs to orchestrate its own defence against host immune surveillance. Studies indicating that there may be two populations of CD4<sup>+</sup> regulatory T cells suggest the latter (119). In contrast to natural thymus-derived Tregs which arise under homeostatic conditions as a safeguard against autoimmunity, adaptive Tregs (T<sub>R</sub>1 cells) are induced during inflammatory processes like infection or cancer. Interestingly, while natural Tregs are characterized as CD4<sup>+</sup> CD25<sup>+</sup> FOXP3<sup>+</sup> (119), T<sub>R</sub>1 cells are characterized as CD4<sup>+</sup> IL-10<sup>+</sup> FOXP3<sup>-</sup> (120).

The tumor microenvironment can promote the accumulation of regulatory T cells through several mechanisms, including: trafficking, differentiation, expansion, and conversion. Tumor cells and cells within the tumor microenvironment express CC-chemokine ligand 22 (CCL22), which facilitates the migration of natural Tregs from the thymus, lymph node, bone marrow, and periphery to the tumor bed via CC-chemokine receptor 4 (CCR4) (121-123). Furthermore, the secretion of various cytokines and growth factors (ex. IL-10, TGFβ, VEGF) can suppress the differentiation/activation of DCs, which in turn induces the differentiation and expansion of regulatory T cells (124, 125). Lastly, the secretion of TGFβ may be responsible for the conversion of conventional CD4<sup>+</sup> CD25<sup>+</sup> T cells into CD4<sup>+</sup> CD25<sup>+</sup> FOXP3<sup>+</sup> Tregs (126-128). It should also be mentioned that the presence of tumor-infiltrating plasmacytoid DCs as well as IL-10 in the tumor microenvironment can play a contributing role towards the induction of T<sub>R</sub>1 cells (124, 129, 130).

All things considered, the tumor microenvironment might contain natural and converted Tregs as well as T<sub>R</sub>1 cells. These regulatory T cells require TCR triggering to become functional; however, once activated, they suppress T cells in a non-specific manner. Tregs can induce immunosuppression by a variety of mechanisms, including: secretion of immunosuppressive cytokines (131-134), competitive consumption of IL-2 (135-137), direct killing via perforin and granzyme pathways (138, 139), and direct subversion of antigen-presenting cell (APC) function through down-regulation of co-stimulatory

molecules (121, 140-142).  $T_{R1}$  cells primarily suppress immune activity through the production of IL-10 (119).

Interestingly, active vaccination of patients with cancer may induce TAA-specific Tregs. This may not be surprising since Tregs can be considered as another type of antigen-specific T cell elicited during an immune response. It has been suggested that dysfunctional DCs that express TAA might induce regulatory T-cell differentiation within the tumor microenvironment or within tumor draining lymph nodes (143-145). Furthermore, while natural Tregs express FOXP3 but not IL-10 and TGF $\beta$ , and  $T_{R1}$  cells express IL-10 but not FOXP3, TAA-specific Tregs may express both FOXP3 and IL-10 (119). The expression of IL-10 from these cells has been hypothesized to play a profound role in suppressing APC and T cell function (146).

### 1.3.3 Myeloid-Derived Suppressor Cells (MDSCs)

Early studies focused on the characterization of immature myeloid cells (IMCs), which were comprised of immature macrophages, granulocytes, DCs and other myeloid cells at early differentiation stages. In mice, they are phenotypically defined as Gr-1<sup>+</sup> CD11b<sup>+</sup> cells (147). These cells are normally present in the bone marrow and spleen of healthy mice where they eventually undergo differentiation into mature myeloid cells. However, during cancer, differentiation is partially inhibited and they accumulate at secondary lymphoid tissues as well as the tumor site (148-152). They suppress antigen-specific T cell activity through a variety of mechanisms, including inhibition of IFN $\gamma$  production by CD8<sup>+</sup> T cells through direct cell-cell contact (151, 153), secretion of immune suppressive factors (102), induction of T cell anergy (154, 155), and promotion of Treg development (155). Furthermore, Gr-1<sup>+</sup> IMCs can differentiate into F4/80<sup>+</sup> tumor-associated macrophages (TAM), which are able to inhibit T-cell-mediated immune responses by apoptosis (arginase 1 (ARG1) and NO) and suppression (signal transducer and activator of transcription 1 (STAT1)) (156). More interestingly, the release of immune suppressive factors within the tumor microenvironment may expand another IMC population with suppressive capacity: myeloid-derived suppressor cells.

Recent studies demonstrate that MDSCs consist of two main subsets: polymorphonuclear (PMN-MDSCs) and monocytic MDSCs (M-MDSCs). M-MDSCs are characterized by CD11b<sup>+</sup> Ly6G<sup>-</sup>/Ly6C<sup>+</sup> in mice and HLA-DR<sup>-</sup>, CD11b<sup>+</sup>, CD33<sup>+</sup>, CD14<sup>+</sup> in humans. PMN-MDSCs are characterized by CD11b<sup>+</sup> Ly6G<sup>+</sup>/Ly6C<sup>lo</sup> in mice and HLA-DR<sup>-</sup>, CD11b<sup>+</sup>, CD33<sup>+</sup>, CD15<sup>+</sup> in humans. In tumor-free mice, these subsets are referred to as polymorphonuclear neutrophils and inflammatory monocytes, respectively. PMN-MDSCs comprise the majority of MDSCs in cancer despite M-MDSCs having a longer lifespan and

higher proliferative capacity. Since the expansion of M-MDSCs was barely detectable in cancer, it was postulated that PMN-MDSCs may be replenished from M-MDSCs. It has been shown that monocytes differentiate into DCs and macrophages in non-pathological conditions, but preferentially differentiate into PMN-MDSCs in a tumor environment. This suggests that during cancer, regular monocyte differentiation is subverted in order to generate PMN-MDSCs from M-MDSCs. Extensive investigation correlated this process with the loss of retinoblastoma protein (Rb1) in MDSCs, which is coupled with the recruitment of histone deacetylase 2 (HDAC2) to the Rb1 promoter. (157-159)

MDSCs migrate to the tumor site via CCL2, CXCL12 and CXCL5 (160) and orchestrate a variety of immunosuppressive processes to inhibit tumor-specific immune attack (161). Activated MDSCs produce high levels of inducible nitric oxide synthase (iNOS) and ARG1. This in turn increases the production of urea and accelerates the depletion of essential amino acids in the tumor microenvironment (162). For instance, a deficit of L-arginine and cysteine can inhibit T cell proliferation and activation, respectively (163). MDSCs also increase intratumoral levels of NO and ROS (164). NO inhibits E-selectin expression on endothelial cells and thus obstructs T cell recruitment to the tumor (165). In addition, NO and ROS are associated with peroxynitrite production, which in turn causes nitration of TCRs and suppression of CD8<sup>+</sup> T cell responses (166, 167). PGE2 is the main receptor found in MDSCs and up-regulates ARG1 production as well as MDSC recruitment to the tumor (168-171). Lastly, MDSCs are also a major source of TGFβ production, which promotes tumor cell invasion/metastasis and induces anergy in immune effector cells (via membrane-bound TGFβ1) (172, 173).

### **1.3.4 Immune Selection and Escape**

As previously described, tumor cells can evade host immunosurveillance through successful immunoediting. The process of Darwinian selection and tumor escape does not only occur during endogenous host immune responses against increasingly malignant tumors. It can be applied to suboptimal or partially successful antitumor immunotherapies as well. In the context of cancer, natural selection is a process by which the survival of individual tumor cells is dependent on genetic and epigenetic traits that can confer a survival advantage. The outcome of this selection process is determined by multiple factors, including growth factors, nutrient supply, and immune pressure (174). Several of these outcomes will be described below.

Descriptions of MHC loss have had a great deal of intuitive appeal (175), but were correlative and indirect. At present time, there is little controlled evidence in humans or animals that a loss of MHC class I molecules can lead to immunoresistance and increased

incidence of spontaneous tumors in unmanipulated hosts. However, studies in mice (with pre-existing immunity induced by immunization) (176) and humans (with partial responses to immunotherapies) (177) have shown that recurring tumors can down-regulate MHC class I expression. Dysfunctional antigen processing machinery has been implicated with a loss of MHC. For instance, defects in antigen processing components (ex. proteasome multicatalytic complex subunits, low molecular mass protein (LMP) 2 and 7) or peptide transporters (ex. transporter associated with antigen processing (TAP) 1 and 2) were shown to induce MHC class I down-regulation (178-181). Additionally, mutations in one copy of the  $\beta$ 2-microglobulin in association with loss of heterozygosity (LOH) involving the second allele on chromosome 6 have resulted in loss of the MHC class I haplotype (182).

Loss of surface antigen expression can occur independently from MHC class I dysfunction. Due to the heterogeneity of tumor antigen expression within the same tumor, immunological pressures may promote the proliferation of non- or low-antigen expressing tumor cells and lead to disease progression. Unfortunately, the exact mechanisms of tumor antigen down-regulation are not known; however, outgrowth of antigen loss variants may be facilitated by epitope immunodominance, which is defined as the preferential detection of one or a few epitopes among many on a given target (183). Antigen loss variants within a tumor are shielded from immune pressure because parental tumor cells carry the immunodominant epitope and thus divert immune attack away from variant cells. Elimination of the parental cell establishes a new hierarchy of immunodominant epitopes among the remaining subpopulations.

### 1.3.5 T cell exhaustion

T cell exhaustion is a broad term that is often seen as a dysfunctional response of T cells to chronic antigen stimulation or inadequate activating signals in the context of chronic viral infection or tumor growth (184). Exhausted T cells are heterogeneous and express distinct epigenetic and metabolic states (185). Upon encountering antigen, effector T cells display a reduced capacity for cytokine secretion and proliferation, and increased expression of multiple inhibitor receptors, including PD1, TIM3, LAG3, CTLA4 and TIGIT (185). Recently, it has been demonstrated that the unique expression of transcription factor TOX in exhausted cells facilitates an altered transcriptional programme (186).

Developmentally, exhausted T cells share features with effector and memory T cells. Indeed, heterogeneous exhausted T cells are often dichotomized into relevant subsets: terminally differentiated exhausted cells (PD1<sup>hi</sup> TIM3<sup>hi</sup> TCF1<sup>-</sup>) and progenitor exhausted cells (PD1<sup>hi</sup> TIM3<sup>lo</sup> TCF1<sup>+</sup>) that have the ability to self-renew and maintain the former (187). Functional rescue of exhausted T cells is dependent on tumor antigen chronicity,

whereby increased exposure results in further chromatin remodeling and initial plastic dysfunctional states give way to fixed dysfunctional states. Indeed, PD-1 blockade-dependent reinvigoration of exhausted T cells can fail with increased epigenetic stability (188).

Currently, it is not clearly understood how the chromatin and transcriptional changes of exhaustion can be reversed in a deterministic manner in dysfunctional T cells to restore therapeutic efficacy during cancer immunotherapy.

#### **1.4 The Prospect of Combination Therapy**

Most cancer immunotherapeutic strategies fail to fully account for the seventh hallmark of cancer: immune escape. Tumors employ a myriad of mechanisms in order to suppress, subvert, and evade immune attack. As previously stated, optimal cancer immunotherapy should target these mechanisms while inducing sufficient stimulation of tumor-specific effector responses. More recent vaccination modalities have begun to take advantage of this concept. Some pleiotropic chemotherapeutic agents such as cyclophosphamide have been combined with cancer vaccines to induce a tumor-specific immune attack with multiple contingencies. For instance, cyclophosphamide has been shown to induce direct cytotoxicity, deplete immunosuppressive Tregs, activate and mediate the proliferation of T and B cells, and promotes T cell infiltration into the tumor (189-192). Monoclonal antibodies to CTLA4 and PD-1 as immune checkpoint blockers have been combined with vaccines to induce antitumor responses in many poorly immunogenic tumor models (193-196). Lastly, chemotherapeutics such as paclitaxel (TAX), cisplatin (CIS), and doxorubicin (DOX), in combination with several cancer vaccines and even adoptive T cell transfer approaches have resulted in the sensitization of tumor cells to tumor antigen-specific immune attack (197) and even resulted in bystander killing of non-targeted tumor cells (198). Consequently, there is therapeutic value in a combinatorial approach. Currently, there is an increasing interest in utilizing epigenetic modifying agents in combination with cancer immunotherapeutic modalities to synergize antitumor attack.

##### **1.4.1 Histone Acetylation as a Target for Gene Regulation**

Histone proteins organize DNA into repeating structures of chromatin called nucleosomes. The acetylation status of histones alters chromatin structure and regulates gene expression on an epigenetic level (199, 200). Two classes of enzymes can affect histone acetylation status: histone acetyltransferases (HATs) and histone deacetylases (HDACs) (201).



Nucleosomes contain 146 base pairs of DNA wrapped around a core histone octamer which is composed of an H3-H4 tetramer and two H2A-H2B dimers. These proteins are highly conserved and each contains a lysine rich amino (N)-terminal tail which is the site of post-translational modification. The N-terminal histone tail is enveloped by the DNA double helix and modification of these structures by acetylation or deacetylation affects the interaction of DNA with transcription-regulatory non-nucleosomal protein complexes. (202)

HATs can be divided into several families on the basis of highly conserved structural motifs (ex. Gcn5-related *N*-acetyl transferase (GNAT) family (203-207)). These families can be further subdivided into Type A HATs, which are involved in the regulation of gene expression, and Type B HATs, which are involved in the assembly of nascent histones into chromosomes. HATs engage in complex association patterns with protein complexes that can include other HATs, transcriptional co-activators and co-repressors in order to regulate gene expression (202). This results in the acetylation of specific histone lysine substrates by transfer of an acetyl group from acetyl CoA to form  $\epsilon$ -*N*-acetyllysine. The process neutralizes the positively charged lysine residues and reduces their affinity for DNA, unwinding the nucleosomal array and allowing for gene transcription to occur (208). HATs may also target non-histone protein substrates, including transcription factors and are termed, factor acetyltransferases (FATs) (209).

The acetylation status of chromatin is also dependent on HDAC activity. Four classes of HDAC have been described depending on yeast homology; however, Class I and II are considered “classical” HDACs due to their mechanism of action. Class I human HDACs (HDAC 1, HDAC2, HDAC3, and HDAC8) are found within the nucleus and seem to be ubiquitously expressed in human tissues (201). Class II human HDACs (IIa: HDAC4, HDAC5, HDAC7, HDAC9; IIb: HDAC6, HDAC10) have been shown to localize either in the nucleus or cytoplasm, suggesting a role in the deacetylation of nonhistone proteins (202). As with HATs, Class I HDACs are also constituents of multiprotein transcriptional complexes which include nuclear-hormone corepressors (NCOR) and silencing mediator for retinoid and thyroid hormone receptors (SMRT) (210, 211). Class I and II HDACs possess highly conserved catalytic domains and deacetylate histone lysine substrates by activating a water molecule with a divalent cation in cooperation with histidine-aspartate residues. The removal of charge-neutralizing acetyl groups from histone lysine tails results in the compaction of chromatin structure and repression of gene transcription (210).

Tumorigenic mutations can modify the expression of genes (ex. Ras, p53) that are normally controlled by epigenetic modification. Genetic abnormalities can also impact HATs/HDACs directly and affect their targeting to certain loci (212). Since cell development and differentiation is governed by sequential gene activation, disruptions in

chromatin remodelling can induce the proliferation of undifferentiated cells and cancer. It has been proposed that restoration of epigenetic control over endogenous differentiation and apoptotic programmes can be achieved using histone deacetylase inhibitors (HDACi) (202, 212). Consequently, the original application of HDACi was in transcription-based anticancer therapy.

#### 1.4.2 The Therapeutic Potential of HDAC Inhibitors

HDAC inhibitors (HDACi) have shown much promise as direct anticancer agents and many have progressed to clinical development (213-223). HDACi can impact several cellular processes that are dysregulated in neoplastic cells. Induction of cell cycle arrest (G1/S, G2/M) results in a disruption of normal differentiation programmes and leads to cytostatic effects (219, 224, 225). Direct treatment with HDACi can directly induce tumor cell death through the activation of death-receptor and intrinsic (ex. mitochondrial death pathway (226)) apoptotic pathways and activation of caspase cascades. Furthermore, HDACi have anti-angiogenic (ex. down-regulation of VEGF, basic fibroblast growth factor (bFGF), hypoxia-inducible factor 1 (HIF-1), etc.) and anti-invasive (ex. transcriptional repression of matrix metalloproteinases (MMP) 2 and 9) effects *in vitro* and *in vivo* can obstruct tumor development (227-232). Finally, HDACi can induce apoptosis through indirect regulation of gene expression by modulating the activity of transcriptional factors (E2F1, p53, STAT1/3, and NFκB) (233-237) as well as expression-independent mechanisms. Taken together, it is apparent that the effects conferred by HDACi are as varied as the types of HDACi known, suggesting that there is a correlation between HDACi type and their function.

HDACi can be broadly characterized by a common pharmacophore which includes key elements of inhibitor-enzyme interactions (238). This includes a hydrophobic cap that blocks the entrance to active site, a polar site, and a hydroxamic acid type zinc-binding active site separated by a hydrophobic spacer spanning the hydrophobic pocket on the enzyme (239, 240). The common mechanism of these drugs is to bind a critical Zn<sup>2+</sup> ion required for the catalytic function of HDACs (241, 242). With a few exceptions, HDACi can be divided into specific structural classes, including: carboxylates/short-chain fatty acids (valproic acid, sodium butyrate, 4-phenylbutyrate), small-molecule hydroxyaminic acids (suberoylanilide hydroxamic acid (SAHA), pyroxamide, trichostatin A (TSA), oxamflatin, and cyclic hydroxamic acid-containing peptides (CHAPS)), electrophilic ketones (epoxides), cyclic tetrapeptides (trapoxin, apicidin, and depsipeptide), benzamides (MS-275 and CI-994), and other hybrid compounds. The important clinical implication of these structural variants is their unique specificity and potency for HDAC isoenzymes and

effects on the acetylation of nonhistone substrates, resulting in broad efficacies, toxicities, and therapeutic uses (238). In particular, synthetic benzamides have shown significant promise for anticancer therapy and have been explored further due to its antiviral and anti-inflammatory properties.

### 1.4.3 Benzamides and MS-275 (Entinostat)

These compounds consist of structurally diverse agents that possess a benzamide moiety and inhibit HDAC activity at a micromolar range (243). As with other HDACi, it is postulated to enter the catalytic site and bind the active zinc; however, it is unclear whether or not this binding is reversible (ex. SAHA) or irreversible (epoxides). Diaminophenyl groups expressed on benzamide HDACi may be essential for optimum activity and have been suggested as potential chelators of the metal ion in the catalytic site (244). Several compounds have been described as members of this group (MS-275, CI-994, etc.) and are currently in clinical trials for the treatment of several cancers (245-248).

MS-275 (2-aminophenyl-4-[n-pyridin-3-metyloxycarbonyl]-(aminomethyl)-[benzamide]) is a newly synthesized benzamide derivative that preferentially inhibits HDAC1 with a median inhibitory concentration (IC<sub>50</sub>) of 0.3  $\mu$ M, HDAC3 with an IC<sub>50</sub> of  $\sim$  8  $\mu$ M, and has no inhibitory effect against HDAC8 (217, 249). It has been clinically evaluated in phase I clinical trials as treatment against refractory solid tumors, leukemias, and lymphomas (246, 250-253). Oral administration of the drug showed attractive safety/efficacy profiles and a long half-life (39-80 hours).

It is the first HDACi to be discovered with oral anticancer activity (associated with increased expression of CDKI p21<sup>CIP1/WAF1</sup> and accumulation of cells in G1-phase in preclinical models) (254). It has been found to inhibit tumor proliferation in several cancer lines including breast, colorectal leukemia, lung, ovary, and pancreas (254), and is associated with an extensive gene induction (p21<sup>WAF1</sup>, gelsolin, metallothionein, histone H2B) and repression (thymidylate synthase, importin-b, c-myc) profile (225). In human breast cancer and pediatric solid tumor cell lines, it has been postulated that HDACi-mediated antitumor activity is dependent on the induction of TGF $\beta$ -receptor expression and tumor suppressor activity (255, 256). In hematological malignancies, MS-275 is associated with the activation of death receptor pathways through induction of TNF-related apoptosis-inducing ligand (TRAIL) and FasL as well as up-regulation of co-stimulatory molecules such as 4-1BBL (257, 258).

### 1.4.4 HDACi for Cancer Immunotherapy

Aside from direct tumor control, HDACi have been documented to have extensive immunomodulatory properties. They can transcriptionally activate MHC class I and II proteins, co-stimulatory molecules (CD40, CD80, and CD86), and intracellular adhesion molecule (ICAM1) to augment immune cell recognition and activation (259, 260). It has also been demonstrated that HDACi induce the expression of MICA and MICB on tumor cells, which in turn can induce NKG2D-restricted cytotoxicity from NK cells (261, 262). Furthermore, direct histone hyperacetylation may alter the activity of STAT1 (263), STAT3 (236), and NF $\kappa$ B (237), which are considered “master immune regulatory transcription factors”. Finally, HDACi are capable of potentiating antigen processing and presentation machinery via upregulation of TAP, LMP, and Tapasin (264).

These immunomodulatory properties suggest that HDACi may be complementary to current cancer immunotherapies as a means to further enhance antitumor immune responses. We have previously demonstrated that MS-275 delivery during heterologous prime-boost viral vaccination improved recall responses against the tumor and can abrogate vaccine-induced autoimmunity (265). This was in part achieved through selective lymphopenia leaving the boosted antitumor lymphocytes intact while depleting both conventional lymphocytes and Tregs. This provided early evidence that MS-275-dependent immunomodulation may subvert tumor resistance through the removal of immunosuppressive cell subsets. This thesis further characterizes how MS-275 can be utilized to overcome tumor resistance during cancer immunotherapy.

## **1.5 Thesis Scope and Content**

Herein I describe my doctoral studies which utilize pre-clinical models to describe how resistance to cancer immunotherapy can manifest, the tumor resistance mechanisms at play, and how HDAC inhibition via MS-275 can enhance antitumor immunity to provide lasting tumor regression.

## **2.0 Chapter Two – HDACi Delivery Reprograms Tumor-Infiltrating Myeloid Cells to Eliminate Antigen-Loss Variants**

### **2.1 Introduction**

ACT in solid melanoma tumors promotes acute tumor regression but facilitates the therapeutic selection of immune escape variants, resulting in eventual tumor relapse. This manuscript describes the therapeutic benefit of using of MS-275 in conjunction with ACT.

We observed that combination therapy promotes sustained tumor regression, which is mediated by the reprogramming and functional polarization of tumor-infiltrating myeloid cells from immunosuppressive cells to antitumor effector cells with the ability to reject immune escape variants.

### **2.2 Manuscript Status, Copyright, and Citation**

*Status:* Published manuscript

*Copyright:* © Nguyen A et al. (2018). This article is available under open access and is printed under the terms of the Creative Commons Attribution License 4.0 International License (CC BY 4.0) (<https://creativecommons.org/licenses/by/4.0/>). The only modification made was to fit the published work within the thesis.

*Citation:* Nguyen, A, Ho, L, Workenhe, ST, Chen, L, Samson, J, Walsh, SR, Pol, J, Bramson, JL, Wan, Y (2018). “HDACi Delivery Reprograms Tumor-Infiltrating Myeloid Cells to Eliminate Antigen-Loss Variants.” *Cell Reports* 24(3): 642-654.

### **2.3 Published Journal Article**

Starting on the next page.

**HDACi Delivery Reprograms Tumor-infiltrating Myeloid Cells to Eliminate Antigen-loss Variants**

Nguyen, Andrew<sup>1</sup>; Ho, Louisa<sup>1</sup>; Workenhe, Samuel T<sup>1</sup>; Chen, Lan<sup>1</sup>; Samson, Jonathan<sup>2</sup>; Walsh, Scott R<sup>1</sup>; Pol, Jonathan<sup>1</sup>; Bramson, Jonathan L<sup>1</sup>; Wan, Yonghong<sup>1,3</sup>

- 1 Department of Pathology and Molecular Medicine, McMaster Immunology Research Centre, McMaster University, Hamilton, Ontario L8N 3Z5, Canada.
- 2 Advanced Cell Diagnostics, Toronto, Canada
- 3 Lead Contact

**Correspondence: wanyong@mcmaster.ca (Y.W.)**

## Summary

Immune recognition of tumor-expressed antigens by cytotoxic CD8<sup>+</sup> T cells is the foundation of adoptive T-cell therapy (ACT) and is shown to elicit significant tumor regression. However, therapy-induced selective pressure can sculpt the antigenicity of tumors, resulting in outgrowth of variants that lose the target antigen. We demonstrate that tumor relapse from ACT and subsequent oncolytic viral vaccination can be prevented using Class I HDACi, MS-275. Drug delivery subverted the phenotype of tumor-infiltrating CD11b<sup>+</sup> Ly6Chi Ly6G<sup>-</sup> myeloid cells, favoring NOS2/ROS secretion and pro-inflammatory genes characteristic of M1 polarization. Simultaneously, MS-275 abrogated the immunosuppressive function of tumor-infiltrating myeloid cells and reprogrammed them to eliminate antigen-negative tumor cells in a caspase-dependent manner. Elevated IFN $\gamma$  within the tumor microenvironment suggests that MS-275 modulates the local cytokine landscape to favor antitumor myeloid polarization through the IFN $\gamma$ R/STAT1 signaling axis. Exploiting tumor-infiltrating myeloid cell plasticity thus complements T-cell therapy in targeting tumor heterogeneity and immune escape.

## Introduction

Cancer immunotherapy has seen major advancement with the success of adoptive cell therapy (ACT), wherein autologous tumor antigen-specific CD8<sup>+</sup> T cells expanded *ex vivo* and subsequently reinfused into the cancer patient. While shown to be capable of promoting tumor regression and enhanced clinical outcomes (Fesnak et al., 2016), a loss of responsiveness to ACT has been observed across multiple tumor types or even within the same tumor type due to genetic and epigenetic instability in growing tumors predisposing them to antigenic heterogeneity (Landsberg et al., 2012; Restifo et al., 2016). Since ACT monotherapies often target a single defined tumor antigen, therapy-induced selection of resistant clones induces proliferation of tumor variants with decreased or absent antigen expression. As a result, tumor recurrence is often associated with a loss of recognition by tumor-specific T cells (Junttila and de Sauvage, 2013). To prevent the outgrowth of antigen-loss variants, therapies incorporating non-parallel tumoricidal pathways must be used in combination to supplement T cell-mediated killing.

In addition to CD8<sup>+</sup> T cells, various myeloid cell subsets have been demonstrated to have antitumor effects (Mantovani and Allavena, 2015; Pommier et al., 2013; Powell and Huttenlocher, 2016). It is possible to mobilize these cells in conjunction with ACT to elicit complete tumor destruction and prevent relapse; however, within the immunosuppressive tumor microenvironment, these cells typically exhibit tolerogenic pro-tumor characteristics (Engblom et al., 2016). In particular, the intratumoral myeloid cell compartment comprises a large heterogeneous population of immunosuppressive cells including tumor-associated macrophages, tumor-associated neutrophils, tolerogenic DCs, and myeloid-derived suppressor cells (MDSCs). Interestingly, modulation of the local cytokine milieu can polarize their activation status and functional programming according to classical (M1) or alternatively (M2) activated phenotypes. M1 polarization prototypically involves IFN $\gamma$ /IFN $\gamma$ R ligation leading to the production of pro-inflammatory mediators (NOS2, TNF $\alpha$ , IL-12) through STAT1 signaling, while M2 polarization is dependent on IL4/IL4R or IL13/IL13R ligation and production of anti-inflammatory mediators (Arg1, Fizz1, Ym1) through STAT3/6 signaling (Yang et al., 2013). Since the opposing polarization programs mutually inhibit one another on an epigenetic and transcriptional level (Piccolo et al., 2017), the relative abundance of M1/M2 polarizing cytokines may dictate if tumor-infiltrating myeloid cells will have a pro- or antitumor function.

We observed that the concomitant delivery of HDAC inhibitor, MS-275, in the context of ACT followed by oncolytic viral vaccination could prevent the outgrowth of antigen-loss variants and promote sustained tumor regression. This coincided with a polarization of tumor-infiltrating myeloid cells from an immunosuppressive M2 phenotype to an inflammatory M1 phenotype as a result of increased local production of IFN $\gamma$ . This not



only reduced their suppressive function but allowed the cells to directly eliminate antigen-loss variants, thus demonstrating a multi-mechanistic role for myeloid cell polarization in the context of antitumor immunity.

## Results

### **ACT + OV mediates potent antitumor immunity and tumor regression**

Oncolytic viruses (OVs) can selectively replicate in and kill tumor cells with minimal impact on normal tissue (Russell et al., 2012). By engineering rhabdoviruses to express tumor antigens (termed oncolytic viral vaccines), we demonstrated that OVs could effectively engage and expand pre-existing tumor-specific central memory T cells (TCM) while retaining their beneficial oncolytic properties (Bridle et al., 2016; Bridle et al., 2010; Pol et al., 2013). Since OV vaccines proved to be robust boosting agents, we wanted to see if they could also enhance the proliferation of ACT responses. To test this, C57BL/6 mice were intradermally (i.d.) injected with 10<sup>5</sup> B16-F10 murine melanoma cells that express an immunodominant epitope from the lymphocytic choriomeningitis virus glycoprotein (LCMV GP33-41) (denoted as B16-gp33). GP33-41-specific CD8<sup>+</sup> TCM were generated from donor mice that were infected with LCMV-Armstrong for more than one month. After 5 days of tumor growth, mice were treated with an intravenous (i.v.) injection of 10<sup>4</sup> gp33-specific TCM followed by 2 x 10<sup>8</sup> pfu of VSV-gp33 24 hours later; control mice received either gp33-specific TCM or VSV-gp33 alone. Figure 1A shows that neither TCM nor VSV-gp33 alone had a significant impact on tumor growth, whereas combining TCM and VSV-gp33 boosting induced complete tumor regression. Moreover, gp33-specific TCM + VSV without the gp33 transgene (VSV-MT) was insufficient to control tumor growth, confirming the synergy and complementarity between ACT and antigen-specific OV vaccination. The potency of this combination therapy was further demonstrated in the regression of much larger tumors where treatment did not start until 10 days after B16-gp33 inoculation (Fig. 1B).

Consistent with the efficacy data, significant T cell responses were only evident in mice treated with TCM + VSV-gp33 (Fig. 1C). To confirm that *in vivo* CD8<sup>+</sup> TCM expansion was responsible for tumor regression, we ablated select lymphocyte populations using monoclonal antibodies specific for CD8, CD4, or NK1.1. As expected, depletion of CD8<sup>+</sup> T cells completely abrogated tumor control (Fig. 1D).

To more comprehensively evaluate this combination therapy, we included two additional mouse models targeting dopachrome tautomerase (DCT), a melanocyte-differentiation antigen expressed by murine B16-F10 melanoma cells (Bloom et al., 1997; McGray et al., 2014), and a mutated ERK2-kinase antigen (mERK) that is expressed in CMS-5 fibrosarcoma (Hanson et al., 2000; Ikeda et al., 1997). T cell receptor transgenic mice were used to generate CD8<sup>+</sup> TCM that recognize the immunodominant epitope of DCT180-188 and mERK136-144, respectively. Adoptive transfer of TCM followed by boost with VSV vaccines encoding the relevant epitope elicited robust T cell expansion and complete tumor

regression (Fig. S1), indicating that the potency of this combination therapy is independent of the nature of antigens and the strain of mice.

Interestingly, while tumor regression was durable in both DCT and mERK models, it was short-lived in the gp33 model, with tumor relapse evident after 10-20 days (Fig. 1E). This tumor regrowth could not be prevented by increasing the absolute number of transferred TCM before boosting with VSV-gp33, despite gp33-specific T cell responses as high as ~60% circulating CD8<sup>+</sup> T cells (Fig. 1F and 1G). This suggests that the relapsing tumors developed resistance to targeted T cell therapy. Indeed, prophylactic immunization of C57BL/6 mice with an adenovirus expressing gp33 (Ad-gp33) led to complete protection against challenge with parental B16-gp33 cells but failed to reject relapsed B16-gp33 explants (B16-gp33R) (Fig. 1H), confirming that B16-gp33R cannot be recognized by gp33-specific CD8<sup>+</sup> T cells.

### **Concomitant MS-275 delivery prevents tumor relapse through complete elimination of antigen-loss variants**

We previously demonstrated that MS-275, a Class I HDAC inhibitor, can manipulate secondary CD8<sup>+</sup> T cell responses to potentiate antitumor immunity and improve therapeutic outcomes (Bridle et al., 2013). In the context of ACT + OV, we wondered if incorporating MS-275 could similarly enhance the efficacy of our treatment platform. To test this, we monitored tumor growth in B16-gp33-bearing mice after treatment with ACT + OV + MS-275. MS-275 was administered intraperitoneally after OV-boosting and was given daily for 5 days. Treatment of mice with MS-275 alone or in combination with VSV-gp33 was unable to control the initial tumor, whereas gp33-specific TCM + VSV-gp33 + MS-275 treatment completely regressed the initial tumor and prevented tumor relapse (Fig. 2A), leading to durable cure (Fig. 2B).

By contrast, ACT + OV + MS-275 treatment failed to control the growth of B16-gp33R tumors (Fig. 2C), suggesting that immune escape may be due to irreversible antigen loss. Indeed, PCR analysis of genomic DNA from B16-gp33R cells showed no detectable PCR product compared to B16-gp33 cells (Fig. 2D), confirming the loss of gp33 expression on a genomic level. Our findings thus suggest that concomitant MS-275 delivery may prevent the emergence of antigen-loss variants from selective T-cell pressure and/or inhibit immune escape through direct eradication of pre-existing variants. To investigate these possibilities, we mixed 100 luciferase-expressing B16-F10 (B16-F10-luc) cells with 105 B16-gp33 cells to generate chimeric tumors. As shown in Figure 2F, luciferase signal was clearly detectable 10 days post chimeric tumor implantation confirming B16-F10-luc cell survival and expansion. Consistent with previous observations, gp33-specific TCM + VSV-gp33 only induced transient tumor regression (Fig. 2E) and B16-F10-luc cells continued to

expand in relapsed tumors (increased luciferase signal on day 30; Fig. 2F). Comparatively, treatment with gp33-specific TCM + VSV-gp33 + MS-275 led to durable regression of chimeric tumors (Fig. 2E), suggesting that the addition of MS-275 can directly promote the eradication of antigen-loss variants.

### **ACT + OV + MS-275 subverts the inflammatory status of tumor-infiltrating myeloid cells and reprograms them into killer cells**

One possible mechanism for the therapeutic benefit conferred by MS-275 is the functional improvement of antigen-specific CD8<sup>+</sup> T cells, which could mediate more complete eradication of the tumor to prevent relapse. However, the frequency and functionality of antigen-specific CD8<sup>+</sup> T cells derived from peripheral blood or tumors did not differ between mice receiving ACT + OV and ACT + OV +MS-275 treatment (Fig. S2). Furthermore, qualitative marker expression (TNF $\alpha$ , KLRG1, PD-1) (Fig. S2) and in vitro/in vivo killing (Fig. S3) were relatively unchanged, suggesting that MS-275 may instead leverage alternative cytotoxic cell types or killing mechanisms to eliminate antigen-loss variants.

To gain perspective of the global changes occurring within the tumor microenvironment, we conducted a microarray using tumor RNA from differentially treated mice. Gene ontology term enrichment analyses of differentially expressed genes 5 days post OV-boost indicate a variety of biological processes that were altered as a result of concomitant MS-275 delivery (Table 1); in particular, myeloid leukocyte activation involved in immune response (GO:0002283) and myeloid leukocyte chemotaxis (GO:0030593) along with its associated biological processes seem to show a high degree of enrichment (>100 and 23.07 fold, respectively), indicating that the intratumoral myeloid cell compartment was affected by combination therapy.

Tumor-infiltrating myeloid cells represent a heterogeneous population of CD11b-expressing immune cells with largely immunosuppressive function and can support tumor growth. Cellular subsets can include F4/80<sup>+</sup> tumor-associated macrophages, CD11chi tolerogenic DCs, Gr1<sup>+</sup> tumor-associated neutrophils, Ly6Chi Ly6G<sup>-</sup> monocytic MDSCs, and Ly6Clo Ly6G<sup>+</sup> granulocytic MDSCs (Engblom et al., 2016). While we were unable to observe significant changes to the total number of tumor-infiltrating myeloid cells (Fig. 3A), there was an increased infiltration of CD11chi cells with ACT + OV treatment, though their frequency was unchanged in the presence of MS-275 (Fig. 3B, S8). Indeed, MS-275 did not seem to alter the frequency of any myeloid subset, including CD11c-/lo F4/80<sup>+</sup> cells. Ly6C and Ly6G gating on CD11c-/lo F4/80<sup>+</sup> cells showed that, as was consistent with literature (Haverkamp et al., 2011; Mairhofer et al., 2015), untreated tumor masses were more heavily infiltrated with Ly6Chi Ly6G<sup>-</sup> cells compared to Ly6Clo Ly6G<sup>+</sup> cells

and their relative proportion was unaltered by treatment (Fig. 3B, S8). Interestingly, Ly6Chi Ly6G<sup>+</sup> cells displayed increased expression of Ly6G and fluctuating expression of CD11c upon ACT + OV and, to a larger extent, ACT + OV + MS-275 treatment (Fig. 3C), suggesting that MS-275 may induce a progressive phenotypic shift in tumor-infiltrating myeloid cells. Indeed, morphological analysis of cytopsin preparations derived from purified tumor-infiltrating myeloid cells showed a distinct transition from cells with immature/young monocytic cytological features (fine azurophilic granules, greyish blue cytoplasm, no visible nucleolus) to ones with classically activated macrophage-like characteristics (large distended cytoplasm, rounded rather than elongated shape, phagocytosed cellular debris, highly vacuolated) (Fig. 3D) (Goasguen et al., 2009; McWhorter et al., 2013). Based on these therapy-driven morphological changes, we postulated that tumor-infiltrating myeloid cells were undergoing a pro-inflammatory response. Using established markers of pro-inflammatory (NOS2, ROS) and pro-healing (Arg1) phenotypes typically characterized in macrophage polarization studies (Lopez-Castejon et al., 2011), we observed increased NOS2 (Fig. 3E, F) and ROS (Fig. 3G) and decreased Arg1 (Fig. 3H) expression in tumor-derived Ly6Chi Ly6G<sup>+</sup> gated myeloid cell populations upon ACT + OV treatment. Moreover, in the presence of MS-275, these changes were further pronounced, indicating that the pro-inflammatory status of tumor-infiltrating myeloid cells may be further enhanced. NOS2-related changes (Fig. S4) were also observed in the aforementioned mERK model (Fig. S1), suggesting that these myeloid cell changes were not tumor model or mouse strain specific. Altogether, the data suggest that concomitant MS-275 delivery may potentiate therapy-induced changes to the inflammatory status of tumor-infiltrating myeloid cells.

We next sought to determine if tumor-infiltrating myeloid cells derived from ACT + OV + MS-275-treated mice were functionally dissimilar from those of untreated or ACT + OV-treated mice. We first set up a proliferation assay using CFSE-labeled P14 T cells as responders that were stimulated with gp33 peptide-pulsed dendritic cells. Figure 4A-C shows that tumor-derived myeloid cells from ACT+ OV + MS-275-treated mice possessed a reduced capacity to suppress P14 T cell proliferation compared to those from untreated or ACT + OV-treated mice. We next investigated if tumor-infiltrating myeloid cells, in addition to losing their immunosuppressive function, were directly involved in the killing of antigen-loss variants. Indeed, when co-cultured with B16-F10 cells that do not express gp33, tumor-infiltrating myeloid cells derived from ACT + OV + MS-275-treated mice demonstrated significant killing capacity (Fig. 4E) in a cell contact-dependent manner (Fig. S5). Interestingly, histological staining of tumor tissues showed localized expression of cleaved caspase 3, an apoptosis marker, with CD11b<sup>+</sup> cells following ACT + OV + MS-275 therapy (Fig. 4D), also supporting the notion that MS-275-influenced tumor-infiltrating myeloid cells may provide an antitumor effector role by effectively eradicating antigen-

negative tumor cells. To directly address this hypothesis, we isolated tumor-infiltrating myeloid cells from ACT + OV + MS-275-treated mice (CD11bTVM) and injected them into tumors one day before treatment with ACT + OV. Figure 4F shows that this intratumoral injection was able to recapitulate the therapeutic effects of MS-275 delivery resulting in prolonged survival (Fig. 4G). It is therefore apparent that enhanced inflammatory reprogramming of tumor-infiltrating myeloid cells by MS-275 subverts their immunosuppressive function and confers cytotoxic killing capacity, ultimately preventing tumor relapse.

### **Altered inflammatory status in tumor-infiltrating myeloid cells is representative of M1 polarization**

To better understand the mechanisms by which MS-275 influences the function of tumor-infiltrating myeloid cells in the context of ACT + OV therapy, we sorted CD11b<sup>+</sup> Ly6Chi Ly6G<sup>-</sup> cells from tumor tissues and used an nCounter codeset to quantify the gene expression of 179 inflammation-related mouse genes that are commonly used to define the polarization status of macrophages, namely M1 and M2, a paradigm that has also been observed in other cells within the myeloid lineage (Fridlender et al., 2009; Yang et al., 2013). Gene set enrichment analysis showed enrichment of M2 genes in untreated mice (Table S1) while M1 genes were enriched in both ACT + OV and ACT + OV + MS-275-treated mice (Fig. 5), suggesting that combination treatment in the absence of MS-275 is sufficient to reprogram CD11b<sup>+</sup> Ly6Chi Ly6G<sup>-</sup> cells to express genes congruent with an M1 profile. However, as we previously demonstrated, the extent of NOS2 upregulation and Arg1 downregulation in CD11b<sup>+</sup> Ly6Chi Ly6G<sup>-</sup> cells was more pronounced during concomitant MS-275 delivery. We postulate that the drug enables stronger M1-signaling within the tumor microenvironment, leading to a hyper-polarized state.

### **M1 hyper-polarization is dependent on local IFN $\gamma$ and enhanced Type II-interferon-mediated signaling**

Having delineated the therapeutic role of M1 polarization in T-cell therapy, we set out to answer how concomitant MS-275 delivery alters the tumor microenvironment to promote M1 polarization in tumor-infiltrating myeloid cells. We hypothesized that the functional phenotypes seen in M1 or M2 activation are a dynamic response to combinations of environmental stimuli. Using tumor homogenate from differentially treated mice, the cytokine landscape was assessed with a 31-plex cytokine array and visualized by heat map (Fig. 6A). Principal component analysis indicated that treatment clusters (ACT + OV, ACT + OV + MS-275) were highly removed from untreated clusters (No Tx), confirming that the differential enrichment of M1/M2 genes in CD11b<sup>+</sup> Ly6Chi Ly6G<sup>-</sup> cells corresponded to unique intratumoral cytokine signatures (Fig. 6B). While tightly grouped, ACT + OV

and ACT + OV + MS-275 clusters were also distinct from one another. Indeed, while the relative concentrations of most inflammatory cytokines (including M2-stimulating cytokines IL4 and IL13) did not change between ACT + OV and ACT + OV + MS-275 (Fig. 6A), several inflammatory cytokines were significantly upregulated by MS-275 including M2-related cytokines M-CSF (6.39-fold) and IL10 (2.95-fold) and M1-stimulating cytokine IFN $\gamma$  (6.3-fold) (Fig. 6C). It should be noted that the absolute concentration of M-CSF/IL10 was near the lower limit of detection (Fig. S6), while IFN $\gamma$  was present at high concentrations (~1.5-2.0 ng/mL) upon ACT + OV + MS-275 treatment (Fig. 6D). Coupled with qRT-PCR analysis of IFNG from whole tumor RNA (Fig. 6E), the data suggest that enhanced local production of IFN $\gamma$  from tumor infiltrating lymphocytes such as CD8 $^+$  T cells (Fig. S7) may contribute to the hyper-polarization of tumor-infiltrating myeloid cells towards an enhanced M1 phenotype. This possibility was supported by subsequent analyses where enhanced STAT1 phosphorylation was observed in tumor-derived CD11b $^+$  Ly6Chi Ly6G $^-$  gated cells when MS-275 was present (Fig. 6F). To firmly establish a causal relationship between IFN $\gamma$  signalling and myeloid cell polarization, we included a group of tumor bearing IFN $\gamma$  receptor-deficient mice that were treated with ACT + OV + MS-275. The data in Figure 6G indicate that the effect of MS-275-mediated M1 hyper-polarization was abrogated in IFN $\gamma$  receptor-deficient mice, resulting in a reduced frequency of NOS2-expressing CD11b $^+$  Ly6Chi Ly6G $^-$  cells. Conversely, repeating the study in IFN $\alpha$  receptor-deficient mice did not alter NOS2 expression, suggesting that the role of Type I IFN was not required for myeloid cell polarization (data not shown).

## Discussion

In this study, we describe a treatment platform which incorporates the transfer of tumor-specific central memory T cells (TCM) with a recombinant oncolytic virus (OV) expressing the tumor antigen of interest. This combination induced robust T cell expansion and complete tumor regression in three different models, irrespective of the nature of tumor antigens and strain of mice, confirming the synergy and complementarity between ACT and OV vaccination. While this tumor regression was durable in two models (DCT and mERK), it was transient in the gp33 model, with tumors relapsing after 10-20 days. Genetic analyses revealed that relapsed tumor cells no longer expressed the gp33 gene and failed to be recognized by gp33-specific T cells. Strikingly, concomitant MS-275 delivery with ACT + OV treatment induced complete and durable tumor regression. Though HDAC inhibitors modulate transcription on an epigenetic level and can thus instigate broad biological effects, we observed that MS-275 could help reprogram tumor-infiltrating myeloid cells to directly eliminate antigen-loss tumor cell variants and, by transfusing these cells into ACT+OV-treated mice, the enhanced therapeutic benefits that we observed with MS-275 could be recapitulated. The transcriptional changes mediated by MS-275 on other cell types which may potentiate the efficacy of ACT + OV vaccination remain to be determined.

Tumor-infiltrating myeloid cells broadly represent immunosuppressive cells with pro-tumoral activity. During cancer, they accumulate in secondary lymphoid tissue and tumor sites wherein they suppress antigen-specific T cell activity through direct cell-contact, secretion of soluble factors, or competitive uptake of essential amino acids/cytokines (Gordon et al., 2017; Marvel and Gabrilovich, 2015). As a result, the depletion of tumor-infiltrating myeloid cells to enhance antitumor immune responses has been pursued intensely as a therapeutic strategy (De Henau et al., 2016; Lu et al., 2017). However, identifying selective inhibitors of tumor-infiltrating myeloid cells can be difficult due to their phenotypic heterogeneity and readiness to differentiate into one another (Corzo et al., 2010; Kumar et al., 2016; Strauss et al., 2015).

By contrast, it is known that the local cytokine environment can dictate the functional programming of tumor-infiltrating myeloid cells by influencing M1/M2 activation. While tumor-infiltrating myeloid cells predominantly display M2-like phenotypes (Ochando and Chen, 2012), they have been demonstrated to express arginase and nitric oxide as well as both pro-inflammatory M1 and anti-inflammatory M2 genes (Umemura et al., 2008). This may suggest that polarizing myeloid cell function in favor of a pro-inflammatory phenotype can offer an alternative approach to subverting tumor-infiltrating myeloid cell suppressiveness. Indeed, others have shown that myeloid cell polarizing agents including cationic polymers (He et al., 2016), and inhibitors of CSF-1R (Pyonteck et al., 2013), SHP1



(Ma et al., 2011), TGF $\beta$ R kinase (Fridlender et al., 2009) can reduce local immunosuppression in order to potentiate antitumor immune responses. In our model, we observed that the addition of MS-275 could also enhance M1 polarization, reducing the inhibitory effects of tumor-infiltrating myeloid cells on T cell proliferation. However, it is apparent that prevention of tumor relapse was unlikely mediated through tumor-specific T cell improvement since the magnitude, quality, and killing capacity of gp33-specific CD8<sup>+</sup> T cells were unchanged. In fact, ACT + OV treatment alone was sufficient to completely control the initial tumor, suggesting that local immunosuppression was likely overcome by the rapid and potent therapy-driven antitumor immune response as was suggested by others (McGray et al., 2014). Instead, we observed that concomitant MS-275 delivery with ACT + OV treatment conferred tumoricidal properties to M1-polarized tumor-infiltrating myeloid cells.

Myeloid-derived killer cells have been postulated to suppress tumor growth through the enhanced expression of free radicals and death ligands (Marigo et al., 2016; Pilon-Thomas and Ruffell, 2016); however, until now their clinical relevance has not been clearly defined. In this study, we demonstrate that myeloid-derived killer cells can enhance therapeutic outcomes by directly clearing antigen-loss variants. Interestingly, while ACT + OV + MS-275 can durably regress chimeric tumors that have antigen-negative cells mixed in, B16-gp33R tumors, of which the tumor bulk is composed of antigen-negative cells, cannot be controlled. This suggests that while tumor-infiltrating myeloid cells can decrease the efficacy of ACT through immunosuppression, co-ordinated antitumor responses from both tumor-infiltrating myeloid cells and antigen-specific CD8<sup>+</sup> T cells can mediate complete tumor destruction and prevent relapse. Consequently, the polarization of tumor-infiltrating myeloid cells into myeloid-derived killer cells can multi-mechanistically complement ACT by subverting myeloid suppressiveness and enable the eradication of heterogeneous or therapy-resistant tumor cells.

MS-275 possesses pleiotropic effects and has been investigated as an anticancer agent, either alone or in combination with other targeted therapies (Nguyen et al., 2014). While MS-275 is also under investigation as an anti-inflammatory and immunosuppressive drug in the context of autoimmune diseases and allograft survival (Haberland et al., 2009; Shakespear et al., 2011), it has paradoxically been shown to enhance T-cell therapy (Bridle et al., 2013). Using microarray analysis, we confirmed in this study that OV administration induced acute inflammatory responses within the tumor, which were attenuated by MS-275 (Table 1). However, several local inflammatory signals remained at a high level and even increased in the presence of MS-275, potentially creating a more favourable environment for M1 polarization. This may explain why tumor-derived myeloid cells from both ACT + OV- and ACT + OV + MS-275-treated mice showed enrichment for M1-related genes, yet

only concomitant MS-275 delivery was able to confer tumoricidal capability. In particular, the level of local IFN $\gamma$  was markedly increased and the effect of MS-275-mediated M1 hyper-polarization was abrogated in IFN $\gamma$  receptor-deficient mice, establishing a critical role of IFN $\gamma$  in enhancing the polarization of tumor-infiltrating myeloid cells into myeloid-derived killer cells. Consequently, we suggest that modifying the intratumoral cytokine landscape in favor of selective key pro-inflammatory cytokines (such as IFN $\gamma$ ) is necessary to invoke antigen-independent antitumor mechanisms to help promote durable tumor regression.

IFN $\gamma$  has been well-characterized as an essential component of an effective antitumor immune response. Direct IFN $\gamma$  has been demonstrated to induce tumor senescence or killing (Chin et al., 1997; Ikeda et al., 2002), and defects in IFN $\gamma$  pathway genes have been shown to adversely affect patient responsiveness to anti-CTLA-4 therapy (Gao et al., 2016). IFN $\gamma$  can also have tumor stromal targeting effects leading to regression of tumor vasculature and non-haemorrhagic necrosis (Kammertoens et al., 2017). However, tumor sensing of IFN $\gamma$  can mediate adaptive alterations in gene expression leading to increased resistance to antitumor immune responses. It has been previously reported that immune checkpoints such as PD-L1 are up-regulated in response to IFN $\gamma$  resulting in subsequent deactivation of cytotoxic T cells (McGray et al., 2014). Furthermore, there are even reports suggesting that IFN $\gamma$  facilitates genome immunoediting and the emergence of resistant cancer clones (Takeda et al., 2017). As a result, there is ongoing discussion whether IFN $\gamma$  is necessary for successful antitumor immunity. Interestingly, while ACT + OV + MS-275 therapy is a significant driver of intratumoral IFN $\gamma$ , we did not observe reduced functionality in tumor-infiltrating lymphocytes. We postulate that, relative to the slow activation of antitumor immune responses during traditional cancer vaccination, the rapid expansion and tumor infiltration of transferred T cells during ACT + OV treatment mediates significant de-bulking of the tumor before tumor adaptation can occur. Likewise, due to the enhanced therapeutic benefit we observed during concomitant MS-275 delivery, IFN $\gamma$ 's direct impact on antigen loss may be negligible compared to the potent antitumor response elicited by IFN $\gamma$ -polarized myeloid derived killer cells. Altogether, the combination treatment we described may bypass negative regulation to facilitate an additional antitumor role for IFN $\gamma$  in the elimination of antigen-loss variants.

### **Acknowledgements**

Thank you to Huiyu Xu for providing help with the cytopins and immunofluorescence co-staining, Hong Liang, for her help with sorting tumor-infiltrating myeloid cells by flow cytometry, and Anna Dvorkin, for her assistance in analyzing the microarray, Nanostring, and cytokine array data. This work was made possible through the use of MIRC-supported core facilities including central animal facility, in vivo imaging facility, flow cytometry facility, and genomics facility, and support of the Ontario Institute for Cancer Research (OICR), Canadian Institutes of Health Research (CIHR; FRN 123516 and FRN 152954) and the Canadian Cancer Society (grant #705143).

### **Author Contributions**

A.N. designed and conducted the majority of the experiments described and wrote the manuscript. L.H. prepared the samples for microarray analysis. L.C. monitored the therapeutic efficacy of ACT+OV+MS-275 in DCT and mERK models. J.S. conducted the FISH staining on treated tumor sections. J.P. constructed the VSV-gp33 viral vector and S.R.W. constructed the VSV-mERK viral vector. S.T.W. and J.L.B participated in the conception of experimental designs and manuscript writing. Y.W. supervised the study, and participated in the conception of experimental designs and manuscript writing.

### **Declaration of Interests**

The authors report no conflicts of interest.

### **Data Availability**

The accession numbers for the expression data reported in the paper are GEO: GSE101985.

## References

- Ahmed, R., Salmi, A., Butler, L. D., Chiller, J. M., and Oldstone, M. B. (1984). Selection of genetic variants of lymphocytic choriomeningitis virus in spleens of persistently infected mice. Role in suppression of cytotoxic T lymphocyte response and viral persistence. *The Journal of experimental medicine* 160, 521-540.
- Bassett, J. D., Yang, T. C., Bernard, D., Millar, J. B., Swift, S. L., McGray, A. J., VanSeggelen, H., Boudreau, J. E., Finn, J. D., Parsons, R., et al. (2011). CD8<sup>+</sup> T-cell expansion and maintenance after recombinant adenovirus immunization rely upon cooperation between hematopoietic and nonhematopoietic antigen-presenting cells. *Blood* 117, 1146-1155.
- Benoit, M., Desnues, B., and Mege, J. L. (2008). Macrophage polarization in bacterial infections. *Journal of immunology* 181, 3733-3739.
- Bloom, M. B., Perry-Lalley, D., Robbins, P. F., Li, Y., el-Gamil, M., Rosenberg, S. A., and Yang, J. C. (1997). Identification of tyrosinase-related protein 2 as a tumor rejection antigen for the B16 melanoma. *The Journal of experimental medicine* 185, 453-459.
- Bridle, B. W., Chen, L., Lemay, C. G., Diallo, J. S., Pol, J., Nguyen, A., Capretta, A., He, R., Bramson, J. L., Bell, J. C., et al. (2013). HDAC inhibition suppresses primary immune responses, enhances secondary immune responses, and abrogates autoimmunity during tumor immunotherapy. *Molecular therapy : the journal of the American Society of Gene Therapy* 21, 887-894.
- Bridle, B. W., Nguyen, A., Salem, O., Zhang, L., Koshy, S., Clouthier, D., Chen, L., Pol, J., Swift, S. L., Bowdish, D. M., et al. (2016). Privileged Antigen Presentation in Splenic B Cell Follicles Maximizes T Cell Responses in Prime-Boost Vaccination. *Journal of immunology* 196, 4587-4595.
- Bridle, B. W., Stephenson, K. B., Boudreau, J. E., Koshy, S., Kazdhan, N., Pullenayegum, E., Brunelliere, J., Bramson, J. L., Lichty, B. D., and Wan, Y. (2010). Potentiating cancer immunotherapy using an oncolytic virus. *Molecular therapy : the journal of the American Society of Gene Therapy* 18, 1430-1439.
- Butovsky, O., Siddiqui, S., Gabriely, G., Lanser, A. J., Dake, B., Murugaiyan, G., Doykan, C. E., Wu, P. M., Gali, R. R., Iyer, L. K., et al. (2012). Modulating inflammatory monocytes with a unique microRNA gene signature ameliorates murine ALS. *The Journal of clinical investigation* 122, 3063-3087.

Chin, Y. E., Kitagawa, M., Kuida, K., Flavell, R. A., and Fu, X. Y. (1997). Activation of the STAT signaling pathway can cause expression of caspase 1 and apoptosis. *Molecular and cellular biology* 17, 5328-5337.

Corzo, C. A., Condamine, T., Lu, L., Cotter, M. J., Youn, J. I., Cheng, P., Cho, H. I., Celis, E., Quiceno, D. G., Padhya, T., et al. (2010). HIF-1alpha regulates function and differentiation of myeloid-derived suppressor cells in the tumor microenvironment. *The Journal of experimental medicine* 207, 2439-2453.

De Henau, O., Rausch, M., Winkler, D., Campesato, L. F., Liu, C., Cymerman, D. H., Budhu, S., Ghosh, A., Pink, M., Tchaicha, J., et al. (2016). Overcoming resistance to checkpoint blockade therapy by targeting PI3Kgamma in myeloid cells. *Nature* 539, 443-447.

Du, P., Kibbe, W. A., and Lin, S. M. (2008). lumi: a pipeline for processing Illumina microarray. *Bioinformatics* 24, 1547-1548.

Engblom, C., Pfirschke, C., and Pittet, M. J. (2016). The role of myeloid cells in cancer therapies. *Nature reviews Cancer* 16, 447-462.

Fesnak, A. D., June, C. H., and Levine, B. L. (2016). Engineered T cells: the promise and challenges of cancer immunotherapy. *Nature reviews Cancer* 16, 566-581.

Fridlender, Z. G., Sun, J., Kim, S., Kapoor, V., Cheng, G., Ling, L., Worthen, G. S., and Albelda, S. M. (2009). Polarization of tumor-associated neutrophil phenotype by TGF-beta: "N1" versus "N2" TAN. *Cancer cell* 16, 183-194.

Gao, J., Shi, L. Z., Zhao, H., Chen, J., Xiong, L., He, Q., Chen, T., Roszik, J., Bernatchez, C., Woodman, S. E., et al. (2016). Loss of IFN-gamma Pathway Genes in Tumor Cells as a Mechanism of Resistance to Anti-CTLA-4 Therapy. *Cell* 167, 397-404 e399.

Gautier, L., Cope, L., Bolstad, B. M., and Irizarry, R. A. (2004). affy--analysis of Affymetrix GeneChip data at the probe level. *Bioinformatics* 20, 307-315.

Goasguen, J. E., Bennett, J. M., Bain, B. J., Vallespi, T., Brunning, R., and Mufti, G. J. (2009). Morphological evaluation of monocytes and their precursors. *Haematologica* 94, 994-997.

Gordon, S. R., Maute, R. L., Dulken, B. W., Hutter, G., George, B. M., McCracken, M. N., Gupta, R., Tsai, J. M., Sinha, R., Corey, D., et al. (2017). PD-1 expression by tumour-associated macrophages inhibits phagocytosis and tumour immunity. *Nature* 545, 495-499.

Haberland, M., Montgomery, R. L., and Olson, E. N. (2009). The many roles of histone deacetylases in development and physiology: implications for disease and therapy. *Nature reviews Genetics* 10, 32-42.

Hanson, H. L., Donermeyer, D. L., Ikeda, H., White, J. M., Shankaran, V., Old, L. J., Shiku, H., Schreiber, R. D., and Allen, P. M. (2000). Eradication of established tumors by CD8+ T cell adoptive immunotherapy. *Immunity* 13, 265-276.

Haverkamp, J. M., Crist, S. A., Elzey, B. D., Cimen, C., and Ratliff, T. L. (2011). In vivo suppressive function of myeloid-derived suppressor cells is limited to the inflammatory site. *European journal of immunology* 41, 749-759.

He, W., Liang, P., Guo, G., Huang, Z., Niu, Y., Dong, L., Wang, C., and Zhang, J. (2016). Re-polarizing Myeloid-derived Suppressor Cells (MDSCs) with Cationic Polymers for Cancer Immunotherapy. *Sci Rep* 6, 24506.

Ikeda, H., Ohta, N., Furukawa, K., Miyazaki, H., Wang, L., Kuribayashi, K., Old, L. J., and Shiku, H. (1997). Mutated mitogen-activated protein kinase: a tumor rejection antigen of mouse sarcoma. *Proceedings of the National Academy of Sciences of the United States of America* 94, 6375-6379.

Ikeda, H., Old, L. J., and Schreiber, R. D. (2002). The roles of IFN gamma in protection against tumor development and cancer immunoediting. *Cytokine & growth factor reviews* 13, 95-109.

Irizarry, R. A., Hobbs, B., Collin, F., Beazer-Barclay, Y. D., Antonellis, K. J., Scherf, U., and Speed, T. P. (2003). Exploration, normalization, and summaries of high density oligonucleotide array probe level data. *Biostatistics* 4, 249-264.

Junttila, M. R., and de Sauvage, F. J. (2013). Influence of tumour micro-environment heterogeneity on therapeutic response. *Nature* 501, 346-354.

Kammertoens, T., Friese, C., Arina, A., Idel, C., Briesemeister, D., Rothe, M., Ivanov, A., Szymborska, A., Patone, G., Kunz, S., et al. (2017). Tumour ischaemia by interferon-gamma resembles physiological blood vessel regression. *Nature* 545, 98-102.

Kumar, V., Patel, S., Tcyganov, E., and Gabrilovich, D. I. (2016). The Nature of Myeloid-Derived Suppressor Cells in the Tumor Microenvironment. *Trends in immunology* 37, 208-220.

Landsberg, J., Kohlmeyer, J., Renn, M., Bald, T., Rogava, M., Cron, M., Fatho, M., Lennerz, V., Wolfel, T., Holzel, M., and Tuting, T. (2012). Melanomas resist T-cell therapy through inflammation-induced reversible dedifferentiation. *Nature* 490, 412-416.

Lechner, M. G., Liebertz, D. J., and Epstein, A. L. (2010). Characterization of cytokine-induced myeloid-derived suppressor cells from normal human peripheral blood mononuclear cells. *Journal of immunology* 185, 2273-2284.

Lin, S. M., Du, P., Huber, W., and Kibbe, W. A. (2008). Model-based variance-stabilizing transformation for Illumina microarray data. *Nucleic acids research* 36, e11.

Lopez-Castejon, G., Baroja-Mazo, A., and Pelegrin, P. (2011). Novel macrophage polarization model: from gene expression to identification of new anti-inflammatory molecules. *Cellular and molecular life sciences : CMLS* 68, 3095-3107.

Lu, X., Horner, J. W., Paul, E., Shang, X., Troncoso, P., Deng, P., Jiang, S., Chang, Q., Spring, D. J., Sharma, P., et al. (2017). Effective combinatorial immunotherapy for castration-resistant prostate cancer. *Nature* 543, 728-732.

Ma, G., Pan, P. Y., Eisenstein, S., Divino, C. M., Lowell, C. A., Takai, T., and Chen, S. H. (2011). Paired immunoglobulin-like receptor-B regulates the suppressive function and fate of myeloid-derived suppressor cells. *Immunity* 34, 385-395.

Mairhofer, D. G., Ortner, D., Tripp, C. H., Schaffenrath, S., Fleming, V., Heger, L., Komenda, K., Reider, D., Dudziak, D., Chen, S., et al. (2015). Impaired gp100-Specific CD8(+) T-Cell Responses in the Presence of Myeloid-Derived Suppressor Cells in a Spontaneous Mouse Melanoma Model. *The Journal of investigative dermatology* 135, 2785-2793.

Mantovani, A., and Allavena, P. (2015). The interaction of anticancer therapies with tumor-associated macrophages. *The Journal of experimental medicine* 212, 435-445.

Marigo, I., Zilio, S., Desantis, G., Mlecnik, B., Agnellini, A. H., Ugel, S., Sasso, M. S., Qualls, J. E., Kratochvill, F., Zanovello, P., et al. (2016). T Cell Cancer Therapy Requires CD40-CD40L Activation of Tumor Necrosis Factor and Inducible Nitric-Oxide-Synthase-Producing Dendritic Cells. *Cancer cell* 30, 651.

Martinez, F. O., and Gordon, S. (2014). The M1 and M2 paradigm of macrophage activation: time for reassessment. *F1000Prime Rep* 6, 13.

Marvel, D., and Gabrilovich, D. I. (2015). Myeloid-derived suppressor cells in the tumor microenvironment: expect the unexpected. *The Journal of clinical investigation* 125, 3356-3364.

McGray, A. J., Hallett, R., Bernard, D., Swift, S. L., Zhu, Z., Teoderascu, F., Vanseggelen, H., Hassell, J. A., Hurwitz, A. A., Wan, Y., and Bramson, J. L. (2014). Immunotherapy-induced CD8<sup>+</sup> T cells instigate immune suppression in the tumor. *Molecular therapy : the journal of the American Society of Gene Therapy* 22, 206-218.

McWhorter, F. Y., Wang, T., Nguyen, P., Chung, T., and Liu, W. F. (2013). Modulation of macrophage phenotype by cell shape. *Proceedings of the National Academy of Sciences of the United States of America* 110, 17253-17258.

Nguyen, A., Ho, L., and Wan, Y. (2014). Chemotherapy and Oncolytic Virotherapy: Advanced Tactics in the War against Cancer. *Frontiers in oncology* 4, 145.

Ochando, J. C., and Chen, S. H. (2012). Myeloid-derived suppressor cells in transplantation and cancer. *Immunologic research* 54, 275-285.

Piccolo, V., Curina, A., Genua, M., Ghisletti, S., Simonatto, M., Sabo, A., Amati, B., Ostuni, R., and Natoli, G. (2017). Opposing macrophage polarization programs show extensive epigenomic and transcriptional cross-talk. *Nature immunology* 18, 530-540.

Pilon-Thomas, S., and Ruffell, B. (2016). Tipping the Balancing ACT. *Cancer cell* 30, 367-368.

Pol, J. G., Zhang, L., Bridle, B. W., Stephenson, K. B., Resseguier, J., Hanson, S., Chen, L., Kazhdan, N., Bramson, J. L., Stojdl, D. F., et al. (2013). Maraba Virus as a Potent Oncolytic Vaccine Vector. *Molecular therapy : the journal of the American Society of Gene Therapy*.

Pommier, A., Audemard, A., Durand, A., Lengagne, R., Delpoux, A., Martin, B., Douguet, L., Le Champion, A., Kato, M., Avril, M. F., et al. (2013). Inflammatory monocytes are potent antitumor effectors controlled by regulatory CD4<sup>+</sup> T cells. *Proceedings of the National Academy of Sciences of the United States of America* 110, 13085-13090.

Powell, D. R., and Huttenlocher, A. (2016). Neutrophils in the Tumor Microenvironment. *Trends in immunology* 37, 41-52.

Prevost-Blondel, A., Zimmermann, C., Stemmer, C., Kulmburg, P., Rosenthal, F. M., and Pircher, H. (1998). Tumor-infiltrating lymphocytes exhibiting high ex vivo cytolytic



activity fail to prevent murine melanoma tumor growth in vivo. *Journal of immunology* 161, 2187-2194.

Pyonteck, S. M., Akkari, L., Schuhmacher, A. J., Bowman, R. L., Sevenich, L., Quail, D. F., Olson, O. C., Quick, M. L., Huse, J. T., Teijeiro, V., et al. (2013). CSF-1R inhibition alters macrophage polarization and blocks glioma progression. *Nature medicine* 19, 1264-1272.

Quah, B. J., and Parish, C. R. (2010). The use of carboxyfluorescein diacetate succinimidyl ester (CFSE) to monitor lymphocyte proliferation. *Journal of visualized experiments : JoVE*.

Reich, M., Liefeld, T., Gould, J., Lerner, J., Tamayo, P., and Mesirov, J. P. (2006). GenePattern 2.0. *Nat Genet* 38, 500-501.

Restifo, N. P., Smyth, M. J., and Snyder, A. (2016). Acquired resistance to immunotherapy and future challenges. *Nature reviews Cancer* 16, 121-126.

Ritchie, M. E., Phipson, B., Wu, D., Hu, Y., Law, C. W., Shi, W., and Smyth, G. K. (2015). limma powers differential expression analyses for RNA-sequencing and microarray studies. *Nucleic acids research* 43, e47.

Roederer, M. (2011). Interpretation of cellular proliferation data: avoid the panglossian. *Cytometry A* 79, 95-101.

Russell, S. J., Peng, K. W., and Bell, J. C. (2012). Oncolytic virotherapy. *Nature biotechnology* 30, 658-670.

Shakespeare, M. R., Halili, M. A., Irvine, K. M., Fairlie, D. P., and Sweet, M. J. (2011). Histone deacetylases as regulators of inflammation and immunity. *Trends in immunology* 32, 335-343.

Strauss, L., Sangaletti, S., Consonni, F. M., Szebeni, G., Morlacchi, S., Totaro, M. G., Porta, C., Anselmo, A., Tartari, S., Doni, A., et al. (2015). RORC1 Regulates Tumor-Promoting "Emergency" Granulo-Monocytopenia. *Cancer cell* 28, 253-269.

Subramanian, A., Tamayo, P., Mootha, V. K., Mukherjee, S., Ebert, B. L., Gillette, M. A., Paulovich, A., Pomeroy, S. L., Golub, T. R., Lander, E. S., and Mesirov, J. P. (2005). Gene set enrichment analysis: a knowledge-based approach for interpreting genome-wide expression profiles. *Proceedings of the National Academy of Sciences of the United States of America* 102, 15545-15550.

Takeda, K., Nakayama, M., Hayakawa, Y., Kojima, Y., Ikeda, H., Imai, N., Ogasawara, K., Okumura, K., Thomas, D. M., and Smyth, M. J. (2017). IFN-gamma is required for cytotoxic T cell-dependent cancer genome immunoediting. *Nature communications* 8, 14607.

Umemura, N., Saio, M., Suwa, T., Kitoh, Y., Bai, J., Nonaka, K., Ouyang, G. F., Okada, M., Balazs, M., Adany, R., et al. (2008). Tumor-infiltrating myeloid-derived suppressor cells are pleiotropic-inflamed monocytes/macrophages that bear M1- and M2-type characteristics. *Journal of leukocyte biology* 83, 1136-1144.

Workenhe, S. T., Ketela, T., Moffat, J., Cuddington, B. P., and Mossman, K. L. (2016). Genome-wide lentiviral shRNA screen identifies serine/arginine-rich splicing factor 2 as a determinant of oncolytic virus activity in breast cancer cells. *Oncogene* 35, 2465-2474.

Wu, D., and Yotnda, P. (2011). Production and detection of reactive oxygen species (ROS) in cancers. *Journal of visualized experiments : JoVE*.

Yang, W. C., Ma, G., Chen, S. H., and Pan, P. Y. (2013). Polarization and reprogramming of myeloid-derived suppressor cells. *J Mol Cell Biol* 5, 207-209.

Zhang, L., Bridle, B. W., Chen, L., Pol, J., Spaner, D., Boudreau, J. E., Rosen, A., Bassett, J. D., Lichty, B. D., Bramson, J. L., and Wan, Y. (2013). Delivery of viral-vectored vaccines by B cells represents a novel strategy to accelerate CD8(+) T-cell recall responses. *Blood* 121, 2432-2439.

### Main Figure Titles and Legends

#### **Figure 1: ACT+OV-mediated CD8<sup>+</sup> T cell expansion regressed tumors, but subsequent loss of antigen recognition promotes tumor relapse**

In C57BL/6 mice (n=5 per group), (A) five to (B) ten day old intradermal B16-gp33 tumors were given adoptive cell therapy (ACT, 10<sup>4</sup> gp33-specific TCM delivered i.v.) followed by oncolytic viral (OV) vaccination with 2x10<sup>8</sup> pfu VSV-gp33 i.v. (See also Figure S1). Tumor volumes were calculated based on height, width, and length. (C) Five days post-vaccination, the frequency of gp33-specific CD8<sup>+</sup> T cells, as determined by IFN $\gamma$  expression after ex vivo peptide stimulation, was measured from peripheral blood. (D) Monoclonal antibodies targeting CD8, CD4, and NK1.1 were administered i.p. one day before and after VSV-boosting and every two weeks afterwards. (E) Tumor volumes of ACT+OV-treated mice (n=5) were continuously measured up to 40 days post-tumor challenge. After varying the dose of TCM, (F) the frequency of gp33-specific CD8<sup>+</sup> T cells was measured from peripheral blood and (G) tumor volumes were monitored (n=3-4 per group). (H) C57BL/6 mice (n=3 per group) were pre-treated with Ad-gp33 and challenged with parental or relapsed B16-gp33 after two weeks. Results are mean  $\pm$  SEM. To determine significance one way ANOVA was used (\*\*\*\* p<0.0001); VSV-MT, VSV without transgene

#### **Figure 2: Concomitant MS-275 delivery prevents tumor relapse by mediating the elimination of gene-loss variants**

B16-gp33 tumor-bearing mice (n=5 per group) were treated with ACT+OV. Concomitantly, MS-275 was injected i.p. daily for 5 days. (A) Tumor volumes were used to generate (B) Kaplan-Meier survival curves. (C) B16-gp33R (n=3 per group) or (E) chimeric B16-gp33/B16-F10luc tumor-bearing mice (n=5 per group) were treated with ACT+OV+MS-275. (D) Genomic DNA was used as a template for PCR analysis of gp33 expression. (F) In vivo imaging of B16-F10luc cells in treated mice. Fluorescence signal was quantified by photon flux after i.p. injection of 75 mg/kg D-Luciferin. Results are mean  $\pm$  SEM. B16-gp33R, relapsed B16-gp33 tumor explant; B16-F10luc, luciferase-expressing B16-gp33 cells

#### **Figure 3: Concomitant MS-275 delivery induces a pro-inflammatory phenotype within tumor-infiltrating CD11b<sup>+</sup> Ly6Chi Ly6G<sup>-</sup> myeloid cells**

Five days post-treatment, digested tumors (n=3-5 per group) were enriched for CD11b+ cells. (A) Absolute counts of CD45.2+ CD11b+ cells were quantified and (B) frequencies of myeloid cell subsets were depicted (See also Figure S8). (C) Representative histogram overlays of Ly6G and CD11c are shown for CD11b+ CD11c-/lo F4/80+ Ly6Chi Ly6G- myeloid cells and mean fluorescence intensities were enumerated. (D) CD11b+ cells were Giemsa-Wright stained and imaged at 40x magnification (Scale bar: 5  $\mu$ m). (E) Representative histogram overlays of NOS2 are shown for CD11b+ Ly6Chi Ly6G- and CD11b+ Ly6Clo Ly6G+ cells (See also Figure S4). The frequency of CD11b+ Ly6Chi Ly6G- cells expressing (F) NOS2 and (H) Arg1 was measured. (G) Carboxy-H2DCFDA was used to fluorescently detect reactive oxygen species in tumor-derived CD11b+ cells. Results are mean  $\pm$  SEM. To determine significance one way ANOVA was used (\*\*\*) p=0.0004, \*\*\*\* p=0.0003, \* p=0.0479)

**Figure 4: Pro-inflammatory tumor-infiltrating myeloid cells display decreased suppressiveness and demonstrate tumor killing capacity**

(A-C) Enriched CD11b+ cells (n=3 per group) were co-cultured for 3 days with stimulated CFSE-labeled P14 T cells. CFSE dilution is shown as (A) a representative histogram, (B) cellular division index and (C) percentage of divided cells. (D) B16-F10 tumors (n=3 per group) were co-stained with cleaved caspase 3 and CD11b and imaged at 20x magnification (Scale bar: 25  $\mu$ m). (E) Enriched CD11b+ cells derived from ACT+OV+MS-275-treated mice (CD11bTVM) were co-cultured with B16-F10 target cells at a 10:1 ratio. Killing was measured after 12 hours by MTT reduction and done in triplicate (See also Figure S5). (F, G) CD11bTVM cells were intratumorally injected into B16-gp33 tumor-bearing mice (n=5 per group), treated with ACT+OV, and monitored for (F) tumor growth and (G) survival. Results are mean  $\pm$  SEM. To determine significance one way ANOVA was used (NS=not significant, \*\*\*\* p<0.0001, \*\*\* p=0.0002)

**Figure 5: ACT+OV and ACT+OV+MS-275 reprogram tumor-infiltrating myeloid cells from an M2 phenotype to an M1 phenotype**

Enriched CD11b+ cells (n=3 per group) were pooled and sorted into Ly6Chi Ly6G- and Ly6Clo Ly6G+ fractions. RNA from sorted Ly6Chi Ly6G- cells was analyzed using an nCounter inflammatory gene codeset. Gene set enrichment analysis was conducted using manually curated lists representing M1 and M2 inflammatory profiles (See also Table S1). Enrichment score displays the extent of ‘enrichment’ in a specific list when comparing ACT+OV+/-MS-275 to no treatment. Members of each profile are placed in the rank list

(‘bar code’) which displays the total number of genes in the codeset. A signal-to-noise metric is represented by a red/blue gradient (red represents treated and blue represents untreated). Each comparison demonstrates significant enrichment (false discovery rate, <math><10^{-2}</math>) and data are representative of two independent experiments.

**Figure 6: Concomitant MS-275 delivery enhances M1 polarization further through heightened local IFN $\gamma$ /IFN $\gamma$ R signaling**

Five days post-treatment, B16-gp33 tumors (n=4 per group) were homogenized and sent for multiplex cytokine analysis. (A) Heat map displaying the relative changes in RMA-normalized, log<sub>2</sub> transformed tumor cytokine concentrations. (B) Principal component analysis of tumor cytokine concentrations showing clustering of treatment groups. (C) Revised heat map showing fold concentration changes for cytokines displaying significant differential expression when comparing ACT+OV+MS-275 to ACT+OV treatment (See also Figure S6). (D) Concentration of intratumoral IFN $\gamma$ . (E) qRT-PCR of IFNG expression from whole tumor RNA (n=3 per group) (See also Figure S7). (F) Enrichment of CD11b<sup>+</sup> cells followed by pSTAT1 staining of Ly6Chi Ly6G<sup>-</sup> gated cells (n=5 per group). (G) Enrichment of CD11b<sup>+</sup> cells from IFN $\gamma$ R<sup>-/-</sup> mice followed by NOS2 staining of Ly6Chi Ly6G<sup>-</sup> gated cells (n=5 per group). Results are mean  $\pm$  SEM. To determine significance one way ANOVA was used (\* p=0.0349, \*\* p<0.01, \*\*\* p=0.0033, \*\*\*\* p<0.0001)

**Main Table Titles and Legends**

**Table 1: GO enrichment analysis for differentially expressed genes in ACT+OV+MS-275 vs ACT+OV-treated tumors**

## **Experimental Procedures:**

### **Mice**

Female age-matched (6-8 weeks old) C57BL/6 and Balb/C mice were purchased from Charles River Laboratory, B6.129S7-Ifngr1tm1Agt/J (IFNGR KO) mice were purchased from The Jackson Laboratory, and B6.Cg-Tcratm1Mom Tg(TcrLCMV)327Sdz (P14) mice were purchased from Taconic. DUC18 mice were kindly provided by Dr. Lyse Norian (University of Iowa) and 24H9R mice were kindly provided by Dr. Andy Hurwitz (Frederick National Laboratory for Cancer Research, National Cancer Institute). Mice were housed in the Central Animal Facility at McMaster University and all animal studies complied with the Canadian Council on Animal Care guidelines and were approved by McMaster University's Animal Research Ethics Board.

### **Viral Vectors**

LCMV-Armstrong, VSV-gp33, and Ad-gp33 were described previously (Ahmed et al., 1984; Bassett et al., 2011; Zhang et al., 2013). VSV-MT lacks the gp33 transgene and was utilized as a control vector.

### **Peptides**

The H-2Db-restricted peptide of LCMV-GP33-41 (KAVYNFATM) was purchased from the Dalton Chemical Laboratory and dissolved in ddH<sub>2</sub>O.

### **Cells and Culture Conditions**

B16-gp33 cells were generated as described previously (Prevost-Blondel et al., 1998). B16-gp33, B16-F10, B16-F10luc, B16-gp33R, and CMS-5 cells were grown as previously described (Bridle et al., 2013; Bridle et al., 2016).

### **Tumor Challenge**

Mice were challenged intradermally with 10<sup>5</sup> B16-gp33 cells in 30 µl PBS. Tumor growth was monitored as previously described (Bridle et al., 2016). Chimeric tumors were

generated by mixing B16-gp33 with B16-F10luc cells at a 1000:1 ratio before intradermal injection. In vivo monitoring of these tumors was conducted using an IVIS Spectrum In Vivo Imaging System (Caliper Life Sciences) following intraperitoneal injection of 75 mg/kg D-luciferin (Caliper Life Sciences).

### **Challenge with Relapsed Tumor**

Relapsing tumors (B16-gp33R) were excised and suspended in EDTA at 3 mL/g of tumor before being digested in a mixture of 3 mg/mL collagenase A (Roche) and 0.1% trypsin prepared in complete RPMI (7 mL/g of tumor) at 37°C for 1 hr. B16-gp33R cells were subsequently filtered through a 40 µm strainer, washed, and re-suspended in culture media or PBS.

### **Adoptive T cell Transfer**

Spleens were collected from LCMV-Armstrong-infected mice (>1 month) and a single cell suspension was prepared. Gp33-specific central memory T cells (TCM) were enumerated by staining with H-2Db-GP33 tetramer (Baylor College of Medicine), CD127, and CD62L (BD Biosciences). 10<sup>4</sup> gp33-specific TCM in 200 µL PBS were adoptively transferred into tumor-challenged mice by intravenous injection.

### **Oncolytic Viral Vaccination**

Twenty-four hours post-adoptive T cell transfer, mice were injected intravenously with 2x10<sup>8</sup> pfu of VSV-gp33 in 200 µL PBS. Concomitantly, MS-275 (Sigma-Aldrich) was intraperitoneally injected (100 µg/mouse in 50 µL PBS) daily for five days. Selective lymphocyte depletion was conducted using monoclonal antibodies (produced in-house at McMaster University) specific for CD8<sup>+</sup> T cells, CD4<sup>+</sup> T cells, or NK cells. Mice were injected with 250 µg of mAb in 500 µL PBS on Day -1 and 1 post-vaccination and every two weeks afterwards (150 µg). In some experiments, CD11b-enriched cells (described below) derived from gp33-specific TCM + VSV-gp33 + MS-275-treated mice were injected intratumorally (~3x10<sup>5</sup> cells in 30 µL PBS) at day 0 post-vaccination instead of MS-275.

### **Detection of Antigen-specific Responses**

Five days post-vaccination, PBMCs were stimulated at for 5 hours with gp33 peptide in the presence of brefeldin A (GolgiPlug; BD Biosciences). Following surface staining for CD8 $\alpha$  (BD Biosciences), cells were fixed and permeabilized with Cytofix/Cytoperm (BD Biosciences) and stained for intracellular IFN $\gamma$  (BD Biosciences). Data were acquired using an LSRFortessa flow cytometer with FACSDiva software (BD Biosciences) and analyzed with FlowJo X, version 10.0.7 (Treestar).

### **Genomic DNA Extraction and PCR**

Genomic DNA was extracted from B16-gp33, B16-F10, and B16-gp33R cells using Purelink Genomic DNA Extraction Kits (Life Technologies). PCR was carried out using Taq DNA polymerase (New England Biolabs) using the gp33 primer sequence FWD – GTCCTTTGGGCGCTAACTG, REV – GTGGCGAAATTGTACACAGC.

### **Tumor RNA Extraction and qRT-PCR**

B16-gp33 tumors were excised 5 days post-vaccination and snap-frozen in liquid nitrogen and samples were then homogenized in Trizol (Invitrogen). RNA was extracted and purified using an RNeasy mini kit (Qiagen) and treated with Ambion's DNA-free kit. Reverse transcription was performed with Superscript II First-Strand reverse transcriptase (Thermo Fisher Scientific). qRT-PCR was done as previously described (Workenhe et al., 2016). The primer sequences are as follows: IFNG FWD – CTTGAAAGACAATCAGGCCATC, IFNG REV – CAGCAGCGACTCCTTTTCC; HPRT FWD – ACACCTGCTAATTTTACTGGCAACA, HPRT REV - TGGAAAAGCCAAATACAAAGCCTA

### **Gene Expression Analysis by Microarray**

RNA from B16-gp33 tumors was isolated five days post-vaccination and prepared for profiling on MouseRef8\_V2\_0\_R3\_11278551\_A beadchips (Illumina) according to the manufacturer's protocol. Global expression profiles were preprocessed with the Illumina package in R (Du et al., 2008), and only annotated and present genes were used for further analyses. During the preprocessing, the obtained values were VST transformed (difference variance stabilizing transformation (Lin et al., 2008)) and background correction was



performed; then the obtained data were normalized with quantile normalization. Genes were considered differentially expressed if the fold change was  $>2.0$  and q value was  $<0.1$ . Gene ontology term enrichment analysis was conducted by PANTHER overrepresentation test (release 20160715) using the GO database (released 2016-12-29) with GO biological process complete annotation data set. The reference gene list was the *Mus musculus* genome and expression data analyses include Bonferroni correction for multiple testing. Overrepresented GO terms were sorted hierarchically and displayed results are statistically significant ( $P<0.05$ ).

### **Purification of Tumor-infiltrating Myeloid Cells**

B16-gp33 tumors were excised 5 days post-vaccination and digested in 0.5 mg/mL collagenase Type IV (Gibco), and 0.2 mg/mL DNase (Roche) prepared in complete RPMI (Gibco, 10 mL/250 mg tumor) and incubated at 37°C for 30 min. The digested material was CD11b<sup>+</sup> enriched through magnetic selection with an EasySep Mouse CD11b Positive Selection Kit II (Stemcell Technologies). CD45.2, CD11b, CD11c, F4/80, Ly6C, and Ly6G (BD Biosciences) staining antibodies were used to differentiate myeloid cell subsets, while Nos2 (Thermo Fisher Scientific), Arg1 (R&D Systems), pStat1 (BD Biosciences) were used to characterize their inflammatory status.

### **Cytospin of Tumor-infiltrating Myeloid Cells**

Tumor-infiltrating myeloid cells were isolated, re-suspended in PBS, and cytospun (200  $\mu$ l, 300 rpm, 2 min) in a cytocentrifuge (Cytospin 4; Thermo Fisher Scientific) and differentially stained with Giemsa (Sigma-Aldrich) for morphological analyses. Images were captured at 40X magnification using a Micropublisher 5.0 RTV camera (QImaging) on a Leica DMRA microscope (Leica).

### **Immunofluorescence**

B16-gp33 tumors excised 5 days post-vaccination were snap frozen before cryostat sections were obtained and mounted on gelatin-coated histological slides. The slides were fixed in 4% paraformaldehyde for 20 min at room temperature and blocked with PBS containing 5% goat serum and 0.3% Triton X-100 for 30 min. Anti-Cleaved Caspase-3 (1:400, Cell Signaling Technology) and anti-CD11b (1:400, Thermo Fisher Scientific) were added and incubated overnight at 4°C. Slides were incubated for 1h with biotinylated goat anti-rabbit

IgG (Vector Laboratories) and Texas Red-conjugated goat anti-rat IgG (Cedarlane Labs) followed by Alexa Fluor 488-conjugated streptavidin (Thermo Fisher Scientific). Images were captured at 20X magnification using a Micropublisher 5.0 RTV camera (QImaging) on a Leica DMRA microscope (Leica).

### **ROS assay**

Tumor-infiltrating myeloid cells were isolated and re-suspended in PBS before loading with Carboxy-H2DCFDA as reported by others (Wu and Yotnda, 2011) and measured for fluorescence (435 nm excitation, 535 nm emission) using a Synergy microplate reader (Biotek Instruments). Loaded cells were treated with 1 mM H<sub>2</sub>O<sub>2</sub> for 20 minutes as a positive control.

### **Proliferation assay**

Tumor-infiltrating myeloid cells were isolated and co-cultured for 3 days with gp33-peptide pulsed dendritic cells and CFSE-labeled P14 T cells as previously reported (Quah and Parish, 2010). Tumor-infiltrating myeloid cells were added at a 1:1 or 0.5:1 CD11b to T cell ratio. Proliferation was evaluated using several metrics including the division index and the percentage of cells divided (Roederer, 2011).

### **In vitro Cytotoxicity Assay**

B16-F10 cells (1x10<sup>4</sup> /well) were co-cultured with tumor-infiltrating myeloid cells (1x10<sup>5</sup>/well) in 96-well flat bottom microtiter plates (Corning Inc.) for 12 hours before killing was assessed. Non-adherent cells were washed using warm PBS and 500 µg/mL MTT (3-(4,5-dimethylthiazol-2-yl)-2,5-diphenyltetrazolium bromide, Thermo Fisher Scientific) solution was added before incubating the plates for 4 hours. Solubilization of the formazan by-product was done by aspirating the MTT solution and adding DMSO. The absorbance was measured at 540 nm using a Synergy microplate reader (Biotek).

### **Gene Expression by Nanostring**

Tumor-infiltrating myeloid cells were sorted using a BD FACSAria Flow Cytometer into CD11b<sup>+</sup> Ly6Chi Ly6G<sup>-</sup> and CD11b<sup>+</sup> Ly6Cl<sup>o</sup> Ly6G<sup>-</sup> fractions. Extracted RNA was

analysed using the nCounter Mouse Inflammation Gene Expression CodeSet v2 (Nanostring Technologies). Data was background-subtracted and normalized using nSolver Analysis Software (Nanostring Technologies). Gene Set Enrichment Analysis (GSEA) (Subramanian et al., 2005) was performed using GenePattern Version X (Reich et al., 2006). We examined the enrichment of two manually curated lists: (a) M1 Profile, reflective of the M1 phenotype (34 genes) and (b) M2 Profile, reflective of the M2 phenotype (25 genes) (Table S1) (Benoit et al., 2008; Butovsky et al., 2012; Lechner et al., 2010; Martinez and Gordon, 2014). Two pair-wise comparisons were performed: gp33-specific TCM + VSV-gp33 vs No Tx and gp33-specific TCM + VSV-gp33 + MS-275 vs No Tx.

### **Multiplex Cytokine Analysis**

B16-gp33 tumors were excised 5 days post-vaccination and homogenized in lysing solution (Bioplex Cell Lysing Kit, Bio-Rad Laboratories). The multiplex assay was performed by Eve Technologies using the Bio-Plex 200 system and the Milliplex Mouse Cytokine/Chemokine Magnetic Bead Panel Kit according to their protocol. Multiplex data were preprocessed with the Affymetrix package in R (Gautier et al., 2004) involving RMA background adjustment and quantile normalization (Irizarry et al., 2003). Resulting expression values were transformed to the log<sub>2</sub> scale for further analysis. After preprocessing we performed principal component analysis (princomp function from “stats” package in R) to confirm that samples were clustering into homogeneous groups matching experimental groups. Heat maps were created using the HeatMapImage (version 6) module available on Gene Pattern (<http://genepattern.broadinstitute.org/gp/pages/index.jsf>). To test for differential expression for pre-specified contrasts, linear models were fit for each cytokine using the “limma” package (Ritchie et al., 2015). Obtained p-values were adjusted for multiple comparisons using the Benjamini-Hochberg procedure.

### **Fluorescent in situ Hybridization**

FISH was done at the MIRC Core Histology Facility with the Automated Leica Bond RX and using probes (IFN $\gamma$ , CD3, CD11b) and assay kits obtained from Advanced Cell Diagnostics. Staining and analyses were conducted according to manufacturer instructions.

### **Statistics**

GraphPad Prism version 6.00 for Windows (GraphPad Software) was used for graphing and statistical analyses. One-way analysis of variance (ANOVA) was used to query immune response data. All data were presented as means  $\pm$  SEM and differences between means were considered significant at  $p < 0.05$ . Error bars indicate 95% confidence intervals throughout.

### **Supplementary Figure Titles and Legends**

#### **Figure S1, related to Figure 1A: Efficacy of ACT+OV in additional tumor models**

Balb/c mice or C57BL/6 mice were challenged with CMS-5 or B16-F10 tumors respectively for five days before treatment with ACT+OV (n=5 per group). TCM were derived from TCR-transgenic mice recognizing mERK or DCT (DUC18 and 24H9R mice, respectively).

#### **Figure S2: Concomitant MS-275 does not alter T cell magnitude or phenotype**

Five days post-vaccination, the frequency of gp33-specific CD8<sup>+</sup> T cells was measured (n=5 per group). Functional (CD107, TNF $\alpha$ ) and exhaustion (KLRG1, PD-1) markers were also quantified.

#### **Figure S3: Concomitant MS-275 does not improve T cell killing**

(A) Gp33 peptide-pulsed bulk splenocyte targets were labeled with 5 $\mu$ M CFSE and i.v. injected with an equal number of 0.5 $\mu$ M CFSE unlabeled targets before treatment (n=3 per group). Killing was assessed by CFSE five days post-treatment from individual spleens or pooled tumors. (B) Tumor-enriched CD8<sup>+</sup> T cells were co-cultured with B16-gp33 target cells at a 1:1 ratio (n=3 per group). Killing was measured after 12 hours by MTT reduction and done in triplicate.

#### **Figure S4, related to Figure 3D, E: Reprogrammed pro-inflammatory tumor-infiltrating myeloid cell phenotype in the CMS-5 tumor model**

Five days post-treatment, digested CMS-5 tumors were enriched for CD11b<sup>+</sup> cells. Representative histogram and quantification of NOS2 for Ly6Chi Ly6G<sup>-</sup> gated cells.

#### **Figure S5, related to Figure 4E: Pro-inflammatory tumor-infiltrating myeloid cells kill through cell-contact dependent mechanisms**

Enriched CD11b<sup>+</sup> cells derived from ACT+OV+MS-275-treated mice (CD11bTVM, n=3) were co-cultured with B16-F10 target cells in the presence of iNOS and ROS inhibitors (L-

NIL and SOD/Catalase, respectively) or transwell permeable supports at a 10:1 ratio. Killing was measured after 12 hours by MTT reduction and done in triplicate.

**Figure S6, related to Figure 6C: Concomitant MS-275 delivery alters the intratumoral concentrations of select inflammatory-related cytokines**

Concentrations of cytokines showing significant differential expression when comparing ACT+OV+MS-275 to ACT+OV treatment where n=4 per group.

**Figure S7, related to Figure 6E: Elevated IFN $\gamma$  in the context of MS-275 is attributed to tumor-infiltrating CD8<sup>+</sup> T cells**

B16-gp33 tumor-bearing mice were given gp33-specific TCM one day before vaccination with VSV-gp33 and MS-275. Upon depleting Ab administration, tumor volumes were measured based on height, width, and length (n=5 per group) (A) and the frequency of NOS2-expressing Ly6Chi Ly6G<sup>-</sup> cells was measured by flow cytometry in digested tumors that were purified for CD11b<sup>+</sup> cells (n=3 per group) (B, C). (D) FISH staining of frozen tumor sections derived from ACT+OV+MS-275-treated mice (n=3 per group). (E) In vivo Golgi Plug administration for 6h on day 5 post-ACT+OV+/-MS-275 treatment (n=3 per group) before IFN $\gamma$  staining of tumor-infiltrating CD8<sup>+</sup> T cells and CD11b<sup>+</sup> myeloid cells.

**Figure S8, related to Figure 3B: Enumeration of myeloid cell subsets during ACT + OV + MS-275 treatment**

**Supplementary Table Titles and Legends**

**Table S1: M1/M2 Gene Profile, related to Figure 5**

**Table S2: Differentially expressed genes from the Nanostring nCounter inflammatory gene codeset, related to Figure 5**

**Figure 1**

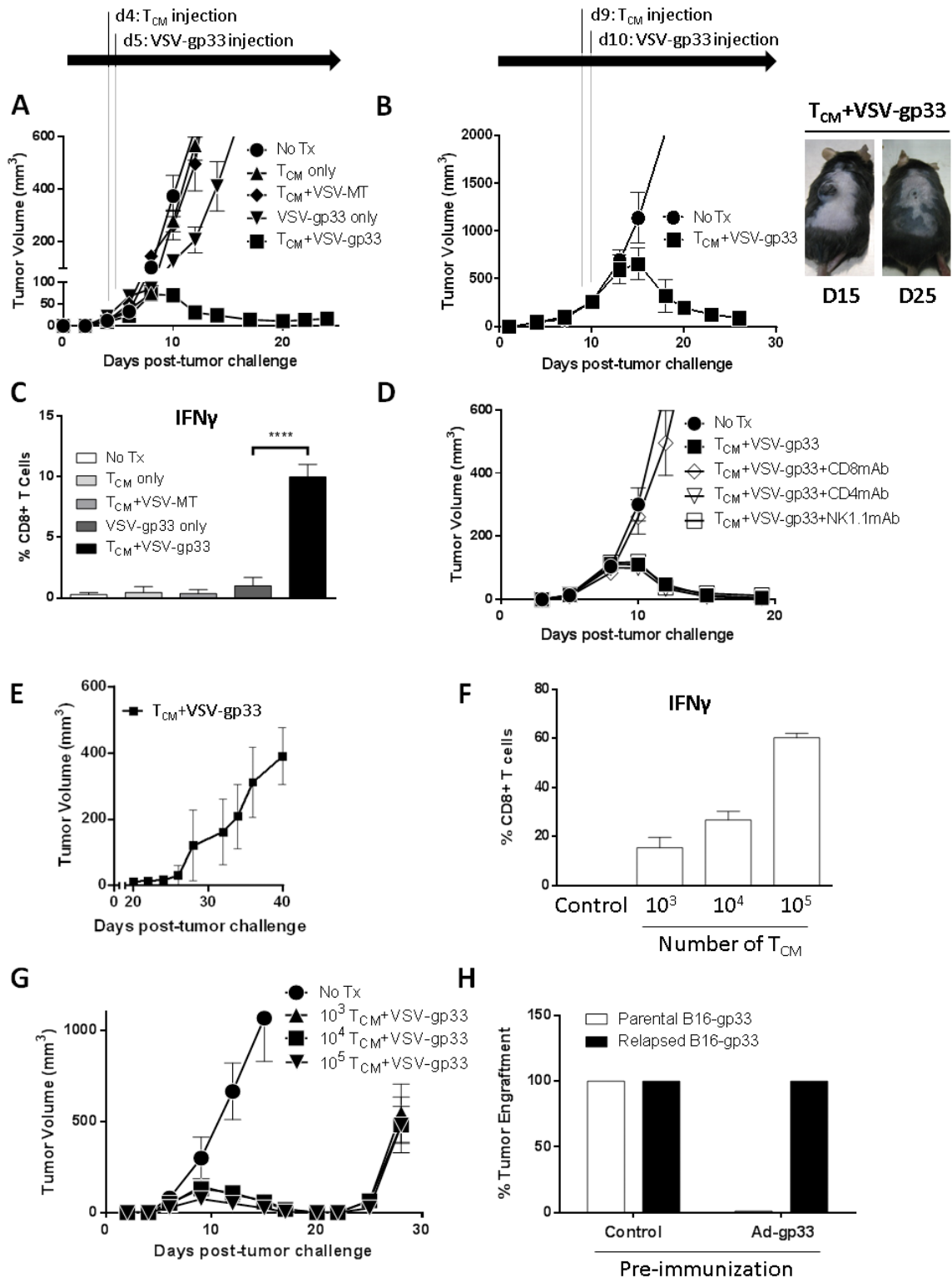


Figure 2

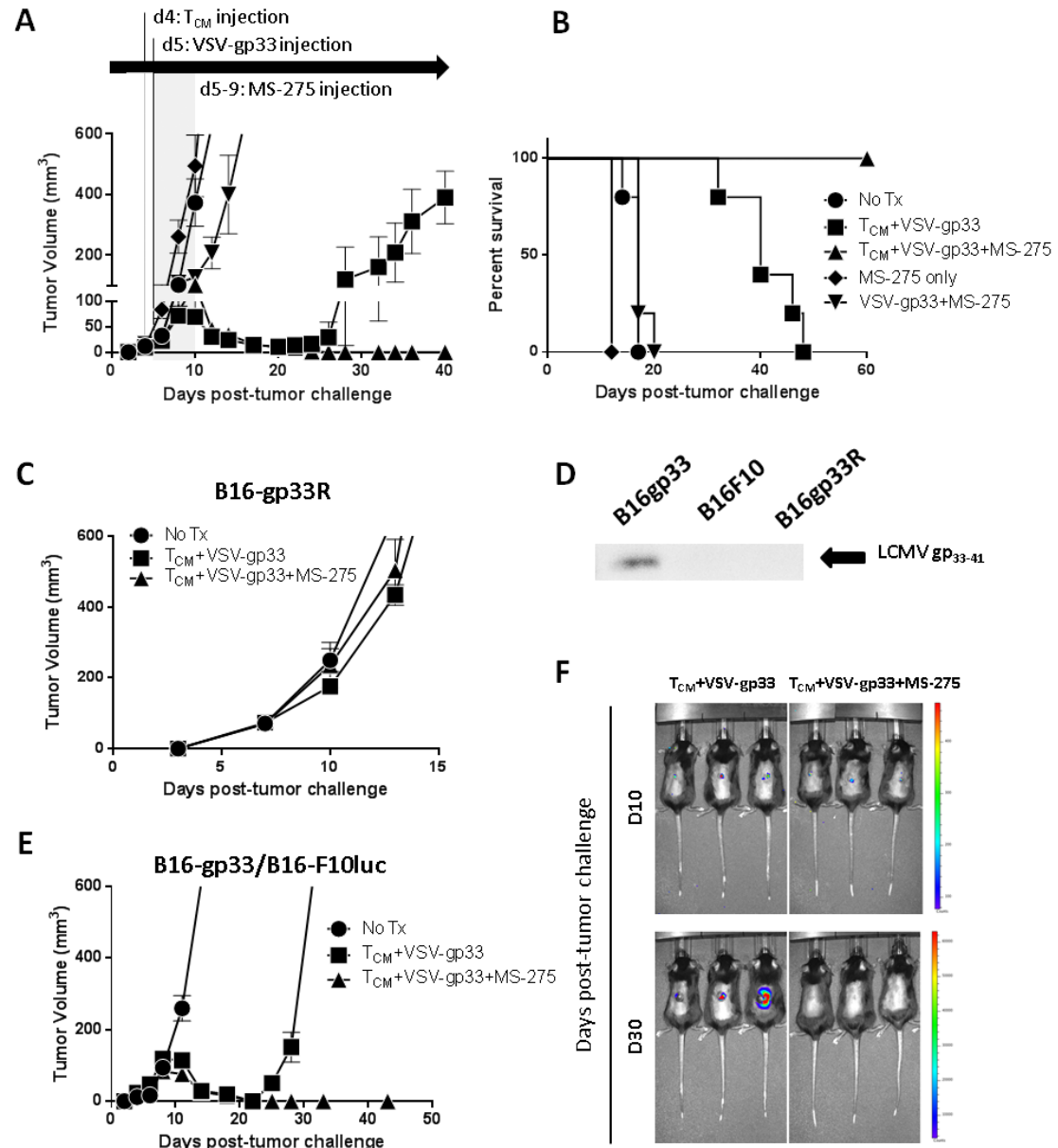




Figure 3

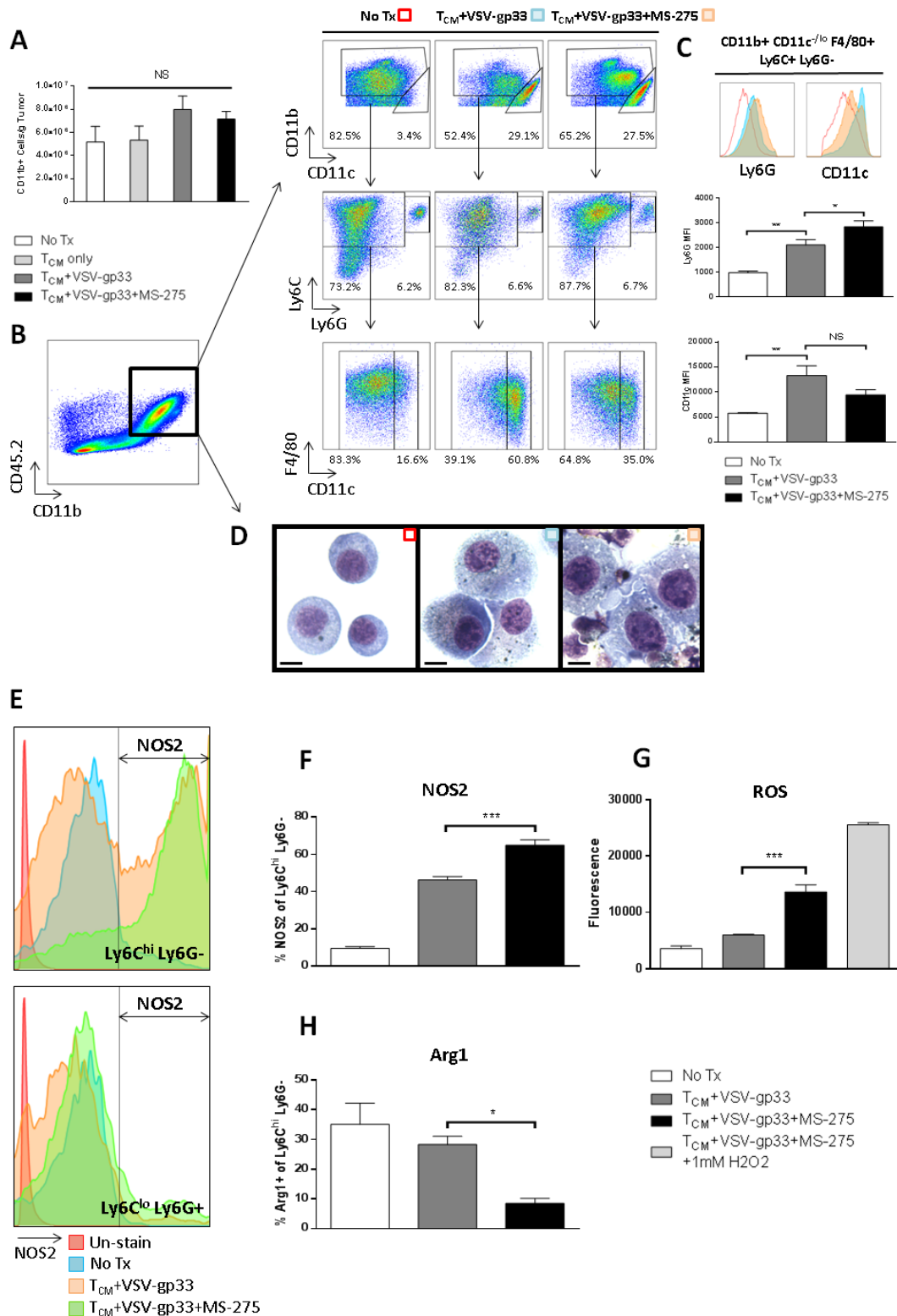


Figure 4

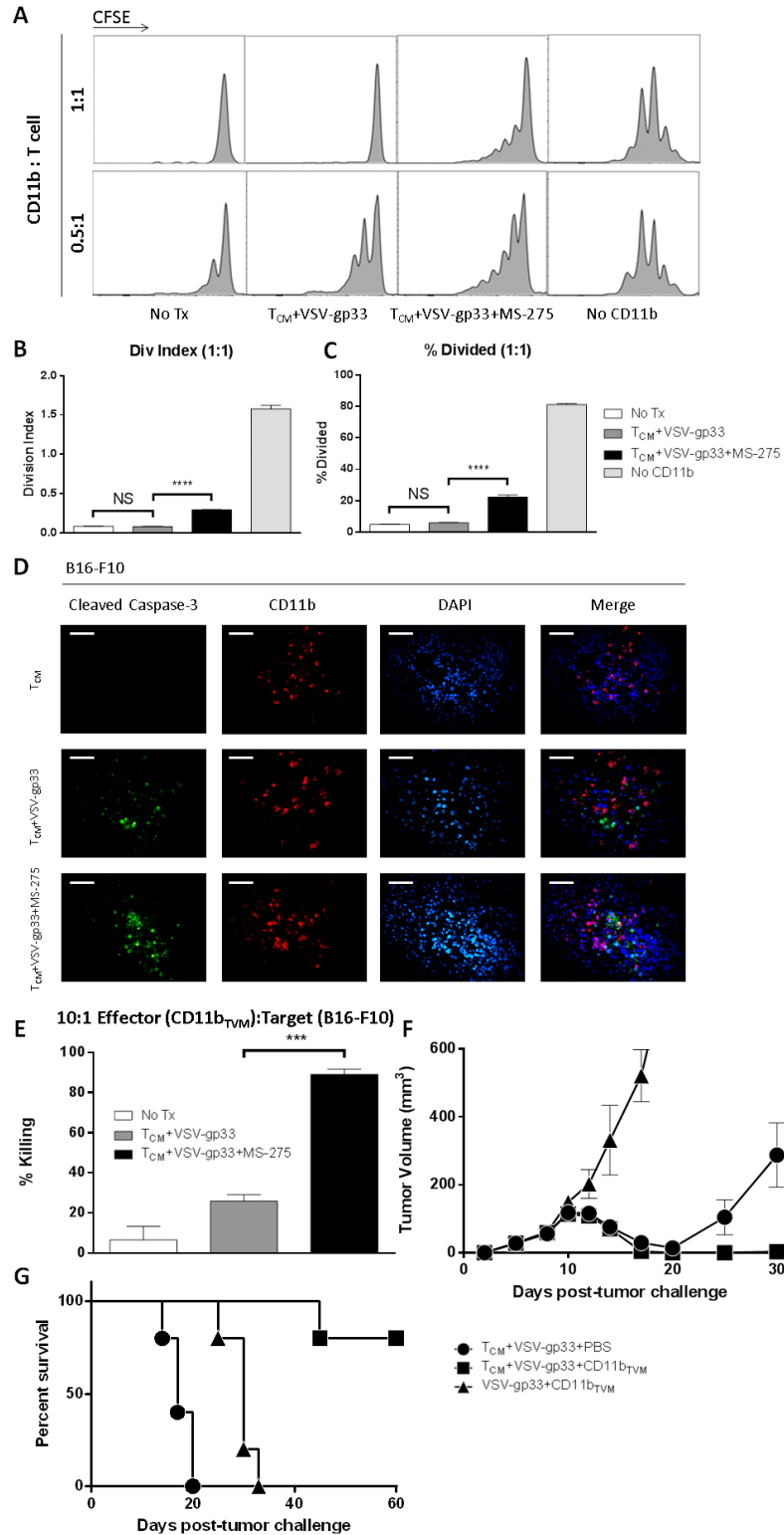


Figure 5

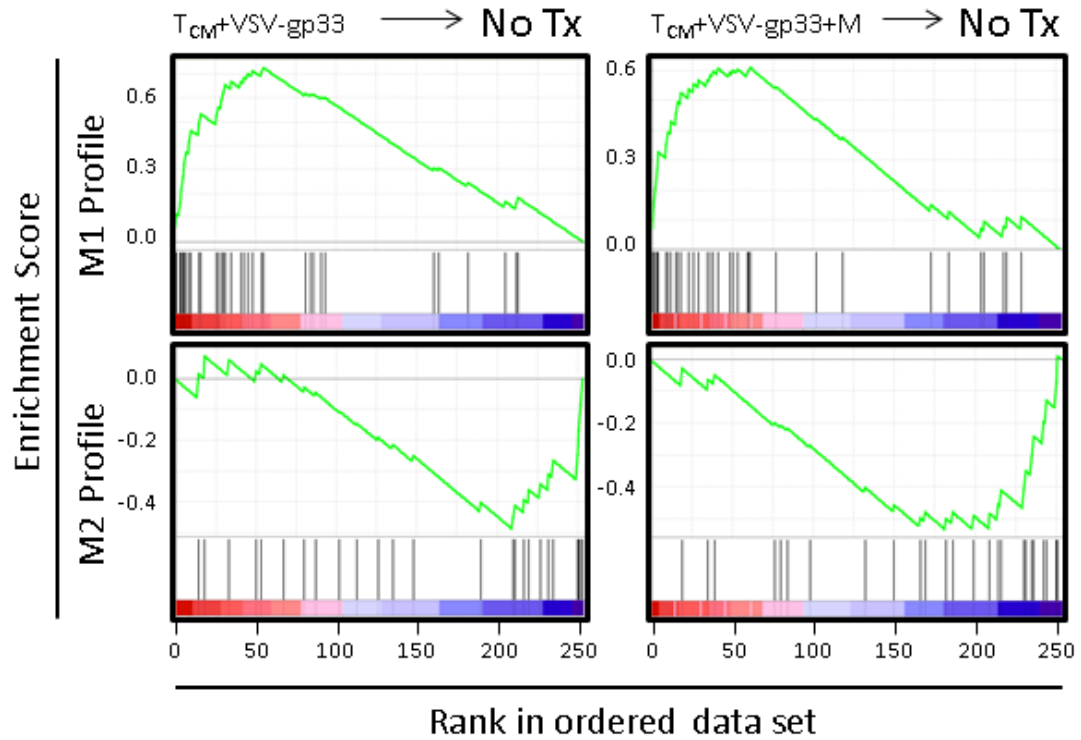
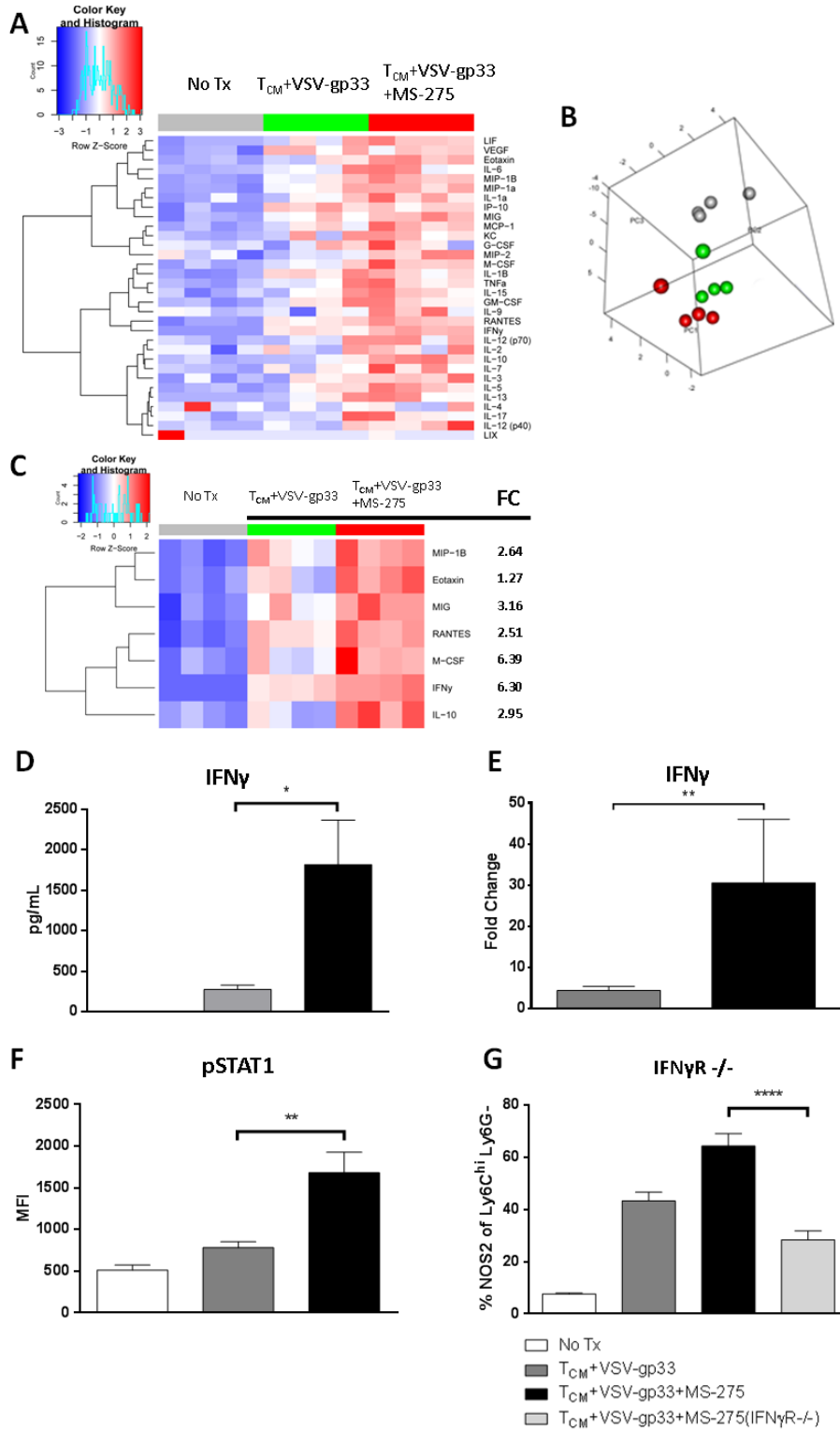


Figure 6

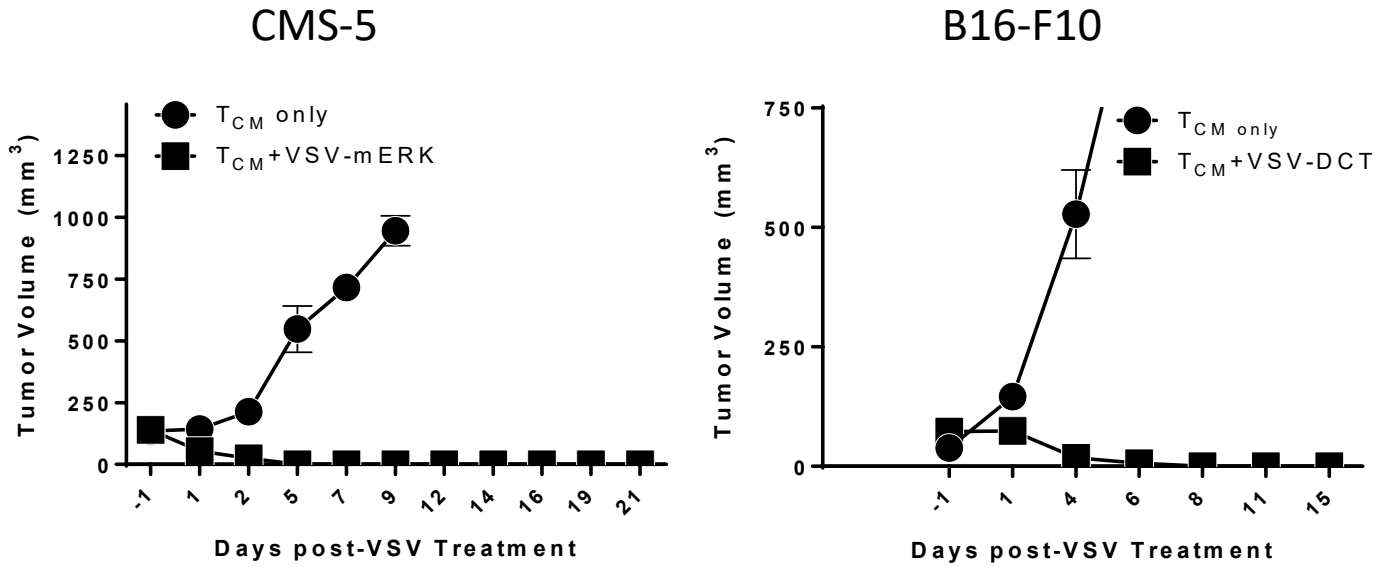


**Table 1**

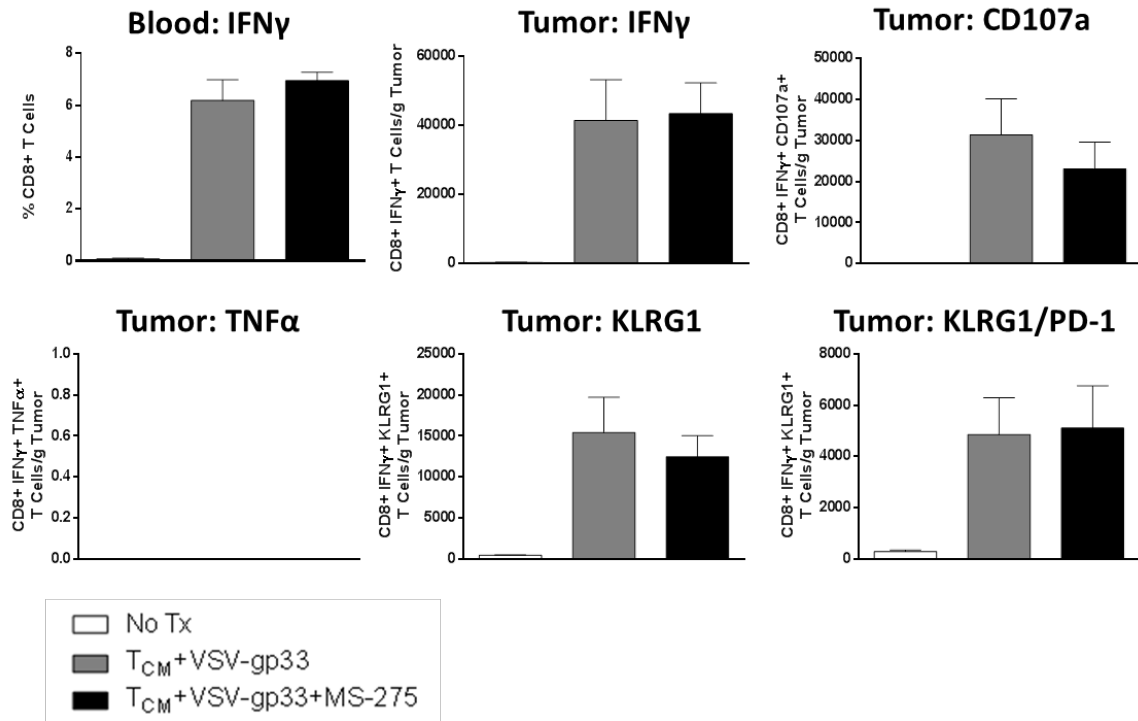
GO Biological Process (Downregulated)	Fold Enrichment	P value
myeloid leukocyte activation involved in immune response (GO:0002283)	> 100	3.15E-02
leukocyte activation involved in immune response (GO:0002366)	12.96	1.05E-02
leukocyte activation (GO:0045321)	9.01	8.90E-07
cell activation (GO:0001775)	7.51	1.07E-05
immune system process (GO:0002376)	6.45	1.84E-19
cell activation involved in immune response (GO:0002263)	12.79	1.15E-02
immune effector process (GO:0002252)	8.91	2.00E-05
immune response (GO:0006955)	8.51	2.49E-14
myeloid leukocyte activation (GO:0002274)	27.5	3.72E-08
neutrophil activation (GO:0042119)	77.78	2.06E-03
granulocyte activation (GO:0036230)	68.05	3.49E-03
positive regulation of acute inflammatory response (GO:0002675)	43.91	1.02E-03
positive regulation of inflammatory response (GO:0050729)	14.98	2.73E-02
regulation of response to stimulus (GO:0048583)	2.56	6.17E-03
positive regulation of response to stimulus (GO:0048584)	3.51	1.19E-03
positive regulation of response to external stimulus (GO:0032103)	9.61	3.62E-03
regulation of acute inflammatory response (GO:0002673)	23.88	1.99E-02
mast cell activation (GO:0045576)	40.33	2.74E-02
myeloid leukocyte chemotaxis (GO:0030593)	23.07	2.35E-02
granulocyte chemotaxis (GO:0071621)	20.94	3.75E-02
leukocyte migration (GO:0050900)	17.01	4.85E-07
leukocyte chemotaxis (GO:0030595)	17.17	1.63E-03
cell chemotaxis (GO:0060326)	16.6	4.79E-06
chemotaxis (GO:0006935)	7.15	3.31E-03
taxis (GO:0042330)	7.11	3.47E-03
response to external stimulus (GO:0009605)	3.88	4.57E-04
neutrophil migration (GO:1990266)	21.27	3.48E-02
lymphocyte mediated immunity (GO:0002449)	15.67	4.23E-04
leukocyte mediated immunity (GO:0002443)	15.74	7.95E-06
immune response-activating cell surface receptor signaling pathway (GO:0002429)	14.08	3.89E-02
immune response-regulating cell surface receptor signaling pathway (GO:0002768)	15.12	3.79E-03
immune response-regulating signaling pathway (GO:0002764)	10.65	3.79E-02
regulation of immune response (GO:0050776)	7.5	2.86E-06
regulation of immune system process (GO:0002682)	5.32	1.77E-06
activation of immune response (GO:0002253)	12.96	4.96E-05
positive regulation of immune response (GO:0050778)	8.73	1.08E-04
positive regulation of immune system process (GO:0002684)	6.92	6.97E-07
adaptive immune response (GO:0002250)	10.01	5.49E-04
innate immune response (GO:0045087)	9.72	1.33E-08
defense response (GO:0006952)	6.95	1.45E-11

response to stress (GO:0006950)	2.9	7.63E-04
inflammatory response (GO:0006954)	8.57	3.19E-05
positive regulation of cytokine production (GO:0001819)	7.8	5.29E-03
response to other organism (GO:0051707)	5.01	3.77E-02
response to external biotic stimulus (GO:0043207)	5.01	3.77E-02
<b>GO Biological Process (Upregulated)</b>	<b>Fold Enrichment</b>	<b>P value</b>
DNA replication	33.62	2.54E-03
cell cycle	9.51	9.77E-04

Supplementary Figure 1

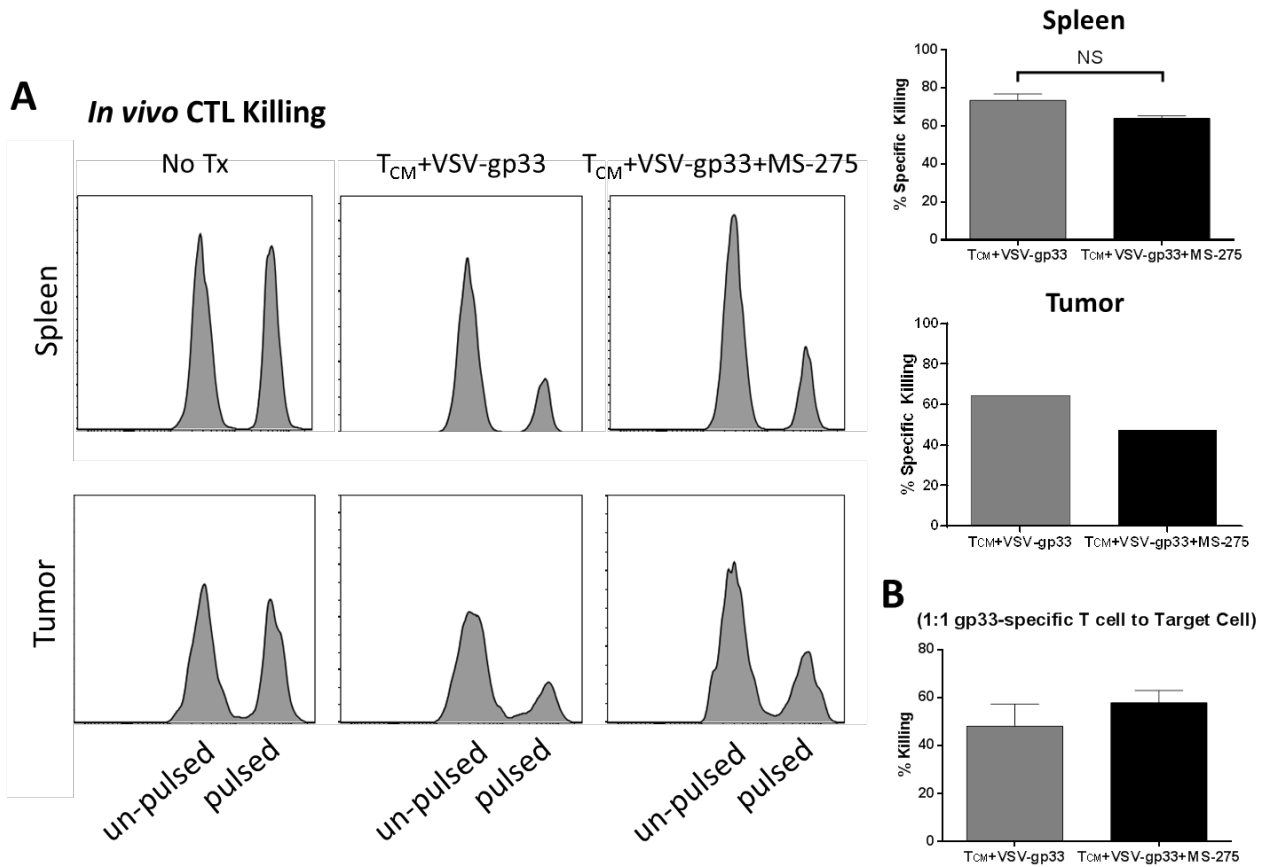


Supplementary Figure 2

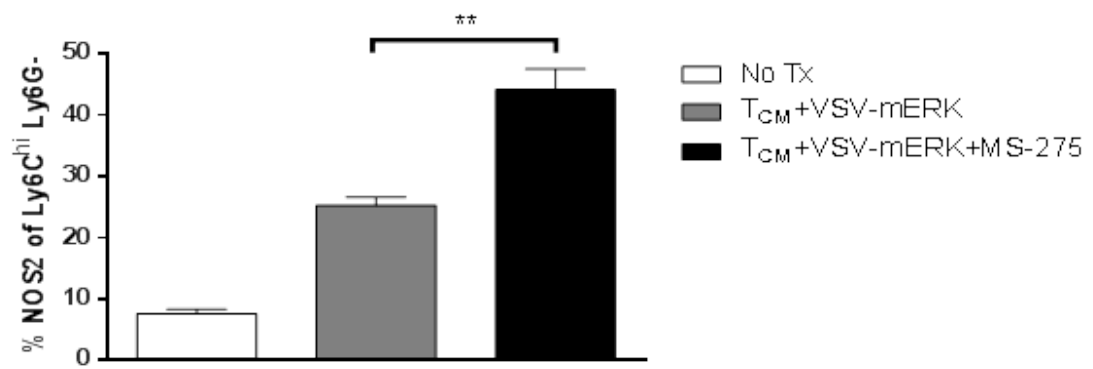
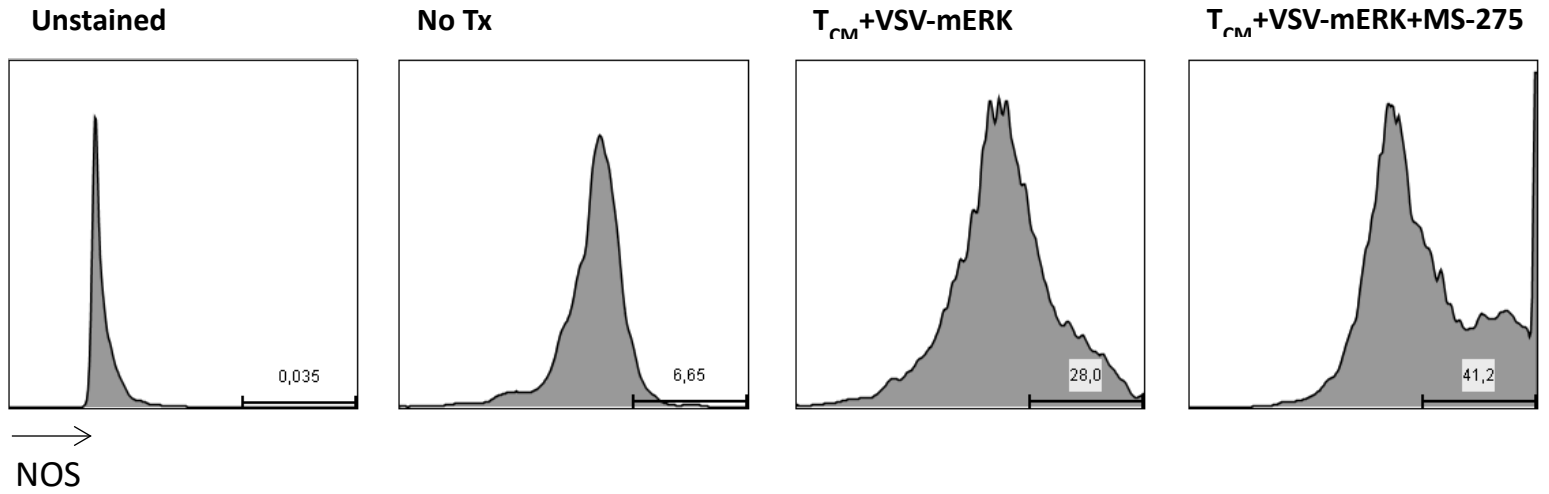




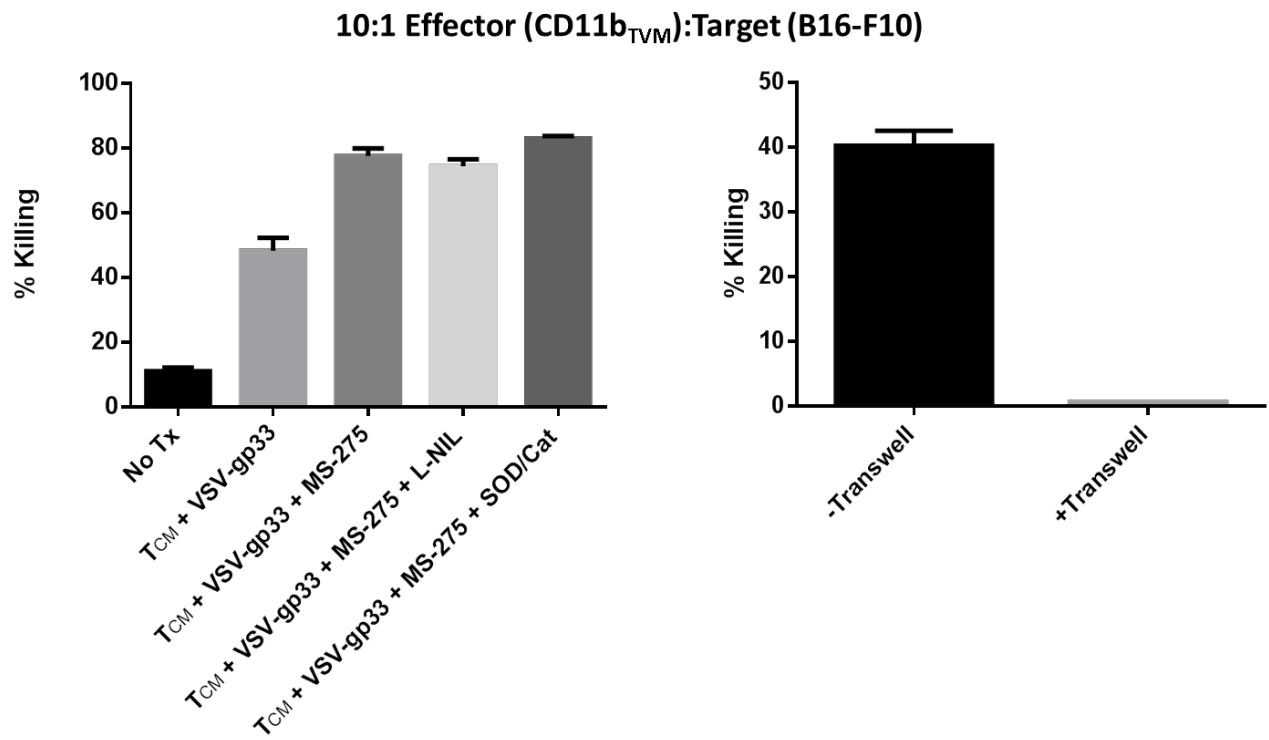
Supplementary Figure 3



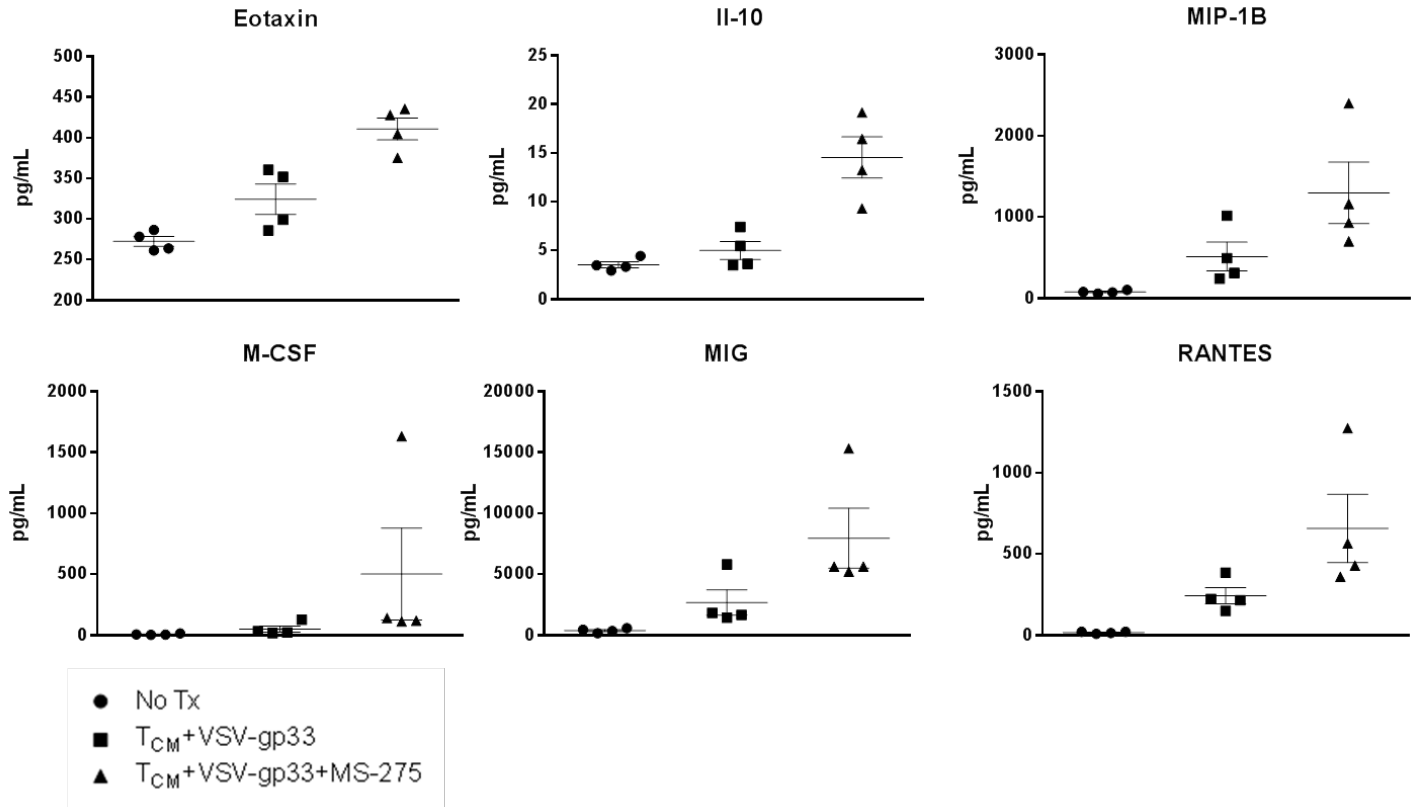
Supplementary Figure 4



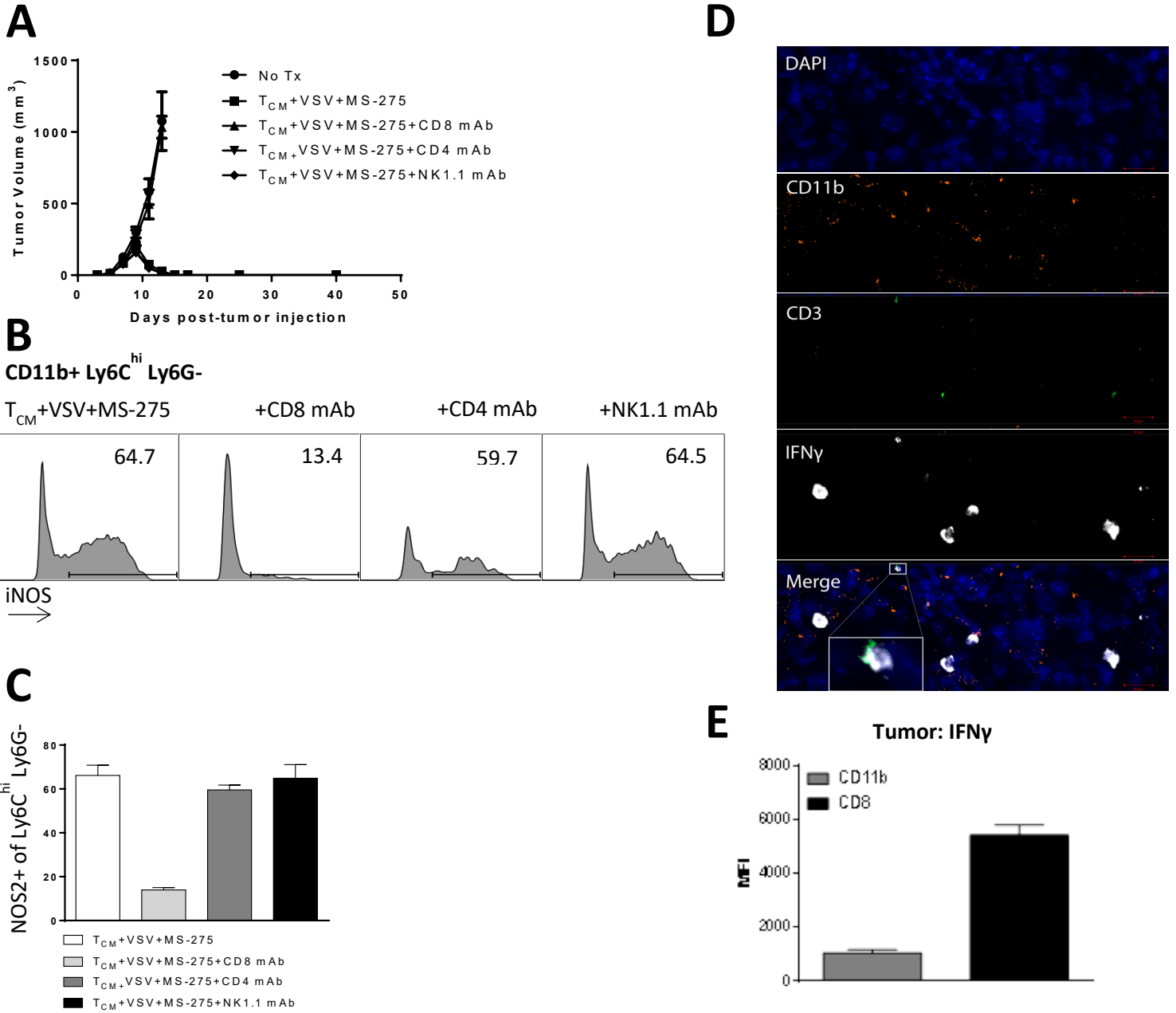
Supplementary Figure 5



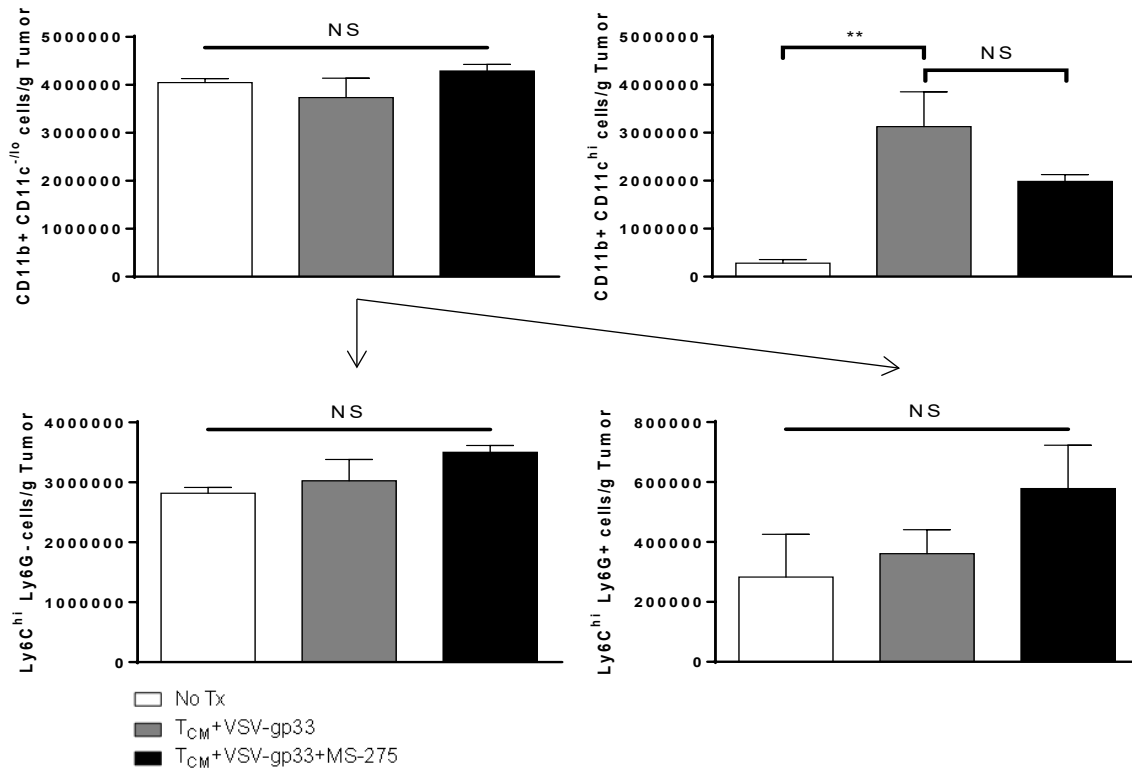
Supplementary Figure 6



Supplementary Figure 7



Supplementary Figure 8



**Supplementary Table 1**

M1 Profile				M2 Profile		
Ccl11	Cxcl10	Iigp1	Nlrp3	Arg1	Cxcr2	Ptgfr
Ccl2	Cxcl2	Il12a	Nos2	Ccl17	Flt1	Ptgir
Ccl3	Cxcl3	Il12b	Tnf	Ccl22	Il10	Retnla
Ccl4	Cxcl5	Il15	Tnfaip3	Ccl24	Il13	Tgfb1
Ccl5	Cxcl9	Il18		Ccr2	Il1rn	Tgfb2
Ccl8	Fasl	Il1a		Cd163	Il4	
Cd40	Hif1a	Il1b		Cebpb	Il6ra	
Cd86	Hmgb1	Il1r1		Chi3l3	Mmp9	
Csf2	Hmgb2	Il23a		Csf1	Mrc1	
Cxcl1	Ifng	Il6		Cxcr1	Ptger3	

**Supplementary Table 2**

Gene Name	TCM+VSV+MS-275 vs. TCM+VSV
Ifng	4.19
Ltb4r1	3.51
Il6ra	3.1
Tnfsf14	2.99
Ccr2	2.88
Oas2	2.82
Chi3l3	2.81
Tlr9	2.76
Cxcr2	2.71
Il18	2.63
Tlr4	2.42
Ifi27l2a	2.4
Tlr1	2.35
Cebpb	2.34
Ccl2	2.32
Il18rap	2.17
Plcb1	2.16
Myd88	2.1
Ccl24	2.07
Mknk1	2.04
Nod2	1.98
Ccr1	1.97
Stat2	1.94
Daxx	1.82
Bcl6	1.76
Ccl5	1.75
Ptger2	1.75
Irf5	1.72
Ltb	1.68
Irf7	1.67
Gngt1	1.65
Ptgs1	1.62
Oas1a	1.61
Prkcb	1.61
Tlr5	1.59
Cd86	1.55



Tlr6	1.51
Igfp1	1.5
Hif1a	1.49
Pla2g4a	1.45
Hsh2d	1.44
Mafk	1.41
Cd40lg	1.38
Flt1	1.38
Fos	1.38
Ccl7	1.37
Stat1	1.36
Tyrobp	1.36
C3ar1	1.34
Nod1	1.34
Irf1	1.33
Twist2	1.33
Map2k4	1.32
Grb2	1.31
Ager	1.29
Ccr4	1.29
Map2k6	1.29
Nfe2l2	1.29
Fasl	1.27
Ripk1	1.26
Cfl1	1.25
Jun	1.25
Rps6ka5	1.25
Ccl20	1.23
Map3k1	1.23
Mafg	1.2
Mef2a	1.19
Rac1	1.19
Fxyd2	1.18
Birc2	1.16
Cxcl9	1.16
Hmgb2	1.15
Limk1	1.15
Cysltr1	1.12
Stat3	1.12

Tradd	1.12
Itgb2	1.11
Mapk14	1.11
Max	1.11
Cysltr2	1.1
Ifit3	1.1
Shc1	1.1
Map3k9	1.09
Csf1	1.08
Prkca	1.08
C1qb	1.06
Mapk1	1.06
C3	1.05
Rhoa	1.05
Cfb	1.04
Il11	1.03
Il7	1.03
Mef2d	1.02
Tlr8	1.02
Cdc42	1.01
Ly96	1.01
Nfatc3	1.01
Lta	-1.01
Alox5	-1.02
Ccr3	-1.02
Cd163	-1.02
Tlr2	-1.02
Bcl2l1	-1.03
Mapkapk2	-1.03
Nos2	-1.03
Masp2	-1.04
C1qa	-1.05
Keap1	-1.05
Mapk3	-1.07
Oasl1	-1.07
Ifit2	-1.08
Raf1	-1.08
Cd4	-1.09
Gnb1	-1.1

Map3k7	-1.1
Mx1	-1.1
Ifi44	-1.11
Tcf4	-1.11
Il13	-1.12
Ppp1r12b	-1.12
Pik3c2g	-1.13
Traf2	-1.13
Hdac4	-1.14
Ccl19	-1.15
Gnas	-1.15
H2-Ea-ps	-1.16
Gnaq	-1.17
Nr3c1	-1.18
Tgfb1	-1.18
C4a	-1.19
H2-Eb1	-1.19
Il10rb	-1.19
Il21	-1.19
C7	-1.21
Hmgb1	-1.21
Il9	-1.21
Tollip	-1.22
Tnfaip3	-1.23
Myc	-1.24
Hspb1	-1.26
Mx2	-1.26
Rapgef2	-1.26
Smad7	-1.27
Ptk2	-1.28
Cfd	-1.29
Irf3	-1.29
C1ra	-1.3
Tgfb3	-1.3
Il1rap	-1.31
Mrc1	-1.32
Nfkb1	-1.32
Il1r1	-1.33
Map2k1	-1.34

Knk1	-1.35
Alox15	-1.37
C9	-1.37
Map3k5	-1.37
Elk1	-1.39
Il15	-1.39
Ptger3	-1.39
Atf2	-1.4
Cxcr4	-1.4
Ddit3	-1.41
Il2	-1.41
Tlr7	-1.41
Il4	-1.42
Relb	-1.43
Rela	-1.45
Nox1	-1.48
Ccl8	-1.49
Ccl11	-1.5
Crp	-1.5
Cxcl3	-1.5
Mmp9	-1.51
Hspb2	-1.52
Ptgir	-1.52
Ifna1	-1.53
Csf2	-1.55
Hmgn1	-1.55
Tlr3	-1.55
Trem2	-1.56
Mapk8	-1.57
Ptger1	-1.58
Il22	-1.61
Il5	-1.61
Cxcl10	-1.63
C8b	-1.73
Il23r	-1.74
Cxcl2	-1.76
C1s	-1.77
Masp1	-1.77
Ccl4	-1.78

Ptger4	-1.79
Cd55	-1.85
Myl2	-1.86
Ccl3	-1.87
Hras1	-1.87
Rock2	-1.89
Mef2c_Mm	-1.91
Tgfbr1	-1.92
Cxcr1	-1.93
Ripk2	-1.95
Ccl17	-2.02
Tbxa2r	-2.02
Hc	-2.1
Il17a	-2.1
Retnla	-2.15
Mbl2	-2.18
Il10	-2.19
Tslp	-2.2
Cxcl5	-2.21
Nlrp3	-2.22
Il1b	-2.24
Defa-rs1	-2.3
Maff	-2.35
Mmp3	-2.36
Ptgfr	-2.36
Creb1	-2.37
Il22ra2	-2.42
Il3	-2.45
Gpr44	-2.46
C6	-2.54
Mapkapk5	-2.58
Mef2b	-2.66
Ccl21a	-2.67
Cd40	-2.68
Ltb4r2	-2.83
Ifit1	-2.85
Il1rn	-2.91
C2	-3.18
Tgfb2	-3.22

C8a	-3.39
Il12a	-3.55
Tnf	-4.13
Areg	-4.31
Il23a	-4.53
Cxcl1	-4.67
Ccr7	-4.78
Ptgs2	-4.81
Arg1	-5.15
Alox12	-5.8
Il6	-5.8
Pdgfa	-5.91
Ifnb1	-6.29
Il1a	-6.45
Il12b	-8.81
Ccl22	-11.02
Csf3	-14.59

### **3.0 Chapter Three – HDACi promotes inflammatory remodeling of the tumor microenvironment to enhance epitope spreading and antitumor immunity**

#### **3.1 Introduction**

Given that HDACi have been documented to induce co-stimulatory molecule expression and up-regulate antigen processing and presentation machinery, we questioned whether MS-275 was capable of altering the inflammatory tumor landscape to promote local immunoactivation and if this was clinically beneficial in our model of tumor relapse.

Utilizing the same tumor model and treatment platform as Chapter Two, we observed that MS-275 changed the inflammatory microenvironment to support the maturation of cross-presenting dendritic cells while discouraging the accumulation of regulatory T cells. This corresponded with an activation of endogenous antitumor T cell responses targeting non-target tumor antigens.

#### **3.2 Manuscript Status, Copyright, and Citation**

*Status:* Submitted to Science Advances

*Copyright:* © Nguyen A et al. (2021). This article would be available under open access and printed under the terms of the Creative Commons Attribution License 4.0 International License (CC BY 4.0) (<https://creativecommons.org/licenses/by/4.0/>). To safeguard against the possibility of ineligibility of submission to other publications, a temporary hold on the electronic publication of the thesis will be requested.

*Citation:* Nguyen, A, Ho, L, Walsh, S, Hogg, R, Chen, L, Wan, Y (2021). “HDACi promotes inflammatory remodeling of the tumor microenvironment to enhance epitope spreading and antitumor immunity.” *Science Advances*. In submission, under peer-review.

#### **3.3 Preprint of the Journal Article**

Starting on the next page.

**HDACi promotes inflammatory remodeling of the tumor microenvironment to enhance epitope spreading and antitumor immunity**

Andrew Nguyen<sup>1</sup>, Louisa Ho<sup>2</sup>, Scott Walsh<sup>1</sup>, Richard Hogg<sup>3</sup>, Lan Chen<sup>1</sup>, Yonghong Wan<sup>1\*</sup>

<sup>1</sup>Department of Pathology and Molecular Medicine, McMaster Immunology Research Centre, McMaster University; Hamilton, Canada.

<sup>2</sup>Wilfrid Laurier University; Waterloo, Canada.

<sup>3</sup>BC Cancer; Vancouver, Canada.

**\*Corresponding author. Email: [wanyong@mcmaster.ca](mailto:wanyong@mcmaster.ca)**



**Abstract:**

Adoptive cell therapy (ACT) with tumor-specific memory T cells has shown increasing efficacy in regressing solid tumors. However, tumor antigen heterogeneity represents a longitudinal challenge for durable clinical responses due to the therapeutic selective pressure for immune escape variants. Here, we demonstrate that delivery of class I histone deacetylase inhibitor, MS-275, promotes sustained tumor regression by synergizing with ACT in a coordinated manner to enhance cellular apoptosis. We find that MS-275 alters the tumor inflammatory landscape to support antitumor immunoactivation through the recruitment and maturation of cross-presenting CD103<sup>+</sup> and CD8<sup>+</sup> dendritic cells and depletion of regulatory T cells. Activated endogenous CD8<sup>+</sup> T cell responses against non-target tumor antigens was critically required for the prevention of tumor recurrence. Importantly, MS-275 alters the immunodominance hierarchy by directing epitope spreading towards endogenous retroviral tumor-associated antigen, p15E. Our data suggest that MS-275 multi-mechanistically improves epitope spreading to promote long-term clearance of solid tumors.

## Introduction

Adoptive cell therapy (ACT) involves the *ex vivo* expansion and infusion of antigen-specific T cells, tumor-infiltrating lymphocytes (TIL) or engineered T cells expressing TCRs or chimeric antigen receptors (CAR) into tumor-bearing patients (1). These personalized cellular products potentiate tumor recognition and killing and has demonstrated clinical efficacy in the treatment of malignant disease (2). However, incomplete responses and tumor recurrence have been reported following adoptive transfer (3). Since patient tumors can harbor extensive variability in antigen expression, targeted therapies such as ACT may create selective pressure for antigen-negative or antigen-low immune escape variants (4). As a result, tumor antigen heterogeneity may reduce the probability of durable responses. It has been demonstrated that the detection of epitope spreading during ACT is highly correlated with improved clinical outcomes (5-7). ‘Epitope’ or ‘determinant’ spreading during cancer immunotherapy is characterized by early tumor lysis and release of immunogenic tumor-derived antigens (8). Cross-presentation of these antigens by tumor-infiltrating dendritic cells (DC) can engage endogenous T cells to facilitate recognition and killing of a wider tumor antigen repertoire (9). Therefore, deliberate induction of broad-spectrum antitumor immunity during ACT may promote comprehensive eradication of heterogeneous solid tumors.

In opposition, the tumor microenvironment (TME) employs an abundant array of immunoregulatory mechanisms that can suppress the activation of endogenous T cell responses. The secretion of immunosuppressive factors by tumors and tumor-infiltrating leukocytes including myeloid-derived suppressor cells, regulatory T cells, and tumor associated macrophages/neutrophils has been shown to curb the development/survival (eg. VEGF, IL6, PGE2) and function (eg. TGF $\beta$ , IL10) of cross-presenting DCs and render them tolerogenic (10, 11). Additionally, the TME impairs the production of pro-inflammatory DC-activating cytokines (eg. IFN $\alpha/\beta$ , Hmgb1) which further inhibits the *de novo* activation of endogenous T cell responses (12-14). As such, targeting TME immunosuppressiveness may improve epitope spreading and improve the therapeutic impact of ACT. For instance, it has been demonstrated that selective MDSC/Treg depletion (eg. doxorubicin, paclitaxel (15-17)) and targeted molecular inhibition (eg. IDO, STAT3 (18, 19)) can foster DC maturation and activity. Alternatively, several methods have been employed to directly potentiate DC function including local up-regulation of DC-recruiting cytokines (eg. GM-CSF, FLT3L (20-22)) and administration of immunostimulatory adjuvants (eg. TLR/CD40/STING agonists (10)). Overall, while immunosuppressive pressures within the TME present significant barriers to epitope spreading, strategies to enhance DC activation and cross-presentation may propel the advancement of combinatorial ACT approaches.

In this study, we determined that MS-275, a class I histone deacetylase inhibitor, delivered in conjunction with ACT could promote sustained tumor regression and prevent relapse. This was associated with inflammatory remodeling of the TME in favor of recruitment and activation of cross-presenting DCs. Decreased immunosuppressive signaling also corresponded with a depletion of tumor-infiltrating regulatory T cells. These changes collectively promoted epitope spreading to non-target tumor antigens which were critical for long-term tumor control. Overall, MS-275 multi-mechanistically improves epitope spreading to enhance the efficacy of ACT.

## Results

### **MS-275 delivery enhances ACT leading to sustained tumor regression**

During adoptive cell therapy (ACT), the *in vivo* magnitude and persistence of infused tumor-specific T cells are considered determinants of successful clinical responses (23). It has been increasingly accepted that less differentiated subsets of memory T cells contribute to durable antitumor immune responses with exceptional proliferative capacity upon antigenic stimulation (24, 25).

To generate LCMV GP33–41-specific memory T cells (TMEM) for adoptive transfer, we infected C57BL/6 mice with lymphocytic choriomeningitis virus (LCMV, Armstrong strain) and harvested bulk splenocytes after one month. In mice intradermally challenged with B16-F10 murine melanoma cells expressing the immunodominant LCMV GP33-41 epitope (B16-gp33), ACT treatment utilizing TMEM was sufficient to completely regress five-day old tumors; however, the tumors quickly relapsed within one month after initial tumor challenge. Class I histone deacetylase inhibitor (HDACi) MS-275 has been previously shown to potentiate immunotherapeutic outcomes (26, 27), so we speculated whether incorporating the drug could prolong tumor regression. Daily injections of MS-275 were delivered concomitantly with ACT or two days prior/after and continued for four additional days. While MS-275 alone did not provide tumor protection, ACT+MS-275 completely sustained tumor regression relative to ACT alone (Figure 1A). Interestingly, early or late delivery of MS-275 abrogated any therapeutic benefit, signifying that timing-dependent interactions between ACT and MS-275 were necessary to prevent tumor relapse.

Since MS-275 has anticancer properties (28, 29), we considered whether the drug was additively contributing to tumor regression by direct elimination of resistant tumor variants despite being unable to control tumor growth on its own. In frozen tumor sections derived five days post-treatment, immunofluorescence staining for cleaved caspase-3 revealed that MS-275 alone did not seem to directly promote tumor apoptosis (Figure 1B). By contrast, ACT+MS-275 treatment demonstrated drastically higher levels of cleaved caspase-3 relative to ACT alone, suggesting that MS-275 synergizes with ACT to drive tumor apoptosis.

Hematoxylin and eosin staining of tumor tissue revealed that that ACT-treated tumors were heavily infiltrated with leukocytes both in the presence or absence of MS-275 (Figure 1C). To determine whether MS-275 enhances ACT by selectively increasing the total number of tumor-infiltrating CD8<sup>+</sup> T cells, we stained tumor sections with anti-CD8 antibody for immunohistochemistry five days post-treatment. There was no significant difference in total CD8 staining with the addition of MS-275 (Figure 1D), which was further validated by flow cytometric analysis (Figure 1E). Furthermore, the total number of LCMV GP33–

41-specific CD8<sup>+</sup> T cells was not affected by MS-275 (Figure 1F). While MS-275 could mobilize other lymphocytes with antitumor potential, selective depletion of CD4 or NK1.1-expressing cells during ACT+MS-275 treatment provided no loss of sustained tumor regression compared to CD8 depletion (Figure 1G). Taken together, despite tumor control being primarily CD8<sup>+</sup> T cell dependent, the additional therapeutic benefit afforded by concomitant MS-275 delivery may not rely on the additional recruitment of target antigen-specific CD8<sup>+</sup> T cells or other antitumor lymphocyte populations.

### **Inflammatory remodeling of the tumor microenvironment favors immunoactivation**

Since the data suggest that ACT-MS-275 synergy occurs within a restricted time frame, we wanted to investigate the dynamic changes within the tumor microenvironment that could facilitate enhanced tumor killing in the presence of the drug. To accomplish this, we conducted microarray analyses (GSE179337) of bulk tumor RNA from ACT-treated mice with or without MS-275 at one, three, and five-days post-treatment.

Using connectivity mapping (CMap), we first confirmed if the gene changes observed were due to the direct influence of MS-275. Time course analysis was performed by measuring differential gene expression between ACT +/- MS-275 from Day 1 to Day 5 post-treatment. Lists of differentially expressed genes (DEGs) that showed >1.5 or >2.0 absolute fold change (FC) were used to query the CMap library and compared to expression data from chemical perturbation studies. Of the 32 chemicals that showed significant overlap in differential gene expression, chemical studies utilizing MS-275 displayed the highest similarity (Figure S1). As a result, we had confidence that during ACT therapy, MS-275 was altering the local genetic landscape through direct chemical perturbation.

To assess the tumor inflammatory state over the course of treatment, custom gene sets (Table S1) representing specific inflammatory pathways were analyzed for statistical enrichment within the expression data of each treatment group (Figure 2A, Table S2). Relative to ACT alone, ACT+MS-275 up-regulated Type I IFN signaling, inflammatory cytokine signaling, and inflammatory responses at an early timepoint (Day 1) while down-regulating those processes at a later timepoint (Day 5). Despite having a progressive anti-inflammatory effect, qRT-PCR validation showed that ACT+MS-275 also enhanced the expression of select pro-inflammatory cytokines at various time points. In particular, MS-275 up-regulated ISG56 and IL-12 expression at Day 1 and IFNG expression at Day 5 (Figure 2B, S2). Taken together, MS-275-driven modulation of tumor inflammation may activate biological pathways that can facilitate sustained tumor regression.

Gene set enrichment analysis (GSEA) was then used to interrogate the effect of MS-275 on biological pathways derived from curated gene sets (C2) in the Molecular Signatures Database (MSigDB) (Figure 2C). An enrichment map was constructed to group significantly enriched gene sets containing similar genes. Based on the differential enrichment pattern of clustered gene sets, we noted that ACT+MS-275 treatment promoted early up-regulation (Day 1) of TCR signaling, JAK-STAT signaling, and innate immunity followed by late up-regulation (Day 5) of antigen processing, cross-presentation and lymphocyte-dependent antigen-dependent responses. Since ACT-only treatment showed an inverse enrichment pattern with the aforementioned biological processes, the data confirmed that MS-275-induced inflammatory changes correlated with enhanced immunoactivation.

Gene ontology (GO) analysis allowed us to determine if terms representing annotated biological processes were statistically overrepresented in our DEGs and comparable to our GSEA-enriched MSigDB pathways. Using DEGs obtained from comparing ACT+MS-275 vs ACT alone over a time-course (D3 vs D1 and D5 vs D1), a protein-protein interaction (PPI) network was constructed and gene modules were identified from the network (Table S3). GO analysis allowed us to functionally classify the modules according to annotated biological processes. After ordering the modules by the percentage of constituent genes up-regulated by MS-275, we observed that antigen processing and cross-presentation was highly upregulated throughout the time-course (Figure 2D, S3).

Since immunoactivation may represent a crucial mechanism for promoting sustained tumor regression, we hypothesized that MS-275's effect on tumor inflammation may alter the composition and/or activation of tumor-infiltrating antigen-presenting myeloid cells. qRT-PCR analysis of various myeloid chemotactic genes such as CCR5, CCR2, and CXCL12 suggested that MS-275 may influence myeloid cell recruitment to the tumor (Figure 2E). Furthermore, GSEA of immunologic signatures (C7) from the MSigDB revealed that gene sets related to activated myeloid cells from LPS treatment, viral infection, or vaccination were enriched by ACT+MS-275 treatment from Day 1 to Day 5 (Figure 2F, S4). Taken together, further examination of tumor-infiltrating myeloid cells was necessary to determine how enhanced antitumor immunity occurred within the context of MS-275.

### **MS-275 drives myeloid cell recomposition and maturation within the tumor and dLN**

Myeloid cells are a heterogenous group of innate immune cells that exist within varying activation and differentiation states (30, 31). Tumors exploit myeloid cell plasticity through the secretion of soluble factors that can divert myelopoiesis and skew myeloid cell function to support tumor growth (32). In the context of ACT, we questioned whether MS-275 could

reprogram tumor-infiltrating myeloid cells into effective antigen-presenting cells with CD8<sup>+</sup> T cell activating capacity.

Five days post-treatment with ACT+/-MS-275, myeloid populations were characterized in the tumor and draining lymph nodes (dLN) by flow cytometry. After excluding lymphocytes, we identified several cell subsets including monocytic (CD11c<sup>-</sup> CD11b<sup>+</sup> Ly6Chi<sup>+</sup> Ly6G<sup>-</sup>), granulocytic (CD11c<sup>-</sup> CD11b<sup>+</sup> Ly6Clo<sup>+</sup> Ly6G<sup>-</sup>), as well as dendritic cell (DC, CD11c<sup>+</sup> CD11b<sup>+</sup> Ly6C<sup>-</sup> CD8<sup>-</sup>/CD11c<sup>+</sup> CD11b<sup>-</sup> Ly6C<sup>+</sup> CD8<sup>+</sup>/CD11c<sup>+</sup> CD11b<sup>-</sup> CD8<sup>-</sup> CD103<sup>+</sup>) populations (Figure 3A). While we had previously reported MS-275's influence on tumor-infiltrating monocytic/granulocytic myeloid cells (33), we expanded our analysis to include DCs and observed cellular subset recomposition within the tumor and dLN (Figure 3B, C). In the tumor, ACT+MS-275 treatment reduced the frequency of CD11b<sup>+</sup> DCs while increasing the frequency of CD8<sup>+</sup> and CD103<sup>+</sup> DCs (Figure 3D); in draining lymph nodes however, there was a reduced frequency of CD103<sup>+</sup> DCs (Figure 3E). In addition, DCs in the tumor and dLN demonstrated a significant increase in maturation marker expression including MHC Class II (I-Ab) and co-stimulatory ligand CD86 (B7-2) (Figure 3F, G). This coincided with higher immunoactivation potential when we pulsed them with LCMV GP33–41 peptide and co-cultured them with CFSE-labeled LCMV-P14 TCR-transgenic naïve T cells *ex vivo* (Figure 3H, I). Overall, MS-275-dependent tumor remodeling may mobilize immunoactivating DCs to promote endogenous CD8<sup>+</sup> T cell responses.

### **Activation of endogenous CD8<sup>+</sup> T cell responses promote sustained tumor regression**

To confirm that endogenous CD8<sup>+</sup> T cells enhanced the therapeutic efficacy of ACT treatment, lymphocyte-deficient RAG2/Il2rg knockout mice were treated with ACT+MS-275. We observed a failure to recapitulate the therapeutic effects of MS-275, resulting in tumor control similar to that of ACT alone (Figure 4A). The data therefore suggest that endogenous CD8<sup>+</sup> T cells were necessary for tumor clearance.

As demonstrated previously, the magnitude of LCMV GP33–41-specific CD8<sup>+</sup> T cell responses remained unchanged during MS-275 delivery. If cross-presentation of tumor peptides during ACT enhanced endogenous CD8<sup>+</sup> T cell responses against targets other than LCMV GP33–41, then broadening the spectrum of antitumor killing may represent an important mechanism to prolong tumor regression. To confirm that MS-275-potentiated tumor killing transcended LCMV GP33–41 epitope recognition, we investigated whether tumor-infiltrating endogenous CD8<sup>+</sup> T cells derived from ACT+MS-275-treated mice could recognize and kill parental B16F10 cells, which do not express LCMV GP33–41. Using a 10:1 effector to target co-culture approach, we did not observe improvements to

B16-gp33 lysis, but there was a significant increase in B16F10 cell death (Figure 4B). Moreover, the inclusion of MCA102 fibrosarcoma cells as an irrelevant line suggested that enhanced tumor killing was antigen-dependent.

Using a limited epitope screening process, we established the antigen specificity of endogenous CD8<sup>+</sup> T cell responses during ACT+MS-275 treatment. In B16-gp33 tumors, there was an increased frequency of CD8<sup>+</sup> T cells specific for p15E, an endogenous retroviral tumor-associated antigen (Figure 4C). Interestingly, T cell responses against defined melanoma antigens (gp100, svy) and other retroviral gene products (gp70) were unchanged. To confirm if epitope spreading altered the immunodominance hierarchy to disproportionately favor p15E-specific responses, we repeated the experiment with a known p15E-expressing tumor model such as MC38 colon adenocarcinoma. In MC38 tumors expressing LCMV GP33-41<sup>+</sup> (MC38-gp33), MS-275 raised the frequency of T cell responses to p15E as well as to a neo-epitope corresponding to a mutation in ADP-dependent glucokinase (Adpgk) (Figure 4D). Although the extent of epitope spreading may be model dependent, we demonstrated that MS-275 could promote endogenous immune responses against non-target tumor antigens.

However, it was yet unclear whether these responses translated to *in vivo* antigen-specific killing. We pulsed CFSE-labeled bulk splenocytes with p15E peptide and infused them into B16-gp33 tumor-bearing mice five days post-ACT+MS-275 treatment. Interestingly, we observed that enhanced p15E responses correlated with improved killing of p15E-pulsed target cells *in vivo* (Figure 4E, F). Since MC38 tumor cells share an endogenous antigen with B16F10 in the expression of p15E (34, 35), we wondered whether ACT+MS-275-driven p15E responses alone could facilitate tumor rejection. In mice that were cured of B16-gp33 tumors during ACT+MS-275 treatment, re-challenge with parental MC38 tumors resulted in delayed tumor growth and longer survival compared to naïve mice (Figure 4G, H). This suggested that persisting immunity from ACT+MS-275 treatment could have mild protective benefits against tumors expressing p15E. To eliminate cell line differences, we repeated the experiment but re-challenged cured mice with parental MCA102 cells (inherently p15E-negative) or MCA102 cells engineered to express p15E (MCA102-p15E). Again, we demonstrated that MCA102-p15E cells showed delayed tumor growth in cured mice relative to parental MCA102 cells (Figure 4J, I). Ultimately, MS-275-dependent immunoactivation of endogenous CD8<sup>+</sup> T cells allow for tumor rejection beyond target antigen recognition.

### **Intratumoral down-regulation of immunosuppressive signals coincide with Treg depletion**



Regulatory T cells (Tregs) exert indispensable functions in inducing and maintaining self-tolerance and immune homeostasis and their presence is often associated with poor clinical prognosis during cancer (36). Many studies support a mutualistic relationship between immunosuppressive tumor-infiltrating myeloid cells and Tregs. Myeloid cells can secrete IL10 and TGF $\beta$  while Tregs secrete IL4, IL13, and IL10, which result in reciprocal activation (37). Furthermore, nitric oxide synthase and arginase production by myeloid cells have been found to be potent inducers of Treg activity (38-40). Since MS-275 remodels the tumor microenvironment and facilitates myeloid cell reprogramming, we questioned whether that would create a subversive effect on tumor-infiltrating Tregs.

qRT-PCR analysis of bulk tumor RNA indicated that ACT+MS-275 treatment down-regulated ARG1, NOS2, and TGFB1 expression, which may prohibit Treg expansion (Figure 5A). To examine its corresponding impact on Treg abundance, we stained frozen tumor sections with anti-Foxp3 antibody for immunohistochemistry and immunofluorescence imaging. While ACT alone increased Treg numbers relative to untreated mice, ACT+MS-275 increased Tregs initially (Day 1), but decreased their number significantly afterwards (Day 3-5) (Figure 5B, C). These trends were validated by qRT-PCR analysis of FOXP3 gene expression in bulk tumor RNA (Figure 5D). Flow cytometric staining of CD45.2-enriched tumor-derived cells further revealed that depletion of tumor-infiltrating CD4<sup>+</sup> CD25<sup>+</sup> Foxp3<sup>+</sup> Tregs was accompanied by a more general and severe depletion of tumor-infiltrating CD4<sup>+</sup> T cells (Figure 5E, F).

### **Tregs inhibit endogenous CD8<sup>+</sup> T cell responses and prevent long-term tumor control**

Tregs can induce immunosuppression through a variety of mechanisms including: secretion of immunosuppressive cytokines, competitive consumption of IL-2, direct killing via perforin and granzyme pathways, and direct subversion of antigen-presenting cell function through down-regulation of co-stimulatory molecules (41). To evaluate the therapeutic contribution of Treg ablation in the context of ACT, we depleted CD4<sup>+</sup> T cells using monoclonal antibodies or utilized “depletion of regulatory T cell” (DEREG) BAC transgenic mice, which express a simian diphtheria toxin receptor-enhanced green fluorescent protein (DTR-eGFP) fusion protein under control of the endogenous forkhead box P3 promoter/enhancer regions on the BAC transgene (42), to ablate Treg via intraperitoneal diphtheria toxin (DT) administration.

Flow cytometric analysis of peripheral blood five days post-treatment revealed that, while MS-275 induced partial depletion of bulk CD4<sup>+</sup> T cells and CD4<sup>+</sup> CD25<sup>+</sup> Foxp3<sup>+</sup> Tregs, CD4 mAb delivery completely depleted both subsets (Figure 6A, B). Comparatively, DT administration preserved the bulk CD4<sup>+</sup> T cell compartment while completely ablating

CD4<sup>+</sup> CD25<sup>+</sup> Foxp3<sup>+</sup> Tregs. In either scenario, the therapeutic benefit of MS-275 was recapitulated and sustained tumor regression was achieved (Figure 6C, D). Therefore, MS-275's influence on Treg numbers may play a critical role in its therapeutic efficacy. Furthermore, DT administration also increased the frequency of p15E-specific CD8<sup>+</sup> T cells while having negligible impact on LCMV GP33–41-specific CD8<sup>+</sup> T cells (Figure 6E, F), suggesting that Tregs selectively inhibit the magnitude of endogenous CD8<sup>+</sup> T cell responses to facilitate tumor relapse. Indeed, CD11c<sup>+</sup> cells isolated from ACT+DT-treated tumors were able to elicit better proliferation during co-culture with P14 naïve T cells compared to ACT alone. Taken together, MS-275 may be instigating concordant mechanisms of enhanced immunoactivation to promote sustained tumor regression via myeloid reprogramming and Treg depletion.

## Discussion

The density and composition of tumor infiltrating immune cells often predict the efficacy of immunotherapy. Broadly speaking, “cold tumors” are characterized by low pro-inflammatory cytokine production, T cell infiltrate, and molecular signatures of immune activation (43). Furthermore, cold tumors orchestrate the poor cellular fate of tumor-infiltrating lymphocytes by cultivating an immunosuppressive microenvironment. Reciprocal host-tumor interactions lead to the propagation of local anti-inflammatory signals and influx of immunosuppressive cells. In particular, myeloid-derived suppressor cells (MDSC) regulatory T cells (Treg), tumor-associated dendritic cells (TADC), and type 2-polarized macrophages (M2) are intrinsically associated with the developing TME and coordinate anti-inflammatory mechanisms to obstruct the function of cytotoxic CD8<sup>+</sup> T cells and antigen-presenting cells (44). As a result, strategies that promote tumor inflammation (“hot tumors”) may circumvent TME immunosuppressive phenotypes and enhance the efficacy of T cell immunotherapy.

With our ACT platform, we were able to observe significant T-cell infiltration in solid tumors and complete acute regression. ACT alone also induced higher local inflammatory signaling relative to ACT+MS-275, suggesting hot tumor induction; however, this corresponded with worse immunologic/clinical outcomes including reduced antigen-presentation/antigen-dependent responses and tumor relapse. Indeed, tumor inflammation does not always predispose the TME towards immunostimulation and can instead promote immune escape (45). It has been demonstrated that tumor exposure to IFN- $\gamma$  up-regulates PD-L1 expression such that subsequent engagement to PD-1 expressing T-cells attenuates their antitumor response (46). Similarly, PD-L1 up-regulation on CD103<sup>+</sup> DCs from tumor dLNs impaired cross-presentation while PD-L1 and PD-1 blockade mitigated DC dysfunction (47). Finally, inflammation has been shown to drive the accumulation of MDSCs and Tregs (48), enhancing tumor immunosuppressive effects on infiltrating immune cells. Attenuating excessive inflammation in hot tumors may therefore allow immunotherapeutic strategies to have a durable clinical outcome.

Histone acetylation can alter chromatin structure and gene transcription to affect various aspects of the TME including tumor immunogenicity, T-cell infiltration, and immunosuppression (49). In the context of ACT, we demonstrated that class I HDAC inhibitor MS-275 promotes sustained tumor regression. Despite having a broadly anti-inflammatory effect over time relative to ACT-only treatment, ACT+MS-275 enhanced gene signatures related to immunoactivation. We speculate that MS-275 achieves this by altering the composition and dynamics of intratumoral inflammatory signaling with emphasis on early up-regulation of Type I IFN signaling and late up-regulation of Type II IFN signaling. IFN- $\alpha$  has been shown to enhance DC maturation and cross-presentation

through antigen survival, endocytic routing, and processing (50). In support of this, we detected increased ISG56 and IL-12 expression (mature DC-derived cytokines) within 24h of treatment that coincided with an accumulation of inflammatory myeloid gene signatures over time. As previously stated, IFN- $\gamma$  may have deleterious effects on antigen presentation and can potentiate immune escape. During ACT+MS-275 treatment, IFNG expression within the tumor peaked 5 days post-treatment coinciding with peak systemic T cell responses. ACT-only treatment produced peak IFNG expression at Day 3, suggesting that earlier exposure to IFN- $\gamma$  may predispose mice to eventual therapeutic failure. Ultimately, if coordinated expression of select inflammatory signals can curtail tumor immunosuppression and maximize antitumor immunity, MS-275 may promote features of what we term a “warm tumor”.

In the TME, the acquisition, processing and cross-presentation of extracellular tumor antigen released from dying tumor cells by tumor-infiltrating dendritic cells (DC) is critical for antitumor immunity. Mouse conventional DCs (cDCs) comprise two main subsets, CD8<sup>+</sup> or CD103<sup>+</sup> cDC1 subsets and CD11b<sup>+</sup> cDC2 subsets. cDC1s are often associated with superior antigen cross-presentation, stronger CD8<sup>+</sup> T cell immunity, and improved clinical prognosis (10). However, tumors often subvert the maturation and function of infiltrating cDCs such that they become protumorigenic and suppress immune activation. These tolerogenic DCs present tumor antigen without proper co-stimulation (CD80/CD86), express inhibitory molecules (PDL1/CTLA4), and secrete immunosuppressive factors (TGF $\beta$ , IL10, IL27, NO, Arg and IDO) (51). Depletion of tolerogenic DCs has been associated with reduced tumor growth and angiogenesis (52, 53) and as such, targeting these cells may improve the recruitment, infiltration and effector activity of T cells in the TME. During ACT+MS-275 treatment, we observed that intratumoral changes to the chemokine milieu were associated with cDC subset recomposition in the tumor/dLN favoring CD8<sup>+</sup> and CD103<sup>+</sup> cDC1 accumulation within the TME. Additionally, MS-275-induced tumor inflammation was accompanied by an increase in co-stimulatory molecule expression (CD86/I-Ab) and antigen-presenting capability. Overall, MS-275 simultaneously subverts tolerogenic DC activity and promotes immunoactivation by recomposing the TME and providing maturation signals to support tumor-infiltrating cDC1s.

Cross-presentation of tumor antigens by cDCs are a pre-requisite to epitope spreading. In cancer immunotherapy, this process leads to the enhancement and diversification of endogenous T-cell responses against different epitopes from the original target. In the context of ACT and other immunotherapies, epitope spreading was observed in patients achieving remission of metastatic lesions and may thus contribute to treatment responsiveness (54). However, the association between epitope spreading and clinical

benefit has been mostly correlative. It is still unclear if and how therapeutic success is mechanistically dependent on epitope spreading. It has been suggested that epitope spreading can eliminate emergent immune escape variants as a result of therapeutic selective pressure (55). Alternatively, it may prolong antitumor immunity by stimulating endogenous T cell responses that can persist after the contraction of the initial therapy (56). During ACT+MS-275 treatment, we demonstrate that endogenous CD8<sup>+</sup> T cells are critical for preventing tumor relapse and selective enhancement of p15E-specific responses provide long-lived recognition and killing of p15E-expressing tumors. Epitope spreading is therefore critical for the prevention of tumor relapse during adoptive cell therapy.

Regulatory T cells (Treg) exert indispensable functions in inducing and maintaining self-tolerance and immune homeostasis. During cancer, Tregs infiltrate into tumor tissue and their presence is associated with poor clinical prognosis (36, 57). Correspondingly, the systemic removal of Treg cells can invoke effective anti-tumor immunity (58, 59). In this study, we observed that MS-275 directly affected the TME and/or recomposed the myeloid department to reduce intratumoral production of TGF $\beta$ , NO, and Arg leading to partial depletion of Treg. This provided direct therapeutic value since complete ablation of Treg during ACT was able to prevent tumor relapse in lieu of MS-275 treatment. Moreover, Treg ablation did not impact LCMV GP33-41-specific T cell responses but significantly up-regulated p15E-specific responses, suggesting that Treg accumulation in tumors selectively inhibits epitope spreading responses.

**Acknowledgments:** Thank you to Huiyu Xu for providing help with the immunohistochemistry and immunofluorescence co-staining, and Anna Dvorkin, for her assistance in analyzing the microarray data.

**Author contributions:**

A.N. designed and conducted the majority of the experiments described and wrote the manuscript. L.H. prepared the samples for microarray analysis and qRT-PCR. S.W. constructed the VSV-gp33 viral vector. R.H. constructed the MCA102-p15E cell line. L.C. helped monitor the therapeutic efficacy of ACT+MS-275 in the gp33 model. Y.W. supervised the study, and participated in the conception of experimental designs.

**Competing interests:** Authors declare that they have no competing interests.

**Data and materials availability:** The accession number for the expression data reported in the paper is GEO: GSE179337.

## References

1. S. A. Rosenberg, N. P. Restifo, J. C. Yang, R. A. Morgan, M. E. Dudley, Adoptive cell transfer: a clinical path to effective cancer immunotherapy. *Nat Rev Cancer* 8, 299-308 (2008).
2. K. M. Kaluza, R. Vile, Improving the outcome of adoptive cell transfer by targeting tumor escape. *Oncoimmunology* 2, e22059 (2013).
3. M. Morotti et al., Promises and challenges of adoptive T-cell therapies for solid tumours. *Br J Cancer* 124, 1759-1776 (2021).
4. N. Chen, X. Li, N. K. Chintala, Z. E. Tano, P. S. Adusumilli, Driving CARs on the uneven road of antigen heterogeneity in solid tumors. *Curr Opin Immunol* 51, 103-110 (2018).
5. A. G. Chapuis et al., T-Cell Therapy Using Interleukin-21-Primed Cytotoxic T-Cell Lymphocytes Combined With Cytotoxic T-Cell Lymphocyte Antigen-4 Blockade Results in Long-Term Cell Persistence and Durable Tumor Regression. *J Clin Oncol* 34, 3787-3795 (2016).
6. A. B. Hont et al., Immunotherapy of Relapsed and Refractory Solid Tumors With Ex Vivo Expanded Multi-Tumor Associated Antigen Specific Cytotoxic T Lymphocytes: A Phase I Study. *J Clin Oncol* 37, 2349-2359 (2019).
7. M. Heckler, S. K. Dougan, Unmasking Pancreatic Cancer: Epitope Spreading After Single Antigen Chimeric Antigen Receptor T-Cell Therapy in a Human Phase I Trial. *Gastroenterology* 155, 11-14 (2018).
8. J. L. Gulley et al., Role of Antigen Spread and Distinctive Characteristics of Immunotherapy in Cancer Treatment. *J Natl Cancer Inst* 109, (2017).
9. S. Jhunjhunwala, C. Hammer, L. Delamarre, Antigen presentation in cancer: insights into tumour immunogenicity and immune evasion. *Nat Rev Cancer* 21, 298-312 (2021).
10. S. K. Wculek et al., Dendritic cells in cancer immunology and immunotherapy. *Nat Rev Immunol* 20, 7-24 (2020).
11. I. Fricke, D. I. Gabrilovich, Dendritic cells and tumor microenvironment: a dangerous liaison. *Immunol Invest* 35, 459-483 (2006).

12. S. Chiba et al., Tumor-infiltrating DCs suppress nucleic acid-mediated innate immune responses through interactions between the receptor TIM-3 and the alarmin HMGB1. *Nat Immunol* 13, 832-842 (2012).
13. M. M. Xu et al., Dendritic Cells but Not Macrophages Sense Tumor Mitochondrial DNA for Cross-priming through Signal Regulatory Protein alpha Signaling. *Immunity* 47, 363-373 e365 (2017).
14. S. Demoulin, M. Herfs, P. Delvenne, P. Hubert, Tumor microenvironment converts plasmacytoid dendritic cells into immunosuppressive/tolerogenic cells: insight into the molecular mechanisms. *J Leukoc Biol* 93, 343-352 (2013).
15. D. Alizadeh et al., Doxorubicin eliminates myeloid-derived suppressor cells and enhances the efficacy of adoptive T-cell transfer in breast cancer. *Cancer Res* 74, 104-118 (2014).
16. L. Bracci, G. Schiavoni, A. Sistigu, F. Belardelli, Immune-based mechanisms of cytotoxic chemotherapy: implications for the design of novel and rationale-based combined treatments against cancer. *Cell Death Differ* 21, 15-25 (2014).
17. L. Zhang et al., Differential impairment of regulatory T cells rather than effector T cells by paclitaxel-based chemotherapy. *Clin Immunol* 129, 219-229 (2008).
18. Y. Nefedova et al., Activation of dendritic cells via inhibition of Jak2/STAT3 signaling. *J Immunol* 175, 4338-4346 (2005).
19. Y. W. Moon, J. Hajjar, P. Hwu, A. Naing, Targeting the indoleamine 2,3-dioxygenase pathway in cancer. *J Immunother Cancer* 3, 51 (2015).
20. P. K. Bommareddy, A. Patel, S. Hossain, H. L. Kaufman, Talimogene Laherparepvec (T-VEC) and Other Oncolytic Viruses for the Treatment of Melanoma. *Am J Clin Dermatol* 18, 1-15 (2017).
21. H. Salmon et al., Expansion and Activation of CD103(+) Dendritic Cell Progenitors at the Tumor Site Enhances Tumor Responses to Therapeutic PD-L1 and BRAF Inhibition. *Immunity* 44, 924-938 (2016).
22. T. Saito et al., Combined mobilization and stimulation of tumor-infiltrating dendritic cells and natural killer cells with Flt3 ligand and IL-18 in vivo induces systemic antitumor immunity. *Cancer Sci* 99, 2028-2036 (2008).
23. C. A. Klebanoff et al., Determinants of successful CD8+ T-cell adoptive immunotherapy for large established tumors in mice. *Clin Cancer Res* 17, 5343-5352 (2011).



24. C. A. Klebanoff et al., Memory T cell-driven differentiation of naive cells impairs adoptive immunotherapy. *The Journal of clinical investigation* 126, 318-334 (2016).
25. J. G. Crompton, M. Sukumar, N. P. Restifo, Uncoupling T-cell expansion from effector differentiation in cell-based immunotherapy. *Immunol Rev* 257, 264-276 (2014).
26. B. W. Bridle et al., HDAC inhibition suppresses primary immune responses, enhances secondary immune responses, and abrogates autoimmunity during tumor immunotherapy. *Mol Ther* 21, 887-894 (2013).
27. Y. Kato et al., Synergistic in vivo antitumor effect of the histone deacetylase inhibitor MS-275 in combination with interleukin 2 in a murine model of renal cell carcinoma. *Clin Cancer Res* 13, 4538-4546 (2007).
28. H. Hess-Stumpp, T. U. Bracker, D. Henderson, O. Politz, MS-275, a potent orally available inhibitor of histone deacetylases--the development of an anticancer agent. *Int J Biochem Cell Biol* 39, 1388-1405 (2007).
29. A. Nguyen, L. Ho, Y. Wan, Chemotherapy and Oncolytic Virotherapy: Advanced Tactics in the War against Cancer. *Front Oncol* 4, 145 (2014).
30. D. I. Gabrilovich, S. Nagaraj, Myeloid-derived suppressor cells as regulators of the immune system. *Nat Rev Immunol* 9, 162-174 (2009).
31. V. Bronte et al., Recommendations for myeloid-derived suppressor cell nomenclature and characterization standards. *Nat Commun* 7, 12150 (2016).
32. V. Kumar, S. Patel, E. Tcyganov, D. I. Gabrilovich, The Nature of Myeloid-Derived Suppressor Cells in the Tumor Microenvironment. *Trends Immunol* 37, 208-220 (2016).
33. A. Nguyen et al., HDACi Delivery Reprograms Tumor-Infiltrating Myeloid Cells to Eliminate Antigen-Loss Variants. *Cell reports* 24, 642-654 (2018).
34. H. J. Zeh, 3rd, D. Perry-Lalley, M. E. Dudley, S. A. Rosenberg, J. C. Yang, High avidity CTLs for two self-antigens demonstrate superior in vitro and in vivo antitumor efficacy. *Journal of immunology* 162, 989-994 (1999).
35. M. H. Kershaw et al., Immunization against endogenous retroviral tumor-associated antigens. *Cancer Res* 61, 7920-7924 (2001).

36. B. Shang, Y. Liu, S. J. Jiang, Y. Liu, Prognostic value of tumor-infiltrating FoxP3+ regulatory T cells in cancers: a systematic review and meta-analysis. *Sci Rep* 5, 15179 (2015).
37. S. Nagaraj, J. I. Youn, D. I. Gabrilovich, Reciprocal relationship between myeloid-derived suppressor cells and T cells. *J Immunol* 191, 17-23 (2013).
38. P. Serafini, S. Mgebroff, K. Noonan, I. Borrello, Myeloid-derived suppressor cells promote cross-tolerance in B-cell lymphoma by expanding regulatory T cells. *Cancer Res* 68, 5439-5449 (2008).
39. W. Niedbala, B. Cai, F. Y. Liew, Role of nitric oxide in the regulation of T cell functions. *Ann Rheum Dis* 65 Suppl 3, iii37-40 (2006).
40. L. Verinaud et al., Nitric oxide plays a key role in the suppressive activity of tolerogenic dendritic cells. *Cell Mol Immunol* 12, 384-386 (2015).
41. Y. Togashi, K. Shitara, H. Nishikawa, Regulatory T cells in cancer immunosuppression - implications for anticancer therapy. *Nat Rev Clin Oncol* 16, 356-371 (2019).
42. K. Lahl et al., Selective depletion of Foxp3+ regulatory T cells induces a scurfy-like disease. *J Exp Med* 204, 57-63 (2007).
43. Q. Duan, H. Zhang, J. Zheng, L. Zhang, Turning Cold into Hot: Firing up the Tumor Microenvironment. *Trends Cancer* 6, 605-618 (2020).
44. C. Engblom, C. Pfirschke, M. J. Pittet, The role of myeloid cells in cancer therapies. *Nat Rev Cancer* 16, 447-462 (2016).
45. J. M. Pitt et al., Targeting the tumor microenvironment: removing obstruction to anticancer immune responses and immunotherapy. *Ann Oncol* 27, 1482-1492 (2016).
46. A. H. Sharpe, E. J. Wherry, R. Ahmed, G. J. Freeman, The function of programmed cell death 1 and its ligands in regulating autoimmunity and infection. *Nat Immunol* 8, 239-245 (2007).
47. Q. Peng et al., PD-L1 on dendritic cells attenuates T cell activation and regulates response to immune checkpoint blockade. *Nat Commun* 11, 4835 (2020).
48. D. Lindau, P. Gielen, M. Kroesen, P. Wesseling, G. J. Adema, The immunosuppressive tumour network: myeloid-derived suppressor cells, regulatory T cells and natural killer T cells. *Immunology* 138, 105-115 (2013).

49. X. Pan, L. Zheng, Epigenetics in modulating immune functions of stromal and immune cells in the tumor microenvironment. *Cellular & molecular immunology* 17, 940-953 (2020).
50. F. Spadaro et al., IFN-alpha enhances cross-presentation in human dendritic cells by modulating antigen survival, endocytic routing, and processing. *Blood* 119, 1407-1417 (2012).
51. S. Manicassamy, B. Pulendran, Dendritic cell control of tolerogenic responses. *Immunol Rev* 241, 206-227 (2011).
52. O. Fainaru et al., Tumor growth and angiogenesis are dependent on the presence of immature dendritic cells. *FASEB J* 24, 1411-1418 (2010).
53. J. M. Tran Janco, P. Lamichhane, L. Karyampudi, K. L. Knutson, Tumor-infiltrating dendritic cells in cancer pathogenesis. *Journal of immunology* 194, 2985-2991 (2015).
54. P. Brossart, The Role of Antigen Spreading in the Efficacy of Immunotherapies. *Clin Cancer Res* 26, 4442-4447 (2020).
55. H. J. Jackson, R. J. Brentjens, Overcoming Antigen Escape with CAR T-cell Therapy. *Cancer Discov* 5, 1238-1240 (2015).
56. S. R. Walsh et al., Endogenous T cells prevent tumor immune escape following adoptive T cell therapy. *The Journal of clinical investigation* 129, 5400-5410 (2019).
57. R. Saleh, E. Elkord, FoxP3(+) T regulatory cells in cancer: Prognostic biomarkers and therapeutic targets. *Cancer Lett* 490, 174-185 (2020).
58. M. Onda, K. Kobayashi, I. Pastan, Depletion of regulatory T cells in tumors with an anti-CD25 immunotoxin induces CD8 T cell-mediated systemic antitumor immunity. *Proc Natl Acad Sci U S A* 116, 4575-4582 (2019).
59. A. Tanaka, S. Sakaguchi, Regulatory T cells in cancer immunotherapy. *Cell Res* 27, 109-118 (2017).
60. R. Ahmed, A. Salmi, L. D. Butler, J. M. Chiller, M. B. Oldstone, Selection of genetic variants of lymphocytic choriomeningitis virus in spleens of persistently infected mice. Role in suppression of cytotoxic T lymphocyte response and viral persistence. *J Exp Med* 160, 521-540 (1984).

61. L. Zhang et al., Delivery of viral-vectored vaccines by B cells represents a novel strategy to accelerate CD8(+) T-cell recall responses. *Blood* 121, 2432-2439 (2013).
62. J. D. Bassett et al., CD8+ T-cell expansion and maintenance after recombinant adenovirus immunization rely upon cooperation between hematopoietic and nonhematopoietic antigen-presenting cells. *Blood* 117, 1146-1155 (2011).
63. B. W. Bridle et al., Privileged Antigen Presentation in Splenic B Cell Follicles Maximizes T Cell Responses in Prime-Boost Vaccination. *Journal of immunology* 196, 4587-4595 (2016).
64. P. Du, W. A. Kibbe, S. M. Lin, lumi: a pipeline for processing Illumina microarray. *Bioinformatics* 24, 1547-1548 (2008).
65. M. E. Ritchie et al., limma powers differential expression analyses for RNA-sequencing and microarray studies. *Nucleic Acids Res* 43, e47 (2015).
66. Y. Benjamini, R. Cohen, Weighted false discovery rate controlling procedures for clinical trials. *Biostatistics* 18, 91-104 (2017).
67. G. Wu, L. Stein, A network module-based method for identifying cancer prognostic signatures. *Genome Biol* 13, R112 (2012).
68. P. Shannon et al., Cytoscape: a software environment for integrated models of biomolecular interaction networks. *Genome Res* 13, 2498-2504 (2003).
69. A. Subramanian et al., Gene set enrichment analysis: a knowledge-based approach for interpreting genome-wide expression profiles. *Proc Natl Acad Sci U S A* 102, 15545-15550 (2005).
70. D. Merico, R. Isserlin, O. Stueker, A. Emili, G. D. Bader, Enrichment map: a network-based method for gene-set enrichment visualization and interpretation. *PloS one* 5, e13984 (2010).
71. A. Nguyen, O. Salem, Y. Wan, Functional Analysis of Tumor-Infiltrating Myeloid Cells by Flow Cytometry and Adoptive Transfer. *Journal of visualized experiments : JoVE*, (2021).
72. B. J. Quah, C. R. Parish, The use of carboxyfluorescein diacetate succinimidyl ester (CFSE) to monitor lymphocyte proliferation. *Journal of visualized experiments : JoVE*, (2010).

73. M. Roederer, Interpretation of cellular proliferation data: avoid the panglossian. *Cytometry. Part A : the journal of the International Society for Analytical Cytology* 79, 95-101 (2011).
74. M. Durward, J. Harms, G. Splitter, Antigen specific killing assay using CFSE labeled target cells. *Journal of visualized experiments : JoVE*, (2010).

## Main Figure Titles and Legends

### **Figure 1: Concomitant MS-275 delivery prevents tumor relapse during adoptive cell therapy**

In C57BL/6 mice (n=5 per group), (A) five-day old intradermal B16-gp33 tumors were treated with adoptive cell therapy (ACT, 104 LCMV GP33–41-specific TMEM i.v. followed by viral vaccination). MS-275 was injected i.p. daily for 5 days starting at various timepoints. Tumor volumes were calculated based on height, width, and length. (B) Immunofluorescence-staining with cleaved caspase-3 antibody and TO-PRO-3 nuclear stain, (C) hematoxylin and eosin staining, or (D) immunohistochemical CD8 antibody staining of frozen tumor sections harvested five days post-treatment. Digested tumors (n=5 per group) were enriched for CD45.2+ cells and the (E) frequency of CD45.2+ CD8+ T cells and (F) absolute count of LCMV GP33–41-specific CD8+ T cells as determined by IFN $\gamma$  expression after ex vivo peptide stimulation was measured. (G) Tumor volume measurements following selective lymphocyte depletion prior and during ACT+MS-275 treatment using monoclonal antibodies specific for CD8, CD4, and NK1.1. Data are represented as mean  $\pm$  SEM. NS=not significant, \*\*\*\* p<0.0001; ACT, adoptive cell therapy

### **Figure 2: MS-275 remodels the inflammatory landscape of the tumor microenvironment to promote antigen processing and presentation**

Bulk tumor RNA was derived from ACT-treated mice +/- MS-275 for microarray analysis (n=4 per group). (A) heatmap and gene set enrichment analysis (GSEA) of custom gene sets representing specific inflammatory pathways at D1 and D5 (see also Table S2). (B) qRT-PCR of pro-inflammatory cytokines at specific time points post-treatment (n=3 per group). (C) GSEA of curated gene sets (C2) derived from the Molecular Signatures Database (MSigDB) and displayed as an enrichment map (see also Figure S2). (D) Gene ontology (GO) analysis of modules (see also Table S3) derived from DE genes (D3 vs D1 and D5 vs D1, FDR p<0.05) within a protein-protein interaction (PPI) network. Modules were sorted by ratio of up-regulated to down-regulated genes when comparing ACT+MS-275 to ACT alone (see also Figure S3). (E) qRT-PCR of myeloid-related chemokines at specific time points post-treatment (n=3 per group). (F) GSEA of immunologic signatures (C7) derived from the Molecular Signatures Database (MSigDB) where highlighted groups represent gene sets related to activated myeloid cells (see also Figure S4). Data are represented as mean  $\pm$  SEM. \* p<0.05, \*\* p<0.01, \*\*\* p<0.001, \*\*\*\* p<0.0001; ACT, adoptive cell therapy, DE, differentially expressed

**Figure 3: MS-275 alters myeloid cell composition within the tumor/dLN and enhances co-stimulation**

Five days post-treatment, digested tumors (n=3 per group) were positively enriched for CD45.2 cells. (A) Representative scatter plots outlining the gating strategy for characterizing myeloid populations in the tumor and draining lymph nodes (dLN). Myeloid cell composition changes in the tumor and dLN during ACT +/- MS-275 treatment were depicted by (B, C) representative contour plots and by (D, E) frequency as a percentage of total CD11c+ cells. Maturation marker expression in total CD11c+ cells in the (F) tumor and (G) dLN were determined by MHC Class II (I-Ab) and co-stimulatory ligand CD86 (B7-2)-specific flow staining. (H, I) Enriched CD11c+ cells were pulsed with LCMV GP33–41 peptide and co-cultured with CFSE-labeled LCMV-P14 TCR-transgenic naïve T cells. Representative histograms show CFSE dilution after 3 days and changes in proliferation due to treatment were quantified by division index. Data are represented as mean ± SEM. NS=not significant, \* p<0.05, \*\* p<0.01, \*\*\* p<0.001, \*\*\*\* p<0.0001; ACT, adoptive cell therapy

**Figure 4: Epitope spreading mobilizes tumor-rejecting p15E-specific endogenous CD8+ T cell responses**

(A) In lymphocyte-deficient RAG2/Il2rg knockout mice (n=7-8 per group), five-day old intradermal B16-gp33 tumors were treated with ACT +/- MS-275. Tumor volumes were calculated based on height, width, and length. Using C57BL/6 tumor-bearing mice treated with ACT+MS-275, (B) CD8+ T cells were positively enriched from digested tumors and co-cultured with target cell lines at a 10:1 effector to target ratio. Killing was measured by MTT reduction and done in triplicate. (C, D) Five days post-vaccination, the frequency of tumor antigen-specific CD8+ T cells in peripheral blood was determined by IFN $\gamma$  expression after ex vivo stimulation with peptides (n=3 per group). (E, F) CFSEhi-labeled bulk splenocytes were pulsed with p15E peptide, mixed with CFSElo-labeled, unpulsed splenocytes at a 1:1 ratio, and infused into tumor-bearing mice five days post-ACT+MS-275 treatment. P15E-specific killing was measured by the recovery of labeled, pulsed targets relative to unpulsed targets (n=4 per group). Mice that were cured of B16-gp33 tumors during ACT+MS-275 were re-challenged with (G, H) natural, p15E-expressing MC38 tumors or (I, J) engineered, p15E-overexpressing MC102 tumors and monitored for tumor growth and survival (n=4 per group). The dotted line represents endpoint tumor volume. Data are represented as mean ± SEM. NS=not significant, \* p<0.05, \*\* p<0.01; ACT, adoptive cell therapy

**Figure 5: Reduced local immunosuppressive signals coincide with reduced regulatory T cell infiltration**

(A, D) Bulk tumor RNA was derived from ACT-treated mice +/- MS-275 and qRT-PCR analysis was performed at specific time points post-treatment (n=3 per group). (B, C) Five days post-treatment, frozen tumor sections were stained with anti-Foxp3 antibody for immunohistochemistry and immunofluorescence imaging. (E, F) Positive enrichment of CD45.2+ cells from digested tumors in treated mice was followed by flow cytometric staining and absolute regulatory T cell counts were measured (n=5 per group). Data are represented as mean  $\pm$  SEM. \* p<0.05, \*\* p<0.01, \*\*\*\* p<0.0001; ACT, adoptive cell therapy

**Figure 6: Regulatory T cells selectively obstruct the magnitude of endogenous responses from epitope spreading and their depletion promotes sustained tumor regression**

In “depletion of regulatory T cell” (DEREG) BAC transgenic mice (n=5 per group), five-day old intradermal B16-gp33 tumors were treated with adoptive cell therapy followed by depletion of regulatory T cells using anti-CD4 monoclonal antibodies or diphtheria toxin. (A, B) Five days post-treatment, regulatory T cells were quantified within peripheral blood by flow cytometry. (C, D) Tumor volume measurements following regulatory T cell depletion in the context of ACT. (E, F) Five days post-vaccination, the frequency of tumor antigen-specific CD8+ T cells in peripheral blood was determined by IFN $\gamma$  expression after ex vivo stimulation with peptides. (G) Five days post-treatment, digested tumors (n=3 per group) were positively enriched for CD11c+ cells, pulsed with LCMV GP33–41 peptide and co-cultured with CFSE-labeled LCMV-P14 TCR-transgenic naïve T cells. Representative histograms show CFSE dilution after 3 days and changes in proliferation due to treatment were quantified by division index. Data are represented as mean  $\pm$  SEM. NS=not significant, \* p<0.05, \*\* p<0.01, \*\*\* p<0.001; ACT, adoptive cell therapy, DT, diphtheria toxin



## **Materials and Methods**

### **Study Design**

The overall objective of the study was to determine how epigenetic modification during adoptive T-cell therapy can prevent tumor recurrence. The *in vivo* experiments were conducted to examine the differential therapeutic effect of histone deacetylase inhibitor delivery, to characterize local genetic, inflammatory, and immunological changes, and to determine the therapeutic impact of epitope spreading in the context of tumor recurrence prevention. *In vivo* studies were performed with  $n = 5$  female age-matched (6-8 weeks old) mice. Experiments were repeated at least three times. Tumor-challenged mice were randomized prior to blinded treatments. Mice were monitored for signs of distress and humane endpoints were determined by decreased body condition. Veterinary staff monitored mice daily and alerted researchers when a humane endpoint had been reached. All animal studies complied with the Canadian Council on Animal Care guidelines and were approved by McMaster University's Animal Research Ethics Board.

### **Animals**

C57BL/6 mice were purchased from Charles River Laboratory and B6.Cg-Tcratm1Mom Tg(TcrLCMV)327Sdz (P14) and Rag2/Il2rg Double Knockout (RAG KO) mice were purchased from Taconic. Mice were housed in the Central Animal Facility at McMaster University.

### **Viral Vectors**

LCMV-Armstrong and VSV-gp33 were described previously (60-62).

### **Tumor Challenge**

Naïve C57BL/6 mice were challenged intradermally with 10<sup>5</sup> B16-gp33 or MC38-gp33 cells in 30  $\mu$ l PBS. Cured mice were re-challenged with 10<sup>5</sup> MC38, MCA102, or MCA102-p15E cells in 30  $\mu$ l PBS. Tumor growth was monitored as previously described (63).

### **Adoptive T cell Transfer**

Spleens were collected from LCMV-Armstrong-infected mice (>1 month) and a single cell suspension was prepared. LCMV GP33–41-specific memory T cells (TMEM) were enumerated by staining with H-2Db-GP33 tetramer (Baylor College of Medicine), CD127, and CD62L (BD Biosciences). 10<sup>4</sup> LCMV GP33–41-specific TMEM in 200 µL PBS were adoptively transferred into tumor-challenged mice by intravenous injection. Twenty-four hours post-adoptive T cell transfer, mice were injected intravenously with 2x10<sup>8</sup> pfu of VSV-gp33 in 200 µL PBS. Concomitantly, MS-275 (Sigma-Aldrich) was intraperitoneally injected (100 µg/mouse in 50 µL PBS) daily for five days. Selective lymphocyte depletion was conducted using monoclonal antibodies (Bio X Cell) specific for CD8, CD4, or NK1.1. Mice were injected with 250 µg of mAb in 500 µL PBS on Day -1 and 1 post-vaccination and every two weeks afterwards (150 µg).

### **Detection of Antigen-specific Responses**

Five days post-vaccination, PBMCs were stimulated for 5 hours with LCMV GP33-41 peptide in the presence of brefeldin A (GolgiPlug; BD Biosciences). Following surface staining for CD8 $\alpha$  (BD Biosciences), cells were fixed and permeabilized with Cytofix/Cytoperm (BD Biosciences) and stained for intracellular IFN $\gamma$  (BD Biosciences). Data were acquired using an LSRFortessa flow cytometer with FACSDiva software (BD Biosciences) and analyzed with FlowJo X, version 10.0.7 (Treestar).

### **Tumor RNA Extraction**

B16-gp33 tumors were excised 5 days post-vaccination and snap-frozen in liquid nitrogen and samples were then homogenized in Trizol (Invitrogen). RNA was extracted and purified using a RNeasy mini kit (Qiagen) and treated with Ambion's DNA-free kit.

### **Gene Expression Microarray**

Samples were profiled using Illumina MouseRef8v2 arrays (GSE179337). The obtained data were processed with VST transformation and quantile normalization (lumi package (64)). Only annotated and detected genes were selected yielding a list of 13,088 genes for further analyses. Time course analysis using limma package (65) was performed with the following contrasts: (ACT+MS-275(D5)-ACT+MS-275(D1)) - (ACT only(D5)-ACT only(D1)) and (ACT+MS-275(D3)-ACT+MS-275(D1)) - (ACT only(D3)-ACT only(D1)). Obtained p-values were corrected with Benjamini-Hochberg correction for multiple testing (66); corrected values <0.05 were considered to be significant. All significant genes from

the comparisons were used for Protein-Protein Interaction Network construction, using Reactome FI plugin (67) in Cytoscape environment (68). Next, the modules of nodes in the network were defused and analyzed for Pathway enrichment and GO Biological Process component. The obtained lists of significantly enriched and over-represented pathways and biological processes were used to categorize and label the modules in the network.

Gene set enrichment analysis (GSEA) (69) was performed using the whole gene expression profiles to examine the following comparisons: (a) ACT+MS-275(D1)-ACT only(D1), (b) ACT+MS-275(D3)-ACT only(D3), and (c) ACT+MS-275(D5)-ACT only(D5). We have performed the analysis using 3 sets of gene sets: C2v4 and C7v4 from MSigDB [<https://www.gsea-msigdb.org/gsea/msigdb/index.jsp>], and a custom gene set (Table S1). FDR corrected P-values < 0.05 were considered to be significant. Next, the results obtained for C2v4 and C7v4 were visualized using Enrichment Map plugin (70) in Cytoscape environment.

### **Purification of Tumor-infiltrating Dendritic Cells**

B16-gp33 tumors were excised 5 days post-vaccination and digested in 0.5 mg/mL collagenase Type IV (Gibco), and 0.2 mg/mL DNase (Roche) prepared in complete RPMI (Gibco, 10 mL/250 mg tumor) and incubated at 37°C for 30 min as previously described (71). The digested material was CD45.2 or CD11c-enriched through magnetic selection with an EasySep Mouse Biotin or CD11c Positive Selection Kit (Stemcell Technologies).

### **Histology**

B16-gp33 tumors excised 5 days post-vaccination were snap frozen before cryostat sections were obtained and mounted on gelatin-coated histological slides. The slides were fixed in 4% paraformaldehyde for 20 min at room temperature and blocked with PBS containing 5% goat serum and 0.3% Triton X-100 for 30 min. Slides were pretreated with Leica Bond Epitope Retrieval buffer #2 (Leica Biosystems) for 20 minutes before staining using hematoxylin and eosin (H&E), immunohistochemistry (IHC), or immunofluorescence (IF). IHC: Anti-CD8 (1:1000, Thermo Fisher Scientific) was added and incubated overnight at 4°C. Color was developed using the Leica Bond Polymer Refine Detection Kit (Leica Biosystems) and with rabbit anti-rat antibody (1:100, Vector Laboratories). IF: Anti-Cleaved Caspase-3 (1:400, Cell Signaling Technology) or anti-FoxP3 (1:400, Thermo Fisher Scientific) were added and incubated overnight at 4°C. Slides were incubated for 1h with biotinylated goat anti-rabbit IgG (Vector Laboratories) followed by Alexa Fluor 488-conjugated streptavidin (Thermo Fisher Scientific).

### **Proliferation assay**

Tumor-infiltrating dendritic cells were isolated, pulsed with LCMV GP33-41 peptide and co-cultured for 3 days with CFSE-labeled P14 T cells as previously reported (72). Proliferation was evaluated using several metrics including division index (73).

### **Cytotoxicity Assay**

In vitro: B16-F10 cells ( $1 \times 10^4$  /well) were co-cultured with tumor-infiltrating myeloid cells ( $1 \times 10^5$ /well) in 96-well flat bottom microtiter plates (Corning Inc.) for 12 hours before killing was assessed. Non-adherent cells were washed using warm PBS and 500  $\mu$ g/mL MTT (3-(4,5-dimethylthiazol-2-yl)-2,5-diphenyltetrazolium bromide, Thermo Fisher Scientific) solution was added before incubating the plates for 4 hours. Solubilization of the formazan by-product was done by aspirating the MTT solution and adding DMSO. The absorbance was measured at 540 nm using a Synergy microplate reader (Biotek). In vivo: Target bulk splenocytes were isolated and pulsed with 1  $\mu$ g/mL LCMV GP33-41 peptide for 1 hour and labeled with CFSE at a final concentration of 5  $\mu$ M/mL (CFSE<sub>hi</sub>) in RPMI media 1640 with 2% FBS for 15 min as previously described (74). The cells were mixed at a 1:1 ratio with unpulsed bulk splenocytes labeled with 0.5  $\mu$ M/mL CFSE (CFSE<sub>lo</sub>) and infused i.v. into treated mice 4 days post-treatment. After 24 hours, spleens were harvested and processed for flow cytometric detection of CFSE-expressing cells.

### **Statistics**

GraphPad Prism (GraphPad Software) was used for graphing and statistical analyses. Student's t-test and one-way/two-way analysis of variance (ANOVA) were used to query immune response data. All data were presented as means  $\pm$  SE and differences between means were considered significant at  $p < 0.05$ . Error bars indicate 95% confidence intervals throughout.

### Supplementary Figure Titles and Legends

#### **Figure S1, related to Figure 2: Connectivity mapping of differentially expressed (DE) genes**

(A) DE genes expressed in ACT+MS-275 relative to ACT only treatment over the period of the 5 days (Day 5 vs. Day 1) were used to create two signatures: genes with fold change of at least 1.5, and genes with fold change of at least 2.0 (FDR  $p < 0.05$ ). Both signatures were used to query the Connectivity Map database and overlapped with chemical perturbation gene signatures. (B) Venn diagram of compounds that show significant overlap (C) Ranking of 32 compounds found to overlap both signatures based on similarity to the  $FC \geq 2.0$  signature

#### **Figure S2, related to Figure 2C: Fully-annotated curated gene sets (C2) enrichment map**

Enrichment map with full annotations for every gene set cluster.

#### **Figure S3, related to Figure 2D: Gene module ranking based on MS-275 up-regulation**

(A) Differential gene expression comparison of ACT+MS-275 treatment vs ACT alone from Day 1 to Day 5 (FDR  $p < 0.05$ ). (B) Protein-protein interaction network where clusters of differentially expressed genes (DE) were assembled into gene modules based on D3 vs D1 and D5 vs D1. (C) Expression heatmap and sorting of modules based on percentage of genes up-regulated by MS-275 for D3 vs D1 and D5 vs D1 comparisons (D) GO term assignment to each module and color assignment based on relative up-regulation (red) or down-regulation (green) by MS-275.

#### **Figure S4, related to Figure 2F: Fully-annotated immunologic signatures (C7) enrichment map**

Enrichment map with full annotations for every gene set cluster.

### Supplementary Table Titles and Legends

#### **Table S1: Custom inflammatory gene sets, related to Figure 2A**

**Table S2: Enriched custom gene sets after gene set enrichment analysis (GSEA), related to Figure 2A**

**Table S3: Modules derived from the network of differentially expressed genes, related to Figure 2D**

**Figure 1**

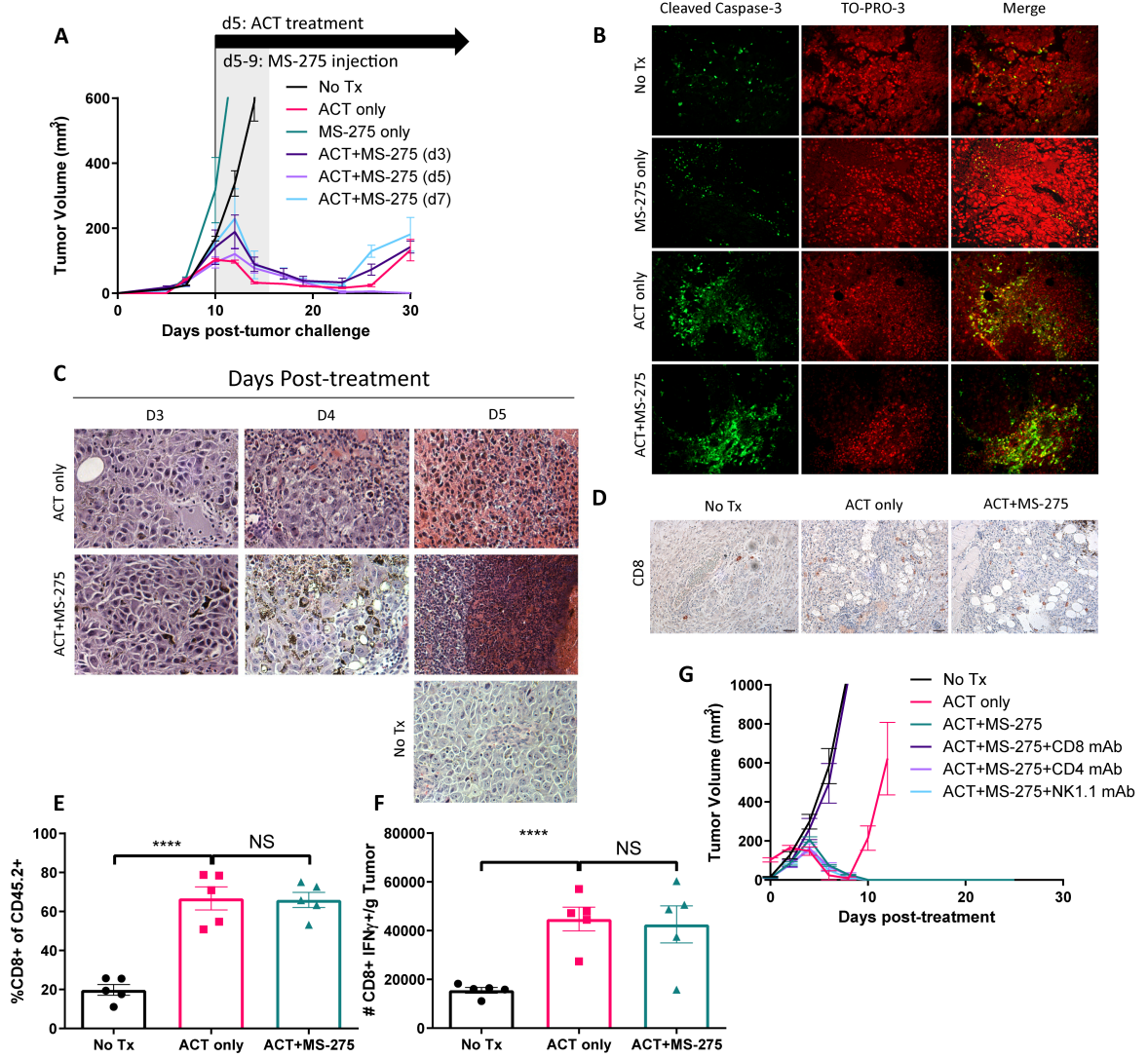
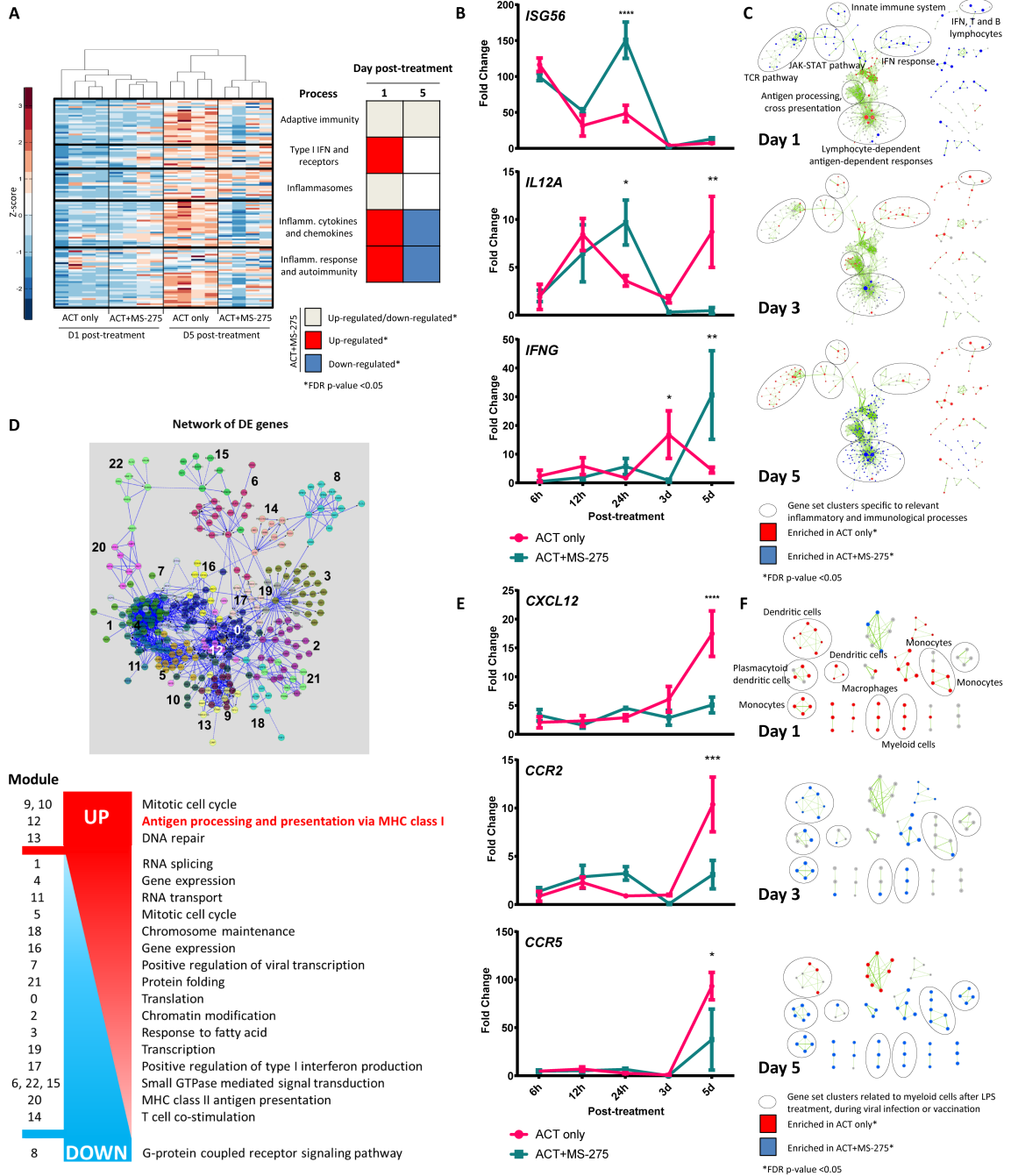
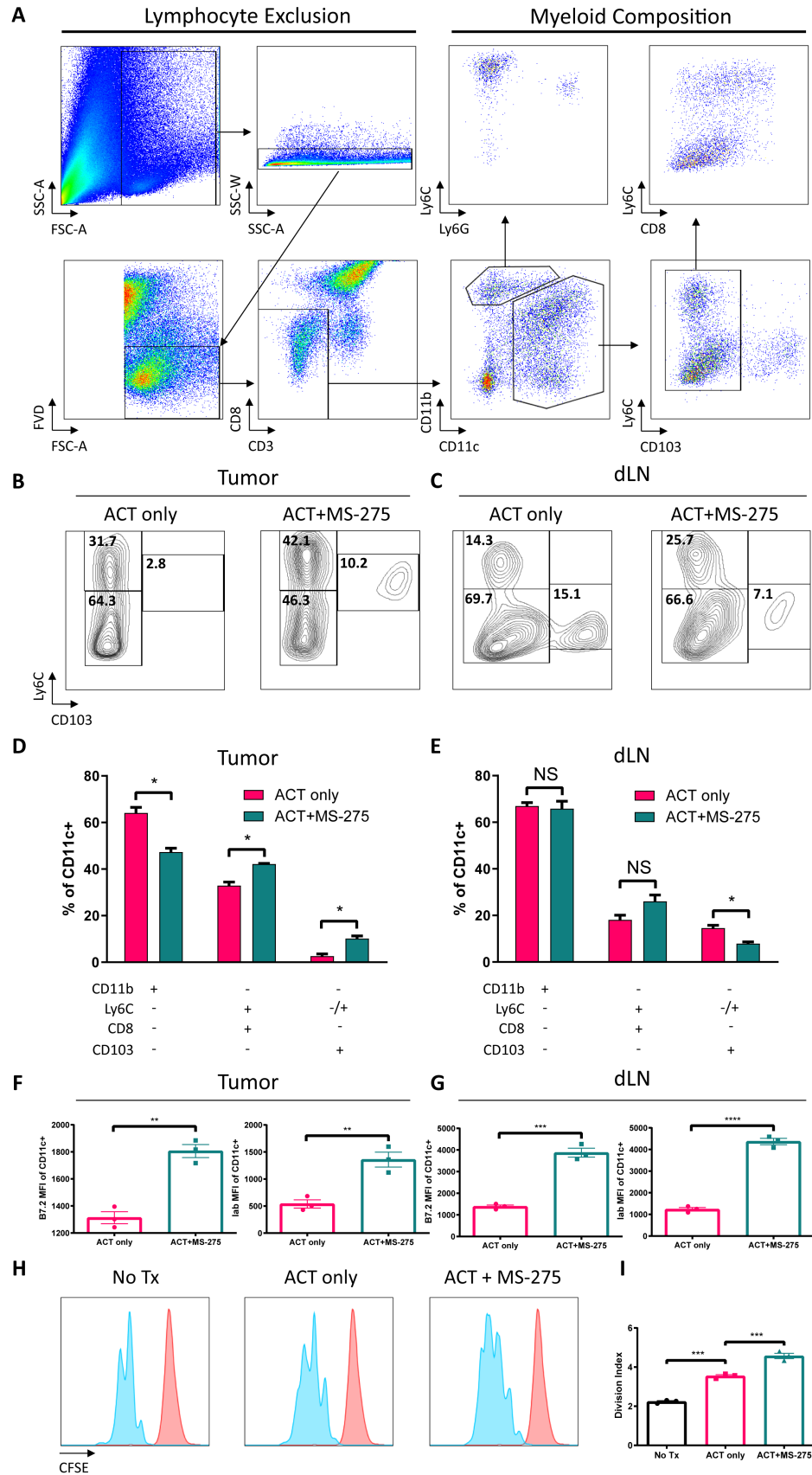


Figure 2





**Figure 3**



**Figure 4**

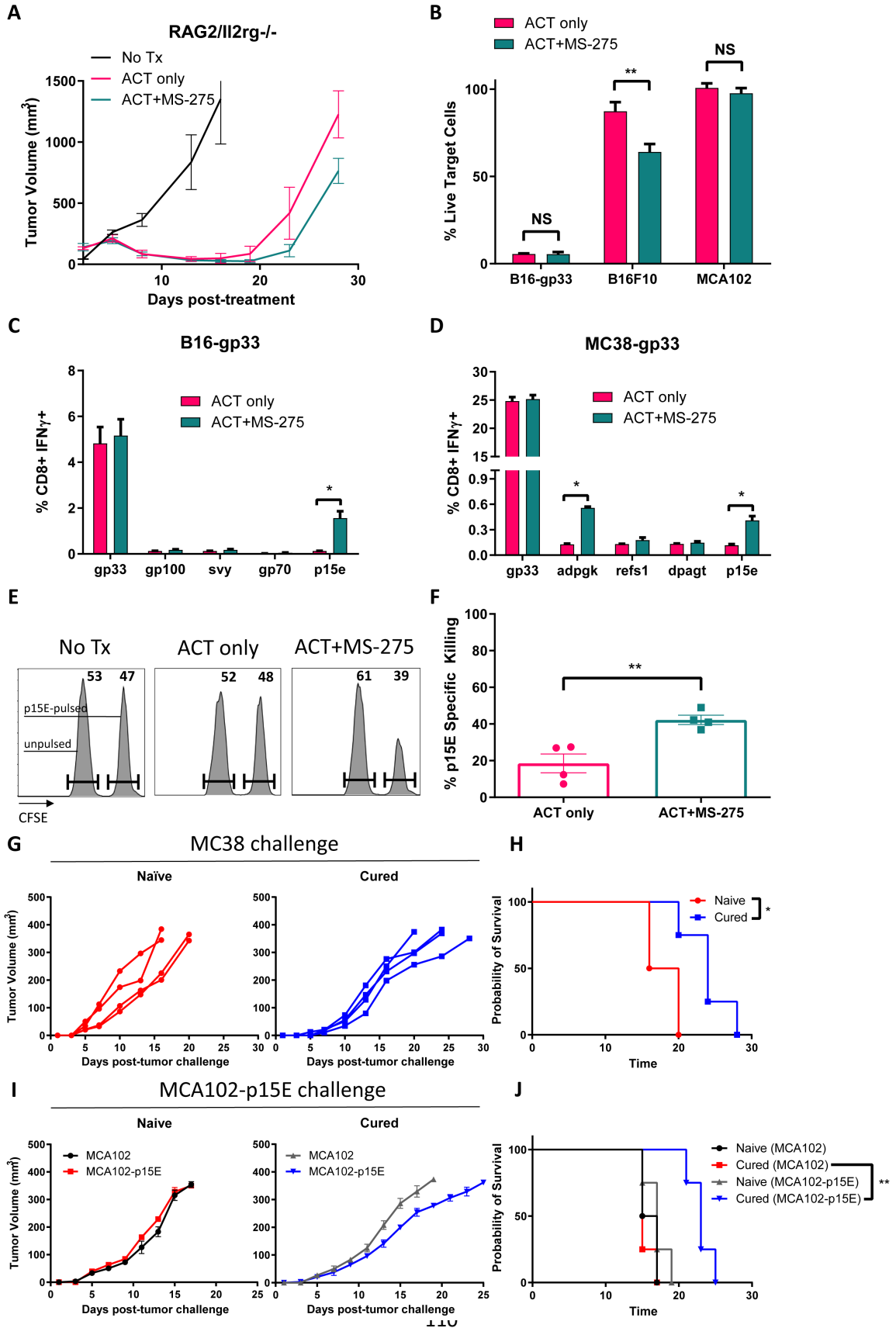


**Figure 5**

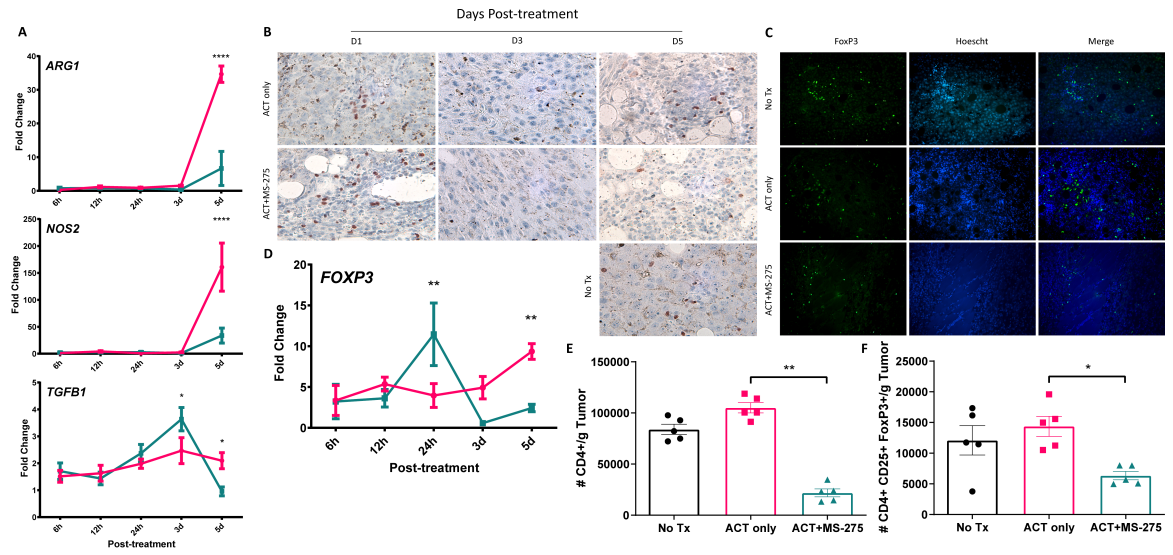
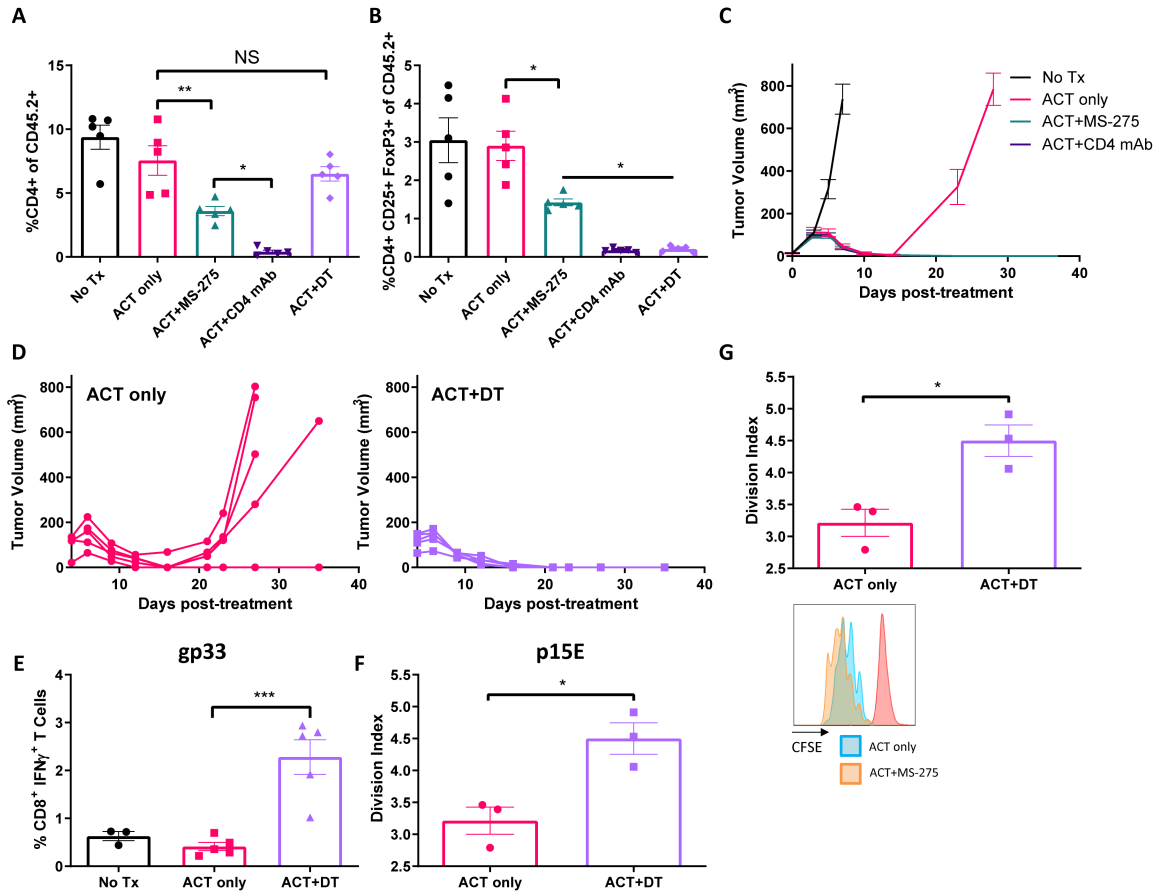
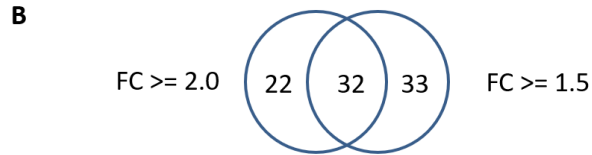
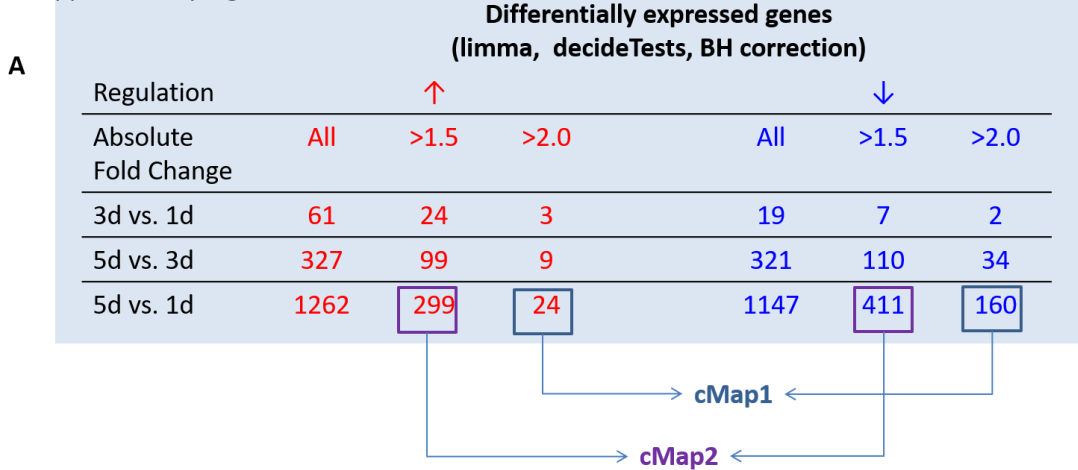


Figure 6



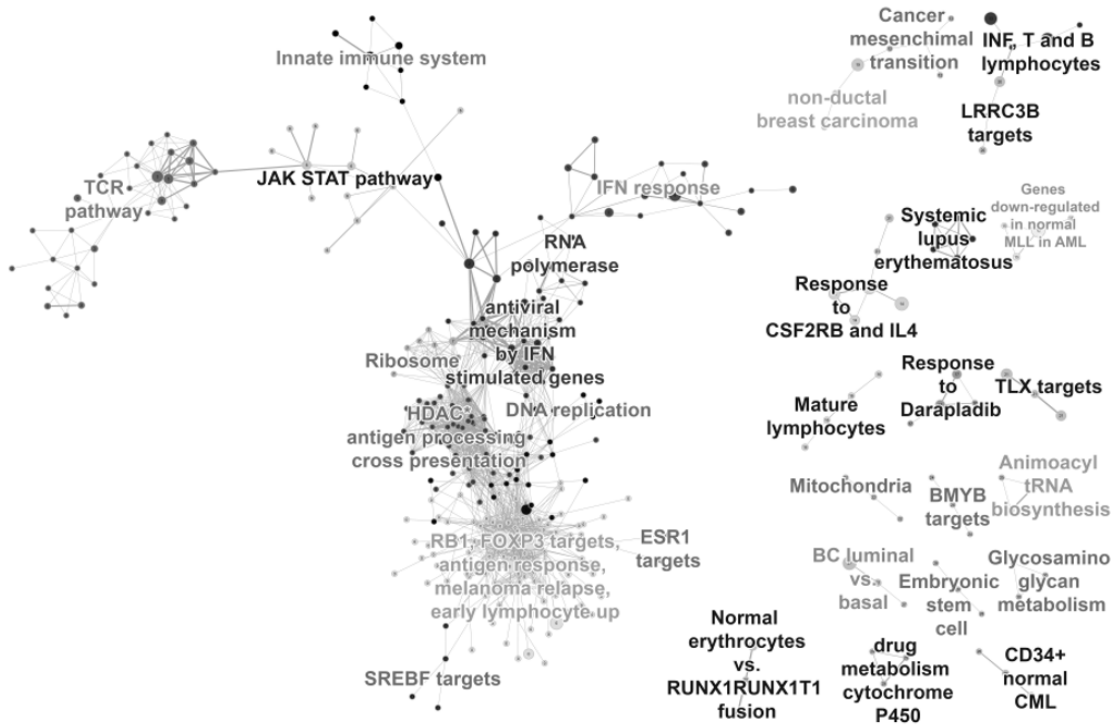
Supplementary Figure 1



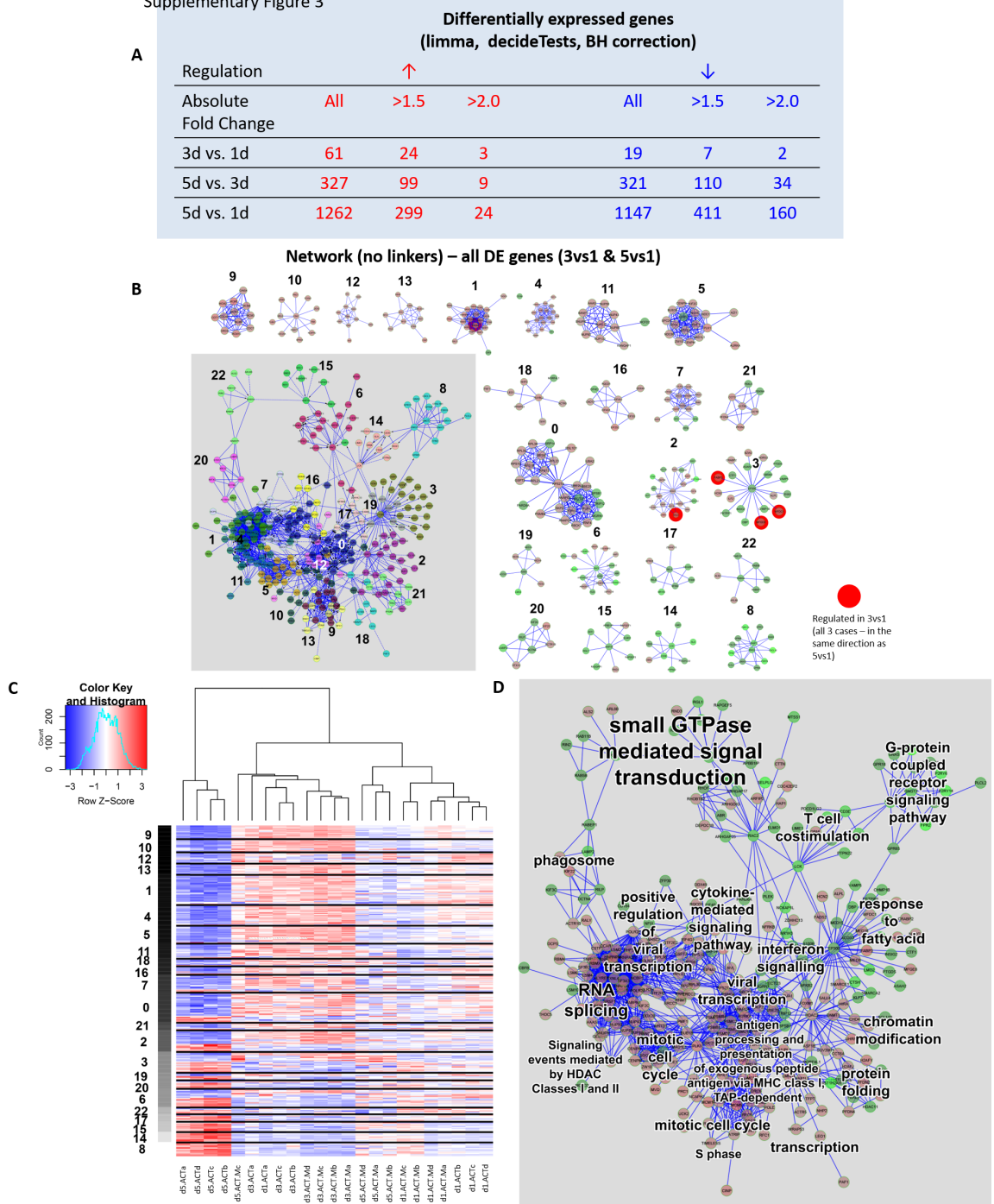
**C**

Compound		Similarity	
		FC2.0	FC1.5
MS-275	HDAC inhibitor	-0.929	-0.782
DL-thiorphan	membrane metalloendopeptidase inhibitor	-0.89	-0.722
quinostatin	PI3K inhibitor	-0.807	-0.87
rottlerin	Enzyme inhibitor	-0.793	-0.729
0297417-0002B		-0.75	-0.829
alexidine		-0.717	-0.573
puromycin	antibiotics	-0.709	-0.65
pyrvinium	anthelmintic	-0.672	-0.717
propafenone	Sodium-channel blocker	-0.665	-0.509
etacrynic acid	Enzyme inhibitor	-0.66	-0.709
ivermectin	Activates chloride channels	-0.658	-0.662
phthalylsulfathiazole		-0.624	-0.593
medrysone	corticosteroid	-0.616	-0.597
methylergometrine	oxytocics	-0.58	-0.644
dequalinium chloride	Disinfectant	-0.567	-0.533
thioridazine	Dopamine antagonist	-0.563	-0.649
levonorgestrel	Synthetic progesterone	-0.558	-0.56
withaferin A		-0.541	-0.61
dipyridamole	phosphodiesterase inhibitor	-0.535	-0.549
trichostatin A	HDAC inhibitor	-0.535	-0.653
flunisolide	corticosteroid	-0.514	-0.487
vorinostat	HDAC inhibitor	-0.512	-0.556
pimozide	Dopamine blocker	-0.51	-0.58
LY-294002	Enzyme inhibitor	-0.507	-0.613
0175029-0000		-0.498	-0.634
chlorpromazine	Dopamine antagonist	-0.458	-0.441
tretinoin	ATRA, retinoic acid	-0.45	-0.427
trifluoperazine	Dopamine antagonist	-0.439	-0.653
sirolimus	Immunosuppressive agent	-0.323	-0.615
wortmannin	Immunosuppressive agent; PI3K inhibitor	-0.3	-0.576
15-delta prostaglandin J2		-0.296	-0.387
valproic acid	HDAC inhibitor	-0.206	-0.307

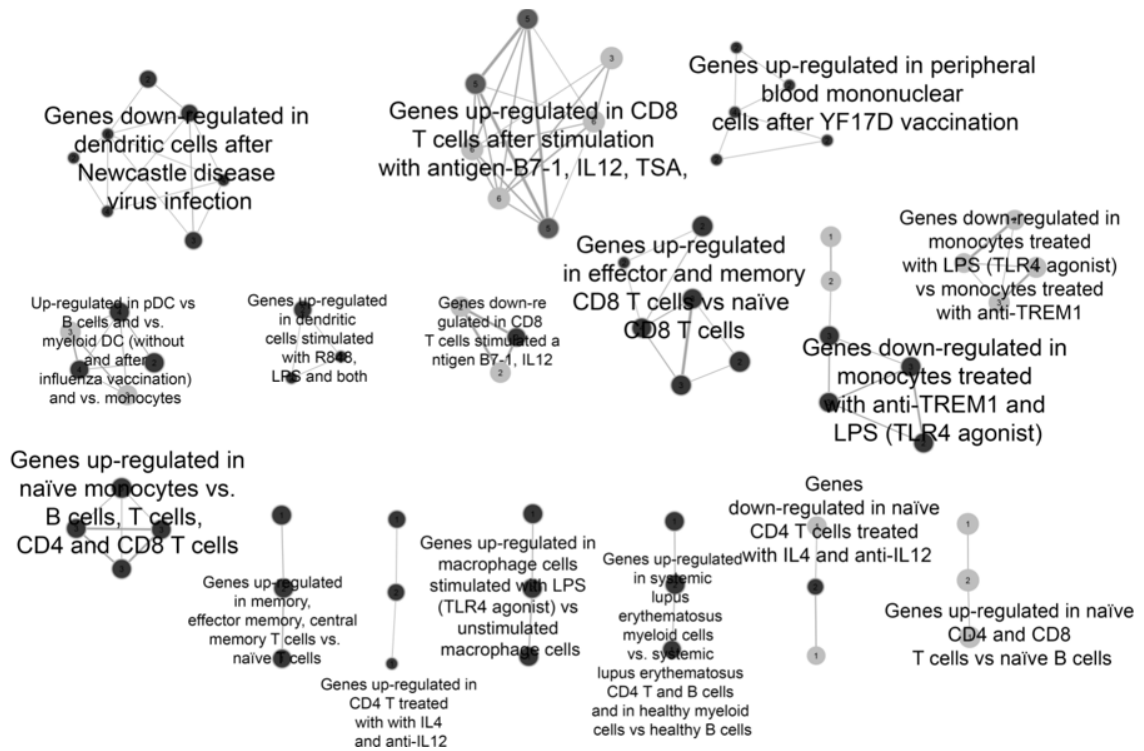
Supplementary Figure 2



Supplementary Figure 3



## Supplementary Figure 4





**Supplementary Table 2**

**Day 1 GSEA - positively enriched in ACT+MS-275 vs ACT only**

NAME	SIZE	FDR q-val	Leading Edge
ADAPTIVEIMMUNITY_DOWN	25	0.001	TLR4, CTLA4, RORC, STAT3, IFNG, TGFB1, SLC11A1, IL18, CXCL10, CCR5, C3
ADAPTIVEIMMUNITY_UP	18	0.001	ICAM1, IFNG, CD83, CD40, PRF1, CD86, CD68, SLC11A1, IL18
ANTIVIRALRESPONSE_UP	74	0.000	MX1, IRAK4, TLR13, AZI2, RELA, IFIH1, TYK2, IFNAR2, CASP8, IFITM2, TLR4, DDX3X, TBK1, RIPK1, DDX58, MAPK3, MAP3K1, MAP2K1, IL15, TLR2, CD40, TLR3, MYD88, TLR7, PSTPIP1, CD86, SPP1, TLR13, CTSB, IRF5, STAT1, CTSS, IL18, CXCL10, CASP1, IFIT2
IFNS_AND_RECEPTORS_DOWN	48	0.000	IFIT3, IRF8, IRF5, IRF1, CXCL10, IFIT2
INFLAMMASOMES_DOWN	46	0.001	MAPK3, IL33, IFNG, BIRC2, MAPK13, NLRX1, MYD88, CCL7, TXNIP, IL18, IRF1, CIITA, NOD1, CASP1
INFLAMMASOMES_UP	9	0.048	BCL2L1, HSP90B1, PSTPIP1, CTSB
INFLAMMATORYCYT_CHE_DOWN	43	0.000	IL33, IL15, CSF1, IFNG, CCL2, IL10RA, CCL3, CXCL13, CXCL16, CXCL9, IL10RB, CCL6, CCL7, TNFRSF11B, CCL9, CXCL10, CCR5
INFLAMMATORYRES	49	0.000	IL1RN, CCL25, FASL, RIPK2, BCL6, TLR4, CCL11, LY96, CSF1, IFNG, TLR2, CCL2, CD40, TLR3, MYD88, CCL3, TLR7, CXCL9, IL10RB, CCL7, C4B, CEBPB, IL18, CXCL10, C3
MELANOMA_UP	18	0.018	ENC1, TRP53INP1, RB1, SOCS2, SOCS3, IRF8

**Day 5 GSEA - negatively enriched in ACT+MS-275 vs ACT only**

NAME	SIZE	FDR q-val	Leading Edge
INFLAMMATORYRESPONSE_AUTOIMMUNITY_DOWN	49	0.000	CCL5, IL1B, CD14, IL1RN, CD40, CCL7, C4B, IL10RB, TLR2, C3, TNF, IL18, NOS2, TLR7, CCL2, BCL6, CEBPB, IL1A, LTB, FASL, ITGB2, CXCR4, NFKB1, CXCL9
INFLAMMATORYCYT_CHE_DOWN	43	0.002	CXCL16, CCR5, CCL6, TNFRSF11B, CCL5, IL1B, IL1RN, CCL7, IL10RB, IL15, IL10RA, TNF, IL2RG, CCL9, CCL2, IL1A, LTB, FASL, CXCL9, IL33, CXCL12, OSM, IL16
ANTIVIRALRESPONSE_UP	74	0.008	CASP1, CCL5, CTSS, TLR13, IL1B, CD14, CD86, CD40, TLR2, IL15, IRF5, TNF, IL18, TLR7, NFKBIA, IL1A, ATG12, NFKB1, AZI2, CTSB
ADAPTIVEIMMUNITY_UP	18	0.008	CD68, SLC11A1, CD86, CD40, CD83, IL18, ICAM1
ADAPTIVEIMMUNITY_DOWN	25	0.016	CCR5, SLC11A1, CCL5, C3, TNF, IL18, NOS2, PDCC1LG2, TGFB1, TLR4, STAT4, TLR6



#### **4.0 Chapter Four – T cell transcriptional reprogramming overcomes tumor burden-induced cellular exhaustion**

##### **4.1 Introduction**

Tumor size or burden is an intrinsic property of solid tumors that has negative clinical implications for cancer immunotherapy. Indeed, systemic immunosuppression associated with increased tumor burden can lead to rapid deletion of transferred cells during ACT. This manuscript characterizes the immunosuppressive pathways associated with tumor burden and illustrates how MS-275 can restore therapeutic efficacy in large tumors.

In this manuscript, large fibrosarcoma tumors are defined by a unique immunosuppressive pathway signature that is conducive to the systemic shutdown of transferred T cell responses through induction of cellular exhaustion. MS-275 promotes tumor tissue normalization by reversing large tumor-intrinsic pathways. This was accompanied by a reprogramming of transferred T cells from an exhausted phenotype to activated effector phenotype.

##### **4.2 Manuscript Status, Copyright, and Citation**

*Status:* Submitted to Immunity

*Copyright:* © Nguyen A et al. (2021). This article would be available under open access and printed under the terms of the Creative Commons Attribution License 4.0 International License (CC BY 4.0) (<https://creativecommons.org/licenses/by/4.0/>). To safeguard against the possibility of ineligibility of submission to other publications, a temporary hold on the electronic publication of the thesis will be requested.

*Citation:* Nguyen, A, Brown, D, Krishnan, R, Walsh, SR, Bastin, D, Deng, L, Chen, L, Bramson, JL, Wan, Y (2021). “T cell transcriptional reprogramming overcomes tumor burden-induced cellular exhaustion.” *Immunity*. In submission.

##### **4.3 Preprint of the Journal Article**

Starting on the next page.

**T cell transcriptional reprogramming overcomes tumor burden-induced cellular exhaustion**

Nguyen, Andrew<sup>1</sup>; Brown, Dominique<sup>2</sup>; Krishnan, Ramya<sup>3</sup>; Walsh, Scott R<sup>1</sup>; Bastin, Donald<sup>4</sup>; Deng, Li<sup>5</sup>; Chen, Lan<sup>1</sup>; Bramson, Jonathan L<sup>1</sup>; Wan, Yonghong<sup>1,6</sup>

- 1 Department of Pathology and Molecular Medicine, McMaster Immunology Research Centre, McMaster University, Hamilton, Ontario L8N 3Z5, Canada.
- 2 Turnstone Biologics, Ontario, Canada
- 3 Public Health Agency of Canada, Ottawa, Ontario, Canada
- 4 Schulich School of Medicine, Western University, London, Ontario, Canada
- 5 Fantasia Biopharma (Zhejiang) Co. Ltd, Zhengjiang, China
- 6 Lead Contact

**Corresponding Author**

Yonghong Wan

Department of Pathology and Molecular Medicine

1280 Main St. W., MDCL 5026

Hamilton, Ontario,

Canada L8S 4K1

Phone: (905) 525-9140 x22461

Fax: (905) 522-6750

E-mail: wanyong@mcmaster.ca

## Summary

Adoptive cell therapy (ACT) for solid tumors is a clinical challenge that is progressively being addressed. However, tumor burden is still an inherent barrier to therapeutic responsiveness. Here we identified that in contrast to small tumors, large syngeneic tumors systemically ablated T cell expansion and mitigated tumor control. This was accompanied by clinically pervasive immunosuppressive pathway changes in the tumor microenvironment. In our study, we demonstrated that Class I histone deacetylase inhibitor MS-275 promoted tumor normalization and in conjunction with ACT restored T cell responses and tumor regression. Transferred CD8<sup>+</sup> T cells displayed higher proliferation and cytotoxicity which we associated with T cell activation-favored transcriptome remodeling. Additionally, Tim-3 was selectively up-regulated, which correlated with reduced signatures of T cell exhaustion and differentiation into a predominantly terminal effector-like Tim3<sup>hi</sup> TCF1<sup>-</sup> CD127<sup>-</sup> KLRG1<sup>+</sup> population. Taken together, concomitant MS-275 delivery may mediate conversion between exhaustion and effector lineage differentiation states.

## **Introduction**

Immunotherapy for the treatment of cancer has gained much attention in recent years for its successes in enabling immune responses that can elicit durable tumor control. One of the major cancer immunotherapy strategies, adoptive cell therapy (ACT), involves the autologous/allogeneic transplant of personalized cellular products that demonstrate potent tumor recognition and killing. These are usually tumor antigen-specific CD8<sup>+</sup> T cells that were derived from tumor-infiltrating lymphocytes or were genetically modified to express specific T-cell receptors or chimeric antigen receptors (Mardiana et al., 2019). ACT and immune checkpoint blockade currently represent the overwhelming number of active trials for immunotherapy and have shown consistent efficacy in the treatment of hematological malignancies (Xin Yu et al., 2019). However, the clinical success of cancer immunotherapy is contingent on a CD8<sup>+</sup> T cell-inflamed tumor microenvironment (TME), and unlike non-solid cancers, solid cancers have often produced compromised T cell responses (Morotti et al., 2021). As a result, the number of clinical trials that have shown success in the treatment of non-melanoma solid cancers is disproportionately low. Currently, the field is looking to address the unique challenges imposed by solid tumors to improve the curative potential of ACT.

The TME in solid tumors presents significant hurdles for T cell inflammation. Tumor secretion of inhibitory chemokines and stromal/vascular changes can impede immune infiltration, while tumor-intrinsic/tumor-extrinsic immunosuppressive factors may reduce their viability and function (Wagner et al., 2020). Furthermore, variability in tumor antigen expression can facilitate therapeutic selective pressure for immune escape variants (Landsberg et al., 2012; Restifo et al., 2016). Fortunately, increasing comprehension of optimal antitumor T cell parameters have fostered improvements to existing ACT protocols. In addition to T cell dose (Hanson et al., 2000), several variables were shown to be determinants of therapeutic efficacy: 1) the differentiation status of adoptively transferred T cells, which is inversely correlated with *in vivo* proliferation capacity (Klebanoff et al., 2011), and 2) the inclusion of post-transfer viral vaccination for *in vivo* antigenic re-stimulation, which enhances cytotoxic effector differentiation and homing of adoptively transferred T cells (Smith et al., 2009). Accordingly, these conditions have been shown to promote the quick accumulation of tumor-infiltrating T cells to bypass TME resistance and regress solid tumors (Nguyen et al., 2018). ACT may also facilitate the induction of secondary endogenous T cell responses against other tumor antigens, resulting in broad spectrum antitumor immunity (Walsh et al., 2019). Taken together, ACT protocols are becoming increasingly efficacious in the control and resolution of solid tumors.

Despite this, the extent of tumor burden presents an additional layer of difficulty for solid tumor eradication. It has been previously demonstrated that successful ACT treatment in small tumors may not be recapturable in large tumors (Kim et al., 2020). This has been attributed to the functional impairment and rapid deletion of transferred cells (Prato et al., 2013). Indeed, increased tumor burden may promote immunosuppressive cytokine/immunoregulatory cell accumulation and dysregulation of antigen presenting cells, which stifles the antigenic re-stimulation of transferred T cells (Hegde et al., 2020; Lin et al., 2020). Deficiencies in cellular activation, along with antigen chronicity, are primary determinants of T cell exhaustion, a broad categorical term that encompasses hyporesponsive effector T cells with unique transcriptional programmes and differentiation states (Blank et al., 2019; Jiang et al., 2015; Thommen and Schumacher, 2018). Therefore, cellular exhaustion may be viewed as a prolific functional consequence of increased tumor burden. While the use of checkpoint blockade and similar strategies can restore the antitumor capacity of exhausted T cells, its therapeutic efficacy in large tumors has been shown to be limited by the degree of reinvigoration relative to the extent of tumor burden (Huang et al., 2017). An alternative strategy is to target the local changes inherent to increased tumor burden that could create systemic immunosuppressive outcomes. However, few studies have examined these upstream biological pathway changes despite large tumors being more clinically representative in terms of size/duration of growth (Wen et al., 2012). Increased comprehension of large tumors may lead to purposeful re-design of the ACT platform to reliably induce positive clinical outcomes.

Here we determined that successful adoptive cell therapy in solid tumors is abrogated by increased tumor burden. Large tumors expressed a unique pathway signature that coincided with the functional exhaustion of transferred T cells. Interestingly, concomitant delivery of Class I histone deacetylase inhibitor, MS-275, restored therapeutic efficacy by promoting tumor tissue homeostasis in large tumors and subverting T cell exhaustion programming. We found that transferred CD8<sup>+</sup> T cells displayed features of heightened activation-dependent signaling and effector differentiation. Overall, our findings suggest that epigenetic remodeling can reliably sensitize large tumors to immunotherapy.

## Results

### **Tumor burden correlates with reduced responsiveness to immunotherapy and negative clinical outcomes**

In a murine CMS5 fibrosarcoma tumor model wherein the immunodominant rejection antigen is mutated ERK2136–144 (mERK2136–144), ex vivo culture of DUC18 T cell receptor (TCR) transgenic T cells into a central memory phenotype (TCM) followed by adoptive transfer and viral vaccination (VSVΔM51-mERK2136–144) sustainably regressed 7-day old (<150 mm<sup>3</sup>) established tumors. However, when we increased the tumor burden to 14 days (>600 mm<sup>3</sup>), our ACT protocol was incapable of controlling tumor growth and prolonging survival (Figure 1A, B). To determine if there was an adverse effect on transferred T cell responses, we harvested peripheral mononuclear blood cells (PBMCs) 5 days post vaccination. In contrast to 7-day old tumors wherein we detected a ~26% circulating mERK2136–144-specific CD8<sup>+</sup> T cell frequency, ACT treatment of 14-day old tumors resulted in complete ablation of the T cell response (Figure 1C).

In addition, 14-day old tumors were surgically removed 24 hours prior to ACT treatment. Unlike intact tumors, surgical resection restored the peripheral T cell response (Figure 1D). As such, we reasoned that increased tumor burden did not induce permanent host biological changes and that the systemic shutdown of antitumor T cell expansion, while potent, was inherently reversible.

To preserve transferred T cell responses during ACT, we first sought to understand the local changes that predisposed large tumors to therapeutic resistance. We harvested RNA from 7- and 14-day old tumors and analyzed them by bulk-cell RNA-seq. 14-day old tumors acquired a distinct transcriptomic signature compared to 7-day tumors by principal component analysis (PCA) (Figure 1E). Correspondingly, gene set enrichment analysis (GSEA) of 14- vs 7-day old tumors using Hallmark, Curated (C2), and Ontology (C5) gene set collections from the Molecular Signatures Database (MSigDB) allowed us to identify biological processes affected by increased tumor burden. Enrichment redundancy across collections affirmed that 14-day old tumors positively enriched pathways related to transcription/translation, cellular metabolism, and hypoxia, and negatively enriched pathways related to inflammatory cytokine signaling and lymphocyte activation (Figure 1F-H). Altogether, unrestrained gene expression and increased bioenergetic demand within large tumors may stimulate pathophysiological signaling processes associated with anti-inflammation and immunosuppression.

If these processes are clinically represented in patients with high tumor burden, it could signify a translational challenge for ACT. We investigated this possibility using human skin cutaneous melanoma (SKCM) cohort data from The Cancer Gene Atlas (TCGA)



project. A training set composed of stratified patient samples based on primary tumor size (T4 vs T1) was used to elucidate overlaps in enriched Hallmark gene sets from 14- vs 7-day old tumors. We found that T4 tumors enriched several pathways previously observed in 14-day old tumors (positive: ‘cholesterol homeostasis’, ‘glycolysis’; negative: ‘KRAS signaling up’, ‘complement’, ‘IL2 STAT5 signaling’, ‘inflammatory response’, ‘IL6 JAK STAT3 signaling’, ‘interferon alpha response’, ‘interferon gamma response’, ‘allograft rejection’) (Figure 1I).

To determine if these enriched pathways could serve as a prognostic signature, single-sample GSEA (ssGSEA) was used to calculate enrichment scores for each sample within the dataset (Figure 1J). Based on the enrichment score and its relative contribution to overall survival per multivariate Cox regression analysis, we developed a prognostic model with the risk score method for survival prediction. The training set was stratified into high- and low-risk groups using the median risk score as a cutoff threshold (Figure 1K). Since the high-risk group had a significantly shorter survival duration compared to the low-risk group (Figure 1L), we confirmed that risk scores derived from our pathway signature had predictive value. While univariate Cox regression indicated that clinical variables ‘pathologic stage’, ‘T stage’, ‘N stage’, and ‘risk score’ were significantly associated with patient survival, multivariate analysis confirmed that only ‘T stage’, or tumor stage, was an independent prognostic factor (Table 1). Interestingly, ‘risk score’ demonstrated the highest hazard ratio (HR = 2.7007) amongst the four prognostic variables. This confirmed our hypothesis that expression of the pathway signature in the context of increased tumor burden contributed to poor clinical outcomes.

Finally, we examined the prevalence of the pathway signature in other tumor cohorts. Using receiver operating characteristic (ROC) curves, we found that risk scores were sensitive and specific in the prediction of tumor burden (T1/T4) in SKCM (AUC = 0.688), head-neck squamous cell carcinoma (HNSC, AUC = 0.709), and breast invasive carcinoma (BRCA, AUC = 0.653) (Figure 1M-O). In each of these studies, T4 patients had a lower survival duration relative to T1 patients. Consequently, large tumor-related pathway changes represent a pervasive clinical issue that should be strategically targeted to improve the efficacy of ACT and other T cell therapies.

### **MS-275 restores tissue homeostasis and promotes tumor clearance during immunotherapy**

Pathway changes observed during tumor progression are often associated with dysregulation of the chromatin landscape which leads to disruption of cellular homeostasis and reconfiguration of the TME (Cheng et al., 2019). This drives local reprogramming of

stromal and immune cell populations to support immunosuppression and resistance to immunotherapy (Pan and Zheng, 2020). By contrast, histone deacetylase inhibitors (HDACi) have been shown to reprogram aberrant regulation of chromatin (Anastas et al., 2019), leading to tumor sensitization and augmentation of antitumor immune responses (Li et al., 2021; McCaw et al., 2019). In this study, we wondered if epigenetic rewriting of the TME using HDACi could promote tissue normalization and prevent shutdown of transferred T cell responses.

We treated 14-day old CMS5 tumors with Class I HDACi MS-275 and harvested tumor RNA for bulk-cell RNA-seq. Interestingly, GSEA of treated vs un-treated 14-day old tumors using MSigDB Hallmark gene sets revealed that the direction of enriched pathways was in complete opposition to that of 14- vs 7-day old tumors (Figure 2A). We validated this observation by analyzing both comparisons ((a) 14- vs 7-day old tumors, (b) treated vs un-treated 14-day old tumors) against the entire database, which comprised the following gene set collections: Positional (C1), Curated (C2), Regulatory target (C3), Computational (C4), Ontology (C5), Oncogenic signature (C6), Immunologic signature (C7), Cell type signature (C8) (Figure 2B). While the number of enriched gene sets was substantially higher in (a) than (b), 77.1% of gene sets in (b) overlapped with (a) with 99.8% opposing enrichment direction (Figure 2C). As a result, MS-275 treatment induced key biological changes that may restore tissue homeostasis within large tumors and improve the outcome of cancer immunotherapy.

Although the treatment of 7-day old CMS5 tumors with ACT+MS-275 did not show additional benefit to tumor regression, survival, and peripheral antitumor immune response (Figure 2D-F), combination therapy completely regressed 14-day old tumors and improved overall survival (Figure 2D, E). Correspondingly, mERK2136–144-specific CD8<sup>+</sup> T cell expansion was restored and comparable to ACT in tumor-free and 7-day old tumors (Figure 2F). Altogether, MS-275-dependent rescue of ablated T cell responses improved the resolution of large, highly immunosuppressive, solid tumors.

Using a different tumor model and treatment modality, we were able to recapitulate the effects of both tumor burden and MS-275 on T cell-dependent therapeutic outcomes. 7-day old MC38 murine colon adenocarcinoma tumors that were engineered to overexpress surrogate tumor antigen LCMV GP33-41 (MC38-gp33) were treated with viral vaccine VSVΔM51-gp33 and found to elicit a sufficient endogenous LCMV GP33-41-specific CD8<sup>+</sup> T cell response to completely regress tumors and prolong survival (Figure 2G-I). By contrast, 14-day old tumors could not be controlled by VSVΔM51-gp33 treatment, which coincided with a significant reduction in antitumor immune response. Concomitant MS-275 delivery was able to restore both tumor regression and immune response resulting in improved overall survival. These findings suggest that MS-275's effects on large tumors

may be widely applicable across tumor types and antigen-specific T cells, both adoptively transferred and endogenously activated.

### **T cells demonstrate increased persistence and cytotoxicity in immunosuppressive large tumors**

Comprehensive analysis of the events which led to the peripheral disappearance of antitumor T cells gave us insight into the consequences of increased tumor burden on T cell fate. We transduced cultured TCM to express luciferase and monitored their accumulation in 14-day old tumor-bearing mice during ACT treatment by in vivo imaging system (IVIS) (Figure 3A). Over the course of 5 days post vaccination, we clearly observed T cell migration to the tumor, axillary lymph nodes, and inguinal lymph nodes (dorsal view) as well as the spleen and cervical lymph nodes (ventral view). Interestingly, ACT treatment was able to elicit early expansion of adoptively transferred T cells which peaked at around day 3-4 (day 4 by tumor flux, Figure 3B); however, by day 5 we were unable to detect a bioluminescent signal, indicating total loss of transferred T cells. Conversely, ACT+MS-275 treatment promoted continuous expansion of adoptively transferred T cells and peak flux at day 5 (Figure 3A, B). Time course analysis of peripheral T cell responses further indicated that tumor-specific CD8<sup>+</sup> T cells persisted beyond day 5 and remained detectable for the length of the study (Figure 3C). Therefore, the disappearance of transferred T cells was likely from large tumors truncating the overall T cell response rather than preventing initial T cell expansion.

To investigate the functional changes incurred by adoptively transferred T cells, we conducted multi-tissue analysis at a timepoint prior to their disappearance (day 4.5). Ki67 and annexin V staining of transferred DUC18-Thy1.1 congenic CD8<sup>+</sup> T cells allowed us to quantify proliferation and early apoptosis during treatment (Figure 3D, E). Thy1.1<sup>+</sup> T cells from 14-day old tumor-bearing mice showed reduced Ki67 expression (blood, tumor) and elevated annexin V expression (tumor) relative to 7-day old tumor-bearing mice. This may suggest that increased tumor burden precipitated T cell dysfunction most severely within the tumor itself while having a disseminated systemic effect. Interestingly, ACT+MS-275 treatment in 14-day old tumors increased Ki67 expression (spleen, blood) compared to ACT alone while having minimal impact on annexin V expression (Figure 3D, E). Since the Ki67 expression level was proportionate to T cell accumulation over time (Figure S1), MS-275 delivery may support the persistence of adoptively transferred T cells by enhancing cellular proliferation.

Although its immune-potentiating capacity was reflected most obviously by increased T cell accumulation, we were curious if MS-275 provided further T cell benefits that could

promote tumor control. We repeated the multi-tissue analysis with P14-Thy1.1 CD8<sup>+</sup> T cells/MC38-gp33 tumors and additionally monitored polyfunctional marker expression to assess degranulation and secretion of multiple inflammatory cytokines. While the frequency of degranulation (CD107a<sup>+</sup>) remained largely unchanged (slightly increased in the tumor), we observed a significant up-regulation of granzyme B (GzB) production (Figure 3F, G). This was accompanied by a slight decrease in interferon  $\gamma$  (IFN $\gamma$ ) and significant down-regulation of tumor necrosis factor  $\alpha$  (TNF $\alpha$ ) production (Figure 3H, I). To determine the net cytotoxic outcome of these polyfunctional changes, we positively enriched Thy1.1<sup>+</sup> cells from bulk splenocytes harvested from treated mice. We then co-cultured them with dye-labeled target cells and measured cell lysis by flow cytometry. At a 0.5:1 effector to target ratio, we observed clear improvement to tumor killing using T cells derived from ACT+MS-275-treated mice (Figure 3J). Overall, MS-275 broadly altered the functional programming of adoptively transferred T cells, which allowed them to persist and demonstrate elevated antitumor activity.

### **T cell transcriptional changes potentiate activation-dependent signaling**

Since MS-275 is an epigenetic agent, we wanted to examine the transcriptional landscape of adoptively transferred CD8<sup>+</sup> T cells during combination treatment. Despite its pleiotropic nature, our aim was to deconvolute the global gene changes associated with MS-275 in order to: 1) discover perturbed biological pathways, 2) correlate them with improved T cell function, and 3) identify prognostic markers of MS-275-induced functional reprogramming.

Bulk splenocytes were harvested from ACT $\pm$ MS-275-treated, 14-day old MC38-gp33 tumor-bearing mice and flow sorted for Thy1.1<sup>+</sup> P14-Thy1.1 cells. T cell RNA was extracted for microarray-based whole transcriptome profiling, whereby PCA revealed that T cells acquired a distinct transcriptomic signature after MS-275 delivery (Figure 4A). GSEA with MSigDB Hallmark gene sets indicated that ACT+MS-275 samples positively enriched pathways related to cell cycle progression, cellular metabolism, and immune response signaling and negatively enriched pathways related to inflammatory cytokine production (Figure 4B). This reinforced our earlier observations that ACT+MS-275 treatment enhanced cellular proliferation and down-regulated IFN $\gamma$  and TNF $\alpha$  production.

Cellular processes are often controlled by interacting proteins that are frequently co-regulated or co-expressed across conditions. Detecting groups of co-expressed genes allow for the identification of novel prognostic markers. To identify markers corresponding to MS-275's effects, we attempted to reproduce our pathway enrichment results using gene co-expression modules. We utilized Co-Expression Module identification Tool

(CEMiTool) analysis for unsupervised dimensionality reduction of the gene expression data to create six modules (M1-M6) of highly correlated genes. Despite the subtle change in median gene activity within each module (Figure 4C), GSEA with M1-M6 gene lists showed positive enrichment of M2 and M3 and negative enrichment of M4 and M6 during ACT+MS-275 treatment (Figure 4D). Of the four gene modules, only M2 showed an overlap in enriched Hallmark pathways (Figure S2). Therefore, it was the module of interest for additional functional characterization and prognostic marker identification.

The co-expressed genes in M2 were submitted as a list for GO-based network construction (Figure 4E). Functional clustering revealed that the majority of overrepresented GO terms associated with M2 were primarily associated with ‘lymphocyte activation’ (Cluster 12, 30.09%) and ‘regulation of cell activation’ (Cluster 13, 31.86%) (Figure 4F) and included relevant biological processes such as ‘positive regulation of lymphocyte activation’ (GO:0051251), ‘positive regulation of lymphocyte proliferation’ (GO:0050671), ‘positive regulation of immune system process’ (GO:0002684), ‘positive regulation of immune response’ (GO:0050778), and ‘positive regulation of reactive oxygen species metabolic process’ (GO:2000379) (Table S1). Since M2 was positively enriched in ACT+MS-275-treated samples, Hallmark GSEA and GO collectively suggested that improvements to T cell functionality were largely driven by enhanced cellular activation.

Hub genes are defined by high module membership and intermodular connectivity, and are often investigated as important prognostic markers (Zhou et al., 2018). We utilized CEMiTool to identify key hub genes within M2 (HAVCR2, PDE8A, MR1, SKAP2, DUSP22), and visualized them in a protein-protein interaction (PPI) network (Figure 4G). Additionally, interactome data integration through GeneMania allowed us to identify several proteins (TNF, CDK1, BRCA1, ASF1B, RRM2, IFI30, CCNB2, PTTG1, BIRC5, CCNA2) with high annotated physical interactivity within M2. All hub genes were highly up-regulated during ACT+MS-275 treatment; in particular, HAVCR2 was one of the top differentially expressed genes in the study (6.754207-fold change) (Figure 4H, S3). Therefore, we reasoned that HAVCR2 and other hub genes comprised a unique gene signature that was conducive to T cell activation.

Gene correlation provides a means by which the roles of poorly characterized proteins can be inferred from better-annotated counterparts. We were curious if individual hub genes participated in any of the aforementioned pathways that potentiated T cell activation during MS-275 delivery. To address this question, we used ssGSEA to calculate enrichment scores for each sample from the Hallmark GSEA analysis (Figure 4I). Using ACT+MS-275 samples, we then constructed a hierarchically-clustered pairwise correlation matrix by combining hub gene expression values with ssGSEA enrichment scores (Figure 4J). After filtering for immunologically relevant pathways, hub genes showed an association with

‘IL2 STAT5 signaling’, ‘MYC targets V1’, ‘oxidative phosphorylation’, and ‘MTORC1 signaling’. In particular, DUSP22 showed weak association with ‘MYC targets V1’ ( $r=0.4053$ ,  $p=0.4984$ ) and ‘oxidative phosphorylation’ ( $r=0.3011$ ,  $p=0.6225$ ) (Figure S4), while HAVCR2 showed moderate association with ‘MYC targets V1’ ( $r=0.5464$ ,  $p=0.3407$ ), ‘oxidative phosphorylation’ ( $r=0.5202$ ,  $p=0.3688$ ), and ‘MTORC1 signaling’ ( $r=0.4926$ ,  $p=0.3992$ ). More importantly, HAVCR2 demonstrated very strong and statistically significant association with ‘IL2 STAT5 signaling’ ( $r=0.9524$ ,  $p=0.0124$ ) (Figure 4K). Thus, HAVCR2 expression may have a role within the IL2/STAT5 signaling axis that contributed to improved T cell activation.

### **Uncoupling Tim-3 expression from cellular exhaustion is associated with terminal effector lineage differentiation**

HAVCR2/Tim-3 is a member of the T-cell immunoglobulin and mucin-domain (TIM) family and has been widely investigated for its involvement in regulating immune responses within autoimmunity and cancer (Ferris et al., 2014). Primarily viewed as checkpoint or co-inhibitory receptor, Tim-3 is often reported in the context of T cell dysfunction or exhaustion (Wolf et al., 2020). However, accumulating evidence suggests it may also have a co-stimulatory role (Avery et al., 2018; Kataoka et al., 2021; Lee et al., 2011). Since our data associated Tim-3 with T cell activation, we wanted to affirm its expression level in the context of increased tumor burden/MS-275 treatment and reconcile its function.

Using DUC18-Thy1.1 CD8<sup>+</sup> T cells for adoptive transfer, we treated 7- or 14-day old CMS5 tumors with ACT±MS-275 and conducted multi-tissue analysis 4.5 days post vaccination. We stained for the expression of Tim-3 as well as PD-1, another exhaustion marker/checkpoint receptor. Thy1.1<sup>+</sup> T cells from ACT-treated 14-day old tumor-bearing mice showed significantly elevated Tim-3 expression (blood, tumor) and PD-1 expression (blood, tumor) relative to 7-day old tumor-bearing mice (Figure 5A, B). This was congruent with the typical T cell exhaustion phenotype, and was reinforced by aforementioned observations of reduced proliferation (blood, tumor). Surprisingly, ACT+MS-275 treatment of 14-day old tumors increased Tim-3 expression further (spleen, blood) compared to ACT alone despite a reduction of PD-1 expression in the spleen. Since MS-275 delivery coincided with enhanced proliferation, Tim-3 expression may have been uncoupled from cellular exhaustion. For further validation, we repeated the experiment and additionally stained for TOX, a potent transcriptional inducer of T cell exhaustion (Khan et al., 2019). In 14-day old tumor-bearing mice, we found no significant change to TOX expression in the spleen, blood, or tumor (Figure 5C). Finally, ssGSEA using a compiled

list of exhausted T cell (TEX) markers allowed us to correlate HAVCR2 expression with TEX gene signature enrichment. There was a strong association in ACT-treated T cells ( $r=0.9123$ ,  $p=0.0308$ ) but none whatsoever in ACT+MS-275-treated T cells ( $r=-0.09578$ ,  $p=0.8782$ ) (Figure 5D). Instead, MS-275 may correspond with activation-dependent changes that influence T cell state.

To better define enhanced cellular activation in the context of T cell state, we utilized GSEA to compare ACT+MS-275- vs ACT-treated T cells using gene lists of known T cell lineages including exhausted (TEX), effector (TEFF), memory (TMEM), memory precursor effector cell (TMPEC), short lived effector cell (TSLEC), and effector memory cells re-expressing CD45A (TEMRA) (Table S2). ACT+MS-275 showed negative enrichment of TEX and TMPEC signatures and positive enrichment of TSLEC and TEMRA signatures (Figure 5E). Heightened activation may therefore have skewed T cell programming away from precursory memory and exhaustion and drove key features of terminal effector differentiation.

In 14-day old MC38-gp33 tumor-bearing mice, ACT±MS-275 treatment with P14-Thy1.1 CD8<sup>+</sup> T cells allowed us to stain splenic Thy1.1<sup>+</sup> cells with a panel of T cell lineage differentiation markers. Following viability, singlet, and exclusion gating as well as artifact removal, a single concatenated sample was created by combining down-sampled events from both ACT and ACT+MS-275 groups. Unsupervised cell clustering was performed with an integrated analysis method using t-stochastic neighbor embedding (t-SNE) and FlowSOM algorithms. Metaclustering revealed extensive heterogeneity in post vaccinated T cells consisting of six major populations (Figure 5F) that underwent significant recombination during MS-275 co-delivery (Figure 5G). Surface marker staining intensity on t-SNE dimension-reduced space showed differential expression patterns that aligned with the territories inhabited by metaclusters (Figure 5H). Unsurprisingly, T cells from ACT+MS-275 treatment were primarily characterized by very high Tim-3 staining intensity as indicated by heatmap hierarchical clustering (Figure 5I). Indeed, T cell phenotype assignment revealed that MS-275 replaced effector-like (Tim-3<sup>+</sup> CD62L<sup>-</sup> TCF1<sup>-</sup> CD127<sup>-</sup>) and memory-like (Tim-3<sup>+</sup> CD62L<sup>-</sup> TCF1<sup>lo</sup> CD127<sup>+</sup>) cells with Tim-3<sup>hi</sup> effector-like (Tim-3<sup>hi</sup> CD62L<sup>-</sup> TCF1<sup>-</sup> CD127<sup>-</sup>) and Tim-3<sup>hi</sup>, TCF1<sup>int</sup> memory-like (Tim-3<sup>hi</sup> CD62L<sup>-</sup> TCF1<sup>int</sup> CD127<sup>+</sup>) cells (Figure 5J). Importantly, 68.42% of adoptively transferred T cells were Tim-3<sup>hi</sup> effector-like cells (TTEC), suggesting that combination treatment facilitated a much more polarized antitumor response.

TSLEC signature enrichment observed during ACT+MS-275 treatment prompted us to explore KLRG1 expression (a defining marker of TSLEC (Herndler-Brandstetter et al., 2018)) in effector-like T cells harvested from multiple tissues post vaccination. Since KLRG1 expression has been shown to be negatively correlated with cellular exhaustion

(Herndler-Brandstetter et al., 2018; Khan et al., 2019; Wherry and Kurachi, 2015), we were interested whether TTEC displayed elevated KLRG1 during ACT+MS-275 treatment compared to ACT alone. Indeed, after gating on CD8<sup>+</sup> Thy1.1<sup>+</sup> CD44<sup>+</sup> Tim-3<sup>+</sup> TCF1<sup>-</sup> CD62L<sup>-</sup> CD127<sup>-</sup> cells (Figure 5K), we observed a systemic increase in KLRG1 expression (spleen, blood, tumor) (Figure 5L). As a result, this phenotypic overlap further suggested that TTEC-restricted Tim-3 expression was uninvolved with exhaustion.



## Discussion

Despite the unprecedented success of adoptive cell therapy for treating hematological malignancies, there are substantial challenges in developing the platform for solid tumors. Improved understanding of the parameters influencing T cell inflammation allowed us to implement a treatment protocol that could durably regress established tumors. However, when we increased the initial tumor burden, we observed a systemic loss of antitumor immunity, enhanced cellular exhaustion, and resistance to immunotherapy. This was associated with tumor microenvironmental (TME) changes that were clinically pervasive in patients with large tumors and were predictive for worse survival outcomes. In this study, we found that histone deacetylase inhibition in conjunction with T cell therapy normalized large tumors to restore immune responses and therapeutic efficacy. This was consistent across multiple tumors and therapeutic modalities. Antitumor T cells underwent transcriptome reprogramming to enhance biological processes associated with cellular activation, which corresponded with improved proliferation and cytotoxicity. Surprisingly, we found that Tim-3 expression was markedly up-regulated but was not functionally correlated with exhaustion; rather, Tim-3hi cells shared genomic and phenotypic features of non-exhausted, terminally differentiated effector lineages. Overall, our findings reveal a novel sensitization approach for effective resolution of highly immunosuppressive large tumors.

Solid tumors are uniquely difficult to treat due to a complexity of multifactorial resistance mechanisms that are further compounded by increased tumor burden. In this study, we determined that large tumors are often driven by an accumulation of key biological pathway changes that predispose them to worse therapeutic responsiveness. In our evaluation of tumor cohort studies, patients with increased primary tumor burden were prone to these changes, which were negative prognostic factors for overall survival. Due to the prevalence of this pathway signature in multiple tumor types, the translational potential of ACT in the treatment of solid tumors may therefore hinge on the subversion of these biological processes. Fortunately, these pathways are well-studied; for instance, cholesterol accumulation, glucose and amino acid deprivation, and hypoxia are known inducers of local T cell hyporesponsiveness (Chang et al., 2015; Franco et al., 2020; Hung et al., 2021; Ma et al., 2019; Scharping et al., 2021). However, concurrent up-regulation of these processes may also facilitate systemic immunosuppressive outcomes. The systemic immune landscape during tumor development has been shown to be quite plastic (Allen et al., 2020), and thus, the prolific dissemination of immunosuppressive factors arising from pathway signature expression may impair the quality of peripheral T cell activation. In our models, we demonstrated that therapy-driven T cell expansion was rapidly ablated in large tumors, resulting in minimal T cell persistence and loss of tumor control. Ultimately, our

data suggest that large tumors worsen the dysfunctional outcomes of cellular exhaustion to enhance the severity of therapeutic resistance.

Despite this, combinatorial approaches may be capable of improving clinical outcomes in large, established tumors. One notable precedent showed that maximal antitumor efficacy could be achieved using a four-component treatment platform consisting of a tumor-targeting antibody, recombinant IL-2, PD-1-blocking antibody, and adjuvanted peptide vaccine (Moynihan et al., 2016). Therapeutic resistance can thus be overwhelmed by effective mobilization of innate and adaptive immune cells to promote broad spectrum antitumor immunity. The authors also demonstrated that concurrent targeting of tumor immunosuppression may be a necessary prerequisite for eradicating large tumors. However, our findings suggested that increased tumor burden was associated with numerous TME pathway changes that can independently promote immunosuppression. As a result, incorporating therapeutic components to target each pathway may not be logistically feasible. By contrast, epigenetic agents have emerged as an increasingly viable combinatorial option for their ability to reprogram the tumor transcriptional landscape to simultaneously affect multiple pathways of therapeutic resistance. In particular, histone deacetylase (HDAC) inhibitors are FDA approved as anti-cancer drugs but also have broad immunopotentiating effects. This includes reducing regulatory T cells, tumor-associated macrophages, and myeloid derived suppressor cells, remodeling the tumor inflammatory landscape, and promoting cross-presentation of tumor antigens (Briere et al., 2018; Li et al., 2021; Ritter et al., 2017; Shen and Pili, 2012; Truong et al., 2021). In our study, we investigated Class I HDAC inhibitor, MS-275 (Entinostat), and found that treatment of large tumors reversed most pathway changes caused by increased burden. In particular, we observed that correction of metabolic, MYC, and MTORC1 signaling was accompanied by restored inflammatory responses. Since MYC and MTORC1 are known regulators of cellular metabolism and have been linked to tumor-driven exhaustion programming (Kim et al., 2017; Topper et al., 2017), MS-275-dependent tumor normalization may prevent T cell exhaustion. Indeed, combination immunotherapy with MS-275 restored T cell fitness and therapeutic efficacy in large tumors.

In addition to tumor normalization, we provide indirect evidence to suggest that MS-275 overwrites the distinct epigenetic features of exhausted T cells to promote effector function. This may address a known issue with exhausted T cells in that intrinsic epigenetic fate inflexibility can limit the durability of reinvigoration strategies such as PD-1 blockade (Ghoneim et al., 2017; Pauken et al., 2016). T cell exhaustion is commonly defined by multiple inhibitory receptor expression (PD1, Tim-3, Lag3, CTLA4, TIGIT) (Blackburn et al., 2009), and in our study, we demonstrated that PD-1 and Tim-3 was up-regulated in transferred T cells in 14-day old tumors compared to 7-day old tumors. However, MS-275

delivery did not reduce Tim-3 expression in 14-day old tumors; rather, Tim-3 was further up-regulated and became correlated with cellular activation rather than exhaustion. Therefore, MS-275's role may not just be corrective, but potentiating as well.

Interestingly, the uncoupling of Tim-3 expression from genomic and functional signatures of cellular exhaustion may suggest that, in certain contexts, Tim-3 may not be a reliable exhaustion marker. Since Tim-3 does not inherently express an inhibitory signaling motif (Wolf et al., 2020), its regulatory role is often conditional. Binding to specific ligands like galectin 9 (Zhu et al., 2005) or co-expression with other regulatory molecules (PD1, CEACAM1) (Huang et al., 2015; Jin et al., 2010; Sakuishi et al., 2010) has been shown to confer inhibitory function. However, the ectopic expression of Tim-3 has been associated with recruitment to the immune synapse and enhanced TCR signaling in a phosphotyrosine-dependent manner (Kataoka et al., 2021; Lee et al., 2011). In our study, MS-275 selectively up-regulated Tim-3 and decorrelated its expression from PD1. Thus, it is possible that combination treatment allowed Tim-3 to exercise its co-stimulatory role to improve the quality of T cell activation and promote a divergent cellular fate. Indeed, Tim-3 expression was strongly associated with the IL-2/STAT5 signaling axis, suggesting its potential involvement in post-activation metabolic reprogramming, proliferation induction, and lineage commitment.

Exhausted T cells exist on a phenotypic continuum like many other differentiation states (Philip et al., 2017). In our study, post-vaccinated antitumor T cells derived from large tumors displayed surface marker heterogeneity while collectively enriching for gene signatures consistent with TEX and TMPEC. These include effector-like Tim3<sup>+</sup> TCF1<sup>-</sup> CD127<sup>-</sup> cells and memory-like Tim3<sup>+</sup> TCF1<sup>lo</sup> CD127<sup>+</sup> cells, which may represent different stages of cellular exhaustion such as terminally exhausted and progenitor exhausted T cells, respectively (Kallies et al., 2020; Siddiqui et al., 2019; Wu et al., 2016). Interestingly, both populations deteriorated over time, which affirmed their dysfunction within large tumors. During MS-275 treatment, T cell heterogeneity was reconciled into a polarized effector response whereby TTEC (Tim3<sup>hi</sup> TCF1<sup>-</sup> CD127<sup>-</sup> KLRG1<sup>+</sup>) was the predominant T cell population and displayed superior post vaccination proliferation and killing. Interestingly, TTEC showed gene signature enrichment for TSLEC and TEMRA, the former of which is a differentiation outcome that has been previously associated with Tim-3 co-stimulation (Avery et al., 2018). We also observed a minor T cell population with memory-like characteristics (TTMC, Tim-3<sup>hi</sup> TCF1<sup>int</sup> CD127<sup>+</sup>). Unlike memory-like Tim3<sup>+</sup> TCF1<sup>lo</sup> CD127<sup>+</sup> cells, TTMC displayed increased proliferation in association with higher Tim-3 and TCF1 expression. Similar to how others have associated the success of immune checkpoint blockade with the proliferation of stem-like tumor-infiltrating lymphocyte subsets (Kallies et al., 2020; Siddiqui et al., 2019), TTMC may represent a

stem-like, self-renewing population that can persist and repopulate TTEC to prolong antitumor immune responses. Ultimately, modulation of the epigenetic landscape may mediate conversion between exhaustion and effector/memory T cell states.

### **Acknowledgements**

Thank you to Omar Salem for the input regarding the RNA-seq and Clariom D array analyses. Y.W. was supported by the Ontario Institute for Cancer Research through funding provided by the Government of Ontario, as well as the Canadian Institutes of Health Research (FRN 123516 and FRN 152954), the Canadian Cancer Society (grant 705143), and the Terry Fox Research Institute (TFRI-1073).

### **Author Contributions**

A.N. designed and performed the majority of the experiments and wrote the manuscript. D.B. and R.K. performed animal experiments. S.R.W. constructed the viral vectors used in the study. D.B. transduced cultured TCM to express luciferase. D.L. performed the cytotoxicity assay. L.C. assisted with in vitro TCM culture and tissue processing. J.L.B. provided guidance during manuscript preparation. Y.W. supervised the study and participated in the conception of experimental designs and manuscript writing.

### **Declaration of Interests**

The authors declare no competing interests.

## References

Allen, B. M., Hiam, K. J., Burnett, C. E., Venida, A., DeBarge, R., TenVooren, I., Marquez, D. M., Cho, N. W., Carmi, Y., and Spitzer, M. H. (2020). Systemic dysfunction and plasticity of the immune macroenvironment in cancer models. *Nat Med* 26, 1125-1134.

Anastas, J. N., Zee, B. M., Kalin, J. H., Kim, M., Guo, R., Alexandrescu, S., Blanco, M. A., Giera, S., Gillespie, S. M., Das, J., et al. (2019). Re-programing Chromatin with a Bifunctional LSD1/HDAC Inhibitor Induces Therapeutic Differentiation in DIPG. *Cancer Cell* 36, 528-544 e510.

Avery, L., Filderman, J., Szymczak-Workman, A. L., and Kane, L. P. (2018). Tim-3 co-stimulation promotes short-lived effector T cells, restricts memory precursors, and is dispensable for T cell exhaustion. *Proc Natl Acad Sci U S A* 115, 2455-2460.

Barbie, D. A., Tamayo, P., Boehm, J. S., Kim, S. Y., Moody, S. E., Dunn, I. F., Schinzel, A. C., Sandy, P., Meylan, E., Scholl, C., et al. (2009). Systematic RNA interference reveals that oncogenic KRAS-driven cancers require TBK1. *Nature* 462, 108-112.

Bindea, G., Mlecnik, B., Hackl, H., Charoentong, P., Tosolini, M., Kirilovsky, A., Fridman, W. H., Pages, F., Trajanoski, Z., and Galon, J. (2009). ClueGO: a Cytoscape plug-in to decipher functionally grouped gene ontology and pathway annotation networks. *Bioinformatics* 25, 1091-1093.

Blackburn, S. D., Shin, H., Haining, W. N., Zou, T., Workman, C. J., Polley, A., Betts, M. R., Freeman, G. J., Vignali, D. A., and Wherry, E. J. (2009). Coregulation of CD8<sup>+</sup> T cell exhaustion by multiple inhibitory receptors during chronic viral infection. *Nat Immunol* 10, 29-37.

Blank, C. U., Haining, W. N., Held, W., Hogan, P. G., Kallies, A., Lugli, E., Lynn, R. C., Philip, M., Rao, A., Restifo, N. P., et al. (2019). Defining 'T cell exhaustion'. *Nat Rev Immunol* 19, 665-674.

Briere, D., Sudhakar, N., Woods, D. M., Hallin, J., Engstrom, L. D., Aranda, R., Chiang, H., Sodre, A. L., Olson, P., Weber, J. S., and Christensen, J. G. (2018). The class I/IV HDAC inhibitor mocetinostat increases tumor antigen presentation, decreases immune suppressive cell types and augments checkpoint inhibitor therapy. *Cancer Immunol Immunother* 67, 381-392.

Broad\_Institute\_TCGA\_Genome\_Data\_Analysis\_Center (2016). Firehose stddata\_2016\_01\_28 run. In Broad Institute of MIT and Harvard, (doi: 10.7908/C11G0KM9).

- Cardozo, L. E., Russo, P. S. T., Gomes-Correia, B., Araujo-Pereira, M., Sepulveda-Hermosilla, G., Maracaja-Coutinho, V., and Nakaya, H. I. (2019). webCEMiTool: Co-expression Modular Analysis Made Easy. *Front Genet* 10, 146.
- Chang, C. H., Qiu, J., O'Sullivan, D., Buck, M. D., Noguchi, T., Curtis, J. D., Chen, Q., Gindin, M., Gubin, M. M., van der Windt, G. J., et al. (2015). Metabolic Competition in the Tumor Microenvironment Is a Driver of Cancer Progression. *Cell* 162, 1229-1241.
- Cheng, Y., He, C., Wang, M., Ma, X., Mo, F., Yang, S., Han, J., and Wei, X. (2019). Targeting epigenetic regulators for cancer therapy: mechanisms and advances in clinical trials. *Signal Transduct Target Ther* 4, 62.
- Deng, M., Bragelmann, J., Kryukov, I., Saraiva-Agostinho, N., and Perner, S. (2017). FirebrowseR: an R client to the Broad Institute's Firehose Pipeline. *Database (Oxford)* 2017.
- Ferris, R. L., Lu, B., and Kane, L. P. (2014). Too much of a good thing? Tim-3 and TCR signaling in T cell exhaustion. *J Immunol* 193, 1525-1530.
- Franco, F., Jaccard, A., Romero, P., Yu, Y. R., and Ho, P. C. (2020). Metabolic and epigenetic regulation of T-cell exhaustion. *Nat Metab* 2, 1001-1012.
- Ghoneim, H. E., Fan, Y., Moustaki, A., Abdelsamed, H. A., Dash, P., Dogra, P., Carter, R., Awad, W., Neale, G., Thomas, P. G., and Youngblood, B. (2017). De Novo Epigenetic Programs Inhibit PD-1 Blockade-Mediated T Cell Rejuvenation. *Cell* 170, 142-157 e119.
- Hammill, J. A., VanSeggelen, H., Helsen, C. W., Denisova, G. F., Eveleigh, C., Tantaló, D. G., Bassett, J. D., and Bramson, J. L. (2015). Designed ankyrin repeat proteins are effective targeting elements for chimeric antigen receptors. *J Immunother Cancer* 3, 55.
- Hanson, H. L., Donermeyer, D. L., Ikeda, H., White, J. M., Shankaran, V., Old, L. J., Shiku, H., Schreiber, R. D., and Allen, P. M. (2000). Eradication of established tumors by CD8<sup>+</sup> T cell adoptive immunotherapy. *Immunity* 13, 265-276.
- Hegde, S., Krisnawan, V. E., Herzog, B. H., Zuo, C., Breden, M. A., Knolhoff, B. L., Hogg, G. D., Tang, J. P., Baer, J. M., Mpooy, C., et al. (2020). Dendritic Cell Paucity Leads to Dysfunctional Immune Surveillance in Pancreatic Cancer. *Cancer Cell* 37, 289-307 e289.
- Herndler-Brandstetter, D., Ishigame, H., Shinnakasu, R., Plajer, V., Stecher, C., Zhao, J., Lietzenmayer, M., Kroehling, L., Takumi, A., Kometani, K., et al. (2018). KLRG1(+) Effector CD8(+) T Cells Lose KLRG1, Differentiate into All Memory T Cell Lineages, and Convey Enhanced Protective Immunity. *Immunity* 48, 716-729 e718.

- Huang, A. C., Postow, M. A., Orlowski, R. J., Mick, R., Bengsch, B., Manne, S., Xu, W., Harmon, S., Giles, J. R., Wenz, B., et al. (2017). T-cell invigoration to tumour burden ratio associated with anti-PD-1 response. *Nature* 545, 60-65.
- Huang, Y. H., Zhu, C., Kondo, Y., Anderson, A. C., Gandhi, A., Russell, A., Dougan, S. K., Petersen, B. S., Melum, E., Pertel, T., et al. (2015). CEACAM1 regulates TIM-3-mediated tolerance and exhaustion. *Nature* 517, 386-390.
- Hung, M. H., Lee, J. S., Ma, C., Diggs, L. P., Heinrich, S., Chang, C. W., Ma, L., Forgues, M., Budhu, A., Chaisaingmongkol, J., et al. (2021). Tumor methionine metabolism drives T-cell exhaustion in hepatocellular carcinoma. *Nat Commun* 12, 1455.
- Ikeda, H., Ohta, N., Furukawa, K., Miyazaki, H., Wang, L., Kuribayashi, K., Old, L. J., and Shiku, H. (1997). Mutated mitogen-activated protein kinase: a tumor rejection antigen of mouse sarcoma. *Proc Natl Acad Sci U S A* 94, 6375-6379.
- Jiang, Y., Li, Y., and Zhu, B. (2015). T-cell exhaustion in the tumor microenvironment. *Cell Death Dis* 6, e1792.
- Jin, H. T., Anderson, A. C., Tan, W. G., West, E. E., Ha, S. J., Araki, K., Freeman, G. J., Kuchroo, V. K., and Ahmed, R. (2010). Cooperation of Tim-3 and PD-1 in CD8 T-cell exhaustion during chronic viral infection. *Proc Natl Acad Sci U S A* 107, 14733-14738.
- Joshi, N. S., Cui, W., Chandele, A., Lee, H. K., Urso, D. R., Hagman, J., Gapin, L., and Kaech, S. M. (2007). Inflammation directs memory precursor and short-lived effector CD8(+) T cell fates via the graded expression of T-bet transcription factor. *Immunity* 27, 281-295.
- Kallies, A., Zehn, D., and Utzschneider, D. T. (2020). Precursor exhausted T cells: key to successful immunotherapy? *Nat Rev Immunol* 20, 128-136.
- Kataoka, S., Manandhar, P., Lee, J., Workman, C. J., Banerjee, H., Szymczak-Workman, A. L., Kvorjak, M., Lohmueller, J., and Kane, L. P. (2021). The costimulatory activity of Tim-3 requires Akt and MAPK signaling and its recruitment to the immune synapse. *Sci Signal* 14.
- Khan, O., Giles, J. R., McDonald, S., Manne, S., Ngiow, S. F., Patel, K. P., Werner, M. T., Huang, A. C., Alexander, K. A., Wu, J. E., et al. (2019). TOX transcriptionally and epigenetically programs CD8(+) T cell exhaustion. *Nature* 571, 211-218.
- Kim, L. C., Cook, R. S., and Chen, J. (2017). mTORC1 and mTORC2 in cancer and the tumor microenvironment. *Oncogene* 36, 2191-2201.



- Kim, S. I., Cassella, C. R., and Byrne, K. T. (2020). Tumor Burden and Immunotherapy: Impact on Immune Infiltration and Therapeutic Outcomes. *Front Immunol* 11, 629722.
- Klebanoff, C. A., Gattinoni, L., Palmer, D. C., Muranski, P., Ji, Y., Hinrichs, C. S., Borman, Z. A., Kerkar, S. P., Scott, C. D., Finkelstein, S. E., et al. (2011). Determinants of successful CD8<sup>+</sup> T-cell adoptive immunotherapy for large established tumors in mice. *Clin Cancer Res* 17, 5343-5352.
- Knaus, H. A., Berglund, S., Hackl, H., Blackford, A. L., Zeidner, J. F., Montiel-Esparza, R., Mukhopadhyay, R., Vanura, K., Blazar, B. R., Karp, J. E., et al. (2018). Signatures of CD8<sup>+</sup> T cell dysfunction in AML patients and their reversibility with response to chemotherapy. *JCI Insight* 3.
- Kucera, M., Isserlin, R., Arkhangorodsky, A., and Bader, G. D. (2016). AutoAnnotate: A Cytoscape app for summarizing networks with semantic annotations. *F1000Res* 5, 1717.
- Landsberg, J., Kohlmeyer, J., Renn, M., Bald, T., Rogava, M., Cron, M., Fatho, M., Lennerz, V., Wolfel, T., Holzels, M., and Tuting, T. (2012). Melanomas resist T-cell therapy through inflammation-induced reversible dedifferentiation. *Nature* 490, 412-416.
- Law, C. W., Chen, Y., Shi, W., and Smyth, G. K. (2014). voom: Precision weights unlock linear model analysis tools for RNA-seq read counts. *Genome Biol* 15, R29.
- Lee, J., Su, E. W., Zhu, C., Hainline, S., Phuah, J., Moroco, J. A., Smithgall, T. E., Kuchroo, V. K., and Kane, L. P. (2011). Phosphotyrosine-dependent coupling of Tim-3 to T-cell receptor signaling pathways. *Mol Cell Biol* 31, 3963-3974.
- Li, X., Su, X., Liu, R., Pan, Y., Fang, J., Cao, L., Feng, C., Shang, Q., Chen, Y., Shao, C., and Shi, Y. (2021). HDAC inhibition potentiates anti-tumor activity of macrophages and enhances anti-PD-L1-mediated tumor suppression. *Oncogene* 40, 1836-1850.
- Liberzon, A., Birger, C., Thorvaldsdottir, H., Ghandi, M., Mesirov, J. P., and Tamayo, P. (2015). The Molecular Signatures Database (MSigDB) hallmark gene set collection. *Cell Syst* 1, 417-425.
- Lin, J. H., Huffman, A. P., Wattenberg, M. M., Walter, D. M., Carpenter, E. L., Feldser, D. M., Beatty, G. L., Furth, E. E., and Vonderheide, R. H. (2020). Type 1 conventional dendritic cells are systemically dysregulated early in pancreatic carcinogenesis. *J Exp Med* 217.
- Ma, X., Bi, E., Lu, Y., Su, P., Huang, C., Liu, L., Wang, Q., Yang, M., Kalady, M. F., Qian, J., et al. (2019). Cholesterol Induces CD8<sup>(+)</sup> T Cell Exhaustion in the Tumor Microenvironment. *Cell Metab*.

- Mardiana, S., Solomon, B. J., Darcy, P. K., and Beavis, P. A. (2019). Supercharging adoptive T cell therapy to overcome solid tumor-induced immunosuppression. *Sci Transl Med* 11.
- McCaw, T. R., Li, M., Starenki, D., Liu, M., Cooper, S. J., Arend, R. C., Forero, A., Buchsbaum, D. J., and Randall, T. D. (2019). Histone deacetylase inhibition promotes intratumoral CD8(+) T-cell responses, sensitizing murine breast tumors to anti-PD1. *Cancer Immunol Immunother* 68, 2081-2094.
- Merico, D., Isserlin, R., Stueker, O., Emili, A., and Bader, G. D. (2010). Enrichment map: a network-based method for gene-set enrichment visualization and interpretation. *PLoS One* 5, e13984.
- Mootha, V. K., Lindgren, C. M., Eriksson, K. F., Subramanian, A., Sihag, S., Lehar, J., Puigserver, P., Carlsson, E., Ridderstrale, M., Laurila, E., et al. (2003). PGC-1 $\alpha$ -responsive genes involved in oxidative phosphorylation are coordinately downregulated in human diabetes. *Nat Genet* 34, 267-273.
- Morotti, M., Albukhari, A., Alsaadi, A., Artibani, M., Brenton, J. D., Curbishley, S. M., Dong, T., Dustin, M. L., Hu, Z., McGranahan, N., et al. (2021). Promises and challenges of adoptive T-cell therapies for solid tumours. *Br J Cancer* 124, 1759-1776.
- Mostafavi, S., Ray, D., Warde-Farley, D., Grouios, C., and Morris, Q. (2008). GeneMANIA: a real-time multiple association network integration algorithm for predicting gene function. *Genome Biol* 9 Suppl 1, S4.
- Moynihan, K. D., Opel, C. F., Szeto, G. L., Tzeng, A., Zhu, E. F., Engreitz, J. M., Williams, R. T., Rakhra, K., Zhang, M. H., Rothschilds, A. M., et al. (2016). Eradication of large established tumors in mice by combination immunotherapy that engages innate and adaptive immune responses. *Nat Med* 22, 1402-1410.
- Nguyen, A., Ho, L., Workenhe, S. T., Chen, L., Samson, J., Walsh, S. R., Pol, J., Bramson, J. L., and Wan, Y. (2018). HDACi Delivery Reprograms Tumor-Infiltrating Myeloid Cells to Eliminate Antigen-Loss Variants. *Cell Rep* 24, 642-654.
- Nguyen, A., Salem, O., and Wan, Y. (2021). Functional Analysis of Tumor-Infiltrating Myeloid Cells by Flow Cytometry and Adoptive Transfer. *J Vis Exp*.
- Pan, X., and Zheng, L. (2020). Epigenetics in modulating immune functions of stromal and immune cells in the tumor microenvironment. *Cell Mol Immunol* 17, 940-953.

- Pauken, K. E., Sammons, M. A., Odorizzi, P. M., Manne, S., Godec, J., Khan, O., Drake, A. M., Chen, Z., Sen, D. R., Kurachi, M., et al. (2016). Epigenetic stability of exhausted T cells limits durability of reinvigoration by PD-1 blockade. *Science* 354, 1160-1165.
- Philip, M., Fairchild, L., Sun, L., Horste, E. L., Camara, S., Shakiba, M., Scott, A. C., Viale, A., Lauer, P., Merghoub, T., et al. (2017). Chromatin states define tumour-specific T cell dysfunction and reprogramming. *Nature* 545, 452-456.
- Piranlioglu, R., Lee, E., Ouzounova, M., Bollag, R. J., Vinyard, A. H., Arbab, A. S., Marasco, D., Guzel, M., Cowell, J. K., Thangaraju, M., et al. (2019). Primary tumor-induced immunity eradicates disseminated tumor cells in syngeneic mouse model. *Nat Commun* 10, 1430.
- Prato, S., Zhan, Y., Mintern, J. D., and Villadangos, J. A. (2013). Rapid deletion and inactivation of CTLs upon recognition of a number of target cells over a critical threshold. *J Immunol* 191, 3534-3544.
- Prevost-Blondel, A., Zimmermann, C., Stemmer, C., Kulmburg, P., Rosenthal, F. M., and Pircher, H. (1998). Tumor-infiltrating lymphocytes exhibiting high ex vivo cytolytic activity fail to prevent murine melanoma tumor growth in vivo. *J Immunol* 161, 2187-2194.
- Rabinovich, B. A., Ye, Y., Etto, T., Chen, J. Q., Levitsky, H. I., Overwijk, W. W., Cooper, L. J., Gelovani, J., and Hwu, P. (2008). Visualizing fewer than 10 mouse T cells with an enhanced firefly luciferase in immunocompetent mouse models of cancer. *Proc Natl Acad Sci U S A* 105, 14342-14346.
- Reich, M., Liefeld, T., Gould, J., Lerner, J., Tamayo, P., and Mesirov, J. P. (2006). GenePattern 2.0. *Nat Genet* 38, 500-501.
- Restifo, N. P., Smyth, M. J., and Snyder, A. (2016). Acquired resistance to immunotherapy and future challenges. *Nat Rev Cancer* 16, 121-126.
- Ritter, C., Fan, K., Paschen, A., Reker Hardrup, S., Ferrone, S., Nghiem, P., Ugurel, S., Schrama, D., and Becker, J. C. (2017). Epigenetic priming restores the HLA class-I antigen processing machinery expression in Merkel cell carcinoma. *Sci Rep* 7, 2290.
- Russo, P. S. T., Ferreira, G. R., Cardozo, L. E., Burger, M. C., Arias-Carrasco, R., Maruyama, S. R., Hirata, T. D. C., Lima, D. S., Passos, F. M., Fukutani, K. F., et al. (2018). CEMiTool: a Bioconductor package for performing comprehensive modular co-expression analyses. *BMC Bioinformatics* 19, 56.

Sakuishi, K., Apetoh, L., Sullivan, J. M., Blazar, B. R., Kuchroo, V. K., and Anderson, A. C. (2010). Targeting Tim-3 and PD-1 pathways to reverse T cell exhaustion and restore anti-tumor immunity. *J Exp Med* 207, 2187-2194.

Scharping, N. E., Rivadeneira, D. B., Menk, A. V., Vignali, P. D. A., Ford, B. R., Rittenhouse, N. L., Peralta, R., Wang, Y., Wang, Y., DePeaux, K., et al. (2021). Mitochondrial stress induced by continuous stimulation under hypoxia rapidly drives T cell exhaustion. *Nat Immunol* 22, 205-215.

Shannon, P., Markiel, A., Ozier, O., Baliga, N. S., Wang, J. T., Ramage, D., Amin, N., Schwikowski, B., and Ideker, T. (2003). Cytoscape: a software environment for integrated models of biomolecular interaction networks. *Genome Res* 13, 2498-2504.

Shen, L., and Pili, R. (2012). Class I histone deacetylase inhibition is a novel mechanism to target regulatory T cells in immunotherapy. *Oncoimmunology* 1, 948-950.

Siddiqui, I., Schaeuble, K., Chennupati, V., Fuertes Marraco, S. A., Calderon-Copete, S., Pais Ferreira, D., Carmona, S. J., Scarpellino, L., Gfeller, D., Pradervand, S., et al. (2019). Intratumoral Tcf1(+)PD-1(+)CD8(+) T Cells with Stem-like Properties Promote Tumor Control in Response to Vaccination and Checkpoint Blockade Immunotherapy. *Immunity* 50, 195-211 e110.

Smith, F. O., Klapper, J. A., Wunderlich, J. R., Rosenberg, S. A., and Dudley, M. E. (2009). Impact of a recombinant fowlpox vaccine on the efficacy of adoptive cell therapy with tumor infiltrating lymphocytes in a patient with metastatic melanoma. *J Immunother* 32, 870-874.

Subramanian, A., Tamayo, P., Mootha, V. K., Mukherjee, S., Ebert, B. L., Gillette, M. A., Paulovich, A., Pomeroy, S. L., Golub, T. R., Lander, E. S., and Mesirov, J. P. (2005). Gene set enrichment analysis: a knowledge-based approach for interpreting genome-wide expression profiles. *Proc Natl Acad Sci U S A* 102, 15545-15550.

Thommen, D. S., and Schumacher, T. N. (2018). T Cell Dysfunction in Cancer. *Cancer Cell* 33, 547-562.

Topper, M. J., Vaz, M., Chiappinelli, K. B., DeStefano Shields, C. E., Niknafs, N., Yen, R. C., Wenzel, A., Hicks, J., Ballew, M., Stone, M., et al. (2017). Epigenetic Therapy Ties MYC Depletion to Reversing Immune Evasion and Treating Lung Cancer. *Cell* 171, 1284-1300 e1221.

Truong, A. S., Zhou, M., Krishnan, B., Utsumi, T., Manocha, U., Stewart, K. G., Beck, W., Rose, T. L., Milowsky, M. I., He, X., et al. (2021). Entinostat induces antitumor immune responses through immune editing of tumor neoantigens. *J Clin Invest* 131.

- Van der Maaten, L. J. P., and Hinton, G. E. (2008). Visualizing High-Dimensional Data Using t-SNE. *Journal of Machine Learning Research* 9(Nov), 2579-2605.
- Van Gassen, S., Callebaut, B., Van Helden, M. J., Lambrecht, B. N., Demeester, P., Dhaene, T., and Saeys, Y. (2015). FlowSOM: Using self-organizing maps for visualization and interpretation of cytometry data. *Cytometry A* 87, 636-645.
- Wagner, J., Wickman, E., DeRenzo, C., and Gottschalk, S. (2020). CAR T Cell Therapy for Solid Tumors: Bright Future or Dark Reality? *Mol Ther* 28, 2320-2339.
- Walsh, S. R., Simovic, B., Chen, L., Bastin, D., Nguyen, A., Stephenson, K., Mandur, T. S., Bramson, J. L., Lichty, B. D., and Wan, Y. (2019). Endogenous T cells prevent tumor immune escape following adoptive T cell therapy. *J Clin Invest* 129, 5400-5410.
- Wen, F. T., Thisted, R. A., Rowley, D. A., and Schreiber, H. (2012). A systematic analysis of experimental immunotherapies on tumors differing in size and duration of growth. *Oncoimmunology* 1, 172-178.
- Wherry, E. J., Ha, S. J., Kaech, S. M., Haining, W. N., Sarkar, S., Kalia, V., Subramaniam, S., Blattman, J. N., Barber, D. L., and Ahmed, R. (2007). Molecular signature of CD8+ T cell exhaustion during chronic viral infection. *Immunity* 27, 670-684.
- Wherry, E. J., and Kurachi, M. (2015). Molecular and cellular insights into T cell exhaustion. *Nat Rev Immunol* 15, 486-499.
- Wolf, Y., Anderson, A. C., and Kuchroo, V. K. (2020). TIM3 comes of age as an inhibitory receptor. *Nat Rev Immunol* 20, 173-185.
- Wu, T., Ji, Y., Moseman, E. A., Xu, H. C., Manglani, M., Kirby, M., Anderson, S. M., Handon, R., Kenyon, E., Elkahloun, A., et al. (2016). The TCF1-Bcl6 axis counteracts type I interferon to repress exhaustion and maintain T cell stemness. *Sci Immunol* 1.
- Xin Yu, J., Hubbard-Lucey, V. M., and Tang, J. (2019). The global pipeline of cell therapies for cancer. *Nat Rev Drug Discov* 18, 821-822.
- Zhang, L., Bridle, B. W., Chen, L., Pol, J., Spaner, D., Boudreau, J. E., Rosen, A., Bassett, J. D., Lichty, B. D., Bramson, J. L., and Wan, Y. (2013). Delivery of viral-vectored vaccines by B cells represents a novel strategy to accelerate CD8(+) T-cell recall responses. *Blood* 121, 2432-2439.
- Zhou, Z., Cheng, Y., Jiang, Y., Liu, S., Zhang, M., Liu, J., and Zhao, Q. (2018). Ten hub genes associated with progression and prognosis of pancreatic carcinoma identified by co-expression analysis. *Int J Biol Sci* 14, 124-136.

Zhu, C., Anderson, A. C., Schubart, A., Xiong, H., Imitola, J., Khoury, S. J., Zheng, X. X., Strom, T. B., and Kuchroo, V. K. (2005). The Tim-3 ligand galectin-9 negatively regulates T helper type 1 immunity. *Nat Immunol* 6, 1245-1252.

## Main Figure Titles and Legends

### **Figure 1: Tumor burden potentiates immunotherapeutic resistance and decreased clinical outcomes through the expression of a unique pathway signature**

BALB/c mice were implanted i.d. with CMS5 tumor cells and allowed to grow for 7 or 14 days. Mice were treated with adoptive cell therapy (ACT) consisting of transferred TCM<sup>-</sup>-cultured DUC18 T cells and vaccination with VSV $\Delta$ M51-mERK2136–144.

(A) Tumor volume in 7-day or 14-day tumors left un-treated or treated with ACT.

(B) Fraction of mice that did not reach endpoint (decreased body condition). No palpable tumors were observed in surviving mice.

(C, D) Frequency of mERK2136–144-specific CD8<sup>+</sup> T cells as determined by ex vivo peptide stimulation and IFN $\gamma$  staining 5 days after vaccination. (D) 14-day tumors were surgically removed 24 hours prior to ACT.

(E) PCA was performed on TMM-normalized counts for bulk tumor RNA-seq samples derived from un-treated tumors.

(F-H) GSEA showing enriched pathways in 7-day (negative enrichment score) or 14-day tumors (positive enrichment score). Analyzed using the MSigDB (F) Hallmark, (G) Curated (C2), and (H) Ontology (C5) gene set collections. (G, H) Enrichment Map and AutoAnnotate were used to identify clusters of enriched gene sets.

(I) Using the MSigDB Hallmark gene set collection, GSEA was used to enrich pathways in SKCM patients stratified by tumor size/extent (T1, negative enrichment score; T4, positive enrichment score). Emphasized pathways were also enriched in the 14-day vs 7-day tumor comparison.

(J) Hierarchically-clustered heatmap of single-sample GSEA (ssGSEA)-determined enrichment scores for each patient in the T1/T4 training set using the commonly enriched pathways, forming a pathway signature.

(K) Multivariate Cox regression analysis was used to create risk scores for survival prediction. The distribution of risk scores within the T1/T4 training set allowed for patient stratification into low- and high-risk groups based on the median value.

(L) Kaplan-Meier curves of overall survival of the low- and high-risk groups.

(M-O) ROC curve for tumor burden prediction by pathway signature and corresponding Kaplan-Meier curve of overall survival based on tumor burden (T1/T4). (M) SKCM as well

as (N, O) two additional representative TCGA tumor types HNSC and BRCA were analyzed.

Data in (A-C) are representative of at least 3 experiments with  $n = 5$  mice per group. Data in (D) was obtained with  $n = 5$  mice per group. Data in (E-H) utilized  $n = 3$  mice per group and statistical significance was defined at (F, I)  $FDR < 0.05$  or (G, H)  $FDR < 0.001$ . Error bars are SEM and statistics were based on log rank test, unpaired T-test, or one-way ANOVA test.

**Figure 2: MS275 promotes tissue homeostasis and in conjunction with ACT restores therapeutic efficacy in large, immunosuppressive tumors**

(A-C) Bulk tumor RNA-seq samples were derived from MS-275-treated 14-day tumors. (A) Using the MSigDB Hallmark gene set collection, GSEA was used to enrich pathways in un-treated (negative enrichment score) or MS-275-treated tumors (positive enrichment score). Corresponding pathways in the 14-day vs 7-day tumor comparison were enriched in the opposing direction.

(B) Pie charts illustrating total enriched gene sets from the complete MSigDB collection.

(C) Venn diagram showing the number of overlapping enriched gene sets. Pie charts were used to show the direction of enrichment for overlapped gene sets.

(D-F) BALB/c mice were implanted i.d. with CMS5 tumor cells and allowed to grow for 7 or 14 days. Mice were treated with ACT with or without concomitant MS-275 delivery. (D) Tumor volume and (E) overall survival curves were plotted. (F) Frequency of mERK2136–144-specific CD8<sup>+</sup> T cells with tumor-free controls.

(G-I) C57BL/6 mice were implanted i.d. with MC38-gp33 tumor cells and treated with VSV $\Delta$ M51-gp33 with or without MS-275 delivery. VSV $\Delta$ M51-GFP was used as a vector control. (D) Tumor volume, (E) overall survival, and (F) frequency of LCMV GP33-41-specific CD8<sup>+</sup> T cells.

Data in (A-C) utilized  $n = 3$  mice per group and statistical significance was defined at (A)  $FDR < 0.05$  or (B, C)  $FDR < 0.001$ . Data in (D-I) are representative of at least 2 experiments with  $n = 5$  mice per group. Error bars are SEM and statistics were based on log rank test or one-way ANOVA test.

**Figure 3: T cell reinvigoration is associated with increased proliferation and cytotoxicity**



(A-B) TCM<sup>-</sup>-cultured DUC18 T cells were transduced to express luciferase prior to ACT and monitored post-vaccination by in vivo imaging. (A) Representative images were selected to illustrate T cell accumulation and persistence for each treatment group. (B) Selective gating of the tumor region for quantitation of local T cell inflammation.

(C) Frequency of mERK2136–144-specific CD8<sup>+</sup> T cells over time.

(D-J) Transferred Thy1.1<sup>+</sup> congenic TCM were analyzed 4.5 days post-vaccination and stained for markers of (D, E) proliferation, cell death, and (J-I) polyfunctionality. Fluorescence intensity was determined by geometric mean. (J) Thy1.1<sup>+</sup> cells were positively enriched from bulk splenocytes and co-cultured with dye-labeled target cells. Percent lysis was determined relative to ‘target-only’ controls.

Data in (A, B) are representative of at least 2 experiments with n = 3 mice per group. Data in (C) was obtained with n = 5 mice per group. Data in (D-J) are representative of at least 2 experiments with n = 4-5 per group. Error bars are SEM and statistics were based on unpaired T-test or one-way ANOVA test.

#### **Figure 4: T cell whole transcriptome analysis reveals enhanced activation-dependent signaling**

Transferred T cells were flow sorted from bulk splenocytes in 14-day MC38-gp33 tumor-bearing mice 4.5 days post-vaccination. RNA samples were analyzed by Clariom D microarray.

(A) PCA was performed on SST-RMA-normalized signal values.

(B) Using the MSigDB Hallmark gene set collection, GSEA was used to enrich pathways in ACT-treated (negative enrichment score) or ACT+MS-275-treated tumors (positive enrichment score).

(C) CEMiTool was used to perform weighted gene-centric network analysis and identify modules of co-expressed genes. Graphs demonstrate median gene expression per module across treatment groups.

(D) Using the module gene sets, GSEA was used to enrich pathways in ACT-treated (negative enrichment score) or ACT+MS-275-treated tumors (positive enrichment score).

(E, F) ClueGO was used to perform Gene Ontology Biological Processes (GOBP) pathway analysis for the M2 module. (E) Overrepresented pathways were functionally clustered. (F) Pie chart detailing the percentage of overrepresented pathways per cluster.

(G) CEMiTool-defined hub genes visualized with other M2 genes in a protein-protein interaction (PPI) network. Additional genes were identified based on the degree of physical interactivity within the module.

(H) Fold change in hub gene expression when comparing ACT+MS-275- to ACT-treated T cells.

(I) Hierarchially-clustered heatmap of ssGSEA-determined enrichment scores using the MSigDB Hallmark gene set collection.

(J) Hierarchical clustering matrix of pairwise correlated pathway enrichment scores and hub gene expression values derived from the ACT+MS-275 sample group. A black square was used to represent a correlated cluster of hub genes and pathways. A white square was used to indicate high gene-pathway correlation involving HAVCR2.

(K) Scatter plots showing correlation between Hallmark pathways and HAVCR2 gene expression.

Data in Figure 4 was obtained with  $n = 5$  mice per group. Statistical significance in (B, D) was defined at  $FDR < 0.05$ . All pathways in (E, F) are at least  $p < 0.05$ .

**Figure 5: Tim-3 up-regulation is associated with reduced exhaustion and polarization towards terminal effector lineage differentiation**

(A-C) Transferred Thy1.1+ congenic TCM were analyzed 4.5 days post-vaccination and stained for typical markers of exhaustion. Fluorescence intensity was determined by (A, B) geometric mean or (C) median.

(D) Scatter plot showing correlation between T cell exhaustion signature and HAVCR2 gene expression for ACT or ACT+MS-275 treatment.

(E) GSEA plots of enriched T cell signatures in ACT+MS-275- vs ACT-treated T cells.

(F-J) tSNE visualization and flowSOM clustering of transferred T cells was created by subsampling and concatenating events from all ACT±MS-275-treated samples. (F) FlowSOM clusters were identified and colored. (G) Visualization separated by treatment group. Protein expression levels of lineage differentiation markers were (G) overlaid onto the tSNE map and (H) used by flowSOM to create hierarchically clustered populations with unique phenotypes. (J) Frequencies of flowSOM populations in each treatment group.

(G) Flow cytometry gating strategy to identify effector-like T cells in ACT±MS-275-treated samples.

(H) Frequency of KLRG1+ cells within effector-like T cell populations.

Data in (A-C) are representative of at least 2 experiments with  $n = 4-5$  mice per group. Data in (D-L) was obtained with  $n = 5$  mice per group and statistical significance in (E) was defined at  $FDR < 0.05$ . Error bars are SEM and statistics were based on unpaired T-test or one-way ANOVA test.

### **Main Table Titles and Legends**

**Table 1: Cox regression analysis of prognostic factors for SKCM T1/T4 patients**

## **STAR Methods**

### **Study design**

The overall objective of the study was to determine how epigenetic modification during adoptive T-cell therapy can reinvigorate exhausted T cell responses in large, immunosuppressive tumors. The *in vivo* experiments were used to examine the immunosuppressive effect of increased tumor burden, the therapeutic benefit of histone deacetylase inhibitor delivery, and the functional improvements to antitumor T cells. *In vivo* studies were performed with female, age-matched (6-8 weeks old) mice. Tumor-challenged mice were randomized prior to blinded treatments. Tumor growth was monitored and measured with calipers. Tumor volume was calculated as the width times the length times the depth. Mice were monitored for signs of distress and humane endpoints were determined by decreased body condition. Veterinary staff monitored mice daily and alerted researchers when a humane endpoint had been reached. All animal studies complied with the Canadian Council on Animal Care guidelines and were approved by McMaster University's Animal Research Ethics Board.

### **Animals**

C57BL/6 and BALB/C mice were purchased from Charles River Laboratories and B6.Cg-TcratmlMom Tg(TcrLCMV)327Sdz (P14) mice were purchased from Taconic. DUC18 mice were provided by Lyse Norian (University of Iowa, Iowa City, Iowa, USA) (Hanson et al., 2000). Mice were housed in a pathogen-free room in the Central Animal Facility at McMaster University.

### **Viral vectors**

Recombinant VSV $\Delta$ M51 was engineered to express an H-2Kd-restricted epitope corresponding to amino acids 136–144 of a mutated ERK2 protein (mERK2136–144), denoted as VSV $\Delta$ M51-mERK2 (Walsh et al., 2019). VSV $\Delta$ M51-gp33 expresses the dominant CD8<sup>+</sup> and CD4<sup>+</sup> T cell epitopes of the lymphocytic choriomeningitis virus glycoprotein (LCMV GP33–41 and LCMV GP61–80, respectively) in a minigene cassette (Zhang et al., 2013).

### **Peptides**

Peptides for mERK2136–144 (QYIHSANVL) and LCMV GP33–41 (KAVYNFATM) were purchased from Biomer Technologies and dissolved in PBS supplemented with 0.5% BSA.

### **Cell lines and tumor challenge**

All cells were maintained at 37°C in a humidified atmosphere with 5% CO<sub>2</sub>. CMS5 (a gift from Lyse Norian) (Ikeda et al., 1997), were cultured in DMEM supplemented with 10% FBS, penicillin/streptomycin (100 U/mL and 100 ng/mL, respectively), and 2 mM l-glutamine (Thermo Fisher Scientific). MC38-gp33 cells (MC38 cells stably transfected with a minigene corresponding to the GP33–41 peptide) (Prevost-Blondel et al., 1998) were maintained in MEM/F11 containing 10% FBS, 2 mM l-glutamine, 5 ml sodium pyruvate, 5 mL nonessential amino acids, 5 mL vitamin solution (Thermo Fisher Scientific), 55 µM 2-mercaptoethanol (Sigma-Aldrich), 100 U/mL penicillin, and 100 ng/ml streptomycin.

Tumor cells were washed twice with PBS and re-suspended in PBS at a concentration of 106 cells/30 µL for CMS5 cells or 105 cells/30 µL for MC38-gp33 cells. Mice were challenged via i.d. injection, and tumors were allowed to grow to a mean volume of ≤150 mm<sup>3</sup> (7-day old) or ≥600 mm<sup>3</sup> (14-day old) prior to treatment.

### **Surgical resection of tumors**

Primary tumors were surgically resected as described (Piranlioglu et al., 2019). Using a scalpel, an incision was made around the tumor mass, which was then carefully removed. Arteries supplying the tumor were cauterized and skin flaps were sutured by metal clips.

### **In vitro TCM differentiation**

Bulk splenocytes from TCR transgenic mice were isolated and cultured for 7 days in RPMI 1640 (GIBCO) supplemented with 10% FBS, penicillin-streptomycin (100 U/ml and 100 ng/ml, respectively), l-glutamine (2 mM), and 2-mercaptoethanol (55 µM). Splenocytes were stimulated with 100 ng/ml mERK2136–144 or LCMV GP33–41 peptide (Biomer Technologies) in the presence of 10 ng/ml IL-15, 10 ng/ml IL-21 (BioLegend), and 20 ng/ml rapamycin (Sigma-Aldrich).

### **Luciferase transduction**

Retrovirus encoding Luciferase (RV2011oFL) (Rabinovich et al., 2008) was prepared and concentrated as previously described (Hammill et al., 2015) and supplemented with 20ug/mL lipofectamine 2000 (Invitrogen) and 16ug/mL polybrene (ABM) for transduction. DUC18 splenocytes were resuspended at  $2 \times 10^6$ /mL in T cell culture media lacking cytokine and inhibitor additives and transduced with RV2011oFL via spinfection before incubation at 37°C for 2 hours. Cells were then utilized for TCM culture. In vivo monitoring of transferred cells was conducted using an IVIS Spectrum In Vivo Imaging System (Caliper Life Sciences) following intraperitoneal injection of 75 mg/kg D-luciferin (Caliper Life Sciences).

### **Adoptive cell therapy**

In vitro-differentiated TCR transgenic CD8<sup>+</sup> TCM were injected i.v. into mice at a dose of  $10^6$  cells/200  $\mu$ L of PBS. After 24 hours, mice were treated i.v. with VSV $\Delta$ M51-mERK2 or VSV $\Delta$ M51-gp33 at  $2 \times 10^8$  pfu. Concomitantly, MS-275 (Sigma-Aldrich) was injected i.p. (100  $\mu$ g/mouse in 50  $\mu$ L PBS) daily for 5 days.

### **Tumor digestion**

For RNA extraction: Tumors were excised, snap-frozen in liquid nitrogen, and homogenized in Trizol (Invitrogen). RNA was extracted and purified using a RNeasy mini kit (QIAGEN).

For T cell studies: Tumors were excised and digested in 0.5 mg/mL collagenase type IV (GIBCO), 0.2 mg/mL DNase (Roche), and 5 mM calcium chloride prepared in RPMI-1640 (GIBCO) supplemented with 10% FBS, penicillin-streptomycin (100 U/ml and 100 ng/ml) and incubated at 37°C with 200 rpm agitation for 30 min on a temperature-controlled orbital shaker. Digestion was neutralized with two volumes of cold RPMI-1640 with 10% FBS and 2 mM ethylenediamine tetraacetic acid (EDTA), and refrigerated for 10 min at 4 °C. Samples were filtered with a 40  $\mu$ m strainer, centrifuged ( $500 \times g$ , 4°C), and re-suspended in PBS with 2% FBS and 1 mM EDTA.

### **Spleen and blood processing**

Harvested spleens were mechanically dissociated with a syringe plunger and treated with ACK lysis buffer (GIBCO) to remove red blood cells. Blood samples were similarly treated

with ACK lysis buffer to extract PBMCs. Cells were re-suspended in PBS with 2% FBS and 1 mM EDTA.

### **T cell enrichment**

For RNA extraction: Re-suspended cells were stained for CD8, Thy1.1, and viability (see below). Stained cells were centrifuged ( $500 \times g$ ,  $4^{\circ}\text{C}$ ) and re-suspended in cold sorting buffer (PBS with 1% w/v BSA, 25 mM 4-(2-hydroxyethyl)-1-piperazineethanesulfonic acid (HEPES), and 1 mM EDTA). Cell sorting was conducted as previously described (Nguyen et al., 2021). RNA was extracted and purified using a RNeasy mini kit (QIAGEN).

For T cell studies: Re-suspended cells were positively enriched for Thy1.1+ cells using an EasySep Mouse Thy1.1+ T Cell Isolation Kit (STEMCELL Technologies).

### **Surface and intracellular staining of T cells**

For surface staining, cells were treated with Fc Block solution (purified rat anti-mouse CD16/CD32, BD Biosciences) and stained for surface markers followed by viability staining. For detection of cytokine production, cells were stimulated with  $1 \mu\text{g/ml}$  mERK2136–144 or LCMV GP33–41 peptide (Biomer Technologies) in culture at  $37^{\circ}\text{C}$  for 4 hours. Brefeldin A (GolgiPlug, BD Biosciences;  $1 \mu\text{g/mL}$ ) was added for the last 3 hours of incubation. Cells were Fc blocked, surface stained, and viability stained before fixation and permeabilization (Cytfix/Cytoperm, BD Biosciences), followed by intracellular staining.

Staining fluorescence was detected using a BD LSRFortessa or LSR II flow cytometer (BD Biosciences). Data were analyzed using FlowJo (version 10) flow cytometry analysis software (Tree Star). Sample data was pre-gated, downsampled (7500 events per sample), and concatenated in FlowJo in preparation for tSNE/flowSOM visualization. tSNE dimensionality reduction (Van der Maaten and Hinton, 2008) was calculated with default parameters: perplexity = 30, max iterations = 1000, learning rate (eta) = 4378, theta = 0.5 using channels corresponding to CD62L, TCFF1, CD127, and Tim3. Resulting data was clustered using the integrated FlowSOM plugin (Van Gassen et al., 2015) with the aforementioned channels and set for automatically generated number of metaclusters.

### **Cytotoxicity assay**

MC38-gp33 cells were labeled with 5  $\mu$ M CFSE (MilliporeSigma), seeded in a 96-well plate at 105 cells per well, and co-cultured for 6 hours with splenocyte-derived Thy1.1-enriched T cells from treated mice at a 0.5:1 effector to target ratio. Cells were stained with eBioscience Fixable Viability Dye eFluor 780 (Thermo Fisher), and staining was evaluated by flow cytometry (see above). The percentage of specific lysis was calculated using the following equation: % specific lysis =  $100 \times ((\% \text{ specific cell death} - \% \text{ basal cell death}) / (100 - \% \text{ basal cell death}))$ , where specific cell death is determined from viability dye staining of CFSE-positive cells in T cell co-culture wells and basal cell death from wells lacking co-cultured T cells.

### **RNA-seq analysis**

Bulk tumor RNA was extracted (see above) and mRNA was enriched using the NEBNext Poly(A) mRNA Isolation Module (New England Biolabs) where each sample had an RNA integrity number (RIN) score of  $>7$ . A NEBNext Ultra II Directional RNA Library kit (New England Biolabs) was used for RNA-seq library construction. Samples were sequenced on the Illumina HiSeq 2500 with the Illumina HiSeq Rapid v2 kit using a single-read 1x50 bp configuration. Gene counts were normalized using trimmed means of M-values (TMM) and converted to log<sub>2</sub> counts per million with the Limma-Voom package (Law et al., 2014). The normalized counts were used for subsequent analyses.

### **Transcriptome microarray analysis**

RNA was extracted from flow sorted CD8<sup>+</sup> Thy1.1<sup>+</sup> T cells (see above) and utilized for gene expression analysis by Clariom D array (Applied Biosystems). Sample preparation for microarray hybridization was conducted according to the GeneChip WT Pico Reagent Kit User Manual (Applied Biosystems). Samples were run on the GeneChip Scanner 3000 instrument system (Applied Biosystems). CEL files were analyzed on the Transcriptome Analysis Console (TAC 4.0) and probe set signals were SST-RMA-normalized prior to further analysis.

### **Gene set enrichment analysis**

Utilizing GSEA4.1 (Mootha et al., 2003; Subramanian et al., 2005), enrichment analysis was conducted using gene sets from the Molecular Signatures Database (MSigDB, version 7.4) in the Hallmark gene category (Liberzon et al., 2015), Curated (C2) gene category, and Ontology (C5) gene category. Enriched gene sets from C2 and C5 were organized into



networks using the EnrichmentMap plugin (Merico et al., 2010) for Cytoscape 3.8.2 (Shannon et al., 2003), and automatic identification and labeling of network clusters was facilitated by the AutoAnnotate plugin (Kucera et al., 2016). The gene lists that were chosen to represent defined T cell signatures were adapted from previously published characterizations of exhausted T cells (TEX), effector T cells (TEFF), memory T cells (TMEM), memory precursor effector cells (TMPEC), short lived effector cells (TSLEC), and effector memory cells re-expressing CD45A (TEMRA) (Joshi et al., 2007; Knaus et al., 2018; Wherry et al., 2007). GSEA was performed with the following parameters: number of permutations: 2000, permutation type: gene set, metric for ranking genes: T-test.

The ssGSEA (v10.0.x) projection module (Barbie et al., 2009) within GenePattern (Reich et al., 2006) was used to calculate separate enrichment scores for individual sample-gene set pairings, independent of phenotype labeling. ssGSEA was performed on untransformed gene expression signal values with the following parameters: sample normalization method: rank, weighting component: 0.75, minimum gene set size: 10. From ACT+MS-275 treated samples, Pearson's correlation coefficient was used to calculate the correlation between enriched Hallmark pathways (ssGSEA enrichment scores) and differentially expressed hub genes (signal values) and visualized as a correlation matrix or individual scatter plots.

### **Unsupervised weighted gene-centric network analysis**

Module identification: Co-expressed modules were identified with the CEMiTool method (Russo et al., 2018) using the web application, webCEMiTool (Cardozo et al., 2019). Analysis was performed with log<sub>2</sub>-transformed gene expression signal values using default parameters: variance filter (p-value): 0.05, correlation method: Pearson, beta: 18, dissimilarity threshold: 0.8. Identified modules were denoted as M1-M6. CEMiTool was then used to generate a protein-protein interaction (PPI) network from the module 2 (M2) gene list based on interactome data provided by Genemania (Mostafavi et al., 2008).

Pathway analysis: A functional network was constructed from the module 2 (M2) gene list utilizing the ClueGO plugin (Bindea et al., 2009) for Cytoscape 3.8.2. The Gene Ontology Biological Processes (GOBP) database was used and overrepresented terms were displayed according to the following parameters: GO Term Fusion: yes, display only pathways with p: <0.05.

### **Survival analysis of TCGA data**

Normalized RNA-seq data from The Cancer Genome Atlas (TCGA) were downloaded from the Broad Genome Data Analysis Center (GDAC) Firehose repository (doi: 10.7908/C11G0KM9) (Broad\_Institute\_TCGA\_Genome\_Data\_Analysis\_Center, 2016) through the Firebrowse portal (Deng et al., 2017). Patients were filtered to select for primary tumor samples and tumor stage I or IV (extent of primary tumor burden), denoted as T1 or T4. ssGSEA analysis was used to determine Hallmark pathway enrichment scores for each patient (see above) and pathways that overlapped with preclinical data were chosen to represent a pathway signature. Pathways were fitted in a multivariate Cox regression model to assess relative contribution to survival prediction. Using the regression coefficients in the model, a prognostic risk score for predicting overall survival was calculated,

$$Risk\ score = \sum_{i=1}^n exp_i * \beta_i$$

where n is the number of prognostic pathways,  $exp_i$  is the enrichment score of pathway i, and  $\beta_i$  is the regression coefficient of pathway i. The median risk score was used to stratify patients into high- and low-risk groups.

### **Statistical analysis**

Statistical analyses were performed using Prism 8.4.3 (Graphpad Software) and MedCalc. Bar graphs depict means  $\pm$  SEM. Un-paired T-tests (two-tailed) and one-way ANOVA was used to query immune response or characterization data. p values  $< 0.05$  were considered significant (\*:  $p < 0.05$ , \*\*:  $p < 0.01$ , \*\*\*:  $p < 0.001$ ); p-values  $> 0.05$ ; non-significant (NS). For survival studies, Kaplan-Meier analysis was used and log-rank test was used to assess the statistical significance ( $p < 0.05$ ).

Univariate and multivariate Cox regression and patient stratification were used to determine whether a pathway signature unique to increased tumor burden was predictive of decreased overall survival and was independent of other clinical features, where  $p < 0.05$ . Receiver operating characteristic (ROC) curves were used to determine sensitivity and specificity of the pathway signature in predicting increased tumor burden in patients. The area under the curve (AUC) is a ROC performance measurement where a higher value corresponds to an increased ability to distinguish between classes.

### **Supplementary Figure Titles and Legends**

#### **Figure S1: Transferred T cell proliferation and cell death over time, related to Figure 3D, E**

Transferred Thy1.1+ congenic TCM were analyzed at several timepoints post-vaccination and stained for markers of proliferation and cell death. Fluorescence intensity was determined by geometric mean. Data was obtained with n = 5 mice per group. Statistics were based on one-way ANOVA test.

#### **Figure S2: Enriched Hallmark pathways using the Module (M2) list, related to Figure 4D**

Using the MSigDB Hallmark gene set collection, GSEA was used to enrich pathways in ACT-treated (negative enrichment score) or ACT+MS-275-treated tumors (positive enrichment score). Gene expression data was filtered from the Module 2 (M2) gene list.

#### **Figure S3: Differentially expressed genes when comparing ACT+MS-275- to ACT-treated T cells, related to Figure 4D**

(A) Scatter plot outlining average log<sub>2</sub> signal values for expressed genes and volcano plot outlining differentially expressed genes (FDR < 0.05) during ACT±MS-275 treatment. (B) Pie charts showing locus type breakdown for differentially expressed genes. (C) Top differentially expressed genes by absolute fold change.

#### **Figure S4: DUSP22-pathway correlation, related to Figure 4I, J**

Scatter plots showing correlation between Hallmark pathways and DUSP22 gene expression.

### **Supplementary Table Titles and Legends**

#### **Table S1: Overrepresented GO terms associated with Module 2 (M2), related to Figure 4E, F**

#### **Table S2: Gene lists of T cell signatures, related to Figure 5E**

**Figure 1**

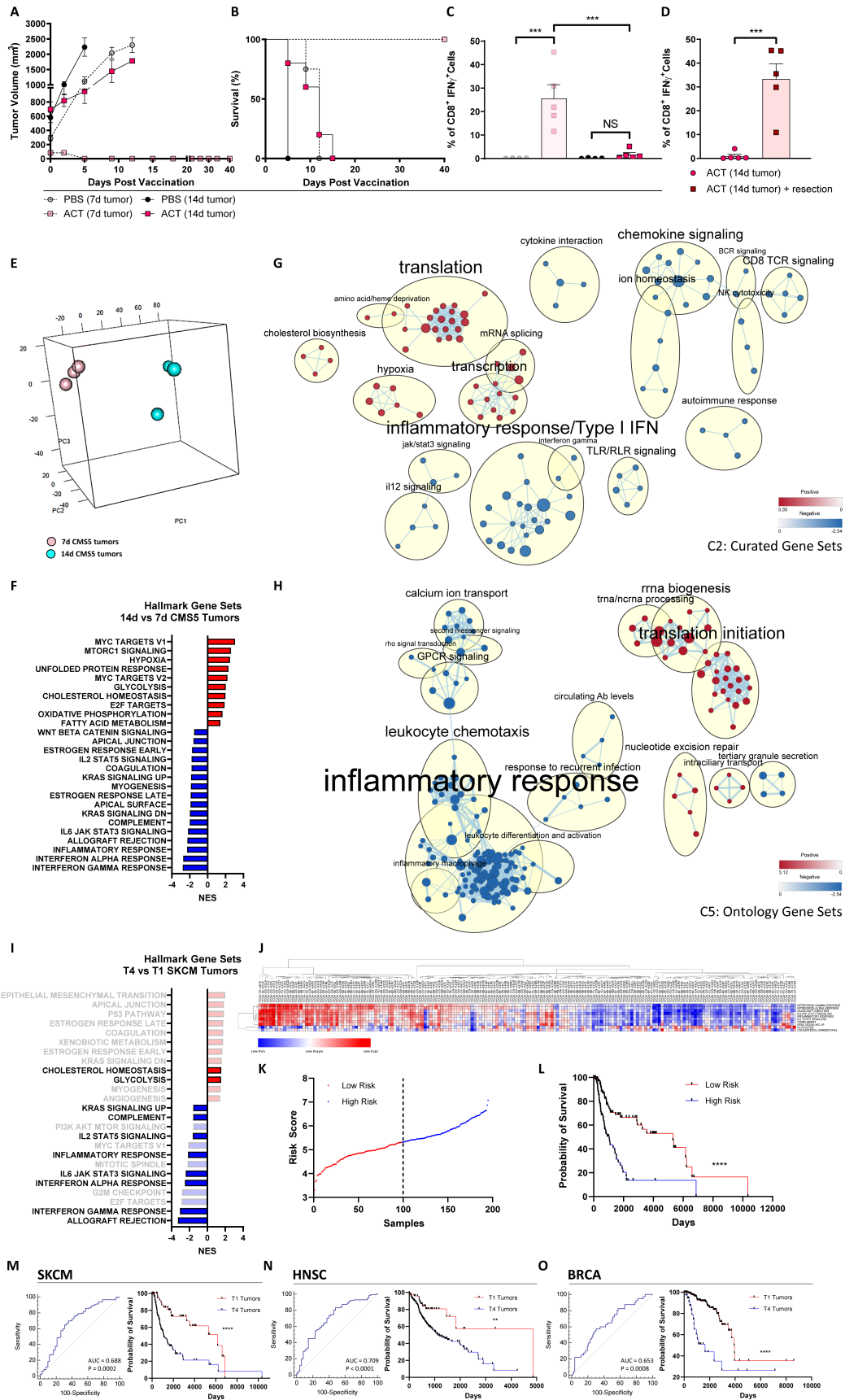
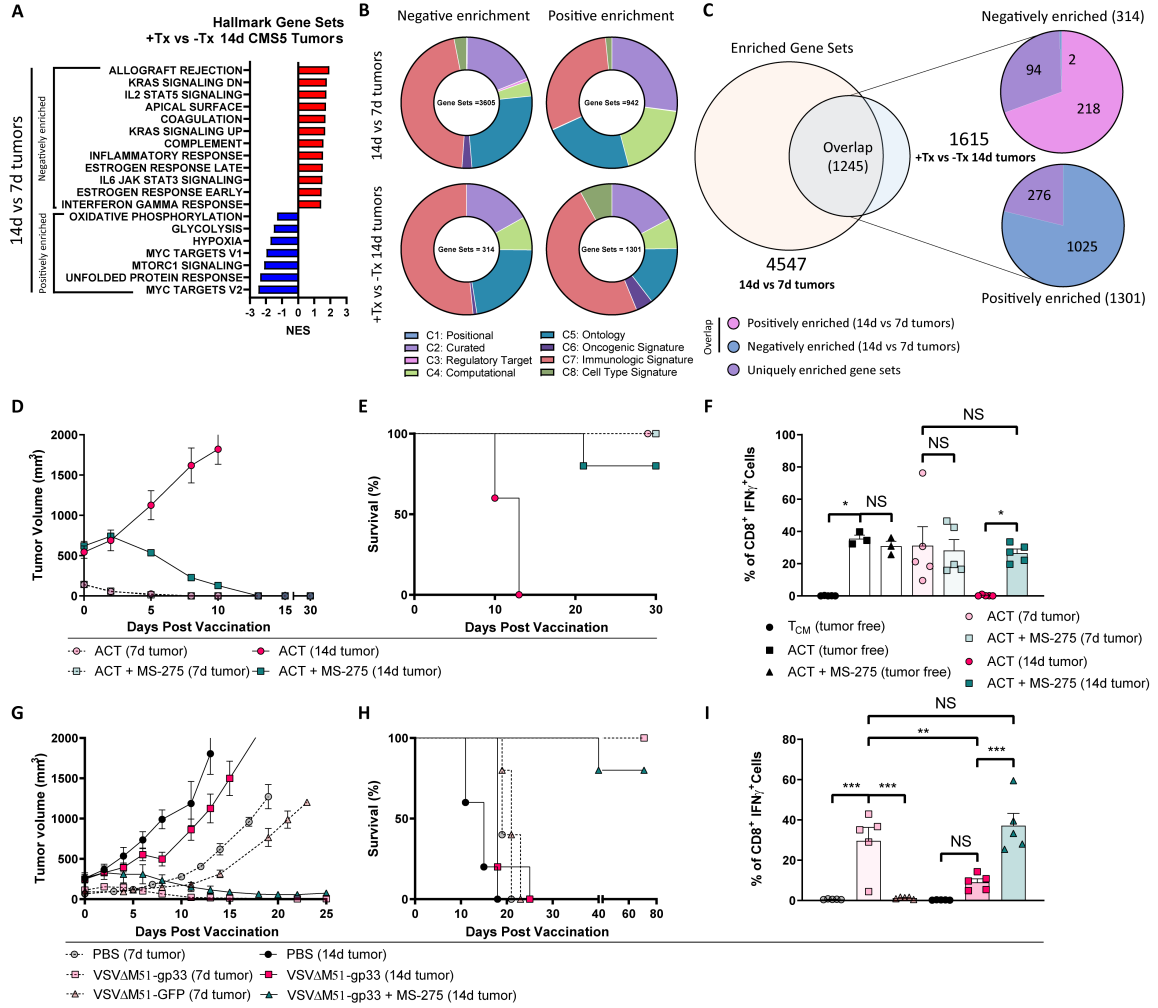


Figure 2



**Figure 3**

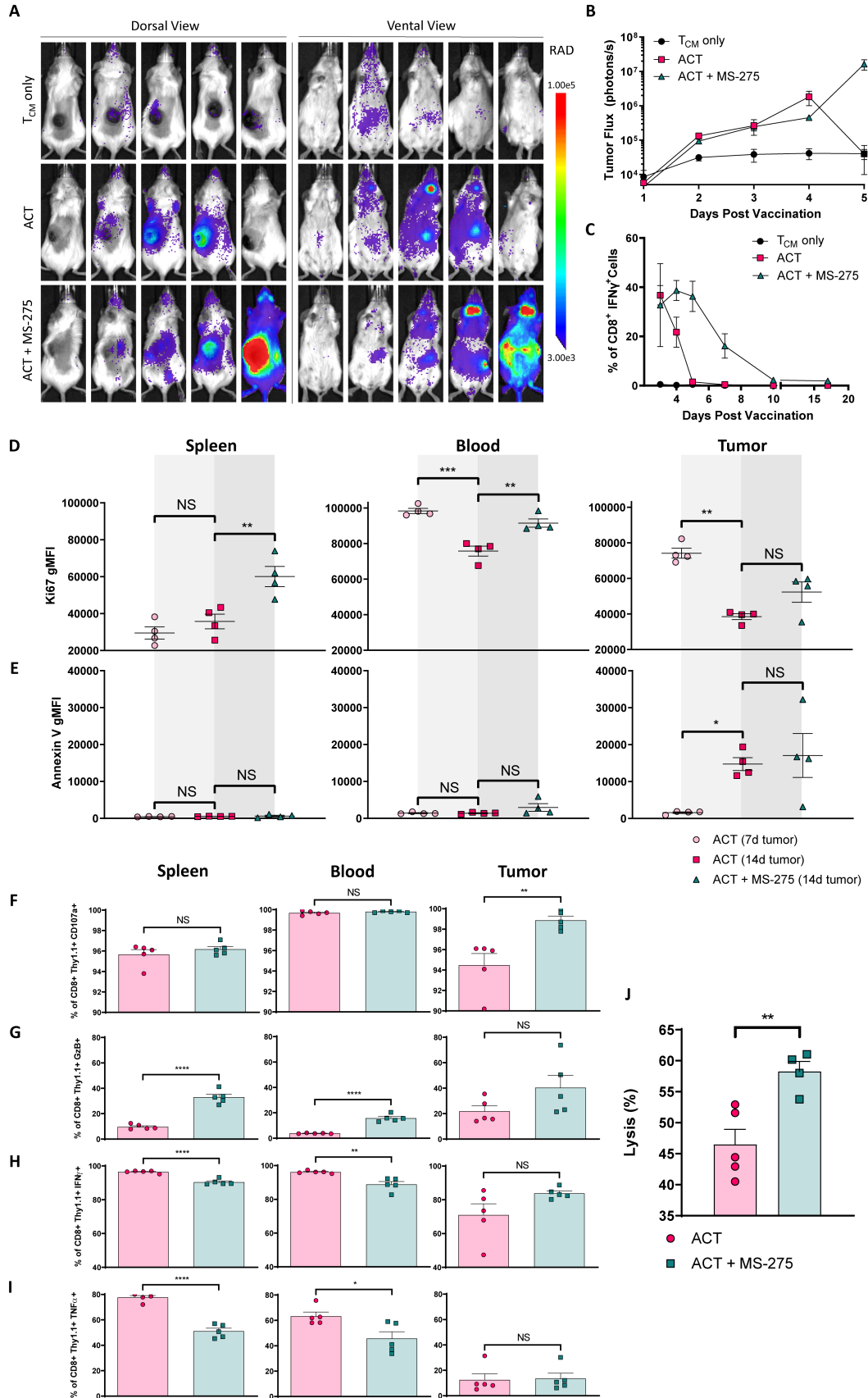


Figure 4

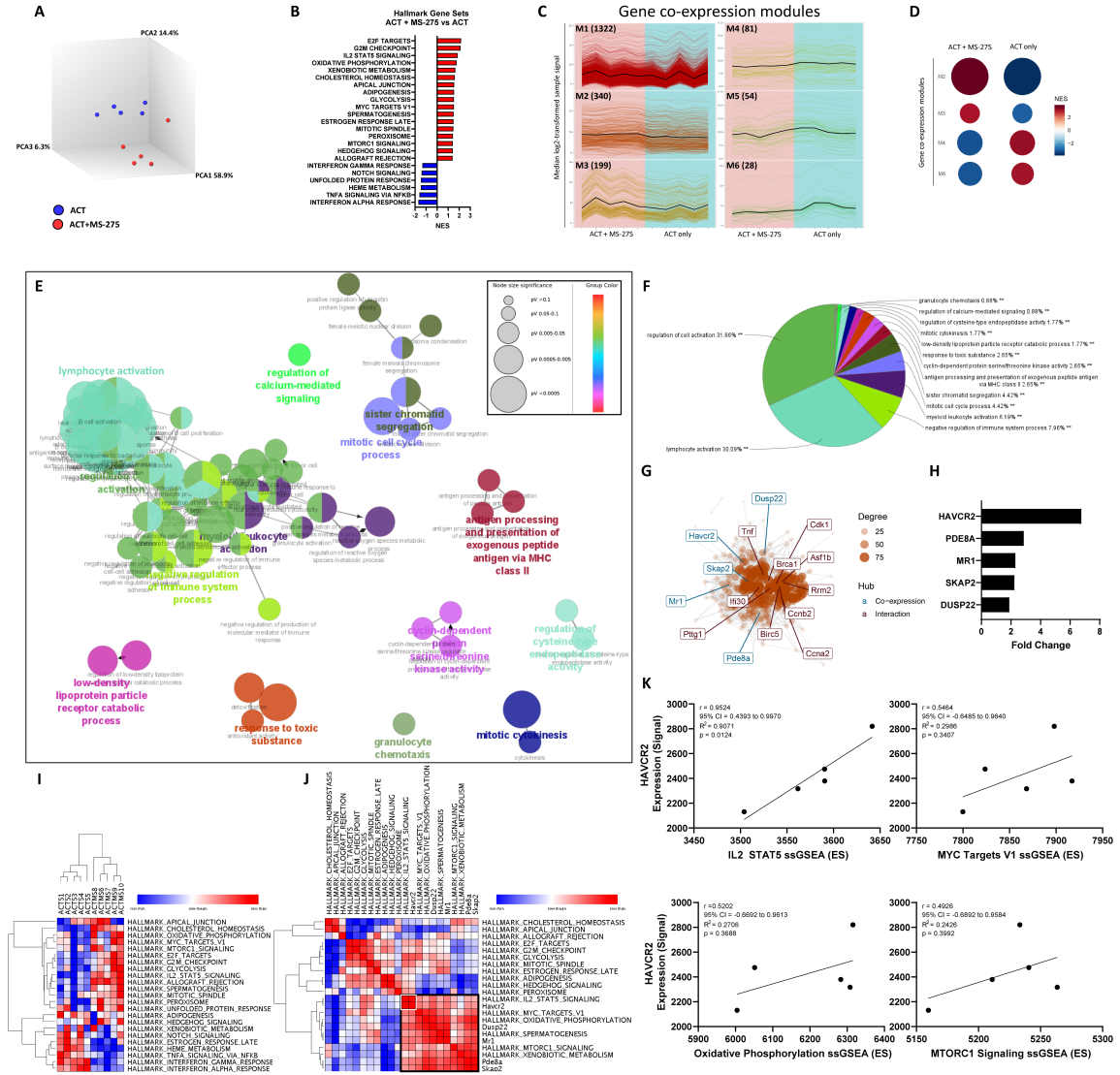
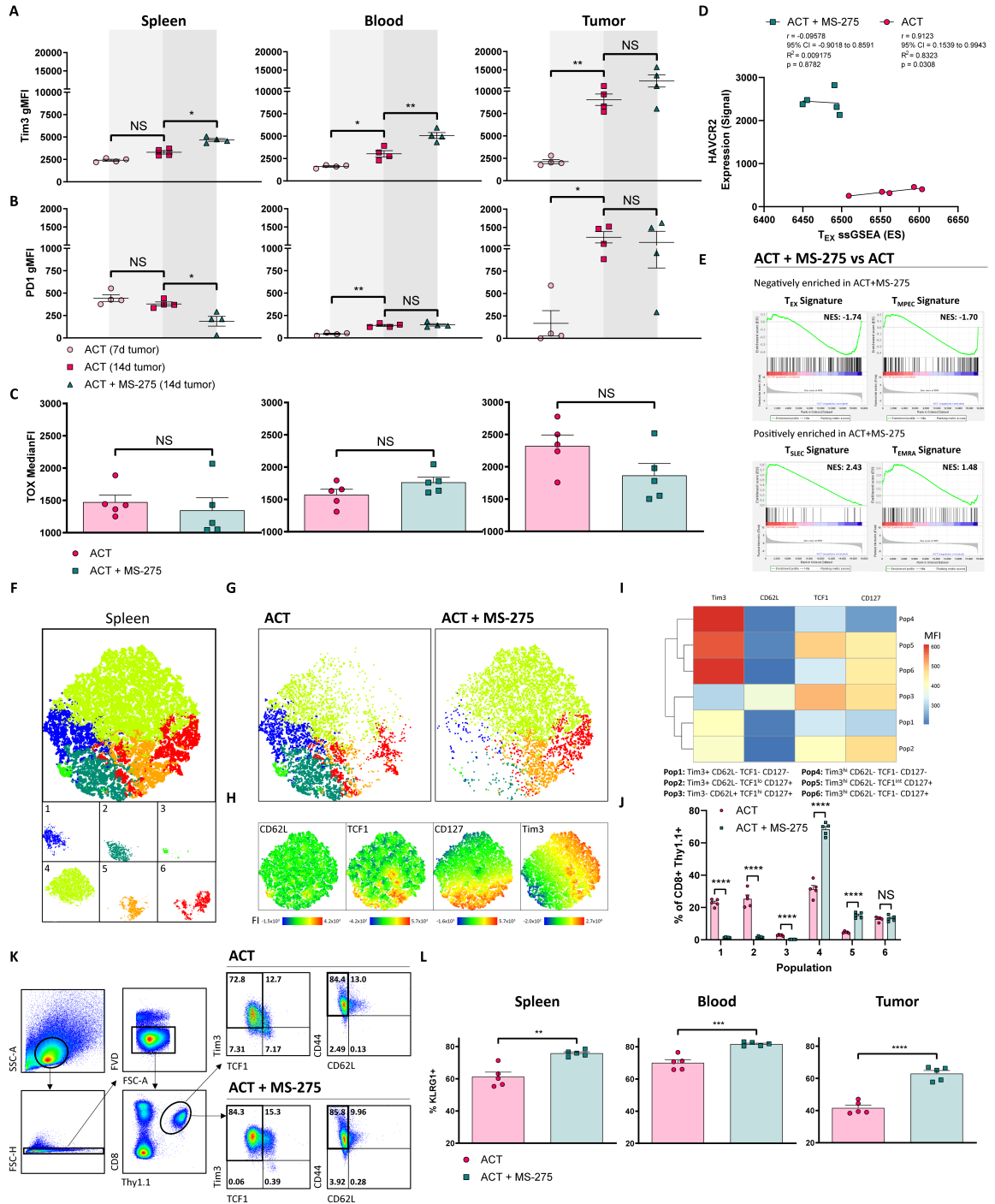


Figure 5



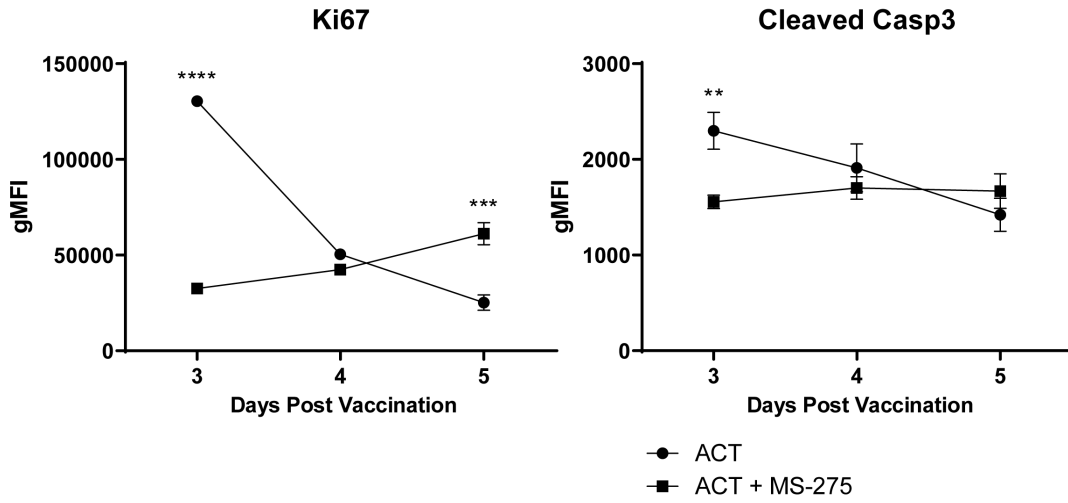


**Table 1**

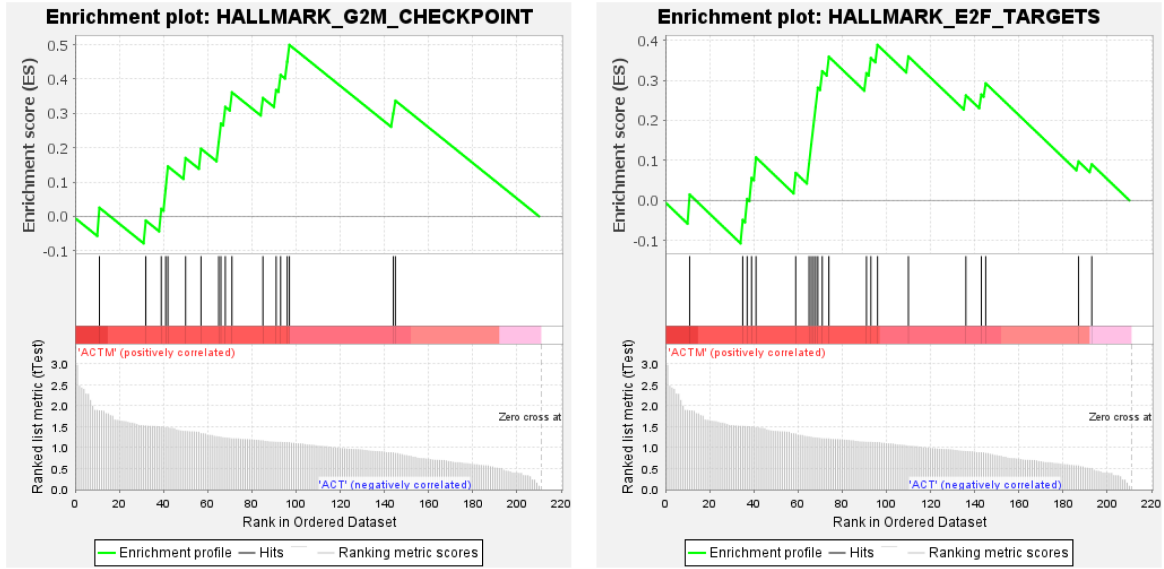
Variables	Patients (N)	Univariate Survival		Multivariate Survival		
		HR (95% CI)	P-value	HR (95% CI)	P-value	
Age	<=61 / >61	99/96	1.4703 (0.9296 to 2.3254)	0.0994		
Gender	Female / Male	82/113	1.3077 (0.8350 to 2.0479)	0.2411		
<b>Pathologic Stage</b>	<b>I-II / III-IV</b>	<b>117/74</b>	<b>2.6947 (1.7179 to 4.2269)</b>	<b>&lt;0.0001</b>	<b>1.6867 (0.4996 to 5.6942)</b>	<b>0.3997</b>
<b>T Stage</b>	<b>T1 / T4</b>	<b>42/153</b>	<b>3.1487 (1.7690 to 5.6046)</b>	<b>0.0001</b>	<b>2.4563 (1.3357 to 4.5172)</b>	<b>0.0038</b>
<b>N Stage</b>	<b>N0 / N1-3</b>	<b>108/67</b>	<b>2.4027 (1.4844 to 3.8891)</b>	<b>0.0004</b>	<b>0.4566 (0.1142 to 1.8257)</b>	<b>0.2676</b>
M Stage	M0 / M1	183/7	1.2430 (0.3905 to 3.9566)	0.7127		
Radiation Therapy	No / Yes	184/11	0.6911 (0.2790 to 1.7118)	0.4247		
<b>Risk Score</b>	<b>Low / High</b>	<b>98/97</b>	<b>2.8692 (1.8019 to 4.5688)</b>	<b>&lt;0.0001</b>	<b>2.7007 (0.7039 to 10.3625)</b>	<b>0.1476</b>

HR, Hazard Ratio; CI, Confidence Interval; T, Tumor; N, Node; M, Metastasis

Supplementary Figure 1

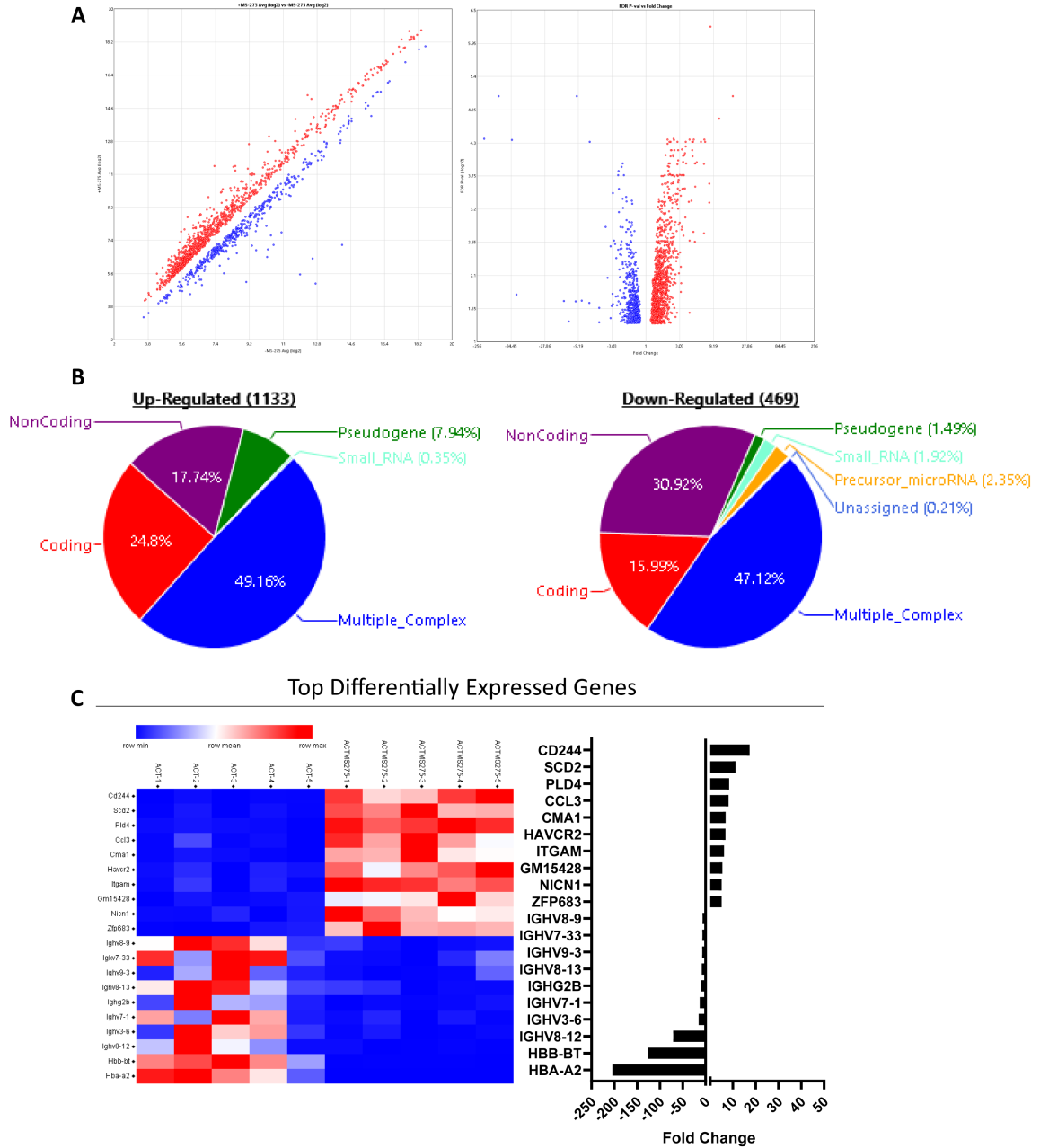


Supplementary Figure 2

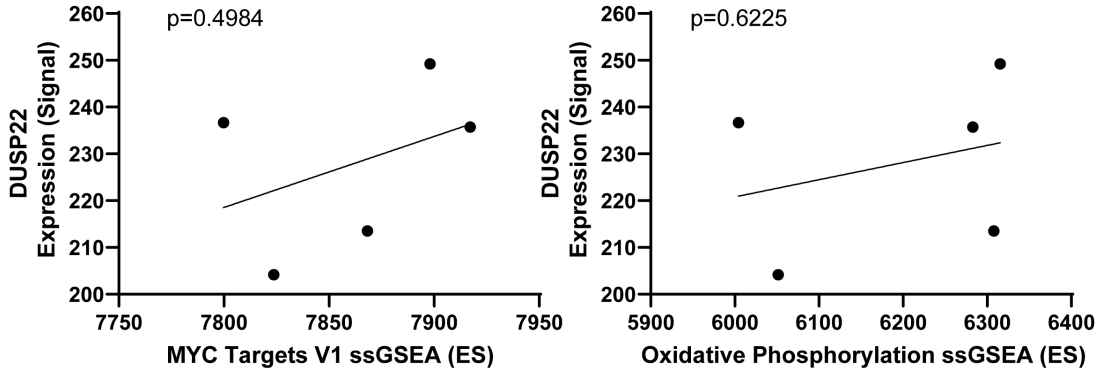


GS	GS DETAILS	ES	NES	NOM p-val	FDR q-val	FWER p-val	RANK AT MAX	LEADING EDGE
1	HALLMARK_G2M_CHECKPOINT	18	0.5	1.7	0.011	0.021	0.019	97
2	HALLMARK_E2F_TARGETS	22	0.39	1.4	0.093	0.092	0.162	96

Supplementary Figure 3



Supplementary Figure 4



	ACT + MS-275		ACT + MS-275
r	0.4053	r	0.3011
95% confidence interval	-0.7425 to 0.9484	95% confidence interval	-0.7914 to 0.9350
R squared	0.1643	R squared	0.09066

### Supplementary Table 1

GO:0071621	granulocyte activation	3.79E-04	3.67E-02	3.79E-04	1.14E-03[5, 6, 7, 8]	Group0	6.80	8.00[C013, C014, C015, Group, S100a11, S100a8, S100a6, S100a9]
GO:0050484	regulation of cytokines	5.31E-04	4.96E-02	5.31E-04	1.06E-03[5, 6, 7, 8]	Group1	7.50	6.00[C013, C014, C022, Ltcam, Tnfrsf16, Tnf]
GO:2000116	regulation of cysteine-type endopeptidase activity	1.15E-04	1.52E-02	1.15E-04	6.74E-04[5, 6, 7, 8, 9, 10, 11, 12]	Group2	4.98	12.00[Ala2, Ala3, Ala4, Ala5, Ala6, Ala7, Ala8, Ala9, Ala10, Ala11, Ala12, Ala13, Ala14, Ala15, Ala16, Ala17, Ala18, Ala19, Ala20, Ala21, Ala22, Ala23, Ala24, Ala25, Ala26, Ala27, Ala28, Ala29, Ala30, Ala31, Ala32, Ala33, Ala34, Ala35, Ala36, Ala37, Ala38, Ala39, Ala40, Ala41, Ala42, Ala43, Ala44, Ala45, Ala46, Ala47, Ala48, Ala49, Ala50, Ala51, Ala52, Ala53, Ala54, Ala55, Ala56, Ala57, Ala58, Ala59, Ala60, Ala61, Ala62, Ala63, Ala64, Ala65, Ala66, Ala67, Ala68, Ala69, Ala70, Ala71, Ala72, Ala73, Ala74, Ala75, Ala76, Ala77, Ala78, Ala79, Ala80, Ala81, Ala82, Ala83, Ala84, Ala85, Ala86, Ala87, Ala88, Ala89, Ala90, Ala91, Ala92, Ala93, Ala94, Ala95, Ala96, Ala97, Ala98, Ala99, Ala100]
GO:0000910	cytokinesis	1.71E-04	1.88E-02	1.71E-04	5.74E-04[5, 6, 7, 8, 9, 10, 11, 12, 13]	Group2	5.77	9.00[Ankrd, Conn, Des, Fgf, Ptkinase, S100a6, S100a9, Tnf, Xp1]
GO:0000201	mitotic cyclin regulation	2.52E-06	3.89E-04	2.52E-06	1.94E-03[5, 6, 7, 8]	Group3	6.45	9.00[Ala3, Ala5, Ala6, Ala7, Ala8, Ala9, Ala10, Ala11, Ala12, Ala13, Ala14, Ala15, Ala16, Ala17, Ala18, Ala19, Ala20, Ala21, Ala22, Ala23, Ala24, Ala25, Ala26, Ala27, Ala28, Ala29, Ala30, Ala31, Ala32, Ala33, Ala34, Ala35, Ala36, Ala37, Ala38, Ala39, Ala40, Ala41, Ala42, Ala43, Ala44, Ala45, Ala46, Ala47, Ala48, Ala49, Ala50, Ala51, Ala52, Ala53, Ala54, Ala55, Ala56, Ala57, Ala58, Ala59, Ala60, Ala61, Ala62, Ala63, Ala64, Ala65, Ala66, Ala67, Ala68, Ala69, Ala70, Ala71, Ala72, Ala73, Ala74, Ala75, Ala76, Ala77, Ala78, Ala79, Ala80, Ala81, Ala82, Ala83, Ala84, Ala85, Ala86, Ala87, Ala88, Ala89, Ala90, Ala91, Ala92, Ala93, Ala94, Ala95, Ala96, Ala97, Ala98, Ala99, Ala100]
GO:0032803	low-density lipoprotein particle receptor catabolic process	3.88E-05	4.90E-03	3.88E-05	2.72E-04[5, 6, 7, 8]	Group4	11.90	3.00[Ala24, Ala25, Ala26]
GO:0008754	classification	1.12E-05	1.55E-03	3.57E-07	2.85E-05[1]	Group5	7.39	10.00[C013, C014, C015, C016, C017, C018, C019, C020, C021, C022, C023, C024, C025, C026, C027, C028, C029, C030, C031, C032, C033, C034, C035, C036, C037, C038, C039, C040, C041, C042, C043, C044, C045, C046, C047, C048, C049, C050, C051, C052, C053, C054, C055, C056, C057, C058, C059, C060, C061, C062, C063, C064, C065, C066, C067, C068, C069, C070, C071, C072, C073, C074, C075, C076, C077, C078, C079, C080, C081, C082, C083, C084, C085, C086, C087, C088, C089, C090, C091, C092, C093, C094, C095, C096, C097, C098, C099, C100]
GO:009636	response to toxic substance	3.57E-07	5.17E-05	3.57E-07	2.85E-06[3]	Group5	5.95	16.00[Ala1, Ala2, Ala3, Ala4, Ala5, Ala6, Ala7, Ala8, Ala9, Ala10, Ala11, Ala12, Ala13, Ala14, Ala15, Ala16, Ala17, Ala18, Ala19, Ala20, Ala21, Ala22, Ala23, Ala24, Ala25, Ala26, Ala27, Ala28, Ala29, Ala30, Ala31, Ala32, Ala33, Ala34, Ala35, Ala36, Ala37, Ala38, Ala39, Ala40, Ala41, Ala42, Ala43, Ala44, Ala45, Ala46, Ala47, Ala48, Ala49, Ala50, Ala51, Ala52, Ala53, Ala54, Ala55, Ala56, Ala57, Ala58, Ala59, Ala60, Ala61, Ala62, Ala63, Ala64, Ala65, Ala66, Ala67, Ala68, Ala69, Ala70, Ala71, Ala72, Ala73, Ala74, Ala75, Ala76, Ala77, Ala78, Ala79, Ala80, Ala81, Ala82, Ala83, Ala84, Ala85, Ala86, Ala87, Ala88, Ala89, Ala90, Ala91, Ala92, Ala93, Ala94, Ala95, Ala96, Ala97, Ala98, Ala99, Ala100]
GO:0193209	antioxidant activity	4.23E-05	5.98E-03	3.57E-07	2.85E-06[7]	Group5	7.82	8.00[Ala28, Ala29, Ala30, Ala31, Ala32, Ala33, Ala34, Ala35, Ala36, Ala37, Ala38, Ala39, Ala40, Ala41, Ala42, Ala43, Ala44, Ala45, Ala46, Ala47, Ala48, Ala49, Ala50, Ala51, Ala52, Ala53, Ala54, Ala55, Ala56, Ala57, Ala58, Ala59, Ala60, Ala61, Ala62, Ala63, Ala64, Ala65, Ala66, Ala67, Ala68, Ala69, Ala70, Ala71, Ala72, Ala73, Ala74, Ala75, Ala76, Ala77, Ala78, Ala79, Ala80, Ala81, Ala82, Ala83, Ala84, Ala85, Ala86, Ala87, Ala88, Ala89, Ala90, Ala91, Ala92, Ala93, Ala94, Ala95, Ala96, Ala97, Ala98, Ala99, Ala100]
GO:0004693	cyclin-dependent protein serine/threonine kinase activity	9.57E-05	9.57E-05	9.57E-05	5.74E-04[5, 6, 7, 8, 9, 10, 11]	Group5	4.78	10.00[C013, C014, C015, C016, C017, C018, C019, C020, C021, C022, C023, C024, C025, C026, C027, C028, C029, C030, C031, C032, C033, C034, C035, C036, C037, C038, C039, C040, C041, C042, C043, C044, C045, C046, C047, C048, C049, C050, C051, C052, C053, C054, C055, C056, C057, C058, C059, C060, C061, C062, C063, C064, C065, C066, C067, C068, C069, C070, C071, C072, C073, C074, C075, C076, C077, C078, C079, C080, C081, C082, C083, C084, C085, C086, C087, C088, C089, C090, C091, C092, C093, C094, C095, C096, C097, C098, C099, C100]
GO:0000979	regulation of cyclin-dependent protein serine/threonine kinase activity	1.18E-04	1.94E-02	9.57E-05	6.74E-04[5, 6, 7, 8, 9, 10, 11, 12]	Group6	8.65	7.00[C013, C014, C015, C016, C017, C018, C019, C020, C021, C022, C023, C024, C025, C026, C027, C028, C029, C030, C031, C032, C033, C034, C035, C036, C037, C038, C039, C040, C041, C042, C043, C044, C045, C046, C047, C048, C049, C050, C051, C052, C053, C054, C055, C056, C057, C058, C059, C060, C061, C062, C063, C064, C065, C066, C067, C068, C069, C070, C071, C072, C073, C074, C075, C076, C077, C078, C079, C080, C081, C082, C083, C084, C085, C086, C087, C088, C089, C090, C091, C092, C093, C094, C095, C096, C097, C098, C099, C100]
GO:0193538	cyclin-dependent protein serine/threonine kinase regulator activity	3.00E-04	3.00E-02	9.57E-05	5.74E-04[5, 6, 7, 8, 9, 10, 11, 12, 13]	Group6	10.64	5.00[C013, C014, C015, C016, C017, C018, C019, C020, C021, C022, C023, C024, C025, C026, C027, C028, C029, C030, C031, C032, C033, C034, C035, C036, C037, C038, C039, C040, C041, C042, C043, C044, C045, C046, C047, C048, C049, C050, C051, C052, C053, C054, C055, C056, C057, C058, C059, C060, C061, C062, C063, C064, C065, C066, C067, C068, C069, C070, C071, C072, C073, C074, C075, C076, C077, C078, C079, C080, C081, C082, C083, C084, C085, C086, C087, C088, C089, C090, C091, C092, C093, C094, C095, C096, C097, C098, C099, C100]
GO:0191868	antigen processing and presentation of exogenous antigen	1.81E-04	1.97E-02	5.67E-04	6.67E-04[3]	Group7	11.80	5.00[C013, C014, C015, C016, C017, C018, C019, C020, C021, C022, C023, C024, C025, C026, C027, C028, C029, C030, C031, C032, C033, C034, C035, C036, C037, C038, C039, C040, C041, C042, C043, C044, C045, C046, C047, C048, C049, C050, C051, C052, C053, C054, C055, C056, C057, C058, C059, C060, C061, C062, C063, C064, C065, C066, C067, C068, C069, C070, C071, C072, C073, C074, C075, C076, C077, C078, C079, C080, C081, C082, C083, C084, C085, C086, C087, C088, C089, C090, C091, C092, C093, C094, C095, C096, C097, C098, C099, C100]
GO:0448032	antigen processing and presentation of peptide antigen	3.75E-04	3.67E-02	5.67E-04	6.67E-04[3]	Group7	8.00	6.00[C013, C014, C015, C016, C017, C018, C019, C020, C021, C022, C023, C024, C025, C026, C027, C028, C029, C030, C031, C032, C033, C034, C035, C036, C037, C038, C039, C040, C041, C042, C043, C044, C045, C046, C047, C048, C049, C050, C051, C052, C053, C054, C055, C056, C057, C058, C059, C060, C061, C062, C063, C064, C065, C066, C067, C068, C069, C070, C071, C072, C073, C074, C075, C076, C077, C078, C079, C080, C081, C082, C083, C084, C085, C086, C087, C088, C089, C090, C091, C092, C093, C094, C095, C096, C097, C098, C099, C100]
GO:0191869	antigen processing and presentation of exogenous peptide antigen via MHC class II	5.22E-05	6.42E-03	5.67E-04	6.67E-04[3]	Group7	23.01	4.00[C013, C014, C015, C016, C017, C018, C019, C020, C021, C022, C023, C024, C025, C026, C027, C028, C029, C030, C031, C032, C033, C034, C035, C036, C037, C038, C039, C040, C041, C042, C043, C044, C045, C046, C047, C048, C049, C050, C051, C052, C053, C054, C055, C056, C057, C058, C059, C060, C061, C062, C063, C064, C065, C066, C067, C068, C069, C070, C071, C072, C073, C074, C075, C076, C077, C078, C079, C080, C081, C082, C083, C084, C085, C086, C087, C088, C089, C090, C091, C092, C093, C094, C095, C096, C097, C098, C099, C100]
GO:0000119	sister chromatid segregation	3.84E-05	4.88E-03	1.64E-07	1.48E-06[14, 5, 6]	Group8	6.67	11.00[Bnc5, E5ocd, Kf8b, Krim, Neap, Neap1, Plx1, Plx1, Spn1, Top2a, Ubr1]
GO:0071474	female meiotic nuclear division	2.28E-04	2.39E-02	1.64E-07	1.48E-06[14, 5, 6, 7, 8]	Group8	11.38	5.00[C013, C014, C015, C016, C017, C018, C019, C020, C021, C022, C023, C024, C025, C026, C027, C028, C029, C030, C031, C032, C033, C034, C035, C036, C037, C038, C039, C040, C041, C042, C043, C044, C045, C046, C047, C048, C049, C050, C051, C052, C053, C054, C055, C056, C057, C058, C059, C060, C061, C062, C063, C064, C065, C066, C067, C068, C069, C070, C071, C072, C073, C074, C075, C076, C077, C078, C079, C080, C081, C082, C083, C084, C085, C086, C087, C088, C089, C090, C091, C092, C093, C094, C095, C096, C097, C098, C099, C100]
GO:0193521	female meiosis chromosome segregation	1.07E-04	1.25E-02	1.64E-07	1.48E-06[14, 5, 6, 7, 8, 9]	Group8	3.97	3.00[Neap, Plx1, Top2a]
GO:0032921	chromosome condensation	2.79E-04	2.62E-02	1.64E-07	1.48E-06[14]	Group8	10.87	5.00[C013, C014, C015, C016, C017, C018, C019, C020, C021, C022, C023, C024, C025, C026, C027, C028, C029, C030, C031, C032, C033, C034, C035, C036, C037, C038, C039, C040, C041, C042, C043, C044, C045, C046, C047, C048, C049, C050, C051, C052, C053, C054, C055, C056, C057, C058, C059, C060, C061, C062, C063, C064, C065, C066, C067, C068, C069, C070, C071, C072, C073, C074, C075, C076, C077, C078, C079, C080, C081, C082, C083, C084, C085, C086, C087, C088, C089, C090, C091, C092, C093, C094, C095, C096, C097, C098, C099, C100]
GO:1904683	positive regulation of ubiquitin protein ligase activity	2.22E-04	2.40E-02	1.64E-07	1.48E-06[14, 5, 6, 7, 8, 9, 10, 11, 12, 13]	Group8	30.00	3.00[C013, C014, C015, C016, C017, C018, C019, C020, C021, C022, C023, C024, C025, C026, C027, C028, C029, C030, C031, C032, C033, C034, C035, C036, C037, C038, C039, C040, C041, C042, C043, C044, C045, C046, C047, C048, C049, C050, C051, C052, C053, C054, C055, C056, C057, C058, C059, C060, C061, C062, C063, C064, C065, C066, C067, C068, C069, C070, C071, C072, C073, C074, C075, C076, C077, C078, C079, C080, C081, C082, C083, C084, C085, C086, C087, C088, C089, C090, C091, C092, C093, C094, C095, C096, C097, C098, C099, C100]
GO:1903047	mitotic cycle process	9.00E-09	1.37E-04	4.61E-09	6.07E-09[1, 4]	Group9	4.20	30.00[Ala1, Ala2, Ala3, Ala4, Ala5, Ala6, Ala7, Ala8, Ala9, Ala10, Ala11, Ala12, Ala13, Ala14, Ala15, Ala16, Ala17, Ala18, Ala19, Ala20, Ala21, Ala22, Ala23, Ala24, Ala25, Ala26, Ala27, Ala28, Ala29, Ala30, Ala31, Ala32, Ala33, Ala34, Ala35, Ala36, Ala37, Ala38, Ala39, Ala40, Ala41, Ala42, Ala43, Ala44, Ala45, Ala46, Ala47, Ala48, Ala49, Ala50, Ala51, Ala52, Ala53, Ala54, Ala55, Ala56, Ala57, Ala58, Ala59, Ala60, Ala61, Ala62, Ala63, Ala64, Ala65, Ala66, Ala67, Ala68, Ala69, Ala70, Ala71, Ala72, Ala73, Ala74, Ala75, Ala76, Ala77, Ala78, Ala79, Ala80, Ala81, Ala82, Ala83, Ala84, Ala85, Ala86, Ala87, Ala88, Ala89, Ala90, Ala91, Ala92, Ala93, Ala94, Ala95, Ala96, Ala97, Ala98, Ala99, Ala100]
GO:0000119	sister chromatid segregation	3.84E-05	4.88E-03	4.61E-09	6.07E-09[1, 4, 5, 6]	Group9	5.67	11.00[Bnc5, E5ocd, Kf8b, Krim, Neap, Neap1, Plx1, Plx1, Spn1, Top2a, Ubr1]
GO:0140214	mitotic nuclear division	9.81E-05	1.18E-02	4.61E-09	6.07E-09[1, 4, 5, 6, 7]	Group9	4.44	13.00[Bnc5, Kf8b, Krim, Neap, Neap1, Plx1, Plx1, Spn1, Top2a, Ubr1]
GO:0000079	mitotic sister chromatid segregation	2.37E-04	2.47E-02	4.61E-09	6.07E-09[1, 4, 5, 6, 7, 8]	Group9	6.92	9.00[Bnc5, Kf8b, Krim, Neap, Neap1, Plx1, Plx1, Spn1, Top2a, Ubr1]
GO:0193521	female meiosis chromosome segregation	1.07E-04	1.25E-02	4.61E-09	6.07E-09[1, 4, 5, 6, 7, 8, 9]	Group9	3.77	3.00[Neap, Plx1, Top2a]
GO:0071593	reactive oxygen species metabolic process	1.31E-05	1.74E-03	5.98E-09	5.98E-09[1]	Group9	4.75	15.00[Ala1, C013, C014, C015, C016, C017, C018, C019, C020, C021, C022, C023, C024, C025, C026, C027, C028, C029, C030, C031, C032, C033, C034, C035, C036, C037, C038, C039, C040, C041, C042, C043, C044, C045, C046, C047, C048, C049, C050, C051, C052, C053, C054, C055, C056, C057, C058, C059, C060, C061, C062, C063, C064, C065, C066, C067, C068, C069, C070, C071, C072, C073, C074, C075, C076, C077, C078, C079, C080, C081, C082, C083, C084, C085, C086, C087, C088, C089, C090, C091, C092, C093, C094, C095, C096, C097, C098, C099, C100]
GO:0001909	leukocyte mediated cytotoxicity	3.48E-05	4.48E-03	5.98E-09	5.98E-09[1, 4]	Group10	7.09	9.00[C013, C014, C015, C016, C017, C018, C019, C020, C021, C022, C023, C024, C025, C026, C027, C028, C029, C030, C031, C032, C033, C034, C035, C036, C037, C038, C039, C040, C041, C042, C043, C044, C045, C046, C047, C048, C049, C050, C051, C052, C053, C054, C055, C056, C057, C058, C059, C060, C061, C062, C063, C064, C065, C066, C067, C068, C069, C070, C071, C072, C073, C074, C075, C076, C077, C078, C079, C080, C081, C082, C083, C084, C085, C086, C087, C088, C089, C090, C091, C092, C093, C094, C095, C096, C097, C098, C099, C100]
GO:0022724	myeloid leukocyte activation	6.74E-07	9.64E-05	5.98E-09	5.98E-09[1, 4]	Group10	6.05	15.00[C013, C014, C015, C016, C017, C018, C019, C020, C021, C022, C023, C024, C025, C026, C027, C028, C029, C030, C031, C032, C033, C034, C035, C036, C037, C038, C039, C040, C041, C042, C043, C044, C045, C046, C047, C048, C049, C050, C051, C052, C053, C054, C055, C056, C057, C058, C059, C060, C061, C062, C063, C064, C065, C066, C067, C068, C069, C070, C071, C072, C073, C074, C075, C076, C077, C078, C079, C080, C081, C082, C083, C084, C085, C086, C087, C088, C089, C090, C091, C092, C093, C094, C095, C096, C097, C098, C099, C100]
GO:0022703	regulation of leukocyte mediated immunity	9.17E-05	5.19E-03	5.98E-09	5.98E-09[1, 4]	Group10	4.78	10.00[C013, C014, C015, C016, C017, C018, C019, C020, C021, C022, C023, C024, C025, C026, C027, C028, C029, C030, C031, C032, C033, C034, C035, C036, C037, C038, C039, C040, C041, C042, C043, C044, C045, C046, C047, C048, C049, C050, C051, C052, C053, C054, C055, C056, C057, C058, C059, C060, C061, C062, C063, C064, C065, C066, C067, C068, C069, C070, C071, C072, C073, C074, C075, C076, C077, C078, C079, C080, C081, C082, C083, C084, C085, C086, C087, C088, C089, C090, C091, C092, C093, C094, C095, C096, C097, C098, C099, C100]
GO:0008620	granulocyte activation	1.81E-04	1.97E-02	5.98E-09	5.98E-09[1, 4]	Group10	11.80	5.00[C013, C01

**Supplementary Table 2**

<b>tex</b>	<b>teff</b>	<b>tmem</b>	<b>tmpec</b>	<b>tslec</b>	<b>temra</b>
1110061A1	FOLR4	ABCA3	2010300C02RIK	44450	ANKDD1A
1500001L2	8430438L05RIK	ABCC4	ABCA3	2610528A11RIK	ARHGEF3
2010200L2	A330103N21RIK	CAMK4	ABI2	4933413G19RIK	BAG2
ABCF2	ATP8A1	DNMT3A	ACPP	AA414768	CASZ1
ACAS2	BC030940	LFNG	ACTN1	ACSS2	CCDC117
ACTB	BCL2	PIGN	ADK	ANXA4	CD244
ACTB	CD2AP	PPM1B	AFF3	APOBEC2	CEP78
ACTR1B	CD69	SNN	AFP	AS3MT	CTBP2
ADD3	CEPT1	TRIM34	AHR	BORCS7	CUL4A
ADD3	D630014A15RIK	ZFP207	ALS2CL	BZRAP1	CX3CR1
ADD3	D630014A15RIK		APOL7B	CAR5B	DGKD
ADNP	DAF1		AR	CCL27A	DOCK5
AGPS	DIRC2		ARHGAP5	CCL3	DPYSL2
AKT2	DIRC2		ARMCX2	CCL6	EMC2
AP1GBP1	DSCR5		ART2B	CCL9	EXOC4
AP3M2	FOXO1		ARXES2	CD244	FAM122B
APEH	FOXP1		AXL	CHIT1	FAM126A
APEH	HSD17B7		BACH2	CMA1	FAM204A
ARCN1	IKBKB		BCL2	CMKLR1	FAM49A
ARFIP1	IRF2BP2		BTBD11	CX3CR1	FAM63B
ARHGAP12	RASA2		BTG1	CYP17A1	FAM69A
ARHGEF18	REV1L		BTLA	DAPK2	FCGR3A
ASH1L	RPL12		CCR6	DIXDC1	FGL2
ATIC	SATB1		CCR7	ESM1	FNIP2
ATP10D	SLC14A1		CCR9	FKBP10	GBP3
ATP11B	TMLHE		CD200	GAS2L3	GNPTAB
ATP8A1	UBE2I		CD2AP	GPX8	GOLIM4
ATP9B	ZFP318		CD55	GSG2	GSAP
AW536289	ZHX2		CD7	GZMA	HDAC8
BCLAF1			CD86	HAVCR2	HENMT1
BFAR			CLYBL	HIST1H2BC	HMG3
BFAR			CMPK2	IFITM10	HSPB11
BRMS1L			CTLA4	INSL6	IDH1
BTBD14A			CXCR5	ITGAM	IGF2R
BTBD5			DAPL1	KCNJ8	ITGAM
CCNT2			DDR1	KLRA21	JAZF1
CCNT2			DDX60	KLRA3	KIR2DL1
CDC14B			DHX58	KLRE1	KIR2DL2

CDC14B	DOCK9	KLRG1	KIR2DL3
CDC27	ELOVL6	MASTL	KIR2DL4
CDC40	EMB	MDM1	KIR2DL5A
CDH11	EVL	MEGF9	KIR2DS1
CDK5RAP1	F2RL1	MIAT	KIR2DS2
CDS2	FAAH	NHSL2	KIR2DS3
CEPT1	FAM101B	NRARP	KIR2DS4
CEPT1	FAM102A	OSBPL3	KIR2DS5
CHC1L	FAM134B	P3H4	KIR3DL1
COMMD8	FAM169B	PRDM1	KIR3DL2
CPNE3	FAM213A	PRF1	KIR3DL3
CPSF1	FAM26F	RACGAP1	KIR3DS1
CREBBP	FAM46C	RAP1GAP2	KLRC3
CRNKL1	FARSB	RHOQ	KLRD1
CTSO	FCHSD2	S1PR5	KLRF1
CUL3	FCRL1	SMPDL3B	LILRB1
CUL3	FILIP1L	SNX10	LUC7L3
CUL3	GBP6	SORD	LYN
CUL4B	GBP9	SPAG1	LYPLA1
CUL5	GM10406	STMN1	MAPK1
D1ERTD762	GM10409	TCRG-C1	MCTP2
DCTN3	GM9706	TKTL1	MDM1
DDX46	GPR183	TPPP3	METTL3
DNM1L	H2-OA	TRAF3IP1	MINPP1
DNMT3A	H2-OB	TSGA10	MYL12A
EDEM1	HVCN1	TSPAN32	NBN
EDEM1	ID3	ZEB2	NFYB
EEF1E1	IER3		OSGEPL1
ELK4	IFI205		P2RX7
ENC1	IFI44		PALLD
ENTPD5	IFIT1		PCID2
EPS8L1	IFIT3		PKD2
FARSLB	IFITM1		PROK2
FBXL12	IFITM3		PRSS23
FBXL4	IGHM		PSTPIP2
FOXK1	IIGP1		PTCH1
FTHFSDC1	IL7R		PTGDS
FVT1	INPP4B		PTPN12
FXVD6	IPO4		PTPN4
GALNT6	IRAK3		RAB29



GMFB	ISG20	RHEBL1
GMPS	JMJD1C	RNF135
GNAI3	KBTBD11	SAMD3
GOSR1	KLF4	SEC23IP
HARSL	LILR4B	SLC15A4
HBP1	LTB	SLFN13
HIPK3	LY6E	SPIN4
IAN4	LYPD6B	SRPK2
INPP5F	LYSMD2	SSBP3
INSIG1	MAP7	STK39
IQGAP1	MS4A4C	STX8
IVNS1ABP	MTMR7	TBK1
JAG2	MYB	TEP1
KATNA1	MYC	TGFBR1
KBTBD2	NCF1	TMEM14A
KCTD4	NRP1	TMEM64
KIF1B	NSG2	TTC38
KLF3	NT5E	TTC39B
KLF7	OAS3	TYROBP
KLHL6	OASL1	UBE2F
LBR	OASL2	USP28
LIN7C	P2RX7	VRK2
LTA4H	PAK6	YME1L1
MADD	PANK1	ZBP1
MAK3	PARP12	ZEB2
MAN1B	PARP8	ZNF600
MAN1B	PDCD1LG2	
ME2	PDK1	
MLL3	PFN2	
MMD	PGS1	
MSL2	PIK3IP1	
MTA3	PIM2	
MTAP	PLEKHA1	
MYO1G	POU2AF1	
NAPG	POU6F1	
NDUFS1	PRMT2	
NEK9	PRSS30	
NFATC1	PTGER2	
NGLY1	PTPN3	
NR2C2	PYDC4	

NRF1	QPCT
NT5C3	QTRTD1
NUP205	RAB37
NUP210	RGS10
OSGEP	RNF144A
PAG	RSAD2
PCCA	RTP4
PCOLN3	SELL
PDE4B	SERPINA3G
PEX13	SESN3
PIGT	SGMS1
PIK3C2A	SH2B3
PITRM1	SH3BP5
PLP2	SIRT5
PPARBP	SLAMF6
PPM1B	SLC14A1
PPP2R5A	SLFN1
PPP3CB	SMAD1
PPP4R2	SOCS3
PRKCN	SOCS5
PRPF4B	SPINT2
PRPS2	SSBP2
PURA	ST6GAL1
RAB14	ST8SIA1
RAB3IP	TACC2
RAD51AP1	TAF4B
RAPGEF2	TBC1D4
RASSF2	TCF12
RASSF3	TCF7
RBM3	TDRP
RBM5	TESPA1
RCOR3	THA1
RNF111	TLR1
RNF111	TNFRSF22
RNF125	TNFRSF25
RNMT	TOX
RPL3L	TPD52
RPP14	TRAF1
RUTBC2	TREML2
SATB1	TRIB2

SATB1	TRIB3
SEN2	TRMT61A
7-Sep	TSC22D1
SERPIN4	UGT1A1
SERTAD3	USP18
SFRS6	USP53
SFRS7	VAV3
SFXN2	VWA5A
SGK3	WDR12
SIRT1	WFIKKN2
SLC35A5	ZBTB18
SLC35B3	ZC3H12D
SLC38A1	ZEB1
SLC39A10	
SLC9A6	
SLCO3A1	
SMAD5	
SP100	
SRPK2	
STAG1	
STAT5B	
SYAP1	
TARDBP	
TAZ	
TBC1D17	
TBPL1	
TGFBR1	
TIA1	
TMOD3	
TNRC15	
TRIM23	
TRP53BP2	
TRPM7	
TTC13	
TTC14	
UBE2D3	
UCHL5	
USP22	
USP28	
UTRN	

VDRIP  
WDR11  
WDR37  
WDR37  
WDR37  
ZC3HDC7  
ZFP148  
ZFP191  
ZFP369  
ZNRF2

## **5.0 Chapter Five – Conclusions**

The findings of this work illustrate the effectiveness of HDAC inhibition in subverting tumor resistance during ACT. MS-275 delivery promoted epigenetic and transcriptional reprogramming within the TME to propagate broad immunomodulatory effects that enhanced the therapeutic efficacy of ACT. Combination therapy can therefore allow for the durable regression of highly immunosuppressive solid tumors.

### **5.1 Tumor resistance can supersede potent therapy-driven antitumor immune responses**

In Chapter Two – Four, our implemented ACT protocol utilized adoptive transfer of memory-cultured tumor-specific T cells followed by viral vaccination. As was previously described, antigen re-stimulation following adoptive transfer potentiates the magnitude of tumor regression; indeed, in B16, MC38, and CMS5 7-day old tumors, we were consistently able to achieve complete acute tumor regression. However, tumor resistance superseded the potency of our vaccination platform in determining clinical outcomes. Resistance to immunotherapy manifested as two separate observations: 1) Acquired resistance, wherein tumor relapse occurred from an outgrowth of immune escape variants (Chapter Two and Three) and 2) primary resistance, wherein increased tumor burden facilitated loss of immediate tumor control due to systemic ablation of antitumor immunity (Chapter Four). In each situation, the rapid expansion of transferred cells failed to prevent loss of tumor recognition or prolific induction of T cell exhaustion. These tumor resistance mechanisms arose independently but are not mutually exclusive; as a result, it is difficult to rationally design immunotherapies to target every manifestation of this multifaceted issue.

### **5.2 TME reprogramming induces a cascade of pro-inflammatory events that disrupt tumor immunosuppression and potentiate antitumor immunity**

MS-275 delivery may provide the conceptual framework to comprehensively address multiple mechanisms of tumor resistance that may not have an overlapping origin. Indeed, the work described suggests that epigenetic reprogramming via HDAC inhibition can reprogram the TME to induce a cascade of immunomodulatory changes that are therapeutically beneficial. In Chapter Four, we showed that MS-275 treatment reversed the expression of unique immunosuppressive pathways in growing tumors to facilitate a pro-inflammatory antitumor response. In Chapter Three, the local inflammatory changes were conducive to the expression of immunoactivating signals and, in Chapter Two, polarization

signals. The net benefits of these microenvironmental changes include subverting tumor immunosuppression and broadening the spectrum of antitumor immunity.

In Chapter Two, tumor-infiltrating myeloid cells were highly immunosuppressive; however, during MS-275 delivery, pro-inflammatory signals including IFN $\gamma$  polarized these cells into cytotoxic effectors with the ability to reject immune escape variants and prevent tumor relapse. In Chapter Three, changes in the local inflammatory milieu promoted the maturation of CD8 $^+$  and CD103 $^+$  cross-presenting DCs, leading to the activation of endogenous T cell responses that targeted p15E, another tumor-rejection antigen. Simultaneously, the reduction of local immunosuppressive factors such as nitric oxide, arginase, and TGF $\beta$  led to partial ablation of Tregs, which were capable of suppressing the magnitude of p15E-specific endogenous T cell responses. In Chapter Four, MS-275 reversed tumor burden-dependent immunosuppressive pathway signatures in the TME to prevent induction of T cell exhaustion in transferred cells and restore tumor control during ACT. Overall, TME reprogramming via HDAC inhibition has interconnecting consequences that ultimately benefit cancer immunotherapies in overcoming a plethora of tumor resistance mechanisms.

### **5.3 Selective inhibition of Class I HDACs may ubiquitously promote antitumor programmes**

Interestingly, despite having broad immunological significance, HDACi have been found to affect only a relatively small number of genes, depending on cell type and HDACi used (266). While different HDACi inhibit different HDAC classes, they share some commonalities in immunotherapeutic potential such as lymphocyte activation and antigen presentation (266). However, HDACi have shown conflicting effects on immunosuppressive cell accumulation and pro-/anti-inflammation (266). As a result, the HDAC inhibition profile likely contributes to the breadth of its subversive potential against tumor immunosuppressiveness. In Chapter Three, we found that MS-275, which selectively inhibits HDAC1 and HDAC3, had a progressive anti-inflammatory effect over time, but showed early and acute pro-inflammatory up-regulation with particular emphasis on Type I IFN and IL-12 production. Additionally, in Chapter Two and Three, IFN $\gamma$  production was up-regulated at later timepoints. It is possible that these selective inflammatory changes can only be observed with MS-275's HDAC inhibition profile. By extension, potentiation of antitumor immunity to overcome tumor resistance can only be observed using MS-275 or similar HDACi.

#### **5.4 Reinvigoration of endogenous T cells is critical for cancer immunotherapy in resistant tumors**

In cancer immunotherapy, endogenously activated CD8<sup>+</sup> T cells are a valuable contributor for effective tumor clearance regardless if they play a primary or secondary therapeutic role. In Chapter Three, ACT targeting a defined tumor antigen can be supplemented by immunoactivating endogenous responses against other tumor antigens to broaden the spectrum of antitumor immune attack and prevent tumor relapse. In Chapter Four, viral vaccination was utilized to mobilize endogenous CD8<sup>+</sup> T cell responses as a primary means of tumor control. Finally, the effectiveness of PD-1 checkpoint therapy has in recent times been less attributed to curbing the tolerizing effect of tumor-expressed PD-L1 on effector T cell function, but rather to promoting the non-specific expansion of endogenous tumor-infiltrating lymphocytes (187).

However, in Chapter Four, we demonstrated that tumor burden facilitates dysfunction within CD8<sup>+</sup> T cells through the systemic induction of cellular exhaustion programmes. Exogenously- and endogenously- derived tumor-specific CD8<sup>+</sup> T cells alike displayed curbed proliferative potential in response to antigen restimulation and their expansion was quickly ablated. Indeed, for PD-1 checkpoint therapy, extent of tumor burden was shown to be a negative determinant of successful clinical outcomes (267). As a result, tumor burden-induced exhaustion is a severe issue for many forms of cancer immunotherapy, not just ACT. By contrast, in Chapter Four we demonstrated that concomitant MS-275 delivery was able to reinvigorate tumor-specific CD8<sup>+</sup> T cells to potentiate their proliferation and persistence in large, solid tumors. This suggests that the effectiveness of MS-275 extends to any cancer immunotherapy that relies on the *in vivo* activation of antitumor CD8<sup>+</sup> T cell responses.

#### **5.5 The Future of HDAC Inhibition in Cancer Immunotherapy**

In Chapter Four, we provided evidence to suggest that MS-275 was able to restore antitumor immune responses and tumor control during ACT. While its effects on tumor normalization confirmed that HDAC inhibition has corrective value in subverting the immunosuppressive pathways being up-regulated within the TME, we also provided some indirect evidence to suggest that HDACi can have a potentiating effect on T cells directly. Indeed, adoptively transferred CD8<sup>+</sup> T cells recovered from tumors treated with MS-275 displayed a unique transcriptional signature, marked by enhanced activation-dependent signaling, up-regulated Tim-3 expression (Tim3<sup>hi</sup>), and terminal effector-like lineage commitment. These characteristics were not expressed in small, ACT-treated tumors in the absence of MS-275 which would have represented a corrective outcome. More importantly,

Tim3<sup>hi</sup> cells showed higher expression of Ki-67, suggesting a proliferative advantage upon antigen re-stimulation. It may be possible that MS-275 may predispose tumor-specific T cells to better functional outcomes post-activation which in turn may allow them to be inert to the immunosuppressiveness of large, solid tumors. If true, then there would be a decreased requirement for cancer immunotherapies to address the plethora of tumor resistance mechanisms or seek a “silver bullet” solution for tumor resistance. HDAC inhibition can be used instead for “T cell doping” which would theoretically create a more powerful antitumor immune response that is resistant to tumor immunosuppression.

## **5.6 Desired Post-activation T Cell Phenotypes for Cancer Immunotherapy**

It has been traditionally accepted that the adoptive transfer of less differentiated T lymphocytes during ACT allowed for higher proliferative potential compared to fully or terminally differentiated effector cells. Although memory cells do not have comparable cytotoxic potential, the increased magnitude of the antitumor immune response upon *in vivo* reactivation and differentiation of these transferred cells into effector cells is what contributes to therapeutic improvement. While the *in vivo* reactivation step thus plays a major role in determining the fate of transferred T cells, it is unclear whether this process can be sculpted to achieve a desired post-activation effector phenotype.

In Chapter Four, it was demonstrated that reinvigoration of endogenous and transferred tumor-specific CD8<sup>+</sup> cells in highly immunosuppressive large tumors correlated with significant up-regulation of Tim-3. Despite being perceived as a checkpoint or co-inhibitory receptor, Tim-3 itself does not inherently express an inhibitory signaling motif. Indeed, our data may suggest that Tim-3 influences T cell activation and differentiation in favor of the short-lived effector lineage. This was functionally associated with higher proliferative potential, persistence, and killing. Moving forward, it would be interesting to examine how epigenetic modulation of memory T cells prior and during re-stimulation influences the expression of Tim-3 and if/how that potentiates T cell function, regardless of tumor burden or resistance.



## **6.0 Chapter Six – References**

1. A. D. Lopez, C. D. Mathers, M. Ezzati, D. T. Jamison, C. J. L. Murray, in *Global Burden of Disease and Risk Factors*, A. D. Lopez, C. D. Mathers, M. Ezzati, D. T. Jamison, C. J. L. Murray, Eds. (Washington (DC), 2006).
2. M. Schuster, A. Nechansky, R. Kircheis, Cancer immunotherapy. *Biotechnology journal* **1**, 138-147 (2006).
3. D. Hanahan, R. A. Weinberg, The hallmarks of cancer. *Cell* **100**, 57-70 (2000).
4. G. P. Dunn, L. J. Old, R. D. Schreiber, The three Es of cancer immunoediting. *Annual review of immunology* **22**, 329-360 (2004).
5. P. Ehrlich, Ueber den jetzigen stand der Karzinomforschung. *Ned.Tijdschr. Geneeskd.* **5**, 273–290 (1909).
6. F. M. Burnet, The concept of immunological surveillance. *Progress in experimental tumor research* **13**, 1-27 (1970).
7. L. J. Old, E. A. Boyse, Immunology of Experimental Tumors. *Annual review of medicine* **15**, 167-186 (1964).
8. G. Klein, Tumor antigens. *Annual review of microbiology* **20**, 223-252 (1966).
9. O. Stutman, Tumor development after 3-methylcholanthrene in immunologically deficient athymic-nude mice. *Science* **183**, 534-536 (1974).
10. H. C. Outzen, R. P. Custer, G. J. Eaton, R. T. Prehn, Spontaneous and induced tumor incidence in germfree "nude" mice. *Journal of the Reticuloendothelial Society* **17**, 1-9 (1975).
11. J. Rygaard, C. O. Povlsen, The mouse mutant nude does not develop spontaneous tumours. An argument against immunological surveillance. *Acta pathologica et microbiologica Scandinavica. Section B: Microbiology and immunology* **82**, 99-106 (1974).
12. A. S. Dighe, E. Richards, L. J. Old, R. D. Schreiber, Enhanced in vivo growth and resistance to rejection of tumor cells expressing dominant negative IFN gamma receptors. *Immunity* **1**, 447-456 (1994).
13. D. H. Kaplan *et al.*, Demonstration of an interferon gamma-dependent tumor surveillance system in immunocompetent mice. *Proceedings of the National Academy of Sciences of the United States of America* **95**, 7556-7561 (1998).

14. S. E. Street, E. Cretney, M. J. Smyth, Perforin and interferon-gamma activities independently control tumor initiation, growth, and metastasis. *Blood* **97**, 192-197 (2001).
15. G. P. Dunn, A. T. Bruce, H. Ikeda, L. J. Old, R. D. Schreiber, Cancer immunoediting: from immunosurveillance to tumor escape. *Nature immunology* **3**, 991-998 (2002).
16. M. Girardi *et al.*, Regulation of cutaneous malignancy by gammadelta T cells. *Science* **294**, 605-609 (2001).
17. M. J. Smyth, D. I. Godfrey, J. A. Trapani, A fresh look at tumor immunosurveillance and immunotherapy. *Nature immunology* **2**, 293-299 (2001).
18. P. Matzinger, Tolerance, danger, and the extended family. *Annual review of immunology* **12**, 991-1045 (1994).
19. W. M. Yokoyama, Now you see it, now you don't! *Nature immunology* **1**, 95-97 (2000).
20. A. Cerwenka *et al.*, Retinoic acid early inducible genes define a ligand family for the activating NKG2D receptor in mice. *Immunity* **12**, 721-727 (2000).
21. A. Diefenbach, E. R. Jensen, A. M. Jamieson, D. H. Raulet, Rae1 and H60 ligands of the NKG2D receptor stimulate tumour immunity. *Nature* **413**, 165-171 (2001).
22. J. F. Bromberg, C. M. Horvath, Z. Wen, R. D. Schreiber, J. E. Darnell, Jr., Transcriptionally active Stat1 is required for the antiproliferative effects of both interferon alpha and interferon gamma. *Proceedings of the National Academy of Sciences of the United States of America* **93**, 7673-7678 (1996).
23. A. Kumar, M. Commane, T. W. Flickinger, C. M. Horvath, G. R. Stark, Defective TNF-alpha-induced apoptosis in STAT1-null cells due to low constitutive levels of caspases. *Science* **278**, 1630-1632 (1997).
24. D. M. Pardoll, Spinning molecular immunology into successful immunotherapy. *Nature reviews. Immunology* **2**, 227-238 (2002).
25. V. Shankaran *et al.*, IFNgamma and lymphocytes prevent primary tumour development and shape tumour immunogenicity. *Nature* **410**, 1107-1111 (2001).
26. W. B. Coley, The treatment of malignant tumors by repeated inoculations of erysipelas. With a report of ten original cases. 1893. *Clinical orthopaedics and related research*, 3-11 (1991).

27. B. Wiemann, C. O. Starnes, Coley's toxins, tumor necrosis factor and cancer research: a historical perspective. *Pharmacology & therapeutics* **64**, 529-564 (1994).
28. A. B. Alexandroff, A. M. Jackson, M. A. O'Donnell, K. James, BCG immunotherapy of bladder cancer: 20 years on. *Lancet* **353**, 1689-1694 (1999).
29. F. G. Perabo *et al.*, Superantigen-activated mononuclear cells induce apoptosis in transitional cell carcinoma. *Anticancer research* **25**, 3565-3573 (2005).
30. R. J. Sylvester, Bacillus Calmette-Guerin treatment of non-muscle invasive bladder cancer. *International journal of urology : official journal of the Japanese Urological Association* **18**, 113-120 (2011).
31. F. M. Burnet, Immunological aspects of malignant disease. *Lancet* **1**, 1171-1174 (1967).
32. F. M. Burnet, Immunological surveillance in neoplasia. *Transplantation reviews* **7**, 3-25 (1971).
33. P. Chaux *et al.*, Identification of five MAGE-A1 epitopes recognized by cytolytic T lymphocytes obtained by in vitro stimulation with dendritic cells transduced with MAGE-A1. *Journal of immunology* **163**, 2928-2936 (1999).
34. P. Chaux *et al.*, Identification of MAGE-3 epitopes presented by HLA-DR molecules to CD4(+) T lymphocytes. *The Journal of experimental medicine* **189**, 767-778 (1999).
35. Y. Kawakami *et al.*, Cloning of the gene coding for a shared human melanoma antigen recognized by autologous T cells infiltrating into tumor. *Proceedings of the National Academy of Sciences of the United States of America* **91**, 3515-3519 (1994).
36. Y. Kawakami *et al.*, Identification of a human melanoma antigen recognized by tumor-infiltrating lymphocytes associated with in vivo tumor rejection. *Proceedings of the National Academy of Sciences of the United States of America* **91**, 6458-6462 (1994).
37. R. F. Wang, E. Appella, Y. Kawakami, X. Kang, S. A. Rosenberg, Identification of TRP-2 as a human tumor antigen recognized by cytotoxic T lymphocytes. *The Journal of experimental medicine* **184**, 2207-2216 (1996).

38. J. G. Houbiers *et al.*, In vitro induction of human cytotoxic T lymphocyte responses against peptides of mutant and wild-type p53. *European journal of immunology* **23**, 2072-2077 (1993).
39. D. I. Gabrilovich, S. Patterson, A. V. Timofeev, J. J. Harvey, S. C. Knight, Mechanism for dendritic cell dysfunction in retroviral infection of mice. *Clinical immunology and immunopathology* **80**, 139-146 (1996).
40. M. Nakagawa *et al.*, Cytotoxic T lymphocyte responses to E6 and E7 proteins of human papillomavirus type 16: relationship to cervical intraepithelial neoplasia. *The Journal of infectious diseases* **175**, 927-931 (1997).
41. N. P. Restifo, M. E. Dudley, S. A. Rosenberg, Adoptive immunotherapy for cancer: harnessing the T cell response. *Nature reviews. Immunology* **12**, 269-281 (2012).
42. S. A. Rosenberg, N. P. Restifo, J. C. Yang, R. A. Morgan, M. E. Dudley, Adoptive cell transfer: a clinical path to effective cancer immunotherapy. *Nat Rev Cancer* **8**, 299-308 (2008).
43. L. Gattinoni, D. J. Powell, Jr., S. A. Rosenberg, N. P. Restifo, Adoptive immunotherapy for cancer: building on success. *Nature reviews. Immunology* **6**, 383-393 (2006).
44. C. A. Klebanoff *et al.*, Central memory self/tumor-reactive CD8<sup>+</sup> T cells confer superior antitumor immunity compared with effector memory T cells. *Proceedings of the National Academy of Sciences of the United States of America* **102**, 9571-9576 (2005).
45. L. Gattinoni *et al.*, Acquisition of full effector function in vitro paradoxically impairs the in vivo antitumor efficacy of adoptively transferred CD8<sup>+</sup> T cells. *The Journal of clinical investigation* **115**, 1616-1626 (2005).
46. C. Berger *et al.*, Adoptive transfer of effector CD8<sup>+</sup> T cells derived from central memory cells establishes persistent T cell memory in primates. *The Journal of clinical investigation* **118**, 294-305 (2008).
47. X. Wang *et al.*, Engraftment of human central memory-derived effector CD8<sup>+</sup> T cells in immunodeficient mice. *Blood* **117**, 1888-1898 (2011).
48. A. G. Chapuis *et al.*, Transferred melanoma-specific CD8<sup>+</sup> T cells persist, mediate tumor regression, and acquire central memory phenotype. *Proceedings of the National Academy of Sciences of the United States of America* **109**, 4592-4597 (2012).

49. M. H. Kershaw, M. W. Teng, M. J. Smyth, P. K. Darcy, Supernatural T cells: genetic modification of T cells for cancer therapy. *Nature reviews. Immunology* **5**, 928-940 (2005).
50. M. S. Topp *et al.*, Restoration of CD28 expression in CD28- CD8+ memory effector T cells reconstitutes antigen-induced IL-2 production. *The Journal of experimental medicine* **198**, 947-955 (2003).
51. J. Charo *et al.*, Bcl-2 overexpression enhances tumor-specific T-cell survival. *Cancer research* **65**, 2001-2008 (2005).
52. K. Liu, S. A. Rosenberg, Interleukin-2-independent proliferation of human melanoma-reactive T lymphocytes transduced with an exogenous IL-2 gene is stimulation dependent. *Journal of immunotherapy* **26**, 190-201 (2003).
53. C. Hsu *et al.*, Primary human T lymphocytes engineered with a codon-optimized IL-15 gene resist cytokine withdrawal-induced apoptosis and persist long-term in the absence of exogenous cytokine. *Journal of immunology* **175**, 7226-7234 (2005).
54. M. H. Kershaw *et al.*, Redirecting migration of T cells to chemokine secreted from tumors by genetic modification with CXCR2. *Human gene therapy* **13**, 1971-1980 (2002).
55. S. A. Rosenberg *et al.*, Durable complete responses in heavily pretreated patients with metastatic melanoma using T-cell transfer immunotherapy. *Clinical cancer research : an official journal of the American Association for Cancer Research* **17**, 4550-4557 (2011).
56. O. Itzhaki *et al.*, Establishment and large-scale expansion of minimally cultured "young" tumor infiltrating lymphocytes for adoptive transfer therapy. *Journal of immunotherapy* **34**, 212-220 (2011).
57. M. J. Besser *et al.*, Clinical responses in a phase II study using adoptive transfer of short-term cultured tumor infiltration lymphocytes in metastatic melanoma patients. *Clinical cancer research : an official journal of the American Association for Cancer Research* **16**, 2646-2655 (2010).
58. G. M. Bendle *et al.*, Lethal graft-versus-host disease in mouse models of T cell receptor gene therapy. *Nature medicine* **16**, 565-570, 561p following 570 (2010).
59. R. A. Morgan *et al.*, Case report of a serious adverse event following the administration of T cells transduced with a chimeric antigen receptor recognizing

- ERBB2. *Molecular therapy : the journal of the American Society of Gene Therapy* **18**, 843-851 (2010).
60. R. Brentjens, R. Yeh, Y. Bernal, I. Riviere, M. Sadelain, Treatment of chronic lymphocytic leukemia with genetically targeted autologous T cells: case report of an unforeseen adverse event in a phase I clinical trial. *Molecular therapy : the journal of the American Society of Gene Therapy* **18**, 666-668 (2010).
  61. M. R. Parkhurst *et al.*, T cells targeting carcinoembryonic antigen can mediate regression of metastatic colorectal cancer but induce severe transient colitis. *Molecular therapy : the journal of the American Society of Gene Therapy* **19**, 620-626 (2011).
  62. L. A. Johnson *et al.*, Gene therapy with human and mouse T-cell receptors mediates cancer regression and targets normal tissues expressing cognate antigen. *Blood* **114**, 535-546 (2009).
  63. M. E. Heffernan, S. M. Garland, M. A. Kane, Global reduction of cervical cancer with human papillomavirus vaccines: insights from the hepatitis B virus vaccine experience. *Sexual health* **7**, 383-390 (2010).
  64. E. Gilboa, DC-based cancer vaccines. *The Journal of clinical investigation* **117**, 1195-1203 (2007).
  65. B. M. Andersen, J. R. Ohlfest, Increasing the efficacy of tumor cell vaccines by enhancing cross priming. *Cancer letters* **325**, 155-164 (2012).
  66. G. S. Salvesen, V. M. Dixit, Caspase activation: the induced-proximity model. *Proceedings of the National Academy of Sciences of the United States of America* **96**, 10964-10967 (1999).
  67. K. Takeda *et al.*, Critical role for tumor necrosis factor-related apoptosis-inducing ligand in immune surveillance against tumor development. *The Journal of experimental medicine* **195**, 161-169 (2002).
  68. S. Dermime, A. Armstrong, R. E. Hawkins, P. L. Stern, Cancer vaccines and immunotherapy. *British medical bulletin* **62**, 149-162 (2002).
  69. B. Moss, Genetically engineered poxviruses for recombinant gene expression, vaccination, and safety. *Proceedings of the National Academy of Sciences of the United States of America* **93**, 11341-11348 (1996).
  70. M. Brown *et al.*, Antigen gene transfer to cultured human dendritic cells using recombinant avipoxvirus vectors. *Cancer gene therapy* **6**, 238-245 (1999).

71. R. Drillien, D. Spehner, A. Bohbot, D. Hanau, Vaccinia virus-related events and phenotypic changes after infection of dendritic cells derived from human monocytes. *Virology* **268**, 471-481 (2000).
72. C. Bonini, S. P. Lee, S. R. Riddell, P. D. Greenberg, Targeting antigen in mature dendritic cells for simultaneous stimulation of CD4<sup>+</sup> and CD8<sup>+</sup> T cells. *Journal of immunology* **166**, 5250-5257 (2001).
73. J. W. Hodge, M. Chakraborty, C. Kudo-Saito, C. T. Garnett, J. Schlom, Multiple costimulatory modalities enhance CTL avidity. *Journal of immunology* **174**, 5994-6004 (2005).
74. S. Yang, K. Y. Tsang, J. Schlom, Induction of higher-avidity human CTLs by vector-mediated enhanced costimulation of antigen-presenting cells. *Clinical cancer research : an official journal of the American Association for Cancer Research* **11**, 5603-5615 (2005).
75. D. Fioretti, S. Iurescia, V. M. Fazio, M. Rinaldi, DNA vaccines: developing new strategies against cancer. *Journal of biomedicine & biotechnology* **2010**, 174378 (2010).
76. C. Larocca, J. Schlom, Viral vector-based therapeutic cancer vaccines. *Cancer journal* **17**, 359-371 (2011).
77. S. J. Draper, J. L. Heeney, Viruses as vaccine vectors for infectious diseases and cancer. *Nature reviews. Microbiology* **8**, 62-73 (2010).
78. S. A. Rosenberg, J. C. Yang, N. P. Restifo, Cancer immunotherapy: moving beyond current vaccines. *Nature medicine* **10**, 909-915 (2004).
79. C. A. Klebanoff, N. Acquavella, Z. Yu, N. P. Restifo, Therapeutic cancer vaccines: are we there yet? *Immunol Rev* **239**, 27-44 (2011).
80. W. W. Overwijk *et al.*, Tumor regression and autoimmunity after reversal of a functionally tolerant state of self-reactive CD8<sup>+</sup> T cells. *J Exp Med* **198**, 569-580 (2003).
81. Y. Lou *et al.*, Dendritic cells strongly boost the antitumor activity of adoptively transferred T cells in vivo. *Cancer Res* **64**, 6783-6790 (2004).
82. M. A. de Witte *et al.*, TCR gene therapy of spontaneous prostate carcinoma requires in vivo T cell activation. *J Immunol* **181**, 2563-2571 (2008).

83. C. A. Klebanoff *et al.*, Programming tumor-reactive effector memory CD8<sup>+</sup> T cells in vitro obviates the requirement for in vivo vaccination. *Blood* **114**, 1776-1783 (2009).
84. S. Ugel *et al.*, In vivo administration of artificial antigen-presenting cells activates low-avidity T cells for treatment of cancer. *Cancer Res* **69**, 9376-9384 (2009).
85. M. A. Pule *et al.*, Virus-specific T cells engineered to coexpress tumor-specific receptors: persistence and antitumor activity in individuals with neuroblastoma. *Nat Med* **14**, 1264-1270 (2008).
86. F. O. Smith, J. A. Klapper, J. R. Wunderlich, S. A. Rosenberg, M. E. Dudley, Impact of a recombinant fowlpox vaccine on the efficacy of adoptive cell therapy with tumor infiltrating lymphocytes in a patient with metastatic melanoma. *J Immunother* **32**, 870-874 (2009).
87. M. E. Dudley *et al.*, Adoptive cell transfer therapy following non-myeloablative but lymphodepleting chemotherapy for the treatment of patients with refractory metastatic melanoma. *J Clin Oncol* **23**, 2346-2357 (2005).
88. C. A. Klebanoff *et al.*, Determinants of successful CD8<sup>+</sup> T-cell adoptive immunotherapy for large established tumors in mice. *Clin Cancer Res* **17**, 5343-5352 (2011).
89. D. I. Gabrilovich *et al.*, Production of vascular endothelial growth factor by human tumors inhibits the functional maturation of dendritic cells. *Nature medicine* **2**, 1096-1103 (1996).
90. J. Y. Shin, I. H. Yoon, J. S. Kim, B. Kim, C. G. Park, Vascular endothelial growth factor-induced chemotaxis and IL-10 from T cells. *Cellular immunology* **256**, 72-78 (2009).
91. A. Ohta *et al.*, A2A adenosine receptor protects tumors from antitumor T cells. *Proceedings of the National Academy of Sciences of the United States of America* **103**, 13132-13137 (2006).
92. Y. Akasaki *et al.*, Induction of a CD4<sup>+</sup> T regulatory type 1 response by cyclooxygenase-2-overexpressing glioma. *Journal of immunology* **173**, 4352-4359 (2004).
93. A. J. Muller, P. A. Scherle, Targeting the mechanisms of tumoral immune tolerance with small-molecule inhibitors. *Nature reviews. Cancer* **6**, 613-625 (2006).



94. G. Gerlini *et al.*, Metastatic melanoma secreted IL-10 down-regulates CD1 molecules on dendritic cells in metastatic tumor lesions. *The American journal of pathology* **165**, 1853-1863 (2004).
95. M. Kurte *et al.*, A synthetic peptide homologous to functional domain of human IL-10 down-regulates expression of MHC class I and Transporter associated with Antigen Processing 1/2 in human melanoma cells. *Journal of immunology* **173**, 1731-1737 (2004).
96. D. A. Thomas, J. Massague, TGF-beta directly targets cytotoxic T cell functions during tumor evasion of immune surveillance. *Cancer cell* **8**, 369-380 (2005).
97. L. Gorelik, R. A. Flavell, Immune-mediated eradication of tumors through the blockade of transforming growth factor-beta signaling in T cells. *Nature medicine* **7**, 1118-1122 (2001).
98. M. Ahmadzadeh, S. A. Rosenberg, TGF-beta 1 attenuates the acquisition and expression of effector function by tumor antigen-specific human memory CD8 T cells. *Journal of immunology* **174**, 5215-5223 (2005).
99. M. Karin, F. R. Greten, NF-kappaB: linking inflammation and immunity to cancer development and progression. *Nature reviews. Immunology* **5**, 749-759 (2005).
100. J. L. Luo, S. Maeda, L. C. Hsu, H. Yagita, M. Karin, Inhibition of NF-kappaB in cancer cells converts inflammation- induced tumor growth mediated by TNFalpha to TRAIL-mediated tumor regression. *Cancer cell* **6**, 297-305 (2004).
101. I. Mellman, G. Coukos, G. Dranoff, Cancer immunotherapy comes of age. *Nature* **480**, 480-489 (2011).
102. G. A. Rabinovich, D. Gabrilovich, E. M. Sotomayor, Immunosuppressive strategies that are mediated by tumor cells. *Annual review of immunology* **25**, 267-296 (2007).
103. A. Facciabene *et al.*, Tumour hypoxia promotes tolerance and angiogenesis via CCL28 and T(reg) cells. *Nature* **475**, 226-230 (2011).
104. A. J. McGray *et al.*, Combined vaccination and immunostimulatory antibodies provides durable cure of murine melanoma and induces transcriptional changes associated with positive outcome in human melanoma patients. *Oncoimmunology* **1**, 419-431 (2012).
105. J. Hamanishi *et al.*, Programmed cell death 1 ligand 1 and tumor-infiltrating CD8+ T lymphocytes are prognostic factors of human ovarian cancer. *Proceedings of the*

- National Academy of Sciences of the United States of America* **104**, 3360-3365 (2007).
106. A. T. Parsa *et al.*, Loss of tumor suppressor PTEN function increases B7-H1 expression and immunoresistance in glioma. *Nature medicine* **13**, 84-88 (2007).
  107. C. Blank, T. F. Gajewski, A. Mackensen, Interaction of PD-L1 on tumor cells with PD-1 on tumor-specific T cells as a mechanism of immune evasion: implications for tumor immunotherapy. *Cancer immunology, immunotherapy : CII* **54**, 307-314 (2005).
  108. Y. Ishida, Y. Agata, K. Shibahara, T. Honjo, Induced expression of PD-1, a novel member of the immunoglobulin gene superfamily, upon programmed cell death. *The EMBO journal* **11**, 3887-3895 (1992).
  109. G. J. Freeman *et al.*, Engagement of the PD-1 immunoinhibitory receptor by a novel B7 family member leads to negative regulation of lymphocyte activation. *The Journal of experimental medicine* **192**, 1027-1034 (2000).
  110. Y. Iwai *et al.*, Involvement of PD-L1 on tumor cells in the escape from host immune system and tumor immunotherapy by PD-L1 blockade. *Proceedings of the National Academy of Sciences of the United States of America* **99**, 12293-12297 (2002).
  111. R. M. Siegel, F. K. Chan, H. J. Chun, M. J. Lenardo, The multifaceted role of Fas signaling in immune cell homeostasis and autoimmunity. *Nature immunology* **1**, 469-474 (2000).
  112. D. R. Green, T. A. Ferguson, The role of Fas ligand in immune privilege. *Nature reviews. Molecular cell biology* **2**, 917-924 (2001).
  113. M. Hahne *et al.*, Melanoma cell expression of Fas(Apo-1/CD95) ligand: implications for tumor immune escape. *Science* **274**, 1363-1366 (1996).
  114. J. O'Connell, A. Houston, M. W. Bennett, G. C. O'Sullivan, F. Shanahan, Immune privilege or inflammation? Insights into the Fas ligand enigma. *Nature medicine* **7**, 271-274 (2001).
  115. G. Andreola *et al.*, Induction of lymphocyte apoptosis by tumor cell secretion of FasL-bearing microvesicles. *The Journal of experimental medicine* **195**, 1303-1316 (2002).
  116. F. H. Igney, P. H. Krammer, Tumor counterattack: fact or fiction? *Cancer immunology, immunotherapy : CII* **54**, 1127-1136 (2005).

117. A. E. Ryan, F. Shanahan, J. O'Connell, A. M. Houston, Addressing the "Fas counterattack" controversy: blocking fas ligand expression suppresses tumor immune evasion of colon cancer in vivo. *Cancer research* **65**, 9817-9823 (2005).
118. D. B. Chappell, T. Z. Zaks, S. A. Rosenberg, N. P. Restifo, Human melanoma cells do not express Fas (Apo-1/CD95) ligand. *Cancer research* **59**, 59-62 (1999).
119. W. Zou, Regulatory T cells, tumour immunity and immunotherapy. *Nature reviews. Immunology* **6**, 295-307 (2006).
120. H. Groux *et al.*, A CD4+ T-cell subset inhibits antigen-specific T-cell responses and prevents colitis. *Nature* **389**, 737-742 (1997).
121. T. J. Curiel *et al.*, Specific recruitment of regulatory T cells in ovarian carcinoma fosters immune privilege and predicts reduced survival. *Nature medicine* **10**, 942-949 (2004).
122. L. Zou *et al.*, Bone marrow is a reservoir for CD4+CD25+ regulatory T cells that traffic through CXCL12/CXCR4 signals. *Cancer research* **64**, 8451-8455 (2004).
123. I. Kryczek *et al.*, CXCL12 and vascular endothelial growth factor synergistically induce neoangiogenesis in human ovarian cancers. *Cancer research* **65**, 465-472 (2005).
124. W. Zou, Immunosuppressive networks in the tumour environment and their therapeutic relevance. *Nature reviews. Cancer* **5**, 263-274 (2005).
125. D. Gajdarova, Mechanisms and functional significance of tumour-induced dendritic-cell defects. *Nature reviews. Immunology* **4**, 941-952 (2004).
126. W. Chen *et al.*, Conversion of peripheral CD4+CD25- naive T cells to CD4+CD25+ regulatory T cells by TGF-beta induction of transcription factor Foxp3. *The Journal of experimental medicine* **198**, 1875-1886 (2003).
127. M. C. Fantini *et al.*, Cutting edge: TGF-beta induces a regulatory phenotype in CD4+CD25- T cells through Foxp3 induction and down-regulation of Smad7. *Journal of immunology* **172**, 5149-5153 (2004).
128. Y. Y. Wan, R. A. Flavell, Identifying Foxp3-expressing suppressor T cells with a bicistronic reporter. *Proceedings of the National Academy of Sciences of the United States of America* **102**, 5126-5131 (2005).

129. P. Yu *et al.*, Intratumor depletion of CD4<sup>+</sup> cells unmasks tumor immunogenicity leading to the rejection of late-stage tumors. *The Journal of experimental medicine* **201**, 779-791 (2005).
130. N. Seo, S. Hayakawa, M. Takigawa, Y. Tokura, Interleukin-10 expressed at early tumour sites induces subsequent generation of CD4<sup>(+)</sup> T-regulatory cells and systemic collapse of antitumour immunity. *Immunology* **103**, 449-457 (2001).
131. F. Ghiringhelli *et al.*, CD4<sup>+</sup>CD25<sup>+</sup> regulatory T cells inhibit natural killer cell functions in a transforming growth factor-beta-dependent manner. *The Journal of experimental medicine* **202**, 1075-1085 (2005).
132. M. L. Chen *et al.*, Regulatory T cells suppress tumor-specific CD8 T cell cytotoxicity through TGF-beta signals in vivo. *Proceedings of the National Academy of Sciences of the United States of America* **102**, 419-424 (2005).
133. Y. Peng, Y. Laouar, M. O. Li, E. A. Green, R. A. Flavell, TGF-beta regulates in vivo expansion of Foxp3-expressing CD4<sup>+</sup>CD25<sup>+</sup> regulatory T cells responsible for protection against diabetes. *Proceedings of the National Academy of Sciences of the United States of America* **101**, 4572-4577 (2004).
134. E. A. Green, L. Gorelik, C. M. McGregor, E. H. Tran, R. A. Flavell, CD4<sup>+</sup>CD25<sup>+</sup> T regulatory cells control anti-islet CD8<sup>+</sup> T cells through TGF-beta-TGF-beta receptor interactions in type 1 diabetes. *Proceedings of the National Academy of Sciences of the United States of America* **100**, 10878-10883 (2003).
135. E. M. Shevach, CD4<sup>+</sup> CD25<sup>+</sup> suppressor T cells: more questions than answers. *Nature reviews. Immunology* **2**, 389-400 (2002).
136. H. von Boehmer, Mechanisms of suppression by suppressor T cells. *Nature immunology* **6**, 338-344 (2005).
137. M. de la Rosa, S. Rutz, H. Dorninger, A. Scheffold, Interleukin-2 is essential for CD4<sup>+</sup>CD25<sup>+</sup> regulatory T cell function. *European journal of immunology* **34**, 2480-2488 (2004).
138. W. J. Grossman *et al.*, Human T regulatory cells can use the perforin pathway to cause autologous target cell death. *Immunity* **21**, 589-601 (2004).
139. D. C. Gondek, L. F. Lu, S. A. Quezada, S. Sakaguchi, R. J. Noelle, Cutting edge: contact-mediated suppression by CD4<sup>+</sup>CD25<sup>+</sup> regulatory cells involves a granzyme B-dependent, perforin-independent mechanism. *Journal of immunology* **174**, 1783-1786 (2005).

140. A. L. Mellor, D. H. Munn, IDO expression by dendritic cells: tolerance and tryptophan catabolism. *Nature reviews. Immunology* **4**, 762-774 (2004).
141. F. Fallarino *et al.*, Modulation of tryptophan catabolism by regulatory T cells. *Nature immunology* **4**, 1206-1212 (2003).
142. D. R. Leach, M. F. Krummel, J. P. Allison, Enhancement of antitumor immunity by CTLA-4 blockade. *Science* **271**, 1734-1736 (1996).
143. H. Nishikawa *et al.*, Definition of target antigens for naturally occurring CD4(+) CD25(+) regulatory T cells. *The Journal of experimental medicine* **201**, 681-686 (2005).
144. M. V. Dhodapkar, R. M. Steinman, J. Krasovsky, C. Munz, N. Bhardwaj, Antigen-specific inhibition of effector T cell function in humans after injection of immature dendritic cells. *The Journal of experimental medicine* **193**, 233-238 (2001).
145. N. G. Chakraborty, S. Chattopadhyay, S. Mehrotra, A. Chhabra, B. Mukherji, Regulatory T-cell response and tumor vaccine-induced cytotoxic T lymphocytes in human melanoma. *Human immunology* **65**, 794-802 (2004).
146. C. M. Hawrylowicz, A. O'Garra, Potential role of interleukin-10-secreting regulatory T cells in allergy and asthma. *Nature reviews. Immunology* **5**, 271-283 (2005).
147. S. Kusmartsev, D. I. Gabrilovich, Inhibition of myeloid cell differentiation in cancer: the role of reactive oxygen species. *Journal of leukocyte biology* **74**, 186-196 (2003).
148. Y. Nefedova *et al.*, Hyperactivation of STAT3 is involved in abnormal differentiation of dendritic cells in cancer. *Journal of immunology* **172**, 464-474 (2004).
149. M. Terabe *et al.*, Transforming growth factor-beta production and myeloid cells are an effector mechanism through which CD1d-restricted T cells block cytotoxic T lymphocyte-mediated tumor immunosurveillance: abrogation prevents tumor recurrence. *The Journal of experimental medicine* **198**, 1741-1752 (2003).
150. V. Bronte *et al.*, Apoptotic death of CD8+ T lymphocytes after immunization: induction of a suppressive population of Mac-1+/Gr-1+ cells. *Journal of immunology* **161**, 5313-5320 (1998).

151. D. I. Gabrilovich, M. P. Velders, E. M. Sotomayor, W. M. Kast, Mechanism of immune dysfunction in cancer mediated by immature Gr-1<sup>+</sup> myeloid cells. *Journal of immunology* **166**, 5398-5406 (2001).
152. Q. Li, P. Y. Pan, P. Gu, D. Xu, S. H. Chen, Role of immature myeloid Gr-1<sup>+</sup> cells in the development of antitumor immunity. *Cancer research* **64**, 1130-1139 (2004).
153. S. Kusmartsev, Y. Nefedova, D. Yoder, D. I. Gabrilovich, Antigen-specific inhibition of CD8<sup>+</sup> T cell response by immature myeloid cells in cancer is mediated by reactive oxygen species. *Journal of immunology* **172**, 989-999 (2004).
154. S. Kusmartsev, S. Nagaraj, D. I. Gabrilovich, Tumor-associated CD8<sup>+</sup> T cell tolerance induced by bone marrow-derived immature myeloid cells. *Journal of immunology* **175**, 4583-4592 (2005).
155. B. Huang *et al.*, Gr-1<sup>+</sup>CD115<sup>+</sup> immature myeloid suppressor cells mediate the development of tumor-induced T regulatory cells and T-cell anergy in tumor-bearing host. *Cancer research* **66**, 1123-1131 (2006).
156. S. Kusmartsev, D. I. Gabrilovich, STAT1 signaling regulates tumor-associated macrophage-mediated T cell deletion. *Journal of immunology* **174**, 4880-4891 (2005).
157. J. I. Youn, D. I. Gabrilovich, New roles of Rb1 in expansion of MDSCs in cancer. *Cell cycle* **12**, 1329-1330 (2013).
158. D. I. Gabrilovich, S. Ostrand-Rosenberg, V. Bronte, Coordinated regulation of myeloid cells by tumours. *Nature reviews. Immunology* **12**, 253-268 (2012).
159. J. I. Youn, S. Nagaraj, M. Collazo, D. I. Gabrilovich, Subsets of myeloid-derived suppressor cells in tumor-bearing mice. *Journal of immunology* **181**, 5791-5802 (2008).
160. Y. Sawanobori *et al.*, Chemokine-mediated rapid turnover of myeloid-derived suppressor cells in tumor-bearing mice. *Blood* **111**, 5457-5466 (2008).
161. B. Almand *et al.*, Increased production of immature myeloid cells in cancer patients: a mechanism of immunosuppression in cancer. *Journal of immunology* **166**, 678-689 (2001).
162. V. Bronte, P. Zanovello, Regulation of immune responses by L-arginine metabolism. *Nature reviews. Immunology* **5**, 641-654 (2005).

163. P. C. Rodriguez, A. H. Zea, A. C. Ochoa, Mechanisms of tumor evasion from the immune response. *Cancer chemotherapy and biological response modifiers* **21**, 351-364 (2003).
164. P. C. Rodriguez, A. C. Ochoa, Arginine regulation by myeloid derived suppressor cells and tolerance in cancer: mechanisms and therapeutic perspectives. *Immunological reviews* **222**, 180-191 (2008).
165. A. E. Gehad *et al.*, Nitric oxide-producing myeloid-derived suppressor cells inhibit vascular E-selectin expression in human squamous cell carcinomas. *The Journal of investigative dermatology* **132**, 2642-2651 (2012).
166. S. Nagaraj *et al.*, Altered recognition of antigen is a mechanism of CD8<sup>+</sup> T cell tolerance in cancer. *Nature medicine* **13**, 828-835 (2007).
167. C. A. Corzo *et al.*, Mechanism regulating reactive oxygen species in tumor-induced myeloid-derived suppressor cells. *J Immunol* **182**, 5693-5701 (2009).
168. M. Fujita *et al.*, COX-2 blockade suppresses gliomagenesis by inhibiting myeloid-derived suppressor cells. *Cancer research* **71**, 2664-2674 (2011).
169. P. C. Rodriguez *et al.*, Arginase I in myeloid suppressor cells is induced by COX-2 in lung carcinoma. *The Journal of experimental medicine* **202**, 931-939 (2005).
170. M. Kamiyama *et al.*, EP2, a receptor for PGE<sub>2</sub>, regulates tumor angiogenesis through direct effects on endothelial cell motility and survival. *Oncogene* **25**, 7019-7028 (2006).
171. N. Obermajer *et al.*, PGE(2)-driven induction and maintenance of cancer-associated myeloid-derived suppressor cells. *Immunological investigations* **41**, 635-657 (2012).
172. J. J. Letterio, A. B. Roberts, Regulation of immune responses by TGF-beta. *Annual review of immunology* **16**, 137-161 (1998).
173. K. Chikamatsu *et al.*, Immunosuppressive activity of CD14<sup>+</sup> HLA-DR<sup>-</sup> cells in squamous cell carcinoma of the head and neck. *Cancer science* **103**, 976-983 (2012).
174. H. T. Khong, N. P. Restifo, Natural selection of tumor variants in the generation of "tumor escape" phenotypes. *Nature immunology* **3**, 999-1005 (2002).
175. A. K. Johnsen *et al.*, Systemic deficits in transporter for antigen presentation (TAP)-1 or proteasome subunit LMP2 have little or no effect on tumor incidence.

- International journal of cancer. Journal international du cancer* **91**, 366-372 (2001).
176. P. Zheng, S. Sarma, Y. Guo, Y. Liu, Two mechanisms for tumor evasion of preexisting cytotoxic T-cell responses: lessons from recurrent tumors. *Cancer research* **59**, 3461-3467 (1999).
177. N. P. Restifo *et al.*, Loss of functional beta 2-microglobulin in metastatic melanomas from five patients receiving immunotherapy. *Journal of the National Cancer Institute* **88**, 100-108 (1996).
178. N. P. Restifo *et al.*, Identification of human cancers deficient in antigen processing. *The Journal of experimental medicine* **177**, 265-272 (1993).
179. P. Korkolopoulou, L. Kaklamanis, F. Pezzella, A. L. Harris, K. C. Gatter, Loss of antigen-presenting molecules (MHC class I and TAP-1) in lung cancer. *British journal of cancer* **73**, 148-153 (1996).
180. M. G. Sanda *et al.*, Molecular characterization of defective antigen processing in human prostate cancer. *Journal of the National Cancer Institute* **87**, 280-285 (1995).
181. B. Seliger *et al.*, Expression and function of the peptide transporters in escape variants of human renal cell carcinomas. *Experimental hematology* **25**, 608-614 (1997).
182. D. J. Hicklin *et al.*, beta2-Microglobulin mutations, HLA class I antigen loss, and tumor progression in melanoma. *The Journal of clinical investigation* **101**, 2720-2729 (1998).
183. H. Schreiber, T. H. Wu, J. Nachman, W. M. Kast, Immunodominance and tumor escape. *Seminars in cancer biology* **12**, 25-31 (2002).
184. D. S. Thommen, T. N. Schumacher, T Cell Dysfunction in Cancer. *Cancer Cell* **33**, 547-562 (2018).
185. C. U. Blank *et al.*, Defining 'T cell exhaustion'. *Nat Rev Immunol* **19**, 665-674 (2019).
186. O. Khan *et al.*, TOX transcriptionally and epigenetically programs CD8(+) T cell exhaustion. *Nature* **571**, 211-218 (2019).



187. I. Siddiqui *et al.*, Intratumoral Tcf1(+)PD-1(+)CD8(+) T Cells with Stem-like Properties Promote Tumor Control in Response to Vaccination and Checkpoint Blockade Immunotherapy. *Immunity* **50**, 195-211 e110 (2019).
188. K. E. Pauken *et al.*, Epigenetic stability of exhausted T cells limits durability of reinvigoration by PD-1 blockade. *Science* **354**, 1160-1165 (2016).
189. F. Moschella, E. Proietti, I. Capone, F. Belardelli, Combination strategies for enhancing the efficacy of immunotherapy in cancer patients. *Annals of the New York Academy of Sciences* **1194**, 169-178 (2010).
190. A. K. Nowak, R. A. Lake, B. W. Robinson, Combined chemoimmunotherapy of solid tumours: improving vaccines? *Advanced drug delivery reviews* **58**, 975-990 (2006).
191. F. Moschella *et al.*, Unraveling cancer chemoimmunotherapy mechanisms by gene and protein expression profiling of responses to cyclophosphamide. *Cancer research* **71**, 3528-3539 (2011).
192. E. S. Antonarakis, M. A. Carducci, Combining low-dose cyclophosphamide with GM-CSF-secreting prostate cancer immunotherapy enhances antitumor immune effects. *Expert opinion on investigational drugs* **19**, 311-314 (2010).
193. W. J. Lesterhuis, J. B. Haanen, C. J. Punt, Cancer immunotherapy--revisited. *Nature reviews. Drug discovery* **10**, 591-600 (2011).
194. A. van Elsas, A. A. Hurwitz, J. P. Allison, Combination immunotherapy of B16 melanoma using anti-cytotoxic T lymphocyte-associated antigen 4 (CTLA-4) and granulocyte/macrophage colony-stimulating factor (GM-CSF)-producing vaccines induces rejection of subcutaneous and metastatic tumors accompanied by autoimmune depigmentation. *The Journal of experimental medicine* **190**, 355-366 (1999).
195. B. Li *et al.*, Anti-programmed death-1 synergizes with granulocyte macrophage colony-stimulating factor--secreting tumor cell immunotherapy providing therapeutic benefit to mice with established tumors. *Clinical cancer research : an official journal of the American Association for Cancer Research* **15**, 1623-1634 (2009).
196. Y. Gao, P. Whitaker-Dowling, J. A. Griffin, M. A. Barmada, I. Bergman, Recombinant vesicular stomatitis virus targeted to Her2/neu combined with anti-CTLA4 antibody eliminates implanted mammary tumors. *Cancer gene therapy* **16**, 44-52 (2009).

197. R. Ramakrishnan *et al.*, Chemotherapy enhances tumor cell susceptibility to CTL-mediated killing during cancer immunotherapy in mice. *The Journal of clinical investigation* **120**, 1111-1124 (2010).
198. R. Ramakrishnan *et al.*, Autophagy induced by conventional chemotherapy mediates tumor cell sensitivity to immunotherapy. *Cancer research* **72**, 5483-5493 (2012).
199. P. D. Gregory, K. Wagner, W. Horz, Histone acetylation and chromatin remodeling. *Experimental cell research* **265**, 195-202 (2001).
200. J. Deckert, K. Struhl, Histone acetylation at promoters is differentially affected by specific activators and repressors. *Molecular and cellular biology* **21**, 2726-2735 (2001).
201. S. G. Gray, T. J. Ekstrom, The human histone deacetylase family. *Experimental cell research* **262**, 75-83 (2001).
202. P. Marks *et al.*, Histone deacetylases and cancer: causes and therapies. *Nature reviews. Cancer* **1**, 194-202 (2001).
203. J. Horiuchi, N. Silverman, G. A. Marcus, L. Guarente, ADA3, a putative transcriptional adaptor, consists of two separable domains and interacts with ADA2 and GCN5 in a trimeric complex. *Molecular and cellular biology* **15**, 1203-1209 (1995).
204. S. P. Baker, P. A. Grant, The SAGA continues: expanding the cellular role of a transcriptional co-activator complex. *Oncogene* **26**, 5329-5340 (2007).
205. R. Candau *et al.*, Identification of human proteins functionally conserved with the yeast putative adaptors ADA2 and GCN5. *Molecular and cellular biology* **16**, 593-602 (1996).
206. Z. Nagy, L. Tora, Distinct GCN5/PCAF-containing complexes function as co-activators and are involved in transcription factor and global histone acetylation. *Oncogene* **26**, 5341-5357 (2007).
207. F. J. Dilworth, K. J. Seaver, A. L. Fishburn, S. L. Htet, S. J. Tapscott, In vitro transcription system delineates the distinct roles of the coactivators pCAF and p300 during MyoD/E47-dependent transactivation. *Proceedings of the National Academy of Sciences of the United States of America* **101**, 11593-11598 (2004).

208. S. Emanuele, M. Lauricella, G. Tesoriere, Histone deacetylase inhibitors: apoptotic effects and clinical implications (Review). *International journal of oncology* **33**, 637-646 (2008).
209. S. Y. Roth, J. M. Denu, C. D. Allis, Histone acetyltransferases. *Annual review of biochemistry* **70**, 81-120 (2001).
210. H. Y. Lin, C. S. Chen, S. P. Lin, J. R. Weng, C. S. Chen, Targeting histone deacetylase in cancer therapy. *Medicinal research reviews* **26**, 397-413 (2006).
211. M. G. Guenther, O. Barak, M. A. Lazar, The SMRT and N-CoR corepressors are activating cofactors for histone deacetylase 3. *Molecular and cellular biology* **21**, 6091-6101 (2001).
212. P. A. Jones, S. B. Baylin, The fundamental role of epigenetic events in cancer. *Nature reviews. Genetics* **3**, 415-428 (2002).
213. J. E. Bolden, M. J. Peart, R. W. Johnstone, Anticancer activities of histone deacetylase inhibitors. *Nature reviews. Drug discovery* **5**, 769-784 (2006).
214. K. N. Bhalla, Epigenetic and chromatin modifiers as targeted therapy of hematologic malignancies. *Journal of clinical oncology : official journal of the American Society of Clinical Oncology* **23**, 3971-3993 (2005).
215. L. M. Butler *et al.*, Inhibition of transformed cell growth and induction of cellular differentiation by pyroxamide, an inhibitor of histone deacetylase. *Clinical cancer research : an official journal of the American Association for Cancer Research* **7**, 962-970 (2001).
216. J. H. Park *et al.*, Class I histone deacetylase-selective novel synthetic inhibitors potently inhibit human tumor proliferation. *Clinical cancer research : an official journal of the American Association for Cancer Research* **10**, 5271-5281 (2004).
217. E. Hu *et al.*, Identification of novel isoform-selective inhibitors within class I histone deacetylases. *The Journal of pharmacology and experimental therapeutics* **307**, 720-728 (2003).
218. R. Furumai *et al.*, FK228 (depsipeptide) as a natural prodrug that inhibits class I histone deacetylases. *Cancer research* **62**, 4916-4921 (2002).
219. S. J. Haggarty, K. M. Koeller, J. C. Wong, C. M. Grozinger, S. L. Schreiber, Domain-selective small-molecule inhibitor of histone deacetylase 6 (HDAC6)-mediated tubulin deacetylation. *Proceedings of the National Academy of Sciences of the United States of America* **100**, 4389-4394 (2003).

220. Z. Zhang *et al.*, Quantitation of HDAC1 mRNA expression in invasive carcinoma of the breast\*. *Breast cancer research and treatment* **94**, 11-16 (2005).
221. A. Vannini *et al.*, Crystal structure of a eukaryotic zinc-dependent histone deacetylase, human HDAC8, complexed with a hydroxamic acid inhibitor. *Proceedings of the National Academy of Sciences of the United States of America* **101**, 15064-15069 (2004).
222. H. J. Kwon, T. Owa, C. A. Hassig, J. Shimada, S. L. Schreiber, Depudecin induces morphological reversion of transformed fibroblasts via the inhibition of histone deacetylase. *Proceedings of the National Academy of Sciences of the United States of America* **95**, 3356-3361 (1998).
223. S. Minucci, P. G. Pelicci, Histone deacetylase inhibitors and the promise of epigenetic (and more) treatments for cancer. *Nature reviews. Cancer* **6**, 38-51 (2006).
224. R. W. Johnstone, Histone-deacetylase inhibitors: novel drugs for the treatment of cancer. *Nature reviews. Drug discovery* **1**, 287-299 (2002).
225. P. A. Marks, T. Miller, V. M. Richon, Histone deacetylases. *Current opinion in pharmacology* **3**, 344-351 (2003).
226. R. W. Johnstone, A. A. Ruefli, S. W. Lowe, Apoptosis: a link between cancer genetics and chemotherapy. *Cell* **108**, 153-164 (2002).
227. D. Z. Qian *et al.*, Targeting tumor angiogenesis with histone deacetylase inhibitors: the hydroxamic acid derivative LBH589. *Clinical cancer research : an official journal of the American Association for Cancer Research* **12**, 634-642 (2006).
228. R. Pili, M. P. Kruszewski, B. W. Hager, J. Lantz, M. A. Carducci, Combination of phenylbutyrate and 13-cis retinoic acid inhibits prostate tumor growth and angiogenesis. *Cancer research* **61**, 1477-1485 (2001).
229. Y. Sasakawa *et al.*, Antitumor efficacy of FK228, a novel histone deacetylase inhibitor, depends on the effect on expression of angiogenesis factors. *Biochemical pharmacology* **66**, 897-906 (2003).
230. M. Michaelis *et al.*, Valproic acid inhibits angiogenesis in vitro and in vivo. *Molecular pharmacology* **65**, 520-527 (2004).
231. L. Rossig *et al.*, Inhibitors of histone deacetylation downregulate the expression of endothelial nitric oxide synthase and compromise endothelial cell function in vasorelaxation and angiogenesis. *Circulation research* **91**, 837-844 (2002).

232. C. F. Deroanne *et al.*, Histone deacetylases inhibitors as anti-angiogenic agents altering vascular endothelial growth factor signaling. *Oncogene* **21**, 427-436 (2002).
233. Y. Zhao *et al.*, Lifespan extension and elevated hsp gene expression in *Drosophila* caused by histone deacetylase inhibitors. *The Journal of experimental biology* **208**, 697-705 (2005).
234. W. Gu, R. G. Roeder, Activation of p53 sequence-specific DNA binding by acetylation of the p53 C-terminal domain. *Cell* **90**, 595-606 (1997).
235. J. Luo, F. Su, D. Chen, A. Shiloh, W. Gu, Deacetylation of p53 modulates its effect on cell growth and apoptosis. *Nature* **408**, 377-381 (2000).
236. Z. L. Yuan, Y. J. Guan, D. Chatterjee, Y. E. Chin, Stat3 dimerization regulated by reversible acetylation of a single lysine residue. *Science* **307**, 269-273 (2005).
237. L. Chen, W. Fischle, E. Verdin, W. C. Greene, Duration of nuclear NF-kappaB action regulated by reversible acetylation. *Science* **293**, 1653-1657 (2001).
238. M. R. Acharya, A. Sparreboom, J. Venitz, W. D. Figg, Rational development of histone deacetylase inhibitors as anticancer agents: a review. *Molecular pharmacology* **68**, 917-932 (2005).
239. T. A. Miller, D. J. Witter, S. Belvedere, Histone deacetylase inhibitors. *Journal of medicinal chemistry* **46**, 5097-5116 (2003).
240. D. C. Drummond, Clinical development of histone deacetylase inhibitors as anticancer agents. *Annu Rev Pharmacol Toxicol* **45**, 495-528 (2004).
241. M. S. Finnin *et al.*, Structures of a histone deacetylase homologue bound to the TSA and SAHA inhibitors. *Nature* **401**, 188-193 (1999).
242. A. A. Lane, B. A. Chabner, Histone deacetylase inhibitors in cancer therapy. *Journal of clinical oncology : official journal of the American Society of Clinical Oncology* **27**, 5459-5468 (2009).
243. R. R. Rosato, S. Grant, Histone deacetylase inhibitors in cancer therapy. *Cancer biology & therapy* **2**, 30-37 (2003).
244. T. Suzuki *et al.*, Synthesis and histone deacetylase inhibitory activity of new benzamide derivatives. *Journal of medicinal chemistry* **42**, 3001-3003 (1999).
245. C. Monneret, Histone deacetylase inhibitors. *European journal of medicinal chemistry* **40**, 1-13 (2005).

246. Q. C. Ryan *et al.*, Phase I and pharmacokinetic study of MS-275, a histone deacetylase inhibitor, in patients with advanced and refractory solid tumors or lymphoma. *Journal of clinical oncology : official journal of the American Society of Clinical Oncology* **23**, 3912-3922 (2005).
247. S. Prakash *et al.*, Chronic oral administration of CI-994: a phase 1 study. *Investigational new drugs* **19**, 1-11 (2001).
248. S. Shankar, R. K. Srivastava, Histone deacetylase inhibitors: mechanisms and clinical significance in cancer: HDAC inhibitor-induced apoptosis. *Advances in experimental medicine and biology* **615**, 261-298 (2008).
249. M. Dokmanovic, P. A. Marks, Prospects: histone deacetylase inhibitors. *Journal of cellular biochemistry* **96**, 293-304 (2005).
250. L. Gore, Updated results from a phase I trial of the histone deacetylase (HDAC) inhibitor MS-275 in patients with refractory solid tumors. *Journal of clinical oncology : official journal of the American Society of Clinical Oncology* **22**, (2004).
251. L. Gore *et al.*, A phase I and pharmacokinetic study of the oral histone deacetylase inhibitor, MS-275, in patients with refractory solid tumors and lymphomas. *Clinical cancer research : an official journal of the American Association for Cancer Research* **14**, 4517-4525 (2008).
252. S. Kummar *et al.*, Phase I trial of MS-275, a histone deacetylase inhibitor, administered weekly in refractory solid tumors and lymphoid malignancies. *Clinical cancer research : an official journal of the American Association for Cancer Research* **13**, 5411-5417 (2007).
253. I. Gojo *et al.*, Phase 1 and pharmacologic study of MS-275, a histone deacetylase inhibitor, in adults with refractory and relapsed acute leukemias. *Blood* **109**, 2781-2790 (2007).
254. A. Saito *et al.*, A synthetic inhibitor of histone deacetylase, MS-27-275, with marked in vivo antitumor activity against human tumors. *Proceedings of the National Academy of Sciences of the United States of America* **96**, 4592-4597 (1999).
255. B. I. Lee *et al.*, MS-275, a histone deacetylase inhibitor, selectively induces transforming growth factor beta type II receptor expression in human breast cancer cells. *Cancer research* **61**, 931-934 (2001).

256. J. Jaboin *et al.*, MS-27-275, an inhibitor of histone deacetylase, has marked in vitro and in vivo antitumor activity against pediatric solid tumors. *Cancer research* **62**, 6108-6115 (2002).
257. B. Vire *et al.*, Anti-leukemia activity of MS-275 histone deacetylase inhibitor implicates 4-1BBL/4-1BB immunomodulatory functions. *PloS one* **4**, e7085 (2009).
258. R. K. Srivastava, R. Kurzrock, S. Shankar, MS-275 sensitizes TRAIL-resistant breast cancer cells, inhibits angiogenesis and metastasis, and reverses epithelial-mesenchymal transition in vivo. *Molecular cancer therapeutics* **9**, 3254-3266 (2010).
259. T. Maeda, M. Towatari, H. Kosugi, H. Saito, Up-regulation of costimulatory/adhesion molecules by histone deacetylase inhibitors in acute myeloid leukemia cells. *Blood* **96**, 3847-3856 (2000).
260. W. J. Magner *et al.*, Activation of MHC class I, II, and CD40 gene expression by histone deacetylase inhibitors. *Journal of immunology* **165**, 7017-7024 (2000).
261. S. Armeanu *et al.*, Natural killer cell-mediated lysis of hepatoma cells via specific induction of NKG2D ligands by the histone deacetylase inhibitor sodium valproate. *Cancer research* **65**, 6321-6329 (2005).
262. S. Skov *et al.*, Cancer cells become susceptible to natural killer cell killing after exposure to histone deacetylase inhibitors due to glycogen synthase kinase-3-dependent expression of MHC class I-related chain A and B. *Cancer research* **65**, 11136-11145 (2005).
263. I. Nusinzon, C. M. Horvath, Interferon-stimulated transcription and innate antiviral immunity require deacetylase activity and histone deacetylase 1. *Proceedings of the National Academy of Sciences of the United States of America* **100**, 14742-14747 (2003).
264. A. N. Khan, C. J. Gregorie, T. B. Tomasi, Histone deacetylase inhibitors induce TAP, LMP, Tapasin genes and MHC class I antigen presentation by melanoma cells. *Cancer Immunol Immunother* **57**, 647-654 (2008).
265. B. W. Bridle *et al.*, HDAC inhibition suppresses primary immune responses, enhances secondary immune responses, and abrogates autoimmunity during tumor immunotherapy. *Mol Ther* **21**, 887-894 (2013).

266. A. N. Khan, T. B. Tomasi, Histone deacetylase regulation of immune gene expression in tumor cells. *Immunol Res* **40**, 164-178 (2008).
267. A. C. Huang *et al.*, T-cell invigoration to tumour burden ratio associated with anti-PD-1 response. *Nature* **545**, 60-65 (2017).



# Functional Analysis of Tumor-Infiltrating Myeloid Cells by Flow Cytometry and Adoptive Transfer

Andrew Nguyen<sup>\*1</sup>, Omar Salem<sup>\*1</sup>, Yonghong Wan<sup>1</sup>

<sup>1</sup> Department of Pathology and Molecular Medicine, McMaster University

\*These authors contributed equally

## Corresponding Author

Andrew Nguyen

nguyea9@mcmaster.ca

## Citation

Nguyen, A., Salem, O.,  
Wan, Y. Functional Analysis of Tumor-  
Infiltrating Myeloid Cells by Flow  
Cytometry and Adoptive Transfer. *J. Vis.  
Exp.* (169), e61511, doi:10.3791/61511  
(2021).

## Date Published

March 5, 2021

## DOI

10.3791/61511

## URL

jove.com/video/61511

## Abstract

The tumor-infiltrating myeloid cell compartment represents a heterogeneous population of broadly immunosuppressive cells that have been exploited by the tumor to support its growth. Their accumulation in tumor and secondary lymphoid tissue leads to the suppression of antitumor immune responses and is thus a target for therapeutic intervention. As it is known that the local cytokine milieu can dictate the functional programming of tumor-infiltrating myeloid cells, strategies have been devised to manipulate the tumor microenvironment (TME) to express a cytokine landscape more conducive to antitumor myeloid cell activity. To evaluate therapy-induced changes in tumor-infiltrating myeloid cells, this paper will outline the procedure to dissociate intradermal/subcutaneous tumor tissue from solid tumor-bearing mice in preparation for leukocyte recovery. Strategies for flow cytometric analysis will be provided to enable the identification of heterogeneous myeloid populations within isolated leukocytes and the characterization of unique myeloid phenotypes. Lastly, this paper will describe a means of purifying viable myeloid cells for functional assays and determining their therapeutic value in the context of adoptive transfer.

## Introduction

The tumor microenvironment (TME) is comprised of rapidly proliferating neoplastic cells and a surrounding heterogeneous stromal cell compartment. As growing tumors are often poorly vascularized, the TME is a peripheral site uniquely characterized by hypoxia, nutrient deprivation, and acidosis<sup>1</sup>. To survive in this landscape, tumor stress responses and metabolic reprogramming result in the secretion of soluble factors that promote tissue remodeling

and angiogenesis as well as the selective recruitment of immune cells<sup>2</sup>. As myeloid cells are one of the most abundant type of hematopoietic cells in the TME, there is increasing interest in examining the role of tumor-infiltrating myeloid cells in the TME.

Myeloid cells are a heterogeneous and plastic group of innate immune cells including monocytes, macrophages, dendritic cells, and granulocytes. Although they have critical

roles in tissue homeostasis and adaptive immune response regulation, their function can be polarizing depending on the composition of activation signals within the local microenvironment<sup>3</sup>. Tumors take advantage of myeloid cell characteristics through the secretion of soluble factors within the TME. These alternative signals can divert myelopoiesis towards immature differentiation and skew the function of existing tumor-infiltrating myeloid cells<sup>3</sup>. Indeed, myeloid cells within the TME often promote cancer progression and can suppress antitumor immune responses, leading to adverse effects on cancer therapy.

Although therapeutic strategies promoting the depletion of immunosuppressive myeloid cells have been shown to delay tumor growth<sup>4</sup>, the lack of target specificity risks the removal of immunostimulatory myeloid cells, which by contrast, aid in the resolution of cancer. These inflammatory myeloid cells can exert profound antitumor effects including direct tumor cell killing and activation of cytotoxic CD8<sup>+</sup> T cells<sup>5</sup>. Alternatively, strategies normalizing the composition and function of myeloid cells in the TME have shown therapeutic success<sup>6</sup>; however, the biological mechanisms underlying their re-education towards an antitumor phenotype have still not been fully understood. Ultimately, a comprehensive characterization of tumor myeloid cells is necessary for further improvement of cancer therapy.

Unfortunately, reproducible disaggregation of tumors for myeloid cell isolation is challenging. Tumor-derived myeloid cells are sensitive to *ex vivo* manipulation compared to other leukocyte subsets, and the aggressiveness of tumor processing can lead to enzymatic epitope cleavage and reduced viability of recovered cells<sup>7</sup>. The purpose of this method is to provide a reliable means of tumor dissociation to preserve surface marker integrity for analysis

and cellular vitality for functional study. In comparison to tumor-infiltrating leukocyte (TIL) isolation protocols that favor harsher enzymatic mixes to enhance the reproducible release of various cellular subsets, this method favors more conservative enzymatic digestion to maximize myeloid cell recovery. High-level multi-color flow gating strategies are also provided to identify murine tumor myeloid cell subsets for further characterization and/or sorting.

## Protocol

**NOTE:** All animal studies complied with the Canadian Council on Animal Care guidelines and were approved by McMaster University's Animal Research Ethics Board.

### 1. Tumor harvest and dissociation

1. Inoculate 6-8-week-old, female, C57BL/6 mice intradermally/subcutaneously with  $2 \times 10^5$  B16 melanoma cells as described by Nguyen *et al.*<sup>8</sup> Allow tumors to grow for 7 days before harvesting.
  2. Euthanize the mouse by cervical dislocation while making sure to not disrupt the tumor when doing so. Spray the mouse down with 70% ethanol before harvesting.
  3. Using a scalpel and scissors, surgically remove the intradermal/subcutaneous tumor from surrounding tissue (including attached tumor-draining lymph nodes), and place the tumors into a preweighed microfuge tube. Keep on ice.
- NOTE:** Conduct tumor harvest in an animal-use biosafety cabinet. Use a 15 mL conical tube for larger tumors.
4. Weigh the tumors, and add 500  $\mu$ L of RPMI-1640 medium with 10% fetal bovine serum (FBS) to each tube,

using scissors to cut the tumors into small pieces within the tube or in a 6-well plate.

**NOTE:** The tumor pieces should be small enough to be mixed by an electric pipettor once the digestion medium has been added.

5. Prepare the dissociation mix by dissolving collagenase type IV at 0.5 mg/mL and DNase at 0.2 mg/mL in RPMI-1640 medium with 10% FBS and 5 mM calcium chloride.

**NOTE:** Dissociation mix must be prepared fresh to maximize collagenase activity.

6. Transfer the minced tumor suspension to a 15 mL conical tube, and add 10 mL of dissociation mix per 0.25 mg of tumor. Place the tube in a temperature-controlled orbital shaker for 30 min at 37 °C with 200 rpm agitation. Neutralize the collagenase activity by adding two volumes of cold RPMI-1640 medium with 10% FBS and 2 mM ethylenediamine tetraacetic acid (EDTA), and refrigerate for 10 min at 4 °C.
7. Briefly vortex and pipette the suspension into a 40 µm strainer on a 50 mL conical tube. Use a syringe plunger and neutralizing media to disaggregate the residual tumor tissue, and wash it through the strainer. Centrifuge the suspension for 5 min (500 × g, 4 °C), discard the supernatant, and resuspend the pellet in phosphate-buffered saline (PBS) with 2% FBS and 1 mM EDTA.

## 2. TIL enrichment and flow cytometric staining (FACS)

1. To enrich TILs for myeloid cell characterization, use a magnetic cell separation kit designed for biotin-positive selection with biotinylated CD45.2 antibodies according to the manufacturer's instructions (see the **Table of Materials**).

2. Resuspend the cells in 200 µL of FACS buffer (PBS with 0.5% w/v bovine serum albumin (BSA)), and transfer them to a 96-well U-bottom plate.

**NOTE:** Do not exceed a staining concentration of  $1 \times 10^8$  cells/mL. Adjust the volume, and split samples into multiple wells to compensate for high cell numbers.

3. Centrifuge the plate for 5 min (500 × g, 4 °C), and discard the supernatant. Add 50 µL of Fc block solution (1:200 dilution of purified rat anti-mouse CD16/CD32 [see the **Table of Materials**]) in FACS buffer, final concentration of 2.5 µg/mL), and resuspend the cells by pipetting. Incubate for 10 min at 4 °C.

4. Add 50 µL of FACS buffer containing 2x concentration of surface-staining antibody (1:50 dilution of CD45.2, NK1.1, CD11c, F4/80, CD8a, Ly6C, CD11b, CD4, Ly6G) and fixable viability stain (FVS, 1:500 dilution), and mix the cells by pipetting. Incubate for 20 min at 4 °C.

**NOTE:** Cover the plate with aluminum foil to minimize light exposure. Antibodies should be titrated prior to the experiment to empirically determine the optimal dilution.

5. Wash the cells twice by adding 200 µL of FACS buffer to each well, centrifuging the suspension (5 min, 500 × g, 4 °C), and discarding the supernatant.
6. Add 100 µL of fixation/permeabilization solution (see the **Table of Materials**) to each well, mix the cells by pipetting, and incubate for 20 min at 4 °C.
7. Add 100 µL of 1x permeabilization buffer (see the **Table of Materials**) to each well, centrifuge the plate for 5 min (500 × g, 4 °C), and discard the supernatant.
8. Wash the cells by adding 200 µL of 1x permeabilization buffer to each well, centrifuging the suspension (5 min, 500 × g, 4 °C), and discarding the supernatant.

**NOTE:** The experiment can be paused overnight after resuspending the cells in permeabilization buffer. Store the sample at 4 °C and protected from light. Resume after briefly mixing the cells before centrifuging.

9. Add 100 µL of permeabilization buffer containing 1x concentration of intracellular staining antibody (1:100 dilution of nitric oxide synthase 2 (NOS2), arginase 1 (Arg1)), and mix the cells by pipetting. Incubate for 20 min at 4 °C.

**NOTE:** Cover the plate with aluminum foil to minimize light exposure. Antibodies should be titrated prior to the experiment to empirically determine the optimal dilution.

10. Add 100 µL of 1x permeabilization buffer to each well, centrifuge the plate for 5 min (500 × g, 4 °C), and discard the supernatant.
11. Wash the cells by adding 200 µL of 1x permeabilization buffer to each well, centrifuging the suspension (5 min, 500 × g, 4 °C), and discarding the supernatant.
12. Resuspend the cells in 300 µL of FACS buffer. Filter the sample through a 5 mL round-bottom polystyrene tube with 40 µm strainer cap before performing flow cytometry analysis.

### 3. Tumor myeloid cell sorting for functional studies

1. After identifying the desired myeloid cell populations by flow cytometry analysis, pre-enrich bulk myeloid cells for sorting with a magnetic cell separation kit designed for CD11b- or CD11c-positive selection according to the manufacturer's instructions (see the **Table of Materials**).
2. Using surface-staining antibodies specific for the desired myeloid cell subsets (1:100 dilution of CD11b, Ly6C,

Ly6G), stain the pre-enriched cells as described in steps 2.2-2.5.

**NOTE:** Include fixable viability stain to ensure the sorting of live myeloid cells. Do not exceed a staining concentration of  $1 \times 10^8$  cells/mL. Adjust the volume, and split the samples into multiple wells to compensate for high cell numbers.

3. Resuspend the cells in cold sorting buffer (PBS with 1% w/v BSA, 25 mM 4-(2-hydroxyethyl)-1-piperazineethanesulfonic acid (HEPES), and 1 mM EDTA). Filter the sample through a 5 mL round-bottom polypropylene tube with a 40 µm strainer cap. Keep the cells on ice, and cover the tube with aluminum foil.

**NOTE:** Adjust the concentration of cells/volume to the desired instrument specification for sorting.

4. Prepare a sample collection tube with capture medium (5 mL round-bottom polypropylene tube containing PBS with 50% FBS).

**NOTE:** Coat tubes with 5 mL capture medium overnight prior to sorting. Discard all but 1-2 mL of the capture medium on the next day before running the sample.

5. Modify the sorter instrument settings to decrease sample pressure and prevent perturbations in droplet formation. Equip the 130 µm nozzle tip, and utilize the 10 psi setting. Run the sample at a low flow rate with periodic sample agitation at 100 rpm, ensuring that the deposition of droplets is in the center of the tube. After the sort, keep the sample on ice.
6. Incubate the sample for 10 min at 4 °C. Centrifuge the tube for 5 min (500 × g, 4 °C), discard the supernatant, and resuspend the pellet in the desired medium for functional assays or adoptive transfer.

#### 4. Adoptive transfer of purified tumor myeloid cells

1. Inoculate 6-8-week-old, female, C57BL/6 mice intradermally with  $1 \times 10^6$  B16 melanoma tumor cells resuspended in 30  $\mu$ L of PBS.

**NOTE:** Inoculate mice in advance such that tumor growth does not exceed 100 mm<sup>3</sup> by the time of adoptive transfer.

2. Resuspend the sorted tumor myeloid cells in PBS with 25 mM HEPES and 1 mM EDTA at a concentration of  $2 \times 10^6$  cells/mL. Filter the sample through a 5 mL round-bottom polystyrene tube with a 40  $\mu$ m strainer cap. Keep on ice.
3. Induce and maintain mice under anesthesia with 3% isoflurane. Apply ophthalmic ointment to prevent ocular dryness/injury.
4. Load a 31 G syringe with 50  $\mu$ L of cell suspension. Dislodge air bubbles by gently flicking the syringe. Clean the injection site using an alcohol swab.
5. Using sterile forceps, lift the skin at the base of the tumor. Insert the needle into the subcutaneous space at a slight upward angle to enter the tumor from below the skin. Use the forceps to pinch the skin surrounding the needle, and slowly dispense the syringe volume. Continue to pinch the skin with the forceps while removing the needle slowly, and use a cotton swab to clean potential leakage.
 

**NOTE:** Proceed with any additional therapeutic treatments if desired.
6. Allow the mice to recover from anesthesia.

#### Representative Results

The results demonstrate that this method produces a high yield of myeloid cells from solid murine tumors. The preservation of receptor integrity and cellular viability facilitates reliable functional analysis of the desired myeloid subsets. These improvements to myeloid cell isolation allowed the discernment of the changing function of intratumoral myeloid cells upon normalization of the TME with the class I histone deacetylase inhibitor (HDACi), MS-275, during adoptive T cell therapy. TIL isolation protocols typically do not take the steps to maximize myeloid cell yield<sup>9</sup>. As a result, enzymatic digestion is typically too harsh and leads to a loss of sample viability. When processed B16 melanoma tumors were treated with collagenase type I for 1 h (a commonly used condition) before positively enriching for CD45.2<sup>+</sup> cells by magnetic selection, the morphology (forward Scatter-area (FSC-A) vs. side scatter-area (SSC-A)) and myeloid cell subgating (CD11b vs. CD11c) indicated that the yield of myeloid cells (CD11b<sup>+</sup> or CD11c<sup>+</sup>) and non-myeloid cells (CD11b<sup>-</sup> CD11c<sup>-</sup>) was extremely low (**Figure 1**). To reduce the potentially excessive specific activity of collagenase, the duration of tumor digestion was decreased to 30 min. While there was a slight improvement in myeloid cell recovery, the overall yield was still low and there was no improvement in non-myeloid cell recovery.

Because lot variation may introduce proteases with specific activity high enough to cause excessive cell death, a separate lot of collagenase type I was requested from a different commercial supplier for comparison. Interestingly, the overall yield of myeloid and non-myeloid cells was much higher, with a slight enhancement in myeloid cell number upon the addition of FBS. Although FBS was added to stabilize the myeloid cells to collagenase-induced damage, this raised

the question as to whether FBS was also neutralizing the tryptic activity of the collagenase type I preparation, which could be impairing cell recovery. As collagenase type I preparations have collagenase, caseinase, clostripain, and tryptic activities<sup>10</sup>, to reduce protease exposure, the digestion was attempted using collagenase type IV, which has higher collagenase-specific activity and lower tryptic activity. This condition resulted in a greater increase in myeloid cell yield, with the addition of FBS resulting in the highest yield. Interestingly, collagenase type I and type IV, with or without FBS, did not markedly change the overall yield of non-myeloid cells.

With these optimized enzymatic digestion conditions, leukocytes were isolated from murine B16 melanoma tumors, and flow cytometry was used to phenotype the different myeloid cell populations within the TME based on their expression of surface markers. Tumors were harvested and processed and the leukocytes isolated using a CD45.2 magnetic selection kit. The cells were then stained using a carefully designed panel of cell surface markers (**Figure 2**). The gating strategy described here starts with a morphological assessment of the cells using FSC-A vs. SSC-A. This allows the exclusion of cellular debris based on their small size. FSC-H vs. FSC-W was used to select single cells and exclude the doublets. Total live leukocytes were then gated based on CD45.2 and viability staining. Lymphocytes were excluded based on NK1.1, CD4, and CD8 staining; note that in BALB/c mice, Asialo-GM1 and/or DX5 can be used to exclude natural killer (NK) cells as NK1.1 is not expressed on BALB/c-derived NK cells. CD11b was then plotted against CD11c to identify tumor-associated dendritic cells (TADCs)/conventional dendritic cells (cDCs).

Cells that are negative for CD11c represent the bulk myeloid cells, which can be further separated based on Ly6C and Ly6G staining. Cells that express intermediate levels of Ly6C and high levels of Ly6G represent the neutrophils. This population shares the same phenotype as the granulocytic myeloid-derived suppressor cells (G-MDSCs). CD11b<sup>+</sup> cells that stain negative for Ly6G, but positive for Ly6C can be divided into Ly6C<sup>hi</sup>, Ly6C<sup>int</sup>, and Ly6C<sup>lo</sup>. Ly6C<sup>int/hi</sup> cells express lower levels of F4/80 and represent inflammatory monocytes. However, Ly6C<sup>hi</sup> cells also share the same phenotype with monocytic myeloid-derived suppressor cells (M-MDSCs). Finally, Ly6C<sup>int</sup> cells express high levels of F4/80 and are usually associated with tumor-associated macrophages (TAMs). While this characterization may not fully identify the myeloid cell subsets of interest, it provides a useful gating strategy to sort myeloid cell populations within the TME for further functional or genomic analyses. Within the context of immunotherapy, adoptive T-cell therapy incorporating epigenetic modifying drugs, such as the class I histone deacetylase inhibitor (HDACi) MS-275, can affect the TME to promote sustained tumor regression, while its absence results in tumor relapse<sup>8</sup>.

Although microarray analysis of bulk tumor RNA suggests a role for tumor-infiltrating myeloid cells, this phenotypic characterization did not indicate major surface marker changes during MS-275 treatment<sup>8</sup>. Interestingly, functional markers present in the flow cytometry staining panel identified a certain myeloid cell subset (CD11b<sup>+</sup> Ly6C<sup>hi</sup> Ly6G<sup>-</sup>) differentially producing nitric oxide synthase 2 (NOS2) and arginase 1 (Arg1), which are implicit readouts of polarizing or divergent functional programming (**Figure 3A**). By sorting CD11b<sup>+</sup> Ly6C<sup>hi</sup> Ly6G<sup>-</sup> cells from differentially treated, tumor-bearing mice, more extensive functional studies could be performed to understand their role. Using carboxyfluorescein

succinimidyl ester (CFSE) labelling to monitor lymphocyte proliferation<sup>11</sup>, sorted myeloid cells derived from naïve and vaccinated mice were found to suppress T cell proliferation *in vitro*, while cells derived from vaccinated + MS-275-treated mice had reduced immunosuppressive function (Figure 3B).

Adoptive transfer of these cells revealed that they instead possessed antitumor capability and promoted sustained regression of tumors during vaccination and prolonged mouse survival (Figure 3C).

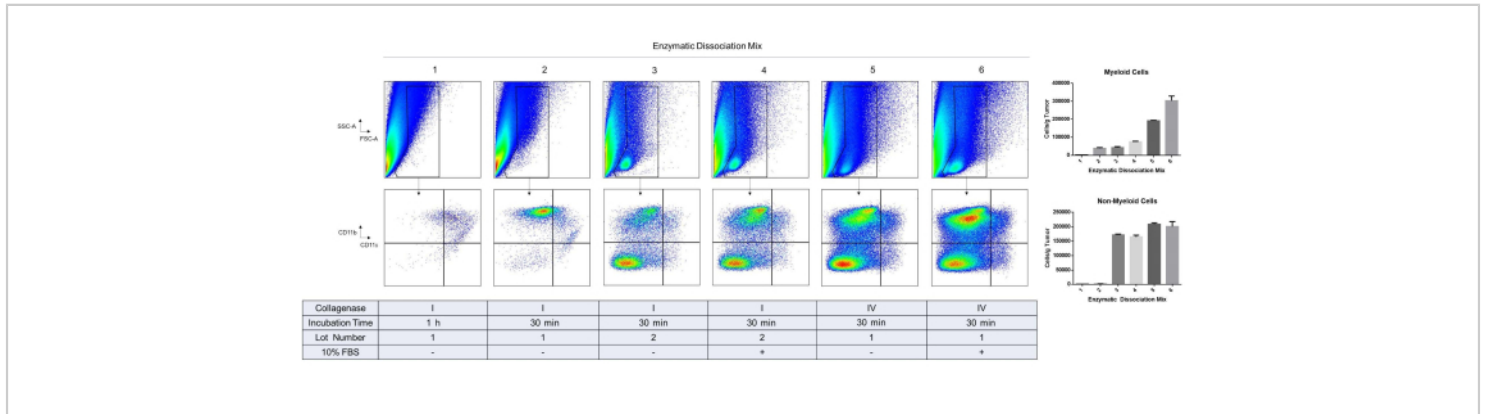


**Figure 1: Representative data showing the effectiveness of varying dissociation conditions.** In C57BL/6 mice (n=3 per group), untreated intradermal B16F10-gp33 tumors were processed and dissociated under various enzymatic conditions before CD45.2 selection. Shown above are the flow cytometry gating strategies used to demonstrate cellular yield differences (FSC-A vs. SSC-A) illustrates tumor-infiltrating leukocyte yield implicitly by cell size/granularity discrimination. (CD11b vs. CD11c ) allows for the quantification of myeloid (CD11b<sup>+</sup> or CD11c<sup>+</sup>) or non-myeloid (CD11b<sup>-</sup> CD11c<sup>-</sup>) cells. Error is defined by standard error of the mean. Abbreviations: CD = cluster of differentiation; SSC-A = side scatter-area; FSC-A = forward scatter area; FBS =fetal bovine serum. [Please click here to view a larger version of this figure.](#)

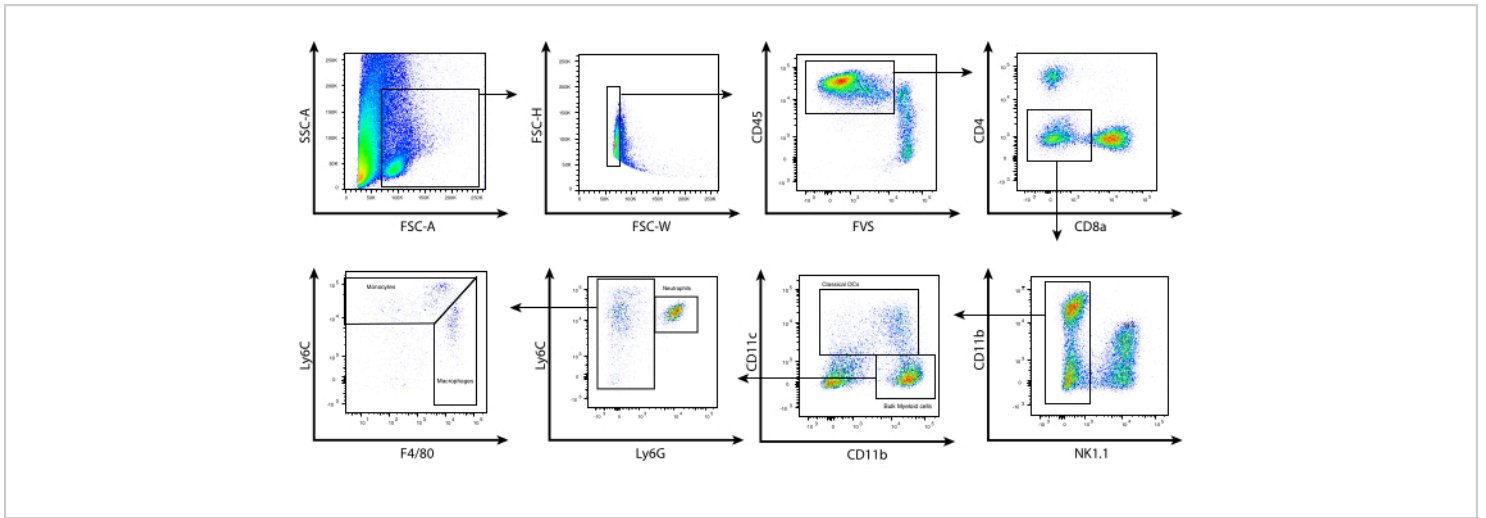


**Figure 2: Representative flow cytometry analysis of tumor-infiltrating myeloid cells.** Following tumor processing and CD45.2 selection, enriched cells were surface-stained as described in the protocol. Shown above is the gating strategy used to exclude the lymphocytes and identify the individual subsets of myeloid cells within the tumor microenvironment. Debris (SSC-A vs. FSC-A) and doublets (FSC-H vs. FSC-W) were excluded, and CD45.2<sup>+</sup> live cells were determined using the fixable viability stain FVS510 (CD45.2 vs. FVS). CD4<sup>+</sup>, CD8<sup>+</sup>, NK1.1<sup>+</sup> cells were gated out. CD11b<sup>hi/lo</sup> CD11c<sup>+</sup> cells represent cDCs. CD11b<sup>+</sup> CD11c<sup>-</sup> were then subgated based on Ly6C and Ly6G expression. Three populations were identified: (i) Ly6C<sup>int</sup> Ly6G<sup>+</sup> (neutrophils/G-MDSCs), (ii) Ly6C<sup>hi</sup> Ly6G<sup>-</sup> F4/80<sup>lo/int</sup> (monocytes/M-MDSCs), (iii) Ly6C<sup>lo/int</sup> Ly6G<sup>-</sup> F4/80<sup>hi</sup> (macrophages/TAMs). Abbreviations: CD = cluster of differentiation; SSC-A = side scatter-area; FSC-A = forward scatter area; FSC-H = forward scatter-height; FSC-W = forward scatter-width; FVS = fixable viability stain; cDCs = conventional dendritic cells; Ly = lymphocyte antigen; G-MDSCs = granulocytic myeloid-derived suppressor cells; M-MDSCs = monocytic myeloid-derived suppressor cells; TAMs= tumor-associated macrophages. [Please click here to view a larger version of this figure.](#)



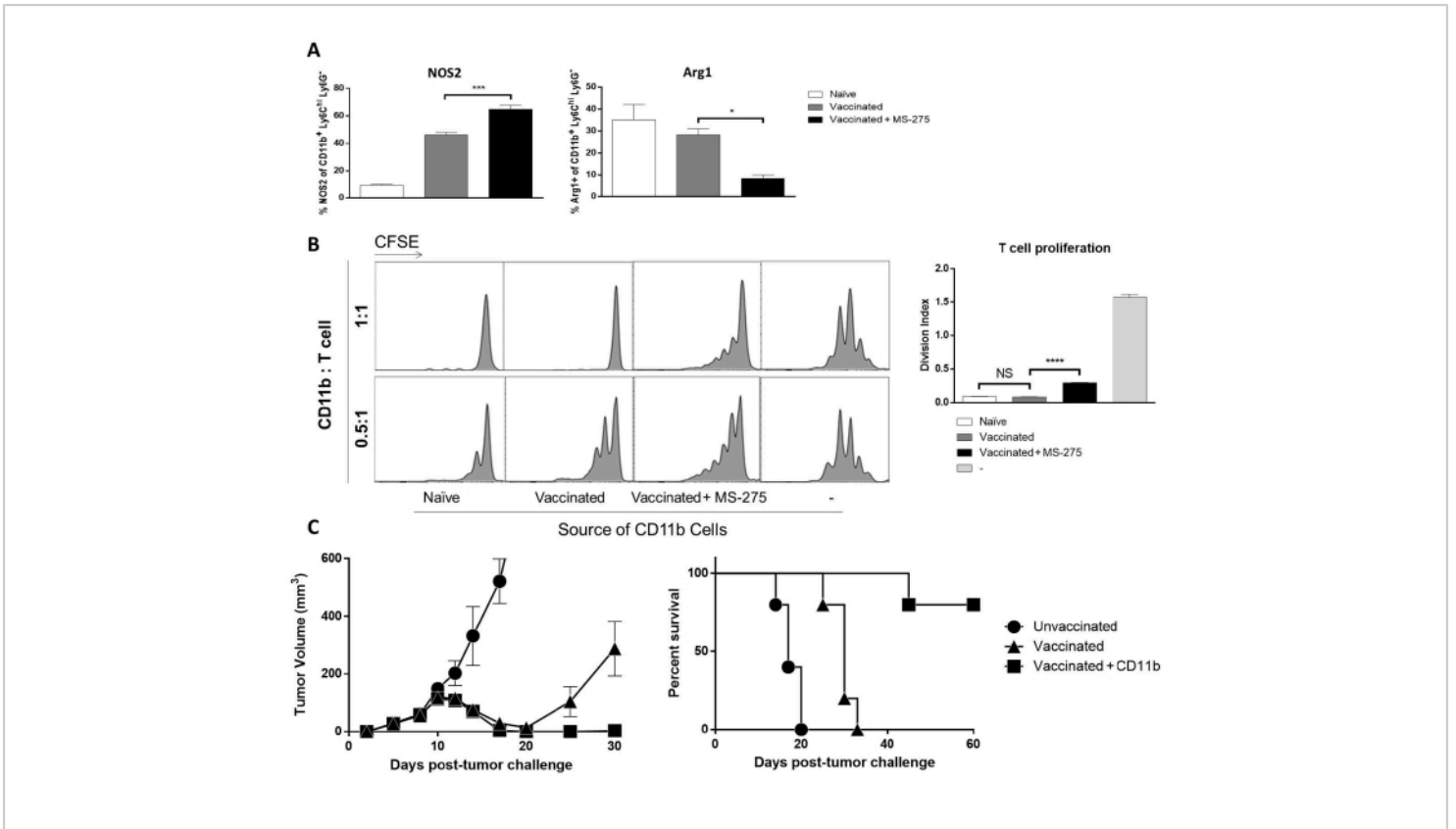


**Figure 3: Functional analyses of purified tumor-infiltrating myeloid cells.** In C57BL/6 mice (n=3-5 per group), intradermal B16F10-gp33 tumors were either unvaccinated or administered adoptive T cell therapy in the presence or absence of the HDAC inhibitor, MS-275. Five days posttreatment, tumors were processed and positively enriched for CD11b<sup>+</sup> cells. The cells were surface-stained to subgate on the desired tumor-infiltrating myeloid cell subset (CD11b<sup>+</sup> Ly6C<sup>hi</sup> Ly6G<sup>-</sup>). **(A)** These cells were further stained intracellularly for markers that can delineate the polarity of functional activation, and the data are presented as the frequency of CD11b<sup>+</sup> Ly6C<sup>hi</sup> Ly6G<sup>-</sup> cells that produce NOS2 or Arg1. Alternatively, the surface-stained CD11b<sup>+</sup>-enriched myeloid cells were sorted to obtain a pure Ly6C<sup>hi</sup> Ly6G<sup>-</sup> cell population. **(B)** These purified cells were peptide-pulsed and cocultured with CFSE-labeled, naïve TCR-transgenic T cells in varying ratios. CFSE dilution, as determined by flow cytometry, is shown as a representative histogram and quantified by cellular division index (1:1). **(C)** Separately purified CD11b<sup>+</sup> Ly6C<sup>hi</sup> Ly6G<sup>-</sup> cells derived from vaccinated + MS-275-treated tumor-bearing mice were adoptively transferred into new tumor-bearing mice (n=5) in conjunction with vaccination and tumor regression, and survival curves were monitored. Error is defined by the standard error of the mean. \*\*\* p=0.0004, \* p=0.0479, \*\*\*\* p<0.0001. This figure has been modified from Nguyen *et al.*<sup>8</sup>. Abbreviations: CD = cluster of differentiation; HDAC = histone deacetylase inhibitor; NOS2 = nitric oxide synthase 2; Arg1 = arginase 1 ; CFSE = carboxyfluorescein succinimidyl ester; TCR = T-cell receptor; Ly = lymphocyte antigen; NS= not significant. [Please click here to view a larger version of this figure.](#)

## Discussion

Although tumor-infiltrating myeloid cells exist in varying activation and differentiation states within the tumor, several subsets have been identified including tumor-associated DCs (TADCs), tumor-associated neutrophils (TANs), myeloid-derived suppressor cells (MDSCs), and tumor-associated macrophages (TAMs)<sup>12</sup>. Unfortunately, the overlapping expression of cell-surface markers used to identify these myeloid cell subsets makes it currently challenging to phenotypically differentiate tumor myeloid cells from other myeloid cells<sup>13</sup>. Similarly, therapy-induced phenotypic changes in tumor-infiltrating myeloid cells may not be easily observed with existing myeloid antibody staining panels. Taken together, the insufficiency of unique surface markers complicates the understanding of myeloid cell biology. To delineate natural, tumor-driven, and therapy-influenced myeloid cells, the evaluation of myeloid cell subsets must be done according to their function in addition to their phenotypic characteristics.

The methods described herein to harvest and dissociate tumor tissue allow for the isolation of myeloid cells with preserved viability and surface marker integrity. As tumor-infiltrating myeloid cells are sensitive to *ex vivo* manipulation<sup>7</sup>, the emphasis of the protocol is on less aggressive mechanical and enzymatic dissociation. However, depending on the tumor tissue type, different samples require variably aggressive treatment to generate a single-cell suspension. For more collagen-rich tumor models (*i.e.*, CMS5 fibrosarcoma), a syringe plunger could be used in addition to scissors to more fully mechanically disaggregate tumor tissue prior to enzymatic treatment. Conversely, less collagen-rich tumor models (*i.e.*, B16 melanoma) do not necessarily require enzymatic treatment. As demonstrated in these results, the type of collagenase preparation and the lot from which it was

derived can significantly influence the variety and potency of proteases that cells are exposed to during enzymatic dissociation.

While non-myeloid leukocytes (*i.e.*, lymphocytes) do not seem to be as sensitive, these data suggest that myeloid cells, in particular, may be very susceptible to excessive protease exposure (**Figure 1**), resulting in damage to membrane proteins and decreased viability. As a result, the use of collagenase type IV over collagenase type I is recommended for its increased collagenase-specific proteolytic activity and the incorporation of FBS into the digestion mix to neutralize residual tryptic activity. Furthermore, utilizing purified collagenase products, as opposed to crude preparations from commercial sources, can increase the reproducibility of cellular recovery. Once the digestion is complete, the addition of EDTA and incubation at 4 °C is mandatory to chelate the Ca<sup>2+</sup> ions and reduce the temperature needed for collagenase activity<sup>14</sup>.

To characterize myeloid cell infiltrate within a heterogeneous TIL population, high-level gating strategies have been provided (**Figure 2**). The polychromatic flow cytometry panel should be designed in such a way that 1) dead and non-myeloid cells are excluded, 2) myeloid cell subsets can be identified, and 3) altered functionality can be implicitly observed across groups of samples (**Figure 3**). Depending on the number of myeloid cell subsets of interest and the depth of functional characterization, these criteria may not be fully accommodated within one staining panel. To free up channels for the panel, markers could be strategically pooled into a single dump channel. Although this method allows for high-dimensional analysis of tumor-infiltrating myeloid cells, it is still constrained by a relatively low parameter limit. More recent technologies using heavy metal reporter ions, such as

mass cytometry, enable up to 40 independent parameters within a single panel, which will allow better study of the cellular and functional diversity of myeloid cells within the TME<sup>15</sup>.

However, the cost of instrumentation limits the ubiquity of its use. Flow cytometry is more accessible and produces reliable characterization data, although the mixing and matching of markers across multiple panels necessitates panel validation as an extremely important step prior to the experiment. Upon identification of tumor-infiltrating myeloid subsets of interest, several researchers<sup>15</sup> describe techniques to sort these cells for functional assays and studies. Sorted cells can be reliably analyzed for their T cell-suppressive capacity *in vitro* as well as their antitumor capability *in vivo* after adoptively transferring them into mouse models of tumor relapse (**Figure 3**). Overall, the significance of the described methods is that, in comparison to other TIL isolation protocols, the conditions of tumor harvest, dissociation, cell enrichment, and cell sorting were tailored towards reproducibly acquiring a high yield of the myeloid cell compartment over all other leukocytes and without compromising their function.

## Disclosures

No conflicts of interest declared.

## Acknowledgments






This work was supported by the Ontario Institute for Cancer Research through funding provided by the Government of Ontario, as well as the Canadian Institutes of Health Research (FRN 123516 and FRN 152954), the Canadian Cancer Society (grant 705143), and the Terry Fox Research Institute (TFRI-1073).

## References

1. Paardekooper, L. M., Vos, W., van den Bogaart, G. Oxygen in the tumor microenvironment: effects on dendritic cell function. *Oncotarget*. **10** (8), 883-896 (2019).
2. Schoupe, E., De Baetselier, P., Van Ginderachter, J. A., Sarukhan, A. Instruction of myeloid cells by the tumor microenvironment: Open questions on the dynamics and plasticity of different tumor-associated myeloid cell populations. *Oncoimmunology*. **1** (7), 1135-1145 (2012).
3. Jahchan, N. S. et al. Tuning the tumor myeloid microenvironment to fight cancer. *Frontiers in Immunology*. **10**, 1611 (2019).
4. Srivastava, M. K. et al. Myeloid suppressor cell depletion augments antitumor activity in lung cancer. *PLoS One*. **7** (7), e40677 (2012).
5. Awad, R. M., De Vlaeminck, Y., Maebe, J., Goyvaerts, C., Breckpot, K. Turn back the TIME: targeting tumor infiltrating myeloid cells to revert cancer progression. *Frontiers in Immunology*. **9**, 1977 (2018).
6. Strauss, L. et al. Targeted deletion of PD-1 in myeloid cells induces antitumor immunity. *Science Immunology*. **5** (43), eaay1863 (2020).
7. Cassetta, L. et al. Deciphering myeloid-derived suppressor cells: isolation and markers in humans, mice and non-human primates. *Cancer Immunology, Immunotherapy*. **68** (4), 687-697 (2019).
8. Nguyen, A. et al. HDACi delivery reprograms tumor-infiltrating myeloid cells to eliminate antigen-loss variants. *Cell Reports*. **24** (3), 642-654 (2018).
9. Newton, J. M., Hanoteau, A., Sikora, A. G. Enrichment and characterization of the tumor immune and non-immune microenvironments in established

- subcutaneous murine tumors. *Journal of Visual Experiments: JoVE*. (136), 57685 (2018).
10. Engfeldt, P., Arner, P., Ostman, J. Nature of the inhibitory effect of collagenase on phosphodiesterase activity. *Journal of Lipid Research*. **26** (8), 977-981 (1985).
  11. Quah, B. J., Parish, C. R. The use of carboxyfluorescein diacetate succinimidyl ester (CFSE) to monitor lymphocyte proliferation. *Journal of Visual Experiments: JoVE*. (44), 2259 (2010).
  12. Schupp, J. et al. Targeting myeloid cells in the tumor sustaining microenvironment. *Cellular Immunology*. **343**, 103713 (2019).
  13. Gabrilovich, D. I., Ostrand-Rosenberg, S., Bronte, V. Coordinated regulation of myeloid cells by tumours. *Nature Reviews Immunology*. **12** (4), 253-268 (2012).
  14. Seglen, P. O. Preparation of isolated rat liver cells. *Methods in Cell Biology*. **13**, 29-83 (1976).
  15. Roussel, M. et al. Mass cytometry deep phenotyping of human mononuclear phagocytes and myeloid-derived suppressor cells from human blood and bone marrow. *Journal of Leukocyte Biology*. **102** (2), 437-447 (2017).

## De novo necroptosis creates an inflammatory environment mediating tumor susceptibility to immune checkpoint inhibitors

Samuel T. Workenhe <sup>1✉</sup>, Andrew Nguyen<sup>2</sup>, David Bakhshinyan<sup>3</sup>, Jiarun Wei<sup>2</sup>, David N. Hare<sup>2</sup>, Kelly L. MacNeill<sup>2</sup>, Yonghong Wan<sup>2</sup>, Andrew Oberst<sup>4</sup>, Jonathan L. Bramson <sup>2</sup>, Jalees A. Nasir <sup>5</sup>, Alyssa Vito<sup>2</sup>, Nader El-Sayes<sup>2</sup>, Sheila K. Singh <sup>3</sup>, Andrew G. McArthur <sup>1,5</sup> & Karen L. Mossman <sup>2✉</sup>

Cancer immunotherapies using monoclonal antibodies to block inhibitory checkpoints are showing durable remissions in many types of cancer patients, although the majority of breast cancer patients acquire little benefit. Human melanoma and lung cancer patient studies suggest that immune checkpoint inhibitors are often potent in patients that already have intratumoral T cell infiltrate; although it remains unknown what types of interventions can result in an intratumoral T cell infiltrate in breast cancer. Using non-T cell-inflamed mammary tumors, we assessed what biological processes and downstream inflammation can overcome the barriers to spontaneous T cell priming. Here we show a specific type of combination therapy, consisting of oncolytic virus and chemotherapy, activates necroptosis and limits tumor growth in autochthonous tumors. Combination therapy activates proinflammatory cytokines; intratumoral influx of myeloid cells and cytotoxic T cell infiltrate in locally treated and distant autochthonous tumors to render them susceptible to immune checkpoint inhibitors.

<sup>1</sup> Department of Pathobiology, Ontario Veterinary College, University of Guelph, Guelph, ON, Canada. <sup>2</sup> McMaster Immunology Research Centre, Institute for Infectious Disease Research, Department of Pathology and Molecular Medicine, McMaster University, Hamilton, ON, Canada. <sup>3</sup> Stem Cell and Cancer Research Institute, Department of Biochemistry and Biomedical Sciences, McMaster University, Hamilton, ON, Canada. <sup>4</sup> Department of Immunology, University of Washington, Seattle, WA 98109, USA. <sup>5</sup> David Braley Centre for Antibiotic Discovery, McMaster University, Hamilton, ON, Canada.  
✉email: [sworkenh@uoguelph.ca](mailto:sworkenh@uoguelph.ca); [mossk@mcmaster.ca](mailto:mossk@mcmaster.ca)

The immune system maintains homeostasis through antigen-specific elimination of tumor cells and preventing tumor growth<sup>1</sup>. Successful generation of T-cell-mediated immunity involves tumor antigen presentation, a process fine-tuned by co-stimulatory/inhibitory signals and cytokines that regulate the activation of tumor-specific naive T cells to become effector T cells<sup>2</sup>. Various types of immunotherapies were developed through the modulation of immune regulatory mechanisms governing antitumor T cells. Of particular interest, the use of monoclonal antibodies to block inhibitory T-cell receptor signaling, collectively called immune checkpoint inhibitors (ICI), are integrated into patient standard of care to treat multiple cancer types<sup>3–6</sup>. However, the overall proportion of patients that respond to ICI is remarkably low owing to numerous adaptive resistance mechanisms orchestrated by tumors to defeat intrinsically developed antitumor immunity<sup>7,8</sup>. There is no definitive biomarker of ICI yet, although correlates such as, neoantigen load<sup>9,10</sup>, expression of inhibitory checkpoint ligands, interferon<sup>11</sup> and proinflammatory signatures<sup>12</sup>, were showed to predict efficacy of ICI.

Certain types of cell death modalities emit proinflammatory signals to stimulate tumor antigen presentation and intratumoral T-cell infiltration. Cell death stimuli initiated by anthracyclines<sup>13</sup>, photodynamic therapy<sup>14</sup>, and oncolytic viruses<sup>15–17</sup> elicit pre-mortem tumor cell endoplasmic reticulum stress leading to calreticulin exposure<sup>18</sup> along with release of ATP<sup>19–21</sup> and high mobility group box 1<sup>20,21</sup>, resulting in potent antigen presentation<sup>22</sup> and adaptive immunity. Although cell death inducers were extensively studied in immune-responsive transplanted tumors<sup>13–22</sup>, it remains largely unknown what types of combination therapies, cell death modalities, and downstream inflammatory signals can heat-up cold and immunosuppressive tumor types such as breast cancer<sup>23,24</sup>.

Genetically engineered mouse models of breast cancer have assisted the functional characterization of biological processes implicated in human breast cancers although they have not been extensively used to develop breast cancer immunotherapies<sup>25,26</sup>. Autochthonous tumors driven by overexpression of the rat oncogene *Neu* (*NeuT*) in BALB-*NeuT* mice are highly immunosuppressive and fail to spontaneously prime T cells or after immunogenic chemotherapy<sup>23</sup>. Consistent with previous reports<sup>25,26</sup>, here we report that monotherapies of chemotherapy and oncolytic virus had significant anticancer activity. The list of ICD-inducing agents is expanding although their immunomodulatory effects when applied in combination are understudied. A combined administration of oHSV-1 and Mitomycin-C extends survival of autochthonous tumor-bearing mice. This immunogenic combination therapy relies on necroptosis to activate immune-dependent anticancer effect during therapy and prophylactic vaccination. Ablation of necrosome formation in the context of therapy and dying tumor cell vaccination results in loss of efficacy. Further characterization of the tumor immune landscape shows that immunogenic therapy activates desirable inflammation and cytokine/chemokine secretion to elicit intracellular T-cell infiltration thereby rendering non-immunogenic tumors susceptible to ICI.

## Results

**A combination of oncolytic virus and chemotherapy extends survival of autochthonous tumor-bearing mice.** We previously used TUBO cells (originally isolated from a spontaneous mammary tumor of BALB-*NeuT* mice<sup>25</sup>) in transplantation experiments to show that oHSV-1 induces markers of ICD and prolongs survival in 50% of tumor-bearing mice<sup>27,28</sup>. To further evaluate the systemic antitumor effects of locally applied ICD-inducing

agents (oHSV-1 and chemotherapeutics) in autochthonous tumors we utilized mouse models of breast carcinogenesis driven by overexpression of the rat oncogene *Neu* (*NeuT*)<sup>25,26</sup>. Female mice that express *NeuT* oncogene acquire highly aggressive mammary tumors<sup>25,26</sup>. In all of the studies, we treated the first palpable tumor and monitored the total tumor burden arising in all of the mammary glands. Although Mitomycin-C (Mito) and Mitoxantrone (MTX) monotherapies slowed tumor growth (Fig. 1b), no monotherapy had significant tumor controlling or survival benefit on their own (Fig. 1a–c). We previously showed that in transplantable TUBO tumors combination therapy of oHSV-1 and MTX results in 69% survival of tumor-bearing mice<sup>29</sup>. Thus, we hypothesized that the combined administration of oHSV-1 with chemotherapeutics would provide multiple danger and pathogen signals for enhanced antitumor effect<sup>27,29–33</sup>. We combined oHSV-1 with ICD-inducing (MTX or Doxorubicin; Dox) or a non-ICD-inducing chemotherapy (Mitomycin-C). Administration of oHSV-1 in combination with MTX or Dox had no significant tumor controlling effect (Fig. 1d) or survival benefit (Fig. 1e). Rather the combined application of oHSV-1 with Mito had a statistically significant tumor controlling effect in BALB-*NeuT* mice (Fig. 1e, f).

**Necroptosis is essential for the therapeutic effect of immunogenic therapy.** To investigate the mechanism by which Mito+oHSV-1 exerts anticancer effect, day 6 tumors were harvested and stained for markers of virus replication, endothelial cell damage, and cell death. Monotherapies of Dox and Mito had insignificant cell death and endothelial cell damage (Fig. 2a–d). Compared with oHSV-1 and Dox+oHSV-1, Mito+oHSV-1 showed a higher level of intratumoral virus replication (Fig. 2a, b) despite in vitro addition of Mito or Dox reducing oHSV-1 replication (Supplementary fig. 1). Mito+oHSV-1 did not alter CD31 levels within tumors (Fig. 2a, c). All the monotherapies (oHSV-1, Dox, Mito) did not affect the level of apoptosis as measured by cleaved caspase 3 (Fig. 2a, d) and necroptosis as assessed by the level of p-MLKL (Fig. 3a). However, Mito+oHSV-1 therapy showed significantly higher apoptosis (Fig. 2a, d) and necroptosis (Fig. 3b, Supplementary fig. 2a, b).

Next, we evaluated which type of cell death is essential for the therapeutic effect of Mito+oHSV-1. Inhibition of caspases using a pan-caspase inhibitor partially offset the therapeutic benefit (Fig. 3c), whereas inhibition of necrosome formation using systemic Nec-1s administration<sup>34</sup> significantly abolished the anticancer effect of Mito+oHSV-1 (Fig. 3c). Nec-1s+Mito+oHSV-1 treatment did not exert a statistically significant change in total lymphocyte numbers (CD4<sup>+</sup> and CD8<sup>+</sup>) in the periphery compared with PBS control and Mito+oHSV-1 treatments (Supplementary fig. 3a, b). An established method for evaluating immune stimulating and antitumor effects of an ICD inducer is to administer in vitro killed cells as a vaccine<sup>35,36</sup>. TUBO cells were previously characterized murine tumor cell line established from spontaneous mammary tumors of BALB-*NeuT* mice<sup>25</sup>. BALB/*NeuT* mice vaccinated with dying TUBO cells treated with Mito+oHSV-1, but not Dox+oHSV-1, showed significant delay in the growth of spontaneous tumors (Fig. 3d). Moreover, Nec-1s treatment or deletion of MLKL (via CRISPR/Cas9-mediated knockout; supplementary fig. S4) abrogates the antitumor effects of the vaccine (Fig. 3e). Overall, these results suggest that necroptosis is an integral part of Mito+oHSV-1 mediated immunotherapeutic effect.

**Combination therapy displays a proinflammatory cytokine signature and T-cell-mediated anticancer effect.** To evaluate the cytokine/chemokine milieu during therapy, we analyzed the level

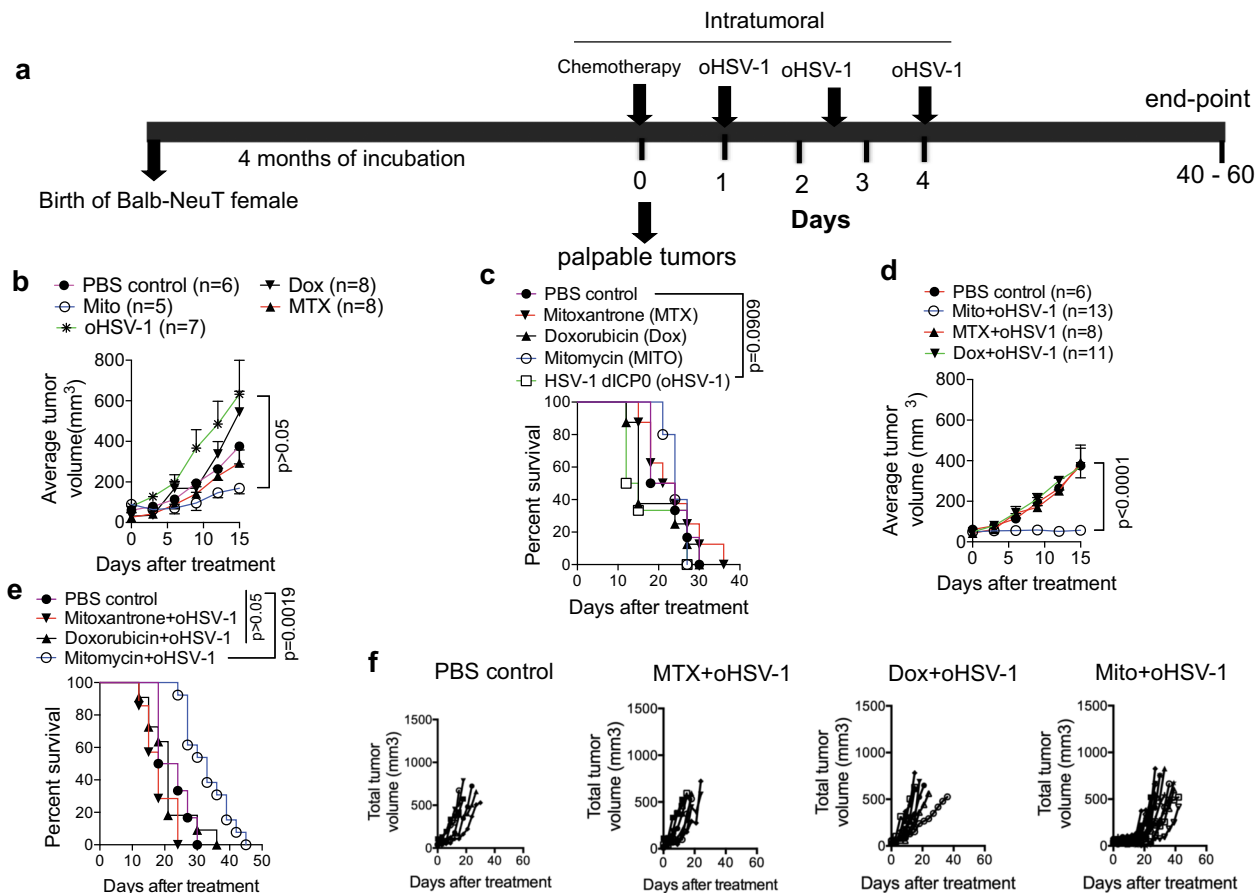


**Fig. 1 ICD-inducing monotherapies fail to limit tumor growth while combination therapy of Mito-C+oHSV-1 extends survival.** **a** Outline of treatment regimens for chemotherapy and oHSV-1 in autochthonous tumors of BALB-NeuT mice. **b, c** Treatment with ICD-inducing monotherapies (MTX, Dox, oHSV-1) and non-ICD-inducing (Mito) neither limit tumor growth nor extend survival of tumor-bearing mice. **d, e** Among the various combinations of oHSV-1 and chemotherapy, Mito+oHSV-1 limits tumor growth and extends survival of tumor-bearing BALB-neuT mice. **f** Individual mice total tumor volumes as a proxy for tumor burden of BALB-NeuT mice treated with various combination therapies. Quantitative data are mean±standard deviation of total tumor volumes (Kruskal-Wallis test) **b, d** and Kaplan-Meier survival (Log-rank, Mantel-Cox test) **c, e**. All the data presented in this figure are pooled from at least two independent experiments done at different times.

of 31 cytokines/chemokines in tumor homogenates in treated and control mice. Untreated BALB-NeuT tumors display higher levels of immunosuppressive cytokines (IL-4 and IL-10) that are significantly downregulated after oHSV-1, Dox+oHSV-1, and Mito+oHSV-1 treatment (Supplementary fig. 5a). Other cytokines commonly upregulated by multiple therapies include Eotaxin, IL-6, and IL-15 (Supplementary fig. 5b). Cytokines/chemokines that did not show significant change include GCSF, granulocyte-macrophage colony-stimulating factor (GM-CSF), IL-1b, IL-2, IL-3, IL-7, IL-9, IL-12, IP-10, CXCL-1, MIG, and VEGF (Supplementary fig. 5c). Proinflammatory cytokines (RANTES, TNF- $\alpha$ , IL-1 $\alpha$ , IL-13, IL-17, LIF, MCSF) and chemokines (Macrophage inhibitory protein 1a (MIP1a) (CCL3), MIP1b (CCL4), Monocyte chemoattractant protein 1) (Fig. 4a) were differentially up-regulated in Mito+oHSV-1 treated tumors. Consistent with the chemokine signature, Mito+oHSV-1 treated tumors showed higher Ly6G<sup>+</sup> (Fig. 4b, c) and F4/80<sup>+</sup> (Fig. 4d, e) immune cell influx 96 h after start of treatment. When Nec-1s is administered along with Mito+oHSV-1, the Ly6G<sup>+</sup> population is significantly reduced (Fig. 4b, c). Moreover, both Mito+oHSV-1 treated and untreated control tumors did not show intratumoral Treg infiltration (Supplementary fig. 6). Overall, these studies show that de novo necroptosis activation results in intratumoral myeloid cell infiltrate.

Given the inflammatory cytokine milieu and the influx of myeloid cells during Mito+oHSV-1, we hypothesized that these early events may contribute to cytotoxic T-lymphocyte infiltration within tumor lesions. To evaluate the intratumoral infiltration of CD8<sup>+</sup> T cells, we isolated day 10 treated and untreated tumors (within the same mouse) for immunohistochemistry (IHC) staining of CD3/CD8 surface markers. While untreated tumors of BALB-NeuT mice lack T-cell infiltration, Mito+oHSV-1 treated and distant untreated tumors within the same mouse show higher levels of CD3<sup>+</sup>CD8<sup>+</sup> T-cell infiltration (Fig. 5a, b). Quantification of the IHC signal shows that distant tumors are significantly infiltrated with CD3<sup>+</sup>CD8<sup>+</sup> T cells. However, Mito+oHSV-1-treated tumors by day 10 show mostly dying tumor cells and loss of tumor architecture. As a result, the IHC quantification did not show significant T-cell infiltration in treated tumors. Inhibiting necrosome formation during Mito+oHSV-1 results in significant reduction of cytotoxic T-lymphocyte infiltration in distantly located untreated tumors (Fig. 5a, b). The abscopal effects of Mito+oHSV-1 is not an outcome of virus replication in untreated tumors, as there is no detectable virus replication in distant tumors following in vivo imaging of virus replication and IHC staining for HSV-1 structural proteins<sup>27</sup> (Supplementary fig. 7).

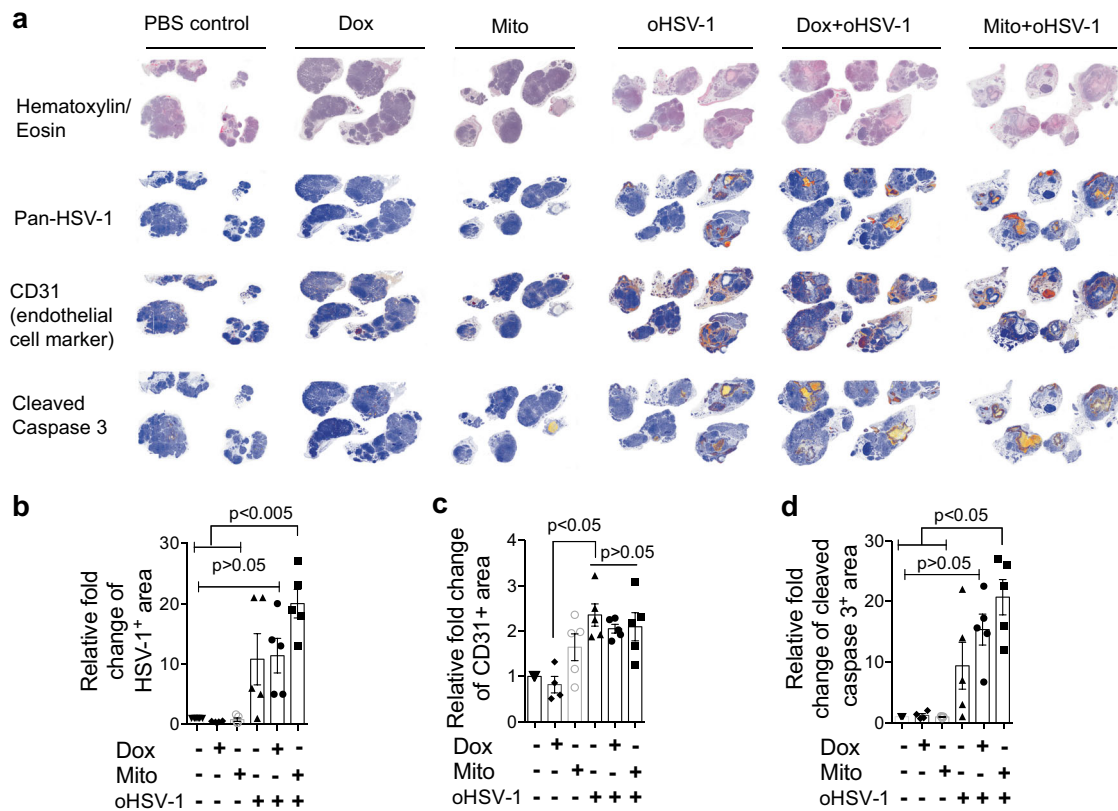


**Fig. 2 Mitomycin+oHSV-1 combination increases virus replication and tumor cell death.** **a** Visualization of oHSV-1 replication (using a polyclonal antibody that detects major HSV-1 structural proteins), vascular damage (using endothelial cell marker CD31), apoptotic cell death (using cleaved caspase 3) on day 6 after start of treatment. **b–d** Immunohistochemistry positive signal were quantified and plotted. Quantitative data are mean±standard deviation of fold changes of positive signal relative to PBS control group. Kruskal-Wallis test with Dunn’s multiple comparison as a post hoc test was used to test statistical significance.

To evaluate the importance of T lymphocytes in the therapeutic outcome of Mito+oHSV-1, we conducted survival studies in the presence or absence of CD4<sup>+</sup> and CD8<sup>+</sup> T cells. Depletion of T cells (CD4<sup>+</sup> and CD8<sup>+</sup>) using monoclonal antibodies reduces the efficacy of Mito+oHSV-1 indicating that the therapeutic efficacy of Mito+oHSV-1 is T-cell mediated (Fig. 5c).

**Therapy-induced necroptosis renders autochthonous tumors susceptible to ICIs.** The extent of tumor-infiltrating CD8<sup>+</sup> T-cell density is significantly associated with improved clinical outcome<sup>37</sup>, although tumor-infiltrating CD8<sup>+</sup> T cells isolated from patient tumors often display exhausted phenotypes characterized by an impaired ability to secrete effector cytokines, high expression of inhibitory receptors and altered signaling pathways<sup>33</sup>. Immunological interventions to block inhibitory receptors at the priming (anti-CTLA-4) and effector (anti-PD-1) stages are able to reinvigorate exhausted T cells, leading to significant therapeutic benefit in multiple human cancer types<sup>3,4,38–40</sup>. Human studies have found that patients harboring non-T-cell-inflamed tumors fare worse during ICI. Moreover, combined anti-CTLA-4+anti-PD-1 therapy has enhanced efficacy that exceeded either of the anti-CTLA-4 and anti-PD-1 monotherapies in melanoma patients<sup>4</sup>. Overall, breast cancer has low mutational load and it has not been intensively investigated for its susceptibility to clinical immunotherapies<sup>41</sup>. ICI using anti-CTLA-4+anti-PDL-1 is undergoing clinical evaluation in breast cancer patients<sup>42</sup>. ICD-inducing agents have a potential to be combined with ICI to treat immunologically cold breast cancer tumors.

As Mito+oHSV-1-mediated necroptosis induce systemic intratumoral cytotoxic T-lymphocyte infiltration, we hypothesized that this treatment may synergize with clinically used anti-CTLA-4+anti-PDL-1 ICI therapy<sup>4</sup>. Untreated tumors of BALB-NeuT mice lack intratumoral cytotoxic T lymphocytes and thus do not benefit from ICI (anti-CTLA-4 and anti-PD-L1). Moreover, Dox+oHSV-1+ICI does not show significant survival or tumor control (Fig. 6a–c, e). However, administration of ICI with Mito+oHSV-1 shows significant anticancer effect evidenced by lower tumor volume (Fig. 6a), tumor multiplicity (Fig. 6b) and prolonged survival of tumor-bearing Balb-NeuT mice (Fig. 6c). Individual mouse tumor plots of Mito+oHSV-1+ICI-treated mice show that a fraction of mice were tumor free for 40 days before relapse (Fig. 6e). Consistent with the essential role of necrosome in Mito+oHSV-1 anticancer immunity, administration of Nec-1s during the triple combination therapy abrogates the survival benefit of Mito+oHSV-1+ICI (Fig. 6d).

## Discussion

Tumors hide from immune recognition and subsequent attack by evading immune-stimulatory cell death<sup>43</sup>, downregulating MHC expression and secreting suppressive chemokines and cytokines<sup>44</sup>. As a result, cell death insults that activate pre-mortem stress and subsequent expression of immunomodulatory molecules can be one of the ways to reinstate immunosurveillance by promoting tumor antigen uptake and presentation<sup>45</sup>. Using autochthonous tumors, our study demonstrates that (1) combining different classes of “bona fide” ICD-inducing agents (oncolytic virus and chemotherapy)



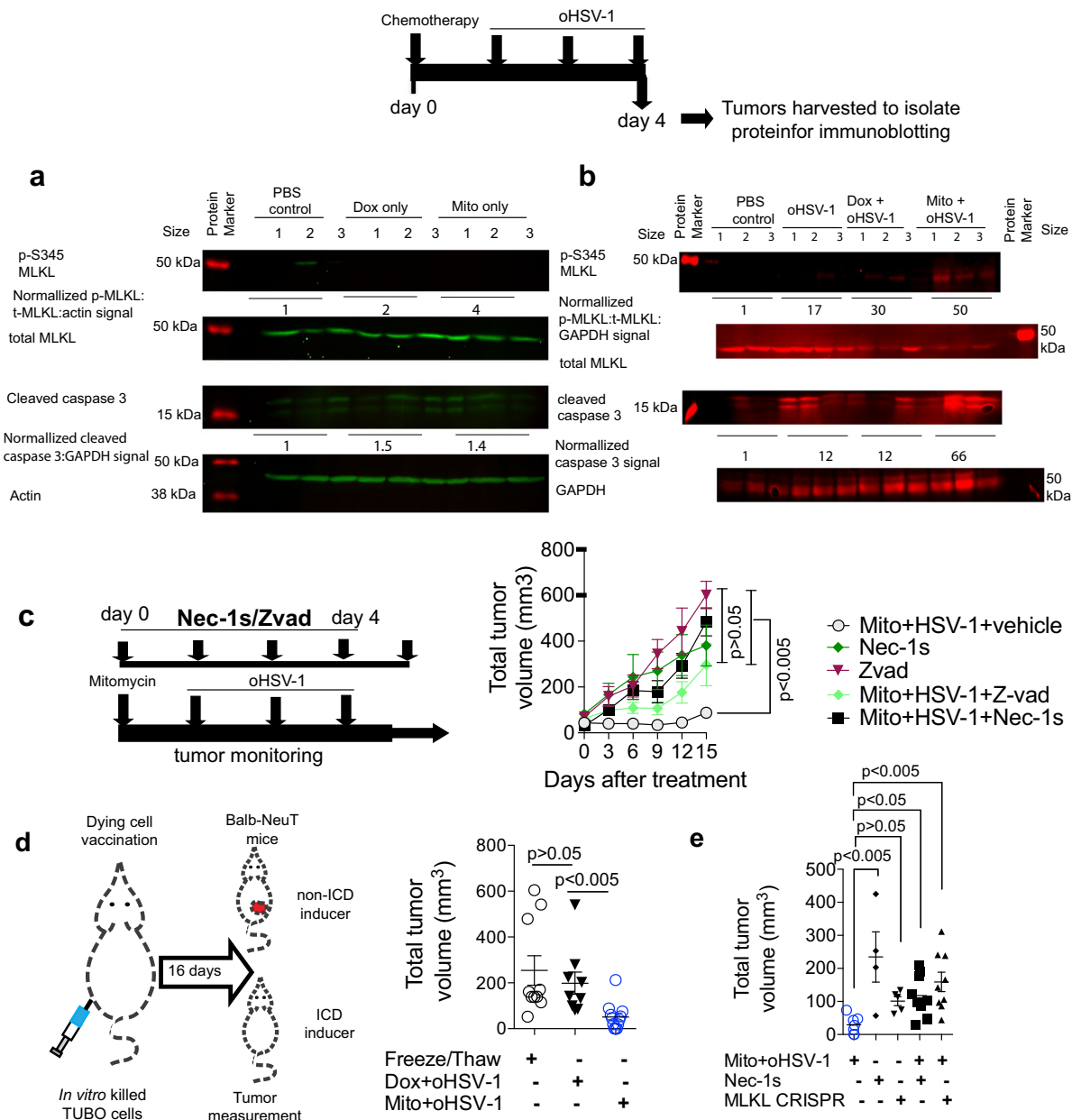


**Fig. 3 Therapeutic efficacy of immunogenic combination therapy relies on necroptosis.** **a, b** Immunoblots of protein harvested from tumors at 96 h after start of Mito+oHSV-1 treatment show higher normalized p-MLKL and cleaved caspase 3 fluorescence intensity ( $n = 3$  per treatment, labeled 1-3). Uncropped images are displayed in Supplementary Fig. 3. **c** Average total tumor volume of mice treated with Mito+oHSV-1 along with daily intraperitoneal administration of Nec-1s or Pan-Caspase inhibitor (ZVad-FMK) from day 1 to day 5. Quantitative data are mean±standard deviation from  $n = 5$  mice per treatment group. **d** Average tumor burden 16 days after vaccination of naïve BALB-NeuT mice with in vitro killed TUBO cells (a cell line isolated from BALB-NeuT spontaneous tumors) (by freeze/thawing ( $n = 10$ ) or 24 h after treatment with Mito+oHSV-1 ( $n = 12$ ) or Dox+oHSV-1 ( $n = 9$ )). Dying TUBO cells were used to vaccinate 110 days old BALB-neuT mice with small palpable tumors. Quantitative data are mean±standard deviation. **e** Total tumor volume of BALB-NeuT mice 16 days after vaccination with dying wild type TUBO cells 24 h after Mito+oHSV-1 ( $n = 7$ ), Mito+oHSV-1+Nec-1s ( $n = 9$ ), and Nec-1s treatment ( $n = 4$ ). Alternatively TUBO cells lacking MLKL (Supplementary fig. 4) were used for vaccination either 24 h after treatment with Mito+oHSV-1 ( $n = 9$ ) or freeze/thawing ( $n = 5$ ). Quantitative data are mean±standard deviation. Statistical significance of mean tumor volumes were tested using Kruskal-Wallis test with Dunn’s multiple comparison as a post hoc test.

provides a rational combinatorial therapy that activates anti-tumor immune response in necroptosis dependent fashion (2) immunogenic Mito+oHSV-1 therapy activates an inflammatory immune contexture associated with proinflammatory cytokine/chemokine signature and influx of myeloid cells and cytotoxic T-lymphocyte infiltrate in distant tumors, and (3) therapy-induced necroptosis is an essential aspect of Mito+oHSV-1 therapy to render tumors susceptible to ICIs.

Autochthonous tumors are highly immune suppressive and lack an intratumoral T-cell infiltrate and thus often monotherapies fail to show immunotherapeutic effect. We found out that locally administered monotherapies of Dox, Mitoxantrone, Mitomycin-C<sup>13</sup>, and oHSV-1<sup>27</sup> fail to extend survival of autochthonous tumor-bearing mice. In support of this, a previous study showed that the anticancer effect of chemotherapies in autochthonous tumors of BALB-NeuT and conditional

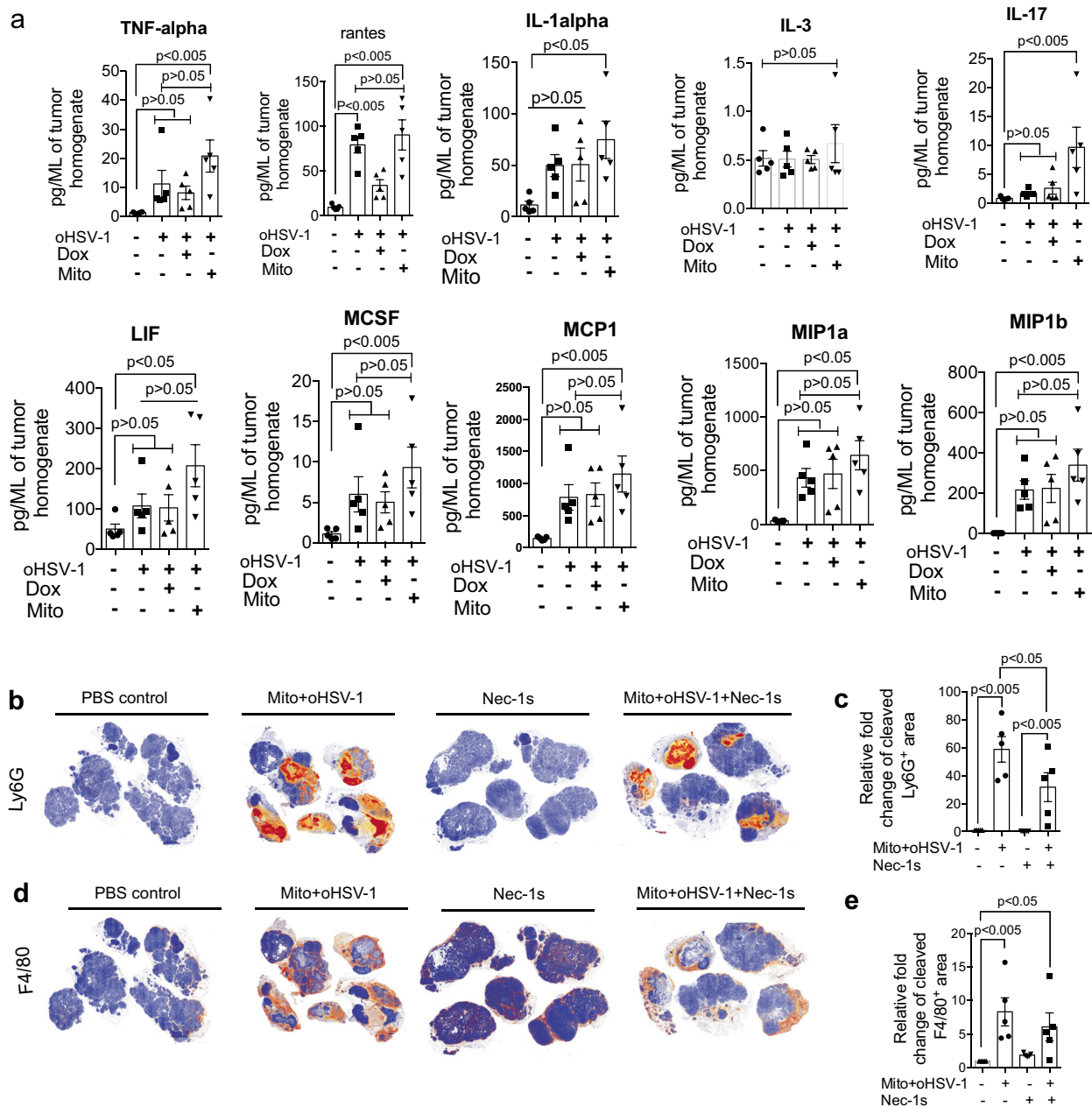


**Fig. 4** Mito+oHSV-1 shows necrosome-dependent proinflammatory signature. **a** Mito+oHSV-1 treated mammary tumors were harvested 96 h post start of treatment and tumor homogenates assayed for expression of 31 cytokines and chemokines. **b–e** Therapy-induced inflammation during Mito+oHSV-1 shows necrosome-dependent Ly6G<sup>+</sup> infiltration. Autochthonous tumors of BALB-NeuT mice treated with Mito+oHSV-1 and/or Nec-1s were harvested 96 h post start of treatment and stained for Ly6G **b, c** and F4/80 **d, e**. Quantitative data are mean±standard deviation. Statistical significance was tested with one-way ANOVA or non-parametric Kruskal–Wallis test with Dunn’s multiple comparison as a post hoc test **a, c, e**. All the experiments in this figure are generated from five mice per treatment group.

*K14cre; Cdh1<sup>fllox/fllox</sup>; Trp53<sup>fllox/fllox</sup>* mice operates independent of the adaptive immune system<sup>23</sup>. However, both of the chemotherapies were able to show intratumoral CD3<sup>+</sup> T-cell infiltrate, although the absence of lymphocytes in Rag<sup>-/-</sup> mice did not change the outcome of mammary tumorigenesis. Among the three combination therapies we tested, only Mito+oHSV-1 treatment showed adaptive immune response in a therapeutic and prophylactic vaccination setting. In support of this findings, a systemic immunogenic combination chemotherapy (cyclophosphamide–oxaliplatin) in *Kras<sup>LSL-G12D/+</sup>; Trp53<sup>fllox/fllox</sup>* lung adenocarcinoma tumors leads to ICD-dependent CD8<sup>+</sup> T-cell infiltration and synergy with ICI<sup>45</sup>. Collectively, these

findings suggest that certain combinations of ICD-inducing therapies can exert immune-mediated anticancer effects in autochthonous tumors.

Compared with transplanted TUBO tumors<sup>29</sup>, autochthonous BALB-NeuT tumors are highly resistant to therapy. The median survival days and percentage of tumor-free mice after combination therapy are higher in transplanted tumors<sup>29</sup> compared with autochthonous tumors in this study. These differences can be attributed to the tumor cell’s ability to sense cell death stimuli and release immunomodulatory molecules<sup>30</sup>, and the tumor immune landscape prior to therapy<sup>46</sup>. Moreover, tumor intrinsic oncogenic events may also dictate the differences in therapeutic

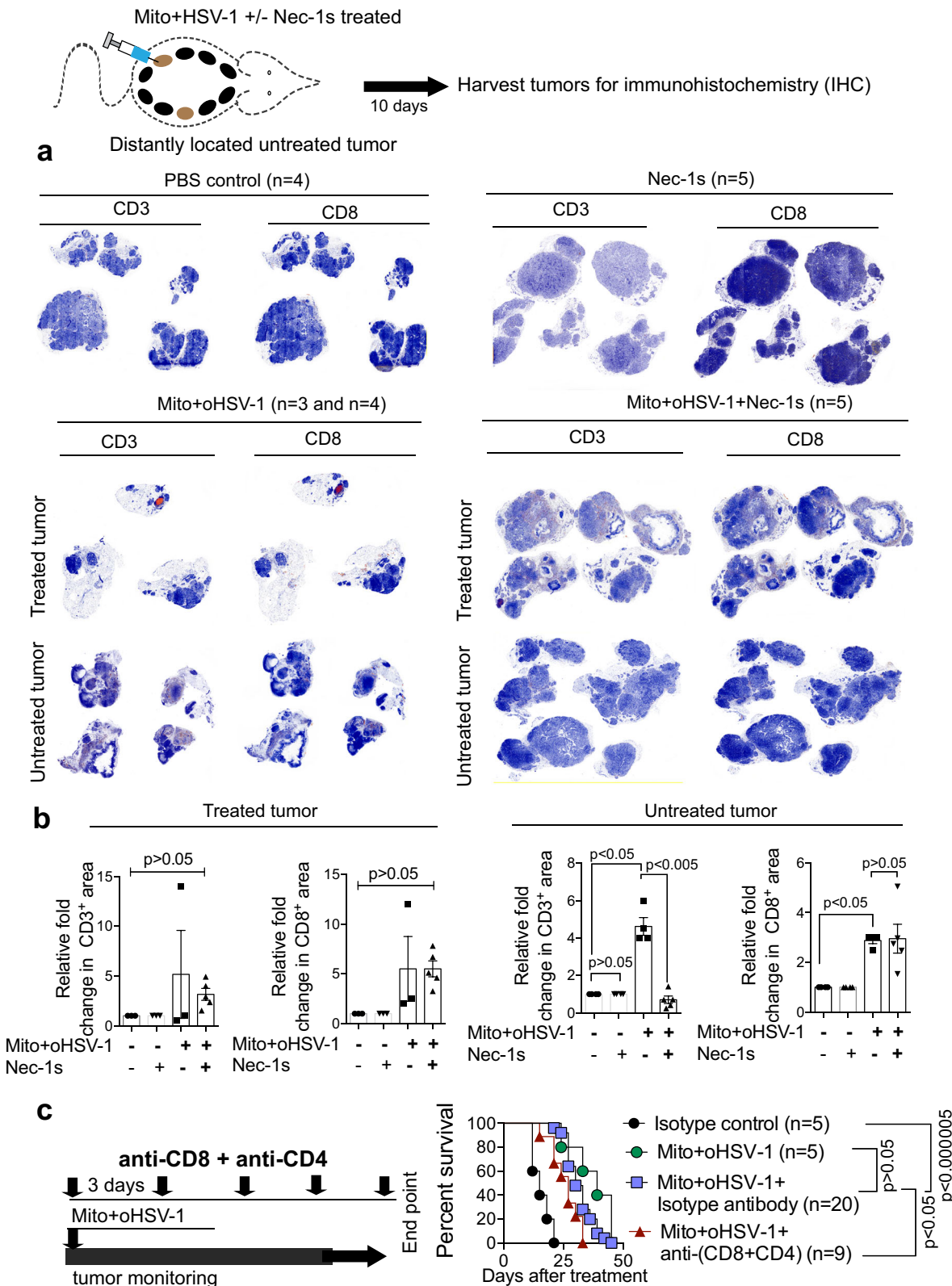


**Fig. 5 Immunogenic Mito+oHSV-1 therapy CD8<sup>+</sup> T-cell infiltration in distant tumor lesions.** **a, b** Ten days after Mito+oHSV-1 treatment treated and distant untreated tumor lesions were processed for IHC staining using CD3 and CD8 antibodies. Fold change in positive signal was calculated relative to the PBS controls. Quantitative data are mean±standard deviation from each treatment group (n = 5) (Statistical significance was tested with one-way ANOVA or non-parametric Kruskal-Wallis test with Dunn’s multiple comparison as a post hoc test). **c** BALB-neuT mice were treated with Mito+oHSV-1 along with monoclonal antibodies to deplete T cells (CD4 and CD8) or isotype control antibody. Quantitative data are Kaplan-Meier survival (Log-rank, Mantel-Cox test).



yet clear<sup>21,49</sup>, utilizing the immunological benefits of therapy-induced necroptosis along with ICIs may have a translational potential. In line with this, several clinically used small molecules, natural compounds and engineered oncolytic viruses that selectively induce necroptosis have a potential for synergy with ICIs<sup>72</sup>. Future studies should aim to characterize the immunotherapeutic potential of therapy-induced necroptosis in human breast cancer patients.

## Methods

**Study design.** The aim of this study was to understand the immune-stimulatory effects of oncolytic virotherapy and various chemotherapeutics in treatment of spontaneously arising mammary tumors. We adopted an autochthonous mouse model that recapitulates a tumor model that fails to undergo spontaneous T-cell priming. We used this model to administer treatments locally at one of the tumor sites and measure systemic effect by measuring tumor volumes arising from all the 10 mammary glands.

For *in vivo* anticancer studies, the primary endpoint is tumor size. We have conducted several previous studies using transplantable and autochthonous tumors and determined that  $n = 5-10$  is an appropriate sample size per treatment group. There were no samples or animals excluded from the analysis. For most of the experiments reported in this manuscript the efficacy of the treatments were assessed in tumor volume as a proxy for tumor growth. As a result, before animals are allocated to any treatment group their tumor volume was measured and mice were randomized to achieve equal tumor volume per treatment group.

**Cells culture.** Human osteosarcoma cells (U2OS; American Type Culture Collection; ATCC, Manassas, VA) were maintained in Dulbecco's modified Eagle's media (DMEM) supplemented with 10% fetal bovine serum (FBS). TUBO is a cell line generated from a spontaneous mammary gland tumor of a BALB-*neuT* mouse<sup>25</sup>. TUBO cells are a generous gift of Dr. Guido Forni, who developed them originally. All the cell lines were mycoplasma tested and they were free of mycoplasma during the study period. TUBO cells were maintained in DMEM with 10% FBS. All media contained 2 mmol/l l-glutamine, 100U/ml penicillin, and 100 µg/ml streptomycin (Gibco). All cell lines were grown at 37 °C under humidified conditions.

**Oncolytic HSV-1.** The oHSV-1 has a deletion of the entire *ICP0*-coding region and has been previously described<sup>27</sup>. Viruses were propagated and tittered on U2OS cells in the presence of 3 mmol/l hexamethylene bisacetamide (Sigma; St. Louis, MO). Virus purification and concentration were done using sucrose cushion ultracentrifugation<sup>27</sup>.

**Western blotting.** Protein samples were harvested after lysing cells in radio-immunoprecipitation buffer (10 mM phosphate pH 7.4, 137 mM NaCl, 1% NP-40, 0.5% sodium deoxycholate and 0.1% sodium dodecyl sulfate) supplemented with protease inhibitor cocktail (Sigma; St. Louis, MO) and phosphatase inhibitors cocktail II and III (Sigma; St. Louis, MO). Protein extracts were resolved in 10–15% sodium dodecyl sulfate polyacrylamide gel electrophoresis and transferred to nitrocellulose membrane (Millipore, Billerica, MA). Blots were blocked in Odessey blocking buffer (LI-COR Biosciences, Lincoln, Nebraska). Western blotting detection was done after incubation with primary antibodies (anti-p-MLKL antibody, Cat#ab196436, Abcam; anti-total-MLKL, Cat#API14272B, Abcepta; anti-cleaved caspase 3 antibody, Cat#9661, Cell Signaling Technology; and anti-beta-actin antibody, Cat#4967, Cell Signaling Technology) infrared dye-conjugated secondary antibody (Donkey-anti-Rabbit IgG-800CW conjugated, Cat#92632213, LI-COR Biosciences) using Odyssey Scanner (LI-COR Biosciences, Lincoln, Nebraska).

**CRISPR knockout cell line.** Design and cloning of sgRNAs targeting mouse MLKL were done as previously described<sup>73</sup>. In brief, the sgRNAs sequences targeting MLKL (Forward 5'-GCACACGGTTTCTAGACGC-3', Reverse 5'-GCGTCTAGGAAACCGTGTGC-3') were cloned into BsmBI digested Lenti-CRISPR v2 plasmid (Addgene, Cambridge, MA). Single guide RNAs-Cas9 cassettes were introduced to TUBO cells by using lentivirus-mediated gene transfer. Lentivirus transduced cells were selected using 1 µg/ml Puromycin for at least 2 weeks and depletion of the protein was verified by immunoblotting.

**Treatment with chemotherapeutics and oHSV-1.** Mice were maintained at the McMaster University Central Animal Facility and all procedures were performed in full compliance with the Canadian Council on Animal Care and approved by the Animal Research Ethics Board of McMaster University. Weaned mice were genotyped for the presence of the transgenes. Transgenic mice (BALB-*NeuT*, Gp/PyMT, FVB-*NeuT*) were allowed to age for 110 days or until the mammary glands start to develop palpable tumors. In the entire study, tumor measurements and treatments were initiated once the first tumor reached palpable size.

Chemotherapeutics were administered once and in the combination setting, chemotherapeutics were administered 1 day prior to intratumoral oncolytic virus treatment (three doses of  $2 \times 10^7$  pfu<sup>27</sup>). Chemotherapeutic doses were 860 mM (1.25 mg/Kg) Dox hydrochloride (Sigma; St. Louis, MO), 6 mM Mito-C (4 mg/Kg) (Sigma; St. Louis, MO) or 5 µM MTX (Sigma; St. Louis, MO) (6.5 mg/Kg)<sup>13,74</sup>, administered intratumorally in 50 µl volume. The RIPK1 inhibitor (Nec-1s) (Bio-Vision, Milpitas, CA) was administered at a dose of 6 mg/kg. The pan-caspase inhibitor ZVAD-FMK (Minneapolis, MN) was used at a dose of 10 mg/kg. Inhibitors or the 5% dimethyl sulphoxide vehicle control were administered intraperitoneally every day for 4 days of Mito+oHSV-1 treatment. All tumors arising from the 10 mammary glands were measured every three days until mice reach endpoint. Mice having a total tumor volume above 525 mm<sup>3</sup> were classified as endpoint and sacrificed<sup>29</sup>.

**Vaccination with dying TUBO cells.** BALB-*NeuT* mice were vaccinated with dying TUBO cells. The control group was vaccinated with TUBO cells that were freeze-thawed. TUBO cells were infected with HSV-1 dICP0 at MOI of 3 for 1 h and then add back media with 25 µM Dox or 30 µM Mito-C was applied<sup>29</sup>. Nec-1s was used in the context of Mito+oHSV-1 treatment at 100 µM. Cells were incubated for 24 hr before scrapping to pellet the cells for vaccination. Each mouse was vaccinated with three million dying cells. Mammary glands were palpated and measured every 3 days.

**Immunohistochemistry.** Treated and control mammary tumors were fixed in 10% formalin for 48 h and then transferred to 70% ethanol until histological processing. Tumor sections were processed for Hematoxylin–Eosin staining or immunohistochemistry using antibodies listed in Supplementary Table 1. All the antibodies used in this study were validated by the supplier as well as independent publications from academic laboratories. However, before we use any of the antibodies, we have validated their suitability by titrating the amount of antibody and running positive and negative controls. All antibodies were stained on the Leica Bond RX Automated Stainer with either Epitope Retrieval Buffer 1 (ER1), Epitope Retrieval Buffer 2 (ER2), or with Enzyme 1 (Leica). All antibodies were diluted in Power Vision Super blocker (Leica). The IHC slides were scanned using Aperio ScanScope slide scanner (Aperio Technologies, CA), and the images were analyzed using Positivity Pixel Count 9.0 algorithm within ImageScope software (Aperio Technologies, CA) as described previously<sup>75</sup>.

**Tumor protein isolation.** Mice were anaesthetized and euthanized before resection of the tumors. Tumors were cut into small pieces and homogenized in the presence of tissue extraction solution (50 mM Tris, pH 7.4, 250 mM NaCl, 5 mM EDTA 2 mM Na<sub>3</sub>VO<sub>4</sub>, 1 mM NaF, 20 mM Na<sub>4</sub>P<sub>2</sub>O<sub>7</sub>, 1 mM beta-glycerophosphate, 1% NP-40). Homogenized tumors were incubated on ice for 30 min. Whole-tumor lysates were clarified by two sequential centrifugations at 13,000 × g for 10 min at 4 °C. Twenty to eighty micrograms of total protein was used for western blot analysis.

**Cytokine analysis.** Cytokine analysis was carried out on tumor homogenates harvested using tissue extraction buffer. Tumor homogenates with equal amounts of protein concentration were shipped to Eve Technologies (Calgary, Alberta, Canada) for 31-Plex murine cytokine/chemokine analysis.

**Antibodies.** The immune checkpoint blockade antibodies anti-CTLA-4 (clone 9H10, BioXcell), and anti-PDL-1 (clone 10 F.9G2, BioXcell) were used alone or in combination with HSV-1+Mito-C. For ICI treatments, mice with palpable tumors volume below 100 mm<sup>3</sup> were injected with 200 µg of the antibodies every 3 days. In the combination treatments ICI antibodies were applied at the same day as the start of HSV-1 treatment. Treatments were continued until mice reached end point. Monoclonal antibodies targeting CD4 (clone GK1.5, BioXcell) and CD8 (Clone 2.43, BioXcell) T cells were administered intraperitoneally at a dose of 250 µg starting 2 days before treatment and applied every other day for the first two weeks and once a week thereafter. Depletion of cells after antibody administration was verified by flow cytometry.

**Statistics and reproducibility.** BALB-*NeuT* female mice tumors take a minimum of 110 days to become palpable and the incidence of macroscopic tumors is a stochastic event making larger experiments difficult to be synchronized. As a result, we conducted experiments with less than five mice per treatment group (while including multiple treatment and controls groups) and pooled experimental results collected from multiple independent experiments.

For each statistical analysis used, normality of the distributions and equality of variance assumptions were tested before running the statistical analyses. One-way analysis of variance, non-parametric Kruskal–Wallis test and *t* test were used to determine the statistical significance of the differences in means. For analyzing the statistical significance of the difference in Kaplan–Meier survival between treatments, the Log-rank (Mantel–Cox) test was used. All the tests were two-sided. The null hypothesis was rejected for *p* values <0.05. All data analyses were carried out using GraphPad Prism (La Jolla, CA, USA).

**Reporting summary.** Further information on research design is available in the Nature Research Reporting Summary linked to this article.

## Data availability

The source data behind the graphs in this paper are available in Supplementary Data 1. All other data are available from the authors upon reasonable request.

Received: 29 August 2019; Accepted: 8 October 2020;

Published online: 04 November 2020

## References

- Shankaran, V. et al. IFN $\gamma$  and lymphocytes prevent primary tumour development and shape tumour immunogenicity. *Nature* **410**, 1107–1111 (2001).
- Sanmamed, M. F. & Chen, L. A paradigm shift in cancer immunotherapy: from enhancement to normalization. *Cell* **175**, 313–326 (2018).
- Hodi, F. S. et al. Improved survival with ipilimumab in patients with metastatic melanoma. *N. Engl. J. Med.* **363**, 711–723 (2010).
- Wolchok, J. D. et al. Nivolumab plus ipilimumab in advanced melanoma. *N. Engl. J. Med.* **369**, 122–133 (2013).
- Antonia, S. J. et al. Durvalumab after chemoradiotherapy in stage iii non-small-cell lung cancer. *N. Engl. J. Med.* **377**, 1919–1929 (2017).
- Motzer, R. J. et al. Nivolumab versus everolimus in advanced renal-cell carcinoma. *N. Engl. J. Med.* **373**, 1803–1813 (2015).
- Topalian, S. L. et al. Immunotherapy: the path to win the war on cancer? *Cell* **161**, 185–186 (2015).
- Fares C. M., Allen E. M. V., Drake C. G., Allison J. P., Hu-Lieskovan S. Mechanisms of resistance to immune checkpoint blockade: why does checkpoint inhibitor immunotherapy not work for all patients? American Society of Clinical Oncology Educational Book, 147–164 (2019).
- Snyder, A. et al. Genetic basis for clinical response to CTLA-4 blockade in melanoma. *N. Engl. J. Med.* **371**, 2189–2199 (2014).
- Le, D. T. et al. PD-1 blockade in tumors with mismatch-repair deficiency. *N. Engl. J. Med.* **372**, 2509–2520 (2015).
- Zaretsky, J. M. et al. Mutations associated with acquired resistance to PD-1 blockade in melanoma. *N. Engl. J. Med.* **375**, 819–829 (2016).
- Zemek, R. M. et al. Sensitization to immune checkpoint blockade through activation of a STAT1/NK axis in the tumor microenvironment. *Sci. Transl. Med.* **11**, eaav7816 (2019).
- Casares, N. et al. Caspase-dependent immunogenicity of doxorubicin-induced tumor cell death. *J. Exp. Med.* **202**, 1691–1701 (2005).
- Mroz, P., Hashmi, J. T., Huang, Y. Y., Lange, N. & Hamblin, M. R. Stimulation of anti-tumor immunity by photodynamic therapy. *Expert Rev. Clin. Immunol.* **7**, 75–91 (2011).
- Lemay, C. G. et al. Harnessing oncolytic virus-mediated antitumor immunity in an infected cell vaccine. *Mol. Ther.* **20**, 1791–1799 (2012).
- Errington, F. et al. Inflammatory tumour cell killing by oncolytic reovirus for the treatment of melanoma. *Gene Ther.* **15**, 1257–1270 (2008).
- Guo, Z. S., Liu, Z. & Bartlett, D. L. Oncolytic immunotherapy: dying the right way is a key to eliciting potent antitumor immunity. *Front. Oncol.* **4**, 74 (2014).
- Obeid, M. et al. Calreticulin exposure dictates the immunogenicity of cancer cell death. *Nat. Med.* **13**, 54–61 (2007).
- Michaud, M. et al. Autophagy-dependent anticancer immune responses induced by chemotherapeutic agents in mice. *Science* **334**, 1573–1577 (2011).
- Yang, H. et al. Contribution of RIP3 and MLKL to immunogenic cell death signaling in cancer chemotherapy. *Oncoimmunology* **5**, e1149673 (2016).
- Yatim, N. et al. RIPK1 and NF-kappaB signaling in dying cells determines cross-priming of CD8(+) T cells. *Science* **350**, 328–334 (2015).
- Ma, Y. et al. Anticancer chemotherapy-induced intratumoral recruitment and differentiation of antigen-presenting cells. *Immunity* **38**, 729–741 (2013).
- Ciampricotti M., Hau C. S., Doornebal C. W., Jonkers J., de Visser K. E. Chemotherapy response of spontaneous mammary tumors is independent of the adaptive immune system. *Nat. Med.* **18**, 344–346 (2012).
- Ciampricotti, M. et al. Development of metastatic HER2(+) breast cancer is independent of the adaptive immune system. *J. Pathol.* **224**, 56–66 (2011).
- Rovero, S. et al. DNA vaccination against rat her-2/Neu p185 more effectively inhibits carcinogenesis than transplantable carcinomas in transgenic BALB/c mice. *J. Immunol.* **165**, 5133–5142 (2000).
- Rahbar, R. et al. B7-H4 expression by nonhematopoietic cells in the tumor microenvironment promotes antitumor immunity. *Cancer Immunol. Res.* **3**, 184–195 (2015).
- Workenhe, S. T. et al. Immunogenic HSV mediated oncolysis shapes the antitumor immune response and contributes to therapeutic efficacy. *Mol. Ther.* **22**, 123–131 (2014).
- Chan, T. A., Wolchok, J. D. & Snyder, A. Genetic basis for clinical response to CTLA-4 blockade in melanoma. *N. Engl. J. Med.* **373**, 1984 (2015).
- Workenhe, S. T., Pol, J. G., Lichty, B., Cummings, D. & Mossman, K. L. Combining oncolytic HSV-1 with immunogenic cell death-inducing drug mitoxantrone breaks cancer immune tolerance and improves therapeutic efficacy. *Cancer Immunol. Res.* **1**, 309–319 (2013).
- van Vloten, J. P., Workenhe, S. T., Wootton, S. K., Mossman, K. L. & Bridle, B. W. Critical interactions between immunogenic cancer cell death, oncolytic viruses, and the immune system define the rational design of combination immunotherapies. *J. Immunol.* **200**, 450 (2018).
- Workenhe, S. T. & Mossman, K. L. Rewiring cancer cell death to enhance oncolytic viro-immunotherapy. *Oncoimmunology* **2**, e27138 (2013).
- Workenhe, S. T. & Mossman, K. L. Oncolytic virotherapy and immunogenic cancer cell death: sharpening the sword for improved cancer treatment strategies. *Mol. Ther.* **22**, 251–256 (2014).
- Workenhe, S. T., Verschoor, M. L. & Mossman, K. L. The role of oncolytic virus immunotherapies to subvert cancer immune evasion. *Future Oncol.* **11**, 675–689 (2015).
- Takahashi, N. et al. Necrostatin-1 analogues: critical issues on the specificity, activity and in vivo use in experimental disease models. *Cell Death Dis.* **3**, e437–e437 (2012).
- Kepp, O. et al. Consensus guidelines for the detection of immunogenic cell death. *Oncoimmunology* **3**, e955691 (2014).
- Pol, J. G. et al. Maraba virus as a potent oncolytic vaccine vector. *Mol. Ther.* **22**, 420–429 (2014).
- DeNardo, D. G. et al. Leukocyte complexity predicts breast cancer survival and functionally regulates response to chemotherapy. *Cancer Discov.* **1**, 54–67 (2011).
- Forde, P. M. et al. Neoadjuvant PD-1 blockade in resectable lung cancer. *N. Engl. J. Med.* **378**, 1976–1986 (2018).
- Gandhi, L. et al. Pembrolizumab plus chemotherapy in metastatic non-small-cell lung cancer. *N. Engl. J. Med.* **378**, 2078–2092 (2018).
- Hellmann, M. D. et al. Nivolumab plus ipilimumab in lung cancer with a high tumor mutational burden. *N. Engl. J. Med.* **378**, 2093–2104 (2018).
- Kroemer, G., Senovilla, L., Galluzzi, L., Andre, F. & Zitvogel, L. Natural and therapy-induced immunosurveillance in breast cancer. *Nat. Med.* **21**, 1128–1138 (2015).
- Wang, H. et al. In silico simulation of a clinical trial with anti-CTLA-4 and anti-PD-L1 immunotherapies in metastatic breast cancer using a systems pharmacology model. *R. Soc. Open Sci.* **6**, 190366–190366 (2019).
- Najafav, A. et al. BRAF and AXL oncogenes drive RIPK3 expression loss in cancer. *PLOS Biol.* **16**, e2005756 (2018).
- Smyth, M. J., Dunn, G. P. & Schreiber, R. D. Cancer immunosurveillance and immunoediting: the roles of immunity in suppressing tumor development and shaping tumor immunogenicity. *Adv. Immunol.* **90**, 1–50 (2006).
- Pfirsckhe, C. et al. Immunogenic chemotherapy sensitizes tumors to checkpoint blockade therapy. *Immunity* **44**, 343–354 (2016).
- Kroemer, G., Galluzzi, L., Kepp, O. & Zitvogel, L. Immunogenic cell death in cancer therapy. *Annu Rev. Immunol.* **31**, 51–72 (2013).
- Galluzzi, L. et al. Autophagy in malignant transformation and cancer progression. *EMBO J.* **34**, 856–880 (2015).
- Spranger, S. & Gajewski, T. F. Impact of oncogenic pathways on evasion of antitumor immune responses. *Nat. Rev. Cancer* **18**, 139 (2018).
- Aaes, T. L. et al. Vaccination with necroptotic cancer cells induces efficient anti-tumor immunity. *Cell Rep.* **15**, 274–287 (2016).
- Snyder, A. G. et al. Intratumoral activation of the necroptotic pathway components RIPK1 and RIPK3 potentiates antitumor immunity. *Sci. Immunol.* **4**, eaaw2004 (2019).
- Seifert, L. et al. The necrosome promotes pancreatic oncogenesis via CXCL1 and Mincle-induced immune suppression. *Nature* **532**, 245–249 (2016).
- Huang, Z. et al. RIP1/RIP3 binding to HSV-1 ICP6 initiates necroptosis to restrict virus propagation in mice. *Cell Host Microbe* **17**, 229–242 (2015).
- Yu, X. et al. Herpes simplex virus 1 (HSV-1) and HSV-2 mediate species-specific modulations of programmed necrosis through the viral ribonucleotide reductase large subunit R1. *J. Virol.* **90**, 1088–1095 (2016).
- Takahashi, N. et al. Necrostatin-1 analogues: critical issues on the specificity, activity and in vivo use in experimental disease models. *Cell Death Dis.* **3**, e437 (2012).
- Cho, Y., McQuade, T., Zhang, H., Zhang, J. & Chan, F. K.-M. RIP1-dependent and independent effects of necrostatin-1 in necrosis and T cell activation. *PLoS ONE* **6**, e23209 (2011).
- Stagg, J. & Allard, B. Immunotherapeutic approaches in triple-negative breast cancer: latest research and clinical prospects. *Ther. Adv. Med Oncol.* **5**, 169–181 (2013).
- Desmedt, C. et al. Biological processes associated with breast cancer clinical outcome depend on the molecular subtypes. *Clin. Cancer Res* **14**, 5158–5165 (2008).

58. Loi, S. Tumor-infiltrating lymphocytes, breast cancer subtypes and therapeutic efficacy. *Oncoimmunology* **2**, e24720 (2013).
59. Loi, S. et al. Prognostic and predictive value of tumor-infiltrating lymphocytes in a phase III randomized adjuvant breast cancer trial in node-positive breast cancer comparing the addition of docetaxel to doxorubicin with doxorubicin-based chemotherapy: BIG 02-98. *J. Clin. Oncol.* **31**, 860–867 (2013).
60. Nanda, R. et al. Pembrolizumab in patients with advanced triple-negative breast cancer: phase Ib KEYNOTE-012 study. *J. Clin. Oncol.* **34**, 2460–2467 (2016).
61. Zamarin, D. et al. Localized oncolytic virotherapy overcomes systemic tumor resistance to immune checkpoint blockade immunotherapy. *Sci. Transl. Med.* **6**, 226ra232 (2014).
62. Saha, D., Martuza, R. L. & Rabkin, S. D. Oncolytic herpes simplex virus immunovirotherapy in combination with immune checkpoint blockade to treat glioblastoma. *Immunotherapy* **10**, 779–786 (2018).
63. Vijayakumar, G., Palese, P. & Goff, P. H. Oncolytic Newcastle disease virus expressing a checkpoint inhibitor as a radioenhancing agent for murine melanoma. *EBioMedicine* **49**, 96–105 (2019).
64. Bourgeois-Daigneault M. C., et al. Neoadjuvant oncolytic virotherapy before surgery sensitizes triple-negative breast cancer to immune checkpoint therapy. *Science translational medicine* **10**, (2018).
65. Samson A., et al. Intravenous delivery of oncolytic reovirus to brain tumor patients immunologically primes for subsequent checkpoint blockade. *Sci. Transl. Med.* **10**, eaao1641 (2018).
66. Passaro, C. et al. Arming an oncolytic herpes simplex virus type 1 with a single-chain fragment variable antibody against pd-1 for experimental glioblastoma therapy. *Clin. Cancer Res.* **25**, 290–299 (2019).
67. Zhu, Y. et al. Enhanced therapeutic efficacy of a novel oncolytic herpes simplex virus type 2 encoding an antibody against programmed cell death 1. *Mol. Ther. Oncolytics* **15**, 201–213 (2019).
68. Rajani, K. et al. Combination therapy with reovirus and anti-pd-1 blockade controls tumor growth through innate and adaptive immune responses. *Mol. Ther.* **24**, 166–174 (2016).
69. Schmid, P. et al. Atezolizumab and nab-paclitaxel in advanced triple-negative breast cancer. *N. Engl. J. Med.* **379**, 2108–2121 (2018).
70. Ribas, A. et al. Oncolytic virotherapy promotes intratumoral T cell infiltration and improves Anti-PD-1 immunotherapy. *Cell* **174**, 1031–1032 (2018).
71. Yatim, N. et al. RIPK1 and NF- $\kappa$ B signaling in dying cells determines cross-priming of CD8<sup>+</sup> T cells. *Science* **350**, 328–334 (2015).
72. Lalaoui, N. & Brumatti, G. Relevance of necroptosis in cancer. *Immunol. Cell Biol.* **95**, 137–145 (2017).
73. Workenhe S. T., Ketela T., Moffat J., Cuddington B. P., Mossman K. L. Genome-wide lentiviral shRNA screen identifies serine/arginine-rich splicing factor 2 as a determinant of oncolytic virus activity in breast cancer cells. *Oncogene* **35**, 2465–2474 (2015).
74. Workenhe, S. T., Pol, J. G., Lichty, B. D., Cummings, D. T. & Mossman, K. L. Combining oncolytic HSV-1 with immunogenic cell death-inducing drug mitoxantrone breaks cancer immune tolerance and improves therapeutic efficacy. *Cancer Immunol. Res.* **1**, 309–319 (2013).
75. Bakhshinyan, D. et al. BMI1 is a therapeutic target in recurrent medulloblastoma. *Oncogene* **38**, 1702–1716 (2019).

## Acknowledgements

We would like to thank Derek Cummings for help with establishing the BALB-NeuT colony in our laboratory. We thank Mary Smith and Mary Bruni of John Mayberry Core Histology Facility, McMaster University for immunohistochemistry staining. Funding support is from Canadian Cancer Society Research Institute (to K.L.M.), Canadian Breast Cancer Foundation (to K.L.M.), and the Joseph and Wolf Lebovic Fellowship Program (to S.T.W.).

## Author contributions

S.T.W., A.N., Y.W., J.L.B. and K.L.M. conceived the study and designed experiments. S.T.W., A.N., A.V., N.E., A.N., D.N.H., J.W., A.O., Kelly L.M., D.N.H. developed the methodologies, conducted the experiments. S.T.W., K.L.M., A.N., A.O., J.A.N., A.G.M., S.K.S., D.B. analyzed and interpreted the experimental results. S.T.W., A.O., Y.W., J.L.B. and K.L.M. wrote and revised the manuscript.

## Competing interests

Authors declare that there are no competing interests.

## Additional information

**Supplementary information** is available for this paper at <https://doi.org/10.1038/s42003-020-01362-w>.

**Correspondence** and requests for materials should be addressed to S.T.W. or K.L.M.

**Reprints and permission information** is available at <http://www.nature.com/reprints>

**Publisher's note** Springer Nature remains neutral with regard to jurisdictional claims in published maps and institutional affiliations.



**Open Access** This article is licensed under a Creative Commons Attribution 4.0 International License, which permits use, sharing, adaptation, distribution and reproduction in any medium or format, as long as you give appropriate credit to the original author(s) and the source, provide a link to the Creative Commons license, and indicate if changes were made. The images or other third party material in this article are included in the article's Creative Commons license, unless indicated otherwise in a credit line to the material. If material is not included in the article's Creative Commons license and your intended use is not permitted by statutory regulation or exceeds the permitted use, you will need to obtain permission directly from the copyright holder. To view a copy of this license, visit <http://creativecommons.org/licenses/by/4.0/>.

© The Author(s) 2020